LATVIJAS UNIVERSITĀTE
FIZIKAS UN MATEMĀTIKAS FAKULTĀTE

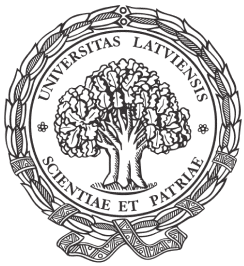

Dmitrijs Bočarovs

VIRSMAS ĪPAŠĪBU UN REAKCIJAS SPĒJU MODELĒŠANA NO PIRMAJIEM PRINCIPIEM NITRĪDU KODOLU DEGVIELAI

Promocijas darba kopsavilkums

Doktora zinātniskā grāda iegūšanai fizikā
Apakšnozare: cietvielu fizika

Rīga, 2012

Promocijas darbs izstrādāts no 2006. gada oktobra līdz 2011. gada augustam Latvijas Universitātes Cietvielu fizikas institūtā.

Darba forma: publikāciju kopa.

Šis darbs izstrādāts ar Eiropas Sociālā fonda atbalstu projektā „Datorzinātnes pielietojumi un tās saiknes ar kvantu fiziku".
Līguma Nr. 2009/0216/1DP/1.1.1.2.0/09/APIA/VIAA/044

Promocijas darba vadītājs: *Dr. chem.* LU Cietvielu fizikas institūta vadošais pētnieks **Jurijs Žukovskis**

Promocijas darba recenzenti:
Dr. lektors **Ģirts Barinovs**, Latvijas Universitātes Fizikas un matemātikas fakultāte
Dr. prof. **Roberto Kačufo** *(Roberto Caciuffo)***,** Eiropas Komisijas Transurāna elementu institūts
Dr. habil. vadošais pētnieks **Linards Skuja**, Latvijas Universitātes Cietvielu fizikas institūts

Promocijas darbs tiks aizstāvēts atklātā sesijā
LU Fizikas, astronomijas un mehānikas specializētajā promocijas padomes sēdē
2012. gada 24. janvārī. plkst. 15.00 Cietvielu fizikas institūtā Ķengaraga ielā 8, Rīgā.

Ar darbu un tā kopsavilkumu var iepazīties Latvijas Universitātes Bibliotēkā Rīgā, Kalpaka bulv. 4, un Latvijas Akadēmiskajā bibliotēkā Rīgā, Rūpniecības ielā 10.

LU Fizikas un astronomijas zinātnes nozares specializētās promocijas padomes priekšsēdētājs: *Dr. habil. phys.* **Ivars Tāle**

ISBN 978-9984-45-436-8

Saturs

Anotācija 5

Saīsinājumu saraksts 6

1. Ievads 7
   - 1.1. Motivācija 7
   - 1.2. Autora ieguldījums 7
   - 1.3. Zinātniskā novitāte 9
2. Literatūras apraksts 10
   - 2.1. UN īpašību eksperimentālie pētījumi 10
   - 2.2. Urāna nitrīda mijiedarbība ar skābekli 12
   - 2.3. Iepriekšējie UN un citu saistīto aktinīdu savienojumu teorētiskie aprēķini 14
3. Teorētiskie pamati 18
   - 3.1. Blīvuma funkcionāļa metodes (DFT) pamati 18
   - 3.2. Apmaiņas–korelācijas funkcionāļi 18
   - 3.3. Pseidopotenciāli 19
   - 3.4. Plakano viļņu formālisms 20
   - 3.5. Aprēķinu parametri *VASP-4* datoru programmā 21
   - 3.6. Aprēķinu parametri LCAO *CRYSTAL-06* datoru programmā 22
   - 3.7. Plātnes modelis un defektu periodiskums 23
4. UN tilpuma modelēšana 25
5. UN (001) un (110) virsmas strukturālās īpašības 27
6. UN ideālas virsmas modelēšana 29
   - 6.1. Bezdefektu UN(001) virsmas PW un LCAO aprēķini 29
   - 6.2. Bezdefektu UN (001) un (110) virsmas PW aprēķini ar spina relaksāciju 31
   - 6.3. Ideālas UN virsmas aprēķini: kopsavilkums 33
7. N un U vakanču modelēšana 34
   - 7.1. Vakances aprēķini: modelis un veidošanās enerģijas 34
   - 7.2. Vakanču radītā virsmas rekonstrukcija 36
   - 7.3. Elektroniskās īpašības: virsmas šūnas ierobežotā izmēra efekti un superšūnas izmēra izvēle 38
   - 7.4. Magnētiskās īpašības 39
   - 7.5. N vakanču aprēķinu rezultātu salīdzinājums UN (001) un (110) virsmai 39
   - 7.6. Vakances aprēķini: kopsavilkums 40

8. O adsorbcijas un migrācijas modelēšana uz UN bezdefektu virsmas 41
8.1. Atomāra skābekļa adsorbcija 41
8.1.1. Modelis un teorētiskie pamati 41
8.1.2. Atomārās adsorbcijas bez spina relaksācijas PW un LCAO aprēķinu salīdzinājums 42
8.1.3. Saites enerģijas, lādiņu un struktūras relaksācijas PW aprēķini 42
8.1.4. Elektronisko īpašību analīze 44
8.1.5. Salīdzinājums skābekļa adsorbcijai virs UN(001) un UN(110) virsmas 45
8.1.6. Atomāra skābekļa adsorbcija: kopsavilkums 46
8.2. Molekulārā skābekļa adsorbcija 46
8.2.1. Modelis un teorētiskais pamatojums 46
8.2.2. Spontānā disociācija 47
8.2.3. Adsorbētās molekulas elektroniskās īpašības 49
8.3. O adatoma migrācijas trajektoriju modelēšana gar UN(001) virsmu 51
9. O atomu migrācija un iekļaušana UN (001) defektīvā virsmā 53
9.1. O adatoma zemo barjeru iekļaušana no pozīcijas virs U_{surf} atoma uz N_{surf} vakanci 53
9.2. Skābekļa iekļaušana virsmas vakancēs 54
9.2.1. Modelis un teorētiskais pamatojums 54
9.2.2. Skābekļa iekļaušanas un šķīdināšanas enerģija 55
9.2.3. Spinu blīvums un lādiņi pēc Badera 57
9.2.4. Lādiņu pārdalījuma analīze: virsmas šūnas ierobežota izmēra efekti un superšūnas izmēra izvēle 57
9.2.5. Iekļautā skābekļa elektronisko stāvokļu blīvums (DOS) 58
9.2.6. Salīdzināšana skābekļa iekļaušanai N vakancē uz UN(001) un (110) virsmas 59
9.2.7. Skābekļa iekļaušanas modelēšana: kopsavilkums 60
10. Kopsavilkums 61
11. Galvenās tēzes 62
12. Literatūra 63
12.1. Autora publicētie darbi par promocijas tēmu 63
12.2. Citi autora publicētie darbi 63
12.3. Literatūras saraksts 63
13. Dalība zinātniskās konferencēs 68
Pateicības 70

Anotācija

Urāna mononitrīds UN ir viens no materiāliem, kuru var izmantot kā perspektīvu degvielu IV paaudzes kodolu reaktoriem. Tā kā UN paraugos vienmēr atrodas ievērojams daudzums skābekļa piemaisījumu, nepieciešams izprast O adsorbcijas mehānismu, kā arī tam sekojošo UN oksidēšanos.

Mēs pirmo reizi veicām UN virsmas un tās mijiedarbības ar skābekli detalizētu pētījumu, izmantojot DFT PAW metodi *VASP* programmas ietvaros. U un N vakances veidošanās enerģijas, kā arī saites enerģijas virs UN virsmas adsorbētajiem skābekļa atomiem un molekulām tika apskatītas kopā ar lādiņu pārdalīšanos, elektronisko stāvokļu blīvumu un O atomu migrācijas trajektorijām. Veiktie aprēķini ļauj piedāvāt enerģētiski iespējamo mehānismu UN(001) virsmas daļējai piesātināšanai ar skābekli. Tas izskaidro eksperimentāli novērojamo vieglo UN oksidāciju gaisā.

Atslēgvārdi: kvantu ķīmija, blīvuma funkcionāļa teorijas aprēķini, urāna mononitrīds, virsmas defekti, skābekļa adsorbcija.

Saīsinājumu saraksts

2D – divdimensiju

3D – trīsdimensiju

AE – pilnelektronu

AFM – antiferomagnētisks stāvoklis

BS – bāzes funkciju komplekts

BZ – Briljuena zona

CASTEP – komerciālā un akadēmiskā programmatūras pakotne, kas balstās uz PW formālismu un pseidopotenciāliem

CFI – Latvijas Universitātes Cietvielu fizikas institūts

CRYSTAL – datoru pakotne periodisko sistēmu un molekulu LCAO aprēķiniem no pirmajiem principiem

DFT – blīvuma funkcionāļa teorija

DOS – stāvokļu blīvums

EC FP-7 – Eiropas Savienības 7. Ietvara programma

EXAFS – rentgenabsorbcijas spektra izstieptā sīkstruktūra

fcc – kubiskā skaldnē centrētā struktūra

FM – feromagnētiskais stāvoklis

GAUSSIAN – datoru pakotne LCAO aprēķiniem no pirmajiem principiem

GGA – vispārinātā gradienta tuvinājums

KKR-GF – Korringa-Kona-Rostokera Grīna funkcija

LAPW – linearizētais paplašinātais plakanais vilnis

LC – lielā serdeņa pseidopotenciāli

LCAO – atomāro orbitāļu lineārā kombinācija

LDA – lokālā blīvuma tuvinājums

LMTO – lineārās „muffin-tin" orbitāles

ML – monoslānis

MT60 – Mosjagina-Titova mazā serdeņa pseidopotenciāls, kas satur 60 elektronus serdenī

MT78 – Mosjagina-Titova lielā serdeņa pseidopotenciāls, kas satur 78 elektronus serdenī

PAW – projicēto paplašināto viļņu metode

PBE – Perdju-Burke-Erncerhofa *(Perdew-Burke-Ernzerhof)* apmaiņas–korelācijas funkcionālis

ppm – daļiņu skaits uz miljonu

PS – pseidoviļņu mīkstā funkcija

PW – plakanie viļņi

PW91 – Perdju-Vanga-91 *(Perdew-Wang-91)* apmaiņas–korelācijas funkcionālis

RBS – Rezenforda apgrieztās izkliedes spektroskopija

RECP – relatīvistiskais efektīva serdeņa pseidopotenciāls

RMM-DIIS – atlikuma minimizācijas metode iteratīvās telpas tiešajā inversijā

SC – mazā serdeņa pseidopotenciāli

SC60 – Štutgartes–Ķelnes grupas pseidopotenciāls SC60 ar 60 elektroniem serdenī

SEM – skenējošā elektronu mikroskopija

UPS – ultravioletā fotoelektronu spektroskopija

US-PP – ultramīkstais pseidopotenciāls

UV – ultravioletais

VASP – Vīnes modelēšanas pakotne no pirmajiem principiem (Vienna *ab initio* simulation package), kas balstās uz PW formālismu un pseidopotenciāliem

XPS – rentgenstaru fotoelektronu spektroskopija

XRD – rentgenstaru difrakcija

1. Ievads

1.1. Motivācija

Urāna mononitrīds (UN) ir viens no daudzsološiem oksīdu nesaturošiem materiāliem, ko varētu izmantot kodolu degvielai t. s. IV paaudzes ātrajos kodolu reaktoros, kuru ieviešana varētu sākties pēc 20–30 gadiem [1, 2]. Urāna nitrīdam tika atklātas vairākas priekšrocības salīdzinājumā ar tradicionālajām UO_2 tipa degvielām (piemēram, augstāka siltumvadītspēja un lielāks metāla blīvums, kā arī augsta šķīdība slāpekļskābē degvielas pārstrādes laikā [2]). Tomēr viena no svarīgākajām aktinīdu nitrīdu problēmām ir to izteiktā oksidācija skābekli saturošā atmosfērā (tajā skaitā pie zemiem parciālajiem spiedieniem), kas ietekmē kodoldegvielas ražīgumu [3, 4]. Tāpēc ir svarīgi saprast UN oksidācijas mehānisma sākotnējo stadiju un atrast veidus, kā uzlabot kodoldegvielas kvalitāti nākotnē.

Galvenais šī promocijas darba mērķis ir iegūt ticamu informāciju par atomāro un elektronisko struktūru gan perfektām, gan defektu saturošām UN virsmas struktūrām, kā arī izprast virsmas oksidēšanās sākotnējo stadiju. Tas tiks darīts, risinot šādus uzdevumus:

- UN tilpuma modelēšana, lai pareizi izvēlētos virsmas aprēķinu parametrus;
- ideālas UN virsmas modelēšana, īpašu uzmanību pievēršot virsmas anizotropajai relaksācijai un pārbūvei;
- atsevišķo N un U vakanču modelēšana, kā arī virsmas defektu veidošanās enerģiju aprēķini;
- molekulārā un atomārā skābekļa adsorbcijas modelēšana uz ideālas UN virsmas;
- skābekļa migrācijas modelēšana pa UN(001) ideālo un defektu saturošo virsmu;
- O adatomu iekļaušanās modelēšana uz virsmas eksistējošās vakancēs;
- UN (001) un (110) virsmām iegūto rezultātu salīdzinājums;
- UN virsmas oksidēšanas atomistiskā modeļa izveide.

Šis pētījums tika veikts sadarbības līguma No. 205343-2006-07 F1ED KAR LV starp Cietvielu fizikas institūtu (Rīgā) un Transurānu elementu institūtu (Karlsrūē, Vācijā) ietvaros, kā arī ir viens no Eiropas Komisijas 7. Ietvara programmas *Basic Research for Innovative Fuel Design for Generation-IV systems (F-BRIDGE)* projektā iekļautajiem uzdevumiem.

1.2. Autora ieguldījums

Aprēķinu galvenie rezultāti, kas apskatīti un izanalizēti promocijas darbā, publicēti piecos rakstos prestižos starptautiskos žurnālos [P1–P5], kā arī prezentēti mutiskajos un stendu referātos starptautiskās un vietējās konferencēs (sk. konferenču sarakstu 13. nodaļā). Autors sniedza būtisku ieguldījumu rakstu un konferenču prezentāciju sagatavošanā un rakstīšanā, kā arī bija korespondējošais autors [P2–P5] rakstiem.

Lielāko rezultātu daļu autors ieguva, izmantojot PW aprēķinus (*VASP* datoru programma) (gandrīz visi aprēķini, kas iegūti [P1–P5] rakstos, izņemot N_2 molekulas un alfa-urāna tilpuma aprēķinus [P4, P5]). Sadarbībā ar Sanktpēterburgas Valsts universitāti (Krievija) tika veikti arī LCAO aprēķini (*CRYSTAL* datoru programma) [P1, P2], lai salīdzinātu abas *ab initio* pieejas, kuras izmantotas UN virsmas un tās ķīmiskās reaktivitātes modelēšanā. Autors instalēja datoru programmatūru parastā un paralēlā režīmā gan Latvijas Supeklasterī (CFI, Rīga), gan Skaitļošanas pētniecības centrā Garhingā (Vācija). Turklāt autors optimizēja ievada parametrus un galvenos uzstādījumus *VASP* aprēķiniem (sīkāku informāciju sk. 3. nodaļā), detalizēti analizēja izejas failus, lai lietotu iegūtos rezultātus tālākai apstrādei un interpretācijai, kā arī uzrakstīja dažādus skriptus, lai vadītu programmatūru un analizētu iegūtos rezultātus (piemēram, lai uzzīmētu DOS no *VASP* izejas failiem, attēlotu zonu struktūru, aprēķinātu magnētiskos momentus, elastības moduli, kā arī ekonomiski sadalītu resursus paralēlajos aprēķinos).

Tā kā līdz šim zinātniskajā literatūrā ir publicēts ierobežots skaits teorētisku un eksperimentālu datu, viena no svarīgām problēmām bija rūpīgi pārbaudīt šajā promocijas darbā aprēķinātos rezultātus. Autors izvēlējās šādas pārbaudes metodes.

1) Iegūto rezultātu salīdzinājums ar citiem eksperimentāliem vai teorētiskiem datiem.

Piemēram, kā uzrādīts literatūrā [1], UN režģa konstante a_0 = 4.886 Å, elastības modulis B = 194 GPa un kohēzijas enerģija E_0 = 13.6 eV. Šie parametri tika izmantoti salīdzināšanai ar vērtībām, kuras iegūtas veiktajos teorētiskajos aprēķinos.

2) Dažādu teorētisko metožu vienlaicīga izmantošana.

Mūsu UN tilpuma un ideālas (001) virsmas PW aprēķini, kā arī rezultāti skābekļa atomu adsorbcijai uz šī substrāta tika salīdzināti ar atbilstošiem LCAO rezultātiem, kas aprēķināti sadarbībā ar prof. R. Evarestova grupu (Sanktpēterburgas Valsts universitāte) [P1, P2]. Kvalitatīva saskaņa, kas iegūta, izmantojot divas dažādas pirmo principu metodes, ievērojami palielina iegūto rezultātu ticamību.

3) Iekšējo konverģences kritēriju meklēšana.

Piemēram, UN vakanču saturošo plātņu aprēķinos ir īpaši svarīgi kontrolēt kopīgo spinu. Vidējam magnētiskam momentam μ_{av} uz U atoma spina relaksētajos aprēķinos jābūt lielākam par 1 μ_B, pretējā gadījumā mēs nevaram panākt defektu veidošanās enerģijas konverģenci atkarībā no UN plātnes biezuma [P4]. Šis efekts ir saistīts ar lokāla minimuma eksistēšanu apskatītajām plātņu konfigurācijām. Globāls enerģijas minimums atbilst spina konfigurācijai ar $\mu_{av} > 1$, savukārt citas spina konfigurācijas neatbilst lokalizācijai globālajā enerģijas minimumā, kas, protams, padara tādus rezultātus par apšaubāmiem.

4) Rezultātiem, kas iegūti vienai un tai pašai sistēmai, salīdzinājumu, variējot skaitļošanas parametrus.

Piemēram, mēs salīdzinām vakances veidošanās enerģijas vienam defekta periodiskumam (2×2 vai 3×3) pie atšķirīgiem plātnes biezumiem (dažāds atomāro slāņu skaits); mēs arī meklējam kritērijus apgriezuma *(cut-off)* enerģijas konverģencei (sīkāk sk. 3. nodaļu) [P4].

1.3. Zinātniskā novitāte

Urāna savienojumu teorētiskie pētījumi ir saistīti ar zināmām grūtībām, jo elektronu kustībai jāievēro relativitātes efekti. Turklāt UN sistēmai ir jaukta metāliski kovalenta ķīmiskā saite: vieglo aktinīdu fizikālās un ķīmiskās īpašības nosaka daļēji lokalizētie *5f* elektroni, kas rada laikietilpīgus aprēķinus. Šajā pētījumā mēs pirmo reizi prezentējam UN virsmas DFT aprēķinus un piedāvājam UN virsmas iespējamo oksidācijas mehānismu. Šie rezultāti pārliecinoši demonstrē kvantu ķīmijas metodes lietošanas iespējas aktinīdu un to virsmas modelēšanā. Iegūtos rezultātus var izmantot urāna nitrīdu citu teorētisko aprēķinu, kā arī saistīto aktinīdu savienojumu (piemēram, urāna monokarbīds UC) aprēķinu pārbaudei. Turklāt DOS analīzes rezultātus, kas prezentēti šajā darbā, var izmantot eksperimentālo ultravioleto fotoelektronu spektru (UPS) kvalitatīvai interpretācijai urāna oksinitrīdiem, kas tiks sintezēti nākotnē.

2. Literatūras apraksts

2.1. UN īpašību eksperimentālie pētījumi

Urāna mononitrīds ir savienojums ar metālisku spīdumu un zemu elektrisko pretestību ($1.6 \cdot 10^{-4}$ cm) [5], kas kristalizējas *fcc* fāzē (tilpuma grupa $Fm\bar{3}m$, 2.1. att.) plašā temperatūru diapazonā. UN režģa konstante ir atkarīga no oglekļa piemaisījumiem [1], bet to neiespaido nelieli skābekļa piemaisījumi [6]. UN augstā kušanas temperatūra (~ 2780 ± 25 K) [1], augsts šķeļamo atomu blīvums (14.32 g/cm^2 pret 10.96 g/cm^2 UO_2 savienojumā [7]) un augsta siltumvadītspēja (13 W/mK) [8] padara urāna mononitrīdu par perspektīvu materiālu atomkodolu reaktoriem [1].

Līdz šim UN ražošanai tika izmantotas dažādas metodes. Urāna nitrīdu paraugi tika ražoti, sākot ar 19. gadsimtu, apdedzinot UCl_4 sāli NH_3 atmosfērā vai urāna bikarbīdu (UC_2) slāpekļa atmosfērā 1100 °C [1]. Visizplatītākās mūsdienu UN ražošanas metodes ir

- urāna nitrēšana N_2 vai NH_3 atmosfērā ~ 800–900 °C. Bieži U_2N_3 tiek izmantots kā starpprodukts, kas pēc tam tiek sadalīts, lai iegūtu UN pulveri ar zemu skābekļa piemaisījumu koncentrāciju [1];
- oglekļtermiskā reducēšana *(Carbothermic reduction)*. UN veidošana karbotermiskā vai nitrifikācijas procesā ir iespējama, izmantojot UO_2 + C presēto maisījumu, kam seko reakcija $UO_2 + 2C + 1/2N_2 \rightarrow UN + 2CO$, kas tiek uzturēta 1700 °C temperatūrā N_2, N_2/H_2 vai NH_3 atmosfērā. Tomēr šie produkti satur lielu O_2 piemaisījumu daudzumu, parasti 0.1 svara procentu [1, 9];
- nitrēšana, kausējot urānu N_2 gāzes atmosfērā ar galvaniskā loka palīdzību pie 3–5 bar spiediena. Ja tiek izmantoti volframa elektrodi, tad iegūtā UN materiāla piesārņojums ar W piemaisījumiem ir neizbēgams. Tāpēc tiek lietoti U elektrodi pie augstāka N_2 spiediena (20 bar) [1]. Reakcijas produkti, savukārt, joprojām ir neviendabīgi;

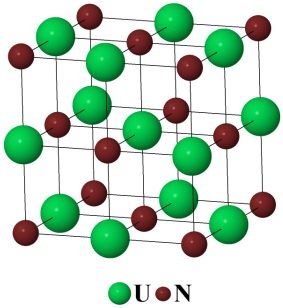

2.1. attēls. Urāna mononitrīda *fcc* struktūra

- hidrēšana *(Hydride route)*. Šīs metodes rezultātā veidojas labas kvalitātes pulveris ar daļiņu izmēru ~ 1 *μm*. Šajā metodē UH_3 izveidojas, reaģējot U un H_2 200–300 °C

temperatūrā. Pēc tam tas tiek sadalīts ($UH_3 \rightarrow U + 3/2H_2$), iegūstot U pulveri inertās gāzes atmosfērā vai vakuumā 400–600 °C temperatūrā. Tālāk, lai iegūtu UN_{1+x}, izraisa urāna pulvera reakciju ar N_2 800 °C. No UN_{1+x} var saražot UN, kā tika aprakstīts iepriekš, sildot to vakuumā 1100–1300 °C temperatūrā. Var arī izmantot tiešo reakciju starp UH_3 un N_2 [1];

- alternatīvie UN izgatavošanas procesi, kas uzsākti no UF_4 vai $UC1_4$ halkogenīdiem, ir mazāk svarīgi rūpnieciskajā ražošanā [1]. Jāatzīmē, ka zinātniskajos pētījumos tiek plaši izmantotas arī alternatīvās metodes. Piemēram, UN virsmu var ražot, bombardējot U metāla virsmu ar slāpekļa atomiem [10].

Aizraujošās un bieži mīklainās UN magnētiskās un elektroniskās īpašības rada U(5*f*) elektroni, kam piemīt pārejas īpašības starp izteikti lokalizētiem lantanoīdu 4*f* elektroniem un stipri delokalizētiem pārejas metālu *d* valences elektroniem [11]. Tiklīdz siltumietilpības mērījumos tiek konstatēts, ka temperatūrās, kas ir zemākas par Nīla *(Neel)* temperatūru (TN ~ 53 K), UN nonāk antiferromagnētiskajā stāvoklī [1]. Urāna nitrīda magnētiskās struktūras noskaidrošana veikta 60. gados, izmantojot neitronu difrakcijas metodes. Tika atrasts, ka urāna nitrīdam piemīt tā sauktā pirmā tipa magnētiskās struktūras sakārtošanās, kurā feromagnētiskie slāņi, kas ir paralēlas (001) plaknei, ir antiferomagnētiski savienoti [5]. Magnētiskā momenta vērtība, kas zemā temperatūrā vienāda ar 0.75 μ_B, ir pārsteidzoši maza (zemākā starp visiem urāna monopniktīdiem UX, kur X = P, As, Sb) [5]. Šeit nepieciešama rūpīga analīze, izmantojot DFT aprēķinus, un rezultātu salīdzināšana ar attiecīgajiem eksperimentālajiem datiem.

Fotoelektronu spektroskopija arī apliecina UN sarežģītību. Tika novērots ļoti augsts elektronisko stāvokļu blīvums Fermī līmeņa tuvumā, kas pierāda, ka U(5*f*) elektroni stipri hibridizējas, piedaloties saites veidošanā ar U(6*d*) elektroniem. U(5*f*) vadāmības stāvokļu apdzīvotība ir 2.2 ± 0.5 *e*, no kuriem ~ 1.8 *e* lokalizējas Fermī līmeņa tuvumā [11]. Ņemot vērā augstas izšķirtspējas leņķa fotoemisijas spektru otros atvasinājumus, referencē [12] tika konstruēta UN zonu struktūra pie 25 K. Stipri izkliedēta josla, centrēta ap Γ(X) punktu, tika novērota Fermī līmeņa tuvumā, kura apakšējā mala atrodas aptuveni pie 2 eV. Pirmie Kerra *(Kerr)* magnetooptiskie UN mērījumi arī norāda uz šauras U(5*f*) joslas veidošanos Fermī līmeņa tuvumā, kā arī uz U(5*f*) stāvokļu hibridizācijas palielināšanos ar U(6*d*) un N(2*p*) stāvokļiem salīdzinājumā ar līdzīgiem datiem par smagākajiem urāna monopniktīdiem [13]. No otras puses, urāna nitrīdam ir vismazākais U-U attālums starp visiem UX savienojumiem (X = N, P, As, Sb, S, Se un Te), kas ir vienāds ar 3.46 Å un ir tuvs kritiskajai 3.4 Å vērtībai, kura pēc Hilla diagrammām *(Hill diagrams)* atdala nemagnētiskos savienojumus no magnētiskiem, līdz ar to ir gaidāma U(5*f*) stāvokļu delokalizācija [14].

Informācijas iegūšana par slāpekļa atomu vai vakanču difūziju urāna nitrīdā ir netriviāla problēma. Diemžēl radioaktīvie slāpekļa izotopi, kuri piemēroti difūzijas mērījumiem, dabā neeksistē. Tāpēc, lai novērtētu slāpekļa difūzijas koeficientu, ir vajadzīgi masu spektrometrijas mērījumi ar ^{15}N atomiem vai arī kodolreakcija, inducēta UN paraugā pēc atkvēlināšanas [1]. No otras puses, termiski radītos un radiācijas izraisītos punktu defektus var pētīt, mērot fizikālos lielumus, kuri ir jutīgi attiecībā pret defektu klātbūtni. Piemēram, aktinīdu savienojumos šim nolūkam var izmantot elektrisko pretestību ρ: konstatētas ļoti lielas ρ izmaiņas atkarībā no vakanču koncentrācijas (piemēram, 12 μΩ·cm 1% C vakancēm UC savienojumā) [1]. Defektu migrācijas enerģiju

var arī noteikt, pētot šo defektu reģenerāciju izohronālās apdedzināšanas laikā vai lietojot „slīpuma izmaiņas metodi" izotermiskā apdedzināšanā ar strauju temperatūras paaugstināšanu. Diemžēl šīs metodes neļauj identificēt ne defekta veidu, ne arī difūzijas procesā iesaistītos atomus (piemēram, C, O un N) atšķirībā no difūzijas pētījumiem ar radioaktīvo marķieri [1].

2.2. Urāna nitrīda mijiedarbība ar skābekli

Urāna mononitrīda oksidācija skābekļa atmosfērā pirmo reizi sistemātiski tika pētītā referencē [15]. Eksperimentiem tika izmantoti divi galvenie UN paraugu veidi: pulverveidīgs UN un gludi pulēti UN gabaliņi. Pēc UN pulveru parauga svara izmaiņas oksidācijas procesā paaugstinātās temperatūrās tika konstatēta stipras eksotermiskas reakcijas sākšanās 250 °C temperatūrā, kuru raksturo strauja skābekļa adsorbcija. Parauga svars palielinājās par 11.5%. Rentgenstaru difrakcijas diagrammā starpproduktiem, veidotiem 250–260 °C, parādās gan vājās difrakcijas līnijas, kas atbilst UN, gan ļoti izteikti līniju paplašinājumi, kas atbilst UO_2 savienojumam. Gludi pulētie UN gabaliņi tika izmantoti, lai pētītu UN oksidēšanās kinētiku. Mērījumi parādīja, ka reakcijas ātrums ir proporcionāls virsmai, kura ir pārklāta ar oksīdu, vai oksidētajam tilpumam. Gan kinētiskie pētījumi, gan rentgenstaru difrakcijas dati norāda uz to, ka UN izotermiskā oksidācija sākas ar $UO_2(N)$ oksīda veidošanos uz parauga virsmas ar vienlaicīgu N_2 gāzes atbrīvošanu, kā arī ar $U_2N_3(O)$ savienojuma veidošanos, atbrīvotajam slāpeklim reaģējot ar UN.

Darbā [16] tiek izpētītas tādas īpašības kā ķīmiskais un fāžu sastāvs, režģa parametri, saķepamība, graudu augšana un siltumvadītspēja paraugos, izmantojot ķīmisko, rentgenstaru un keramogrāfisko analīzi urāna nitrīda karbotermiski iegūtām pulvera granulām, kas satur noteiktu skābekļa daudzumu (~ 0.3, ~ 0.6 un ~ 1.0% no masas). Ir nepieciešams arī pieminēt, ka oksidācijas dēļ UN paraugu vadītspēja pakāpeniski samazinās [16]. Galvenie rezultāti rāda, ka vidējais UN graudu izmērs matricas fāzē samazinās, palielinoties skābekļa saturam. Turklāt siltuma vadītspēja granulām, kas satur skābekli apmēram 1% no masas, ir zemāka nekā parastajām nitrīda granulām, kas satur 1000–2000 skābekļa ppm, attiecīgi par 9–10% pie 1000 un 12–13% pie 1500 K.

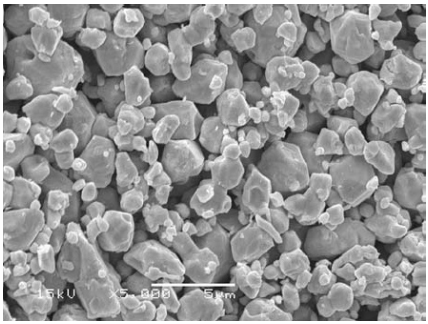

2.2. attēls. UN parauga SEM attēls [9]

Darbā [9] tiešā UF_4 amonolīze *(ammonolysis)* tika izmantota, lai sintezētu UN_2 paraugu, kas tika uzkarsēts inertā atmosfērā līdz 1100 °C temperatūrai 30 minūšu laikā, rezultātā sintezējot UN pulvera paraugus ar UO_2 ieslēgumiem, vienādiem ar 5.0% no masas. Rentgenstaru difrakcijas (XRD) un skenēšanas elektroniskās mikroskopijas (SEM) metodes tika izmantotas šo paraugu morfoloģijas analīzei. SEM attēli liecina par to, ka UN paraugs satur galvenokārt neregulārus graudus ar nepilnīgi kristalizētām skaldnēm (2.2. att.). Novērotais raksturīgais daļiņu izmērs svārstās no 0.1 līdz 6 mm. Izmērītais UN virsmas laukums ir vienāds ar 0.23 m^2/g. Elektronu kūļu mikroraudzes *(electron microprobes)* un rentgenstaru difrakcijas metožu analīze parādīja, ka skābekļa piemaisījumu daudzums UN paraugos ir ļoti liels un sastāv no primārās UN fāzes un sekundārās UO_2 piemaisījumu fāzes. Tas ļauj secināt, ka oksīda piemaisījumi, iespējams, veidojas, pateicoties difūzijas procesam no ķīmiskās apkārtējās vides, un tādējādi tie sakrājas uz daļiņu virsmām. Atrodoties gaisā, skābekļa piemaisījumu koncentrācija pieaug: UN paraugs, kas ir bijis kontaktā ar gaisu 3 mēnešus, uzrāda oksīda piesārņojuma palielināšanos. Kvantitatīvā analīze, kas tika veikta, analizējot XRD ainas, parādīja, ka UO_2 koncentrācija ir pieaugusi šajā laika posmā no 5.0 līdz 14.8% no masas [9].

Plāno UO_2, UN, UO_xN_y un UO_xC_y kārtiņu UPS mērījumi, izmantojot He-II 40.81 eV ierosināto starojumu, kuru rada UV cēlgāzu izlādes avots, tika aprakstīti [17, 18]. Šīs kārtiņas tika sagatavotas ar līdzstrāvas uzputināšanas metodi Ar atmosfērā. 2.3. attēlā redzams, ka U(5*f*) stāvokļi veido pīķi Fermī līmeņa tuvumā (0 eV), kas apstiprina šo stāvokļu pietiekami stipro delokalizācijas raksturu. UO_xN_y valences zonas spektrs liecina par plašas joslas veidošanos, kuru var interpretēt kā šauro O(2*p*) un N(2*p*) joslu superpozīciju. UN paraugam saites enerģijas maksimums pie 6 eV veidojas, pateicoties O(2*p*) stāvokļu ieguldījumiem, bet mazākais maksimums pie 3 eV sakrīt ar N(2*p*) stāvokļu ieguldījumu.

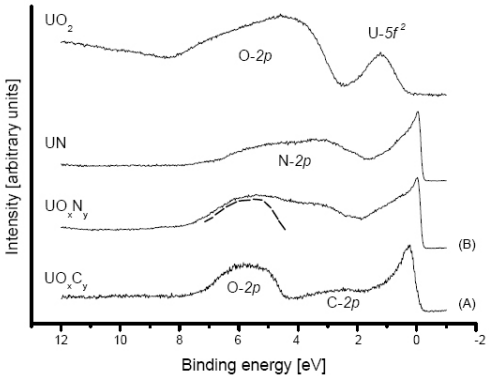

2.3. attēls. He-II valences zonas spektri UO_xC_y, UO_xN_y, UN un UO_2, sk. referenci [18]

Darbā [19] tika izmantotas XPS un XRD metodes, kā arī amonjaka koncentrācijas mērījumi ūdens fāzē pēc katra eksperimenta beigām, lai izpētītu UN koroziju ūdenī. UO_2 plēves veidošanās virsmas reakcijā ar ūdeni tika konstatēta, izmantojot svaigi pulētas

UN tabletes virsmas XPS. Augstā UN korozija ūdenī (928 °C) parādīja, ka UN ir nestabils karstā ūdens vidē. Korozijas ātrums UN ir daudz zemāks nekā metāliskajam urānam, bet augstāks nekā urāna silicīdam.

Biezuma, sastāva, koncentrācijas profila atkarības no dziļuma un jonu starojuma radītie efekti uz urāna nitrīda plānām kārtiņām, kuras uzklātas uz kvarca pamatnēm, tika pētīti [8], izmantojot Rezenforda apgrieztās izkliedes spektroskopiju (*Rutherford Backscattering Spectroscopy*, RBS) ar 2 MeV He^+ joniem. Uzputināšana −200 °C nodrošina biezas stehiomentriskas UN kārtiņas veidošanos. Tika konstatēts, ka šī kārtiņa bija stabila gaisa klātbūtnē. Virsmas oksidācija pastiprinās, kā arī oksidētie virsmas slāņi pakāpeniski kļūst biezāki kārtiņām, kas ir apputinātas augstākās temperatūrās (+25 °C un +300 °C). Tika novērota liela jonu apstarošanas ietekme uz kārtiņu struktūru un sastāvu. Šis pētījums parādīja, ka iespējams ražot stehiometrisko UN plāno kārtiņu ar nepieciešamo urāna saturu, kas vienāds ar 50%, kā arī iegūt nepieciešamo slāņa biezumu, izmantojot kārtiņas apstarošanu ar joniem.

Rezumējot iepriekš teikto, eksperimentālie pētījumi skaidri parādīja, ka skābeklis, kontaktējot ar urāna mononitrīda virsmu, var izraisīt oksīda savienojumu veidošanos, kas pēc sākotnējās stadijas var veidot virsmas slāni, kurš līdzīgs UO_xN oksinitrīdam [14].

2.3. Iepriekšējie UN un citu saistīto aktinīdu savienojumu teorētiskie aprēķini

Tā kā pēdējā laikā ir palielinājusies interese par brīderu reaktoriem un urāna, plutonija un mazāk sastopamo aktinīdu pārvēršanu, mūsdienās ir pievērsta liela uzmanība aktinīdu nitrīdu savienojumu aprēķiniem no pirmajiem principiem, kā arī citiem teorētiskiem aprēķiniem. Tomēr iepriekšējie teorētiskie pētījumi tika veikti galvenokārt par UN tilpumu. Sākot ar 80. gadiem [21–23], aprēķiniem no pirmajiem principiem tika izmantotas galvenokārt DFT aprēķinu metodes.

Pirmajos relatīvistiskajos UN tilpuma aprēķinos tika lietota pilna potenciāla Korringa–Kona–Rostokera (KKR) Grīna funkcijas metode [21] vai lineāro „muffin-tin" orbitāļu metode (LMTO) [22, 23] un galvenā uzmanība tika pievērsta atomārai un elektroniskai struktūrai. Aprēķinātie režģa parametri tika atrasti 3% robežās no eksperimentālām vērtībām, savukārt aprēķinātais elastības modulis sliktāk sakrita ar eksperimentālajiem datiem: bija par 23% lielāks [22] vai atradās 10% robežās [23]. DOS analīze parādīja, ka UN nav spraugas starp valences un vadīšanas zonām. ~ 5–6 eV plata valences zona parādās ~ 2 eV zem Fermī līmeņa. Galvenais maksimums atrodas 1 eV zem Fermī līmeņa [23].

Nesen tika veikti daudzi UN tilpuma DFT aprēķini no pirmajiem principiem. Dažu aktinīdu nitrīdu (AcN, ThN, PaN, UN, NpN, PuN, AmN) pilnelektronu LAPW aprēķini tika veikti, izmantojot PBE *(Perdew-Burke-Ernzerhof)* apmaiņas–korelācijas funkcionāli (ar spin-orbitālās mijiedarbības iekļaušanu vai bez tās iekļaušanas), tas realizēts *WIEN-2k* programmu pakā [20]. Tika novērtētas veidošanās entalpijas, kuru galvenais ieguldījums ir pamatstāvokļa kohēzijas enerģija. Tika konstatēts, ka iegūtās veidošanās entalpijas teicami saskaņojas ar eksperimentālajiem datiem (UN gadījumā labāka korelācija tika panākta ar kalorimetrisko mērījumu rezultātiem: teorētiskā vērtība, vienāda

ar –291.0 kJ·mol^{-1} pret eksperimentālo vērtību, vienādu ar –290.5 ± 1.4 kJ·mol^{-1} [24]). Atsevišķām neatbilstībām ar eksperimentālajiem datiem, kas ir novērotas PuN un ThN, joprojām ir nepieciešama precizēšana.

Referencē [25] GGA tuvinājums tika izmantots tā paša LAPW formālisma ietvaros, lai izpētītu aktinīdu savienojumu strukturālās, elektroniskās un magnētiskās īpašības. Novērotai ķīmiskai saitei starp aktinīdu un slāpekli ir ievērojams jonisks raksturs. Tika konstatēts, ka aprēķinātā kohēzijas enerģija ir tuva eksperimentālām vērtībām (attiecīgi 14.3 eV pret 13.6 eV). Lai gan režģa konstantes tika aprēķinātas labā saskaņā ar eksperimentu (~ 0.4% robežās), UN, AmN, PuN un NpN aprēķini norāda uz šo savienojumu feromagnētisko stāvoli (FM), kas ir pretrunā ar eksperimenta rezultātiem (AFM struktūra eksperimentāli novērota zemās temperatūrās). Aprēķinātais spina blīvums UN FM stāvokļiem ir vienāds ar 0.96 μ_B. No otras puses, NpN aprēķinātā feromagnētiskā struktūra un nemagnētiskā ThN struktūra labi sakrīt ar attiecīgajiem eksperimentālajiem mērījumiem.

Referencē [26] pilno elektronu relativitātes spin-polarizētie DFT aprēķini tika veikti, lai novērtētu kopējo enerģiju, optimizēto ģeometriju, kā arī elektroniskās un termodinamiskās īpašības ideālam stehiometriskajam UN un UN_2 tilpumam. Šim nolūkam tika lietots GGA PW91 apmaiņas–korelācijas funkcionālis un atomiem, smagākiem par ūdeņradi, pievienots skaitliskais dubult-ξ bāzes komplekts ar *d*-tipa polarizācijas funkcijām. Struktūras īpašības, kas nesen tika novērtētas, izmantojot EXAFS un XRD metodes, tika sekmīgi reproducētas teorētiskajos aprēķinos (0.03 Å kļūdas robežās). Aprēķinātais DOS parādīja U(*6d*), U(*5f*) un N(*2p*) stāvokļu hibridizāciju, kā arī U(*5f*) stāvokļu dominēšanu vadīšanas zonā. Šī raksta novitāte ietver sevī fononu frekvences un siltuma jaudas aprēķinus. Šī raksta autori uzskata, ka migrējošie U(*5f*) stāvokļi stipri ietekmē UN termodinamiskās īpašības.

Režģa parametri, elektroniskā struktūra, kā arī termodinamiskās UN īpašības, izmantojot LDA+*U* un GGA+*U* pusempīrisko shēmu ar iekļauto Habarda potenciālu *U*, tika prezentēti referencē [27]. Pilnās enerģijas atkarība no *U*-parametra UN FM un AFM stāvoklī, iegūta attiecīgajos aprēķinos, liecina par to, ka FM stāvoklis ir izdevīgs *U*-parametru diapazonam starp 0 un 2 eV, bet AFM stāvoklis varētu būt izdevīgs *U*-parametriem, lielākiem par 2 eV. Lai gan AFM stāvoklis UN tilpumam ir reproducēts, pamatstāvokli grūti iegūt, lietojot DFT+*U* metodi [28]. Tas var radīt nopietnas kļūdas, aprēķinot defektu veidošanās enerģijas [29, 30]. Mēs nelietojam šo metodi sakarā ar UN virsmas FM raksturu [31], kuru reproducē parastie DFT funkcionāļi.

PW pieeja tika izmantota UN atomāras struktūras aprēķiniem, sākot no [32]. Šajā pētījumā ultramīkstais (US) pseidopotenciāls un PBE apmaiņas–korelācijas funkcionālis tika izmantots, reproducējot eksperimentālās UN un U_2N_3 režģa konstantes ar 3% kļūdu, bet atomu koordinātas ar 5% kļūdu.

Daudz detalizētākos UN tilpuma PW aprēķinos *VASP* un *CASTEP* datoru kodi tika lietoti, izmantojot *Perdew-Wang* (PW91) nelokālo GGA apmaiņas–korelācijas funkcionāli, kombinētu attiecīgi ar US vai PAW pseidopotenciāliem [33, 34]. Abas aprēķinu sērijas liecina par UN ķīmiskās saites jaukto metāliski kovalento būtību, kvalitatīvi reproducējot režģa konstantes, elastības moduli un kohēzijas enerģiju.

PW pieeja, kombinēta ar superšūnas modeli, tika izmantota UN defektu saturoša kristāla ar atsevišķiem punktu defektiem aprēķiniem, kā arī Frenkeļa un Šotki defektu pāriem. Referencē [34] tika parādīts, ka N vakancēm praktiski nav ietekmes uz UN režģa konstanti pat pie koncentrācijām, kas pārsniedz 25%. Ir iegūtas U un N vakances veidošanās enerģijas UN tilpumā, kas vienādas ar 9.1–9.7 eV N vakancei un 9.4–10.3 U vakancei. Aprēķinātā aktivācijas enerģija starpmezglu N atomu migrācijai gar (001) asi tika novērtēta kā samērā zema, 2.73 eV [33]. Šis fakts apstiprina hipotēzi, ka starpmezglu migrācija ir dominējošais N difūzijas mehānisms UN degvielā [1]. Atsevišķi no tukšo vakanču uzvedības tika apskatīta arī O atoma iekļaušana vakancēs UN tilpumā [35]. Tika konstatēts, ka iekļaušana N vakancēs ir enerģētiski labvēlīgāka salīdzinājumā ar iekļaušanu starpmezgla pozīcijā. Tomēr aprēķinātās šķīduma enerģijas parādīja pretēju efektu. Aprēķinātā migrācijas enerģija starpmezglu O atomiem ir ļoti līdzīga (2.84 eV). Šis fakts apstiprina to, ka O atomus var viegli aizstāt ar N atomiem UN struktūrā.

Nesenie UN tilpuma LCAO aprēķini tika veikti [36, 37], izmantojot *GAUSSIAN-03* datora kodu kopā ar PW91 apmaiņas–korelācijas funkcionāli. Kohēzijas enerģijas vērtības, kas aprēķinātas, lietojot relatīvistiskos efektīvās serdes RECP78 un RECP60 potenciālus, ievērojami atšķiras (attiecīgi 9.86 eV un 12.8 eV), tādējādi norādot uz U ārējo čaulu variāciju nozīmi. Grupu teorētiskā analīze, veikta UN joslu struktūras interpretācijai, parādīja, ka vadīšanas zonas apakšā un valences zonas virsotnē veidojas U(*5f*) stāvokļi, kuri nosaka UN metālisko raksturu [36, 37], atšķirībā no UO_2, kas ir pusvadītājs [38]. ± (1.5–2.0) *e* Mullikena efektīvais atomārais lādiņš, kas aprēķināts, izmantojot *GAUSSIAN-03* kodu, apstiprina UN ķīmiskās saites jaukto raksturu un labi saskaņojas ar Badera topoloģisko analīzi, kas dod PW aprēķiniem ± 1.6 *e* lādiņu vērtības [34].

Pēdējos gados publicēti arī daudzi pētījumi par līdzīgiem aktinīdu savienojumiem. Referencē [29] skābekļa vakanču veidošanās enerģijas UO_2 savienojumā tika aprēķinātas, izmantojot Dudareva DFT+*U* pieeju [39]. Atrastas skābekļa vakances veidošanās enerģijas UO_2 tilpumā, kas ir vienādas ar 3.5–5.67 eV. Referencē [40] O un U vakanču veidošanās enerģijas tika aprēķinātas, izmantojot GGA tuvinājumu. Šie aprēķini parādīja nelielu atšķirību starp FM un AFM stāvokli (4.0 eV U vakances veidošanai FM stāvoklim salīdzinājumā ar 4.4 eV AFM stāvokli, kā arī 6.1 eV O vakancei abos gadījumos). Referencē [41] punktu defekti urāna monokarbīda tilpumā tika pētīti, kombinējot PAW metodi ar PBE funkcionāli. Tika konstatēts, kā urāna vakances veidošanās enerģija ir vienāda ar 4.54–4.55 eV, bet analoģiskas oglekļa vakances veidošanas enerģija ir vienāda ar 0.8–0.83 eV. NpN mehāniskās īpašības tika pētītas, izmantojot to pašu GGA PBE funkcionāli [42]. Aprēķinātais NpN elastības modulis mainās intervāla robežās no 147 līdz 227 GPa atkarībā no magnētiskā stāvokļa (AFM, FM vai nemagnētiskais).

Pirmā elektroniskās struktūras modelēšana aktinīdu virsmām un to reakciju spējai attiecībā uz molekulāro un atomāro skābekli tika paveikta tikai nesen. Tomēr tas nav pārsteigums, jo aktinīdu virsmu nevar viegli aprēķināt, izmantojot DFT metodes, sakarā ar lielo elektronu skaitu elementāršūnā. Tomēr daži α-U, δ-Pu un UO_2 virsmu modelēšanas rezultāti ir pieejami zinātniskajā literatūrā. Piemēram, referencē [43] Teilors parādīja, ka PAW metode [44], kas tika lietota arī mūsu pētījumā, ir piemērota (001) virsmas α-U ticamiem aprēķiniem.

Tans *(Tan)* un citi ieguva UO_2 virsmas enerģiju, izmantojot atomu mēroga datoru simulācijas ar starpatomu potenciāliem, kas sistemātiski klasificē 153 unikālas virsmas plaknes konfigurācijas, kuras var uzģenerēt 2×2 superšūnai [45]. Aprēķinātā virsmas enerģija mainās no 2.28 līdz 3.12 eV UO_2 (001) virsmai un no 1.27 līdz 1.54 eV UO_2(111) virsmai. PW91 funkcionālis tika izmantots UO_2 (111), (110) un (100) virsmas modelēšanai [46]. Aprēķini parādīja, ka (111) virsmai ir vismazākā virsmas enerģija (0.461 J/m^2), tai seko (110) virsma (0.846 J/m^2) un (100) virsma (1.194 J/m^2).

Aprēķini, kurus veica Ata-Finns un Rejs *(Atta-Fynn and Ray)* [47, 48], arī apstiprina DFT metodes efektivitāti O, C un N jonu hemisorbcijas modelēšanai virs δ-Pu(111) virsmas. Aprēķini tika veikti, izmantojot GGA PBE apmaiņas–korelācijas funkcionāli. Tika apskatīts 50% virsmas pārklājums ar adatomiem. Aprēķini tika veikti divos līmeņos: bez spin-orbitālās mijiedarbības un ar spin-orbitālo mijiedarbību. Spin-orbītālas mijiedarbības iekļaušana pazemina hemisorbcijas enerģiju par 0.05–0.27 eV, bet, no otras puses, tai ir nenozīmīga ietekme uz hemisorbcijas ģeometriju. Katra atoma efektīvo lādiņu analīze norāda uz to, ka hemisorbcija galvenokārt notiek virsmas slānī. Pu-adatomu hibridizācijā dominē Pu(6*d*) un adatoma 2*p* stāvoklis ar ievērojamu samazinājumu pirmajam pīķim projicētajos Pu(5*f*) stāvokļos, norādot uz dažu Pu(5*f*) elektronu delokalizāciju.

Jebkurā gadījumā šobrīd literatūrā nav publicēti citi UN virsmas aprēķini, izņemot pašreizējos pētījumus, kas tika veikti šajā promocijas darbā [P1–P5].

3. Teorētiskie pamati

UN modelēšanā mēs izmantojām *VASP-4* datoru kodu, komplekso komerciālo datoru pakotni, kas lieto blīvuma funkcionāļa teoriju (DFT) un iekļauj sevī Kona–Šema *(Kohn-Sham)* vienādojumu iteratīvu risināšanu, balstītu uz atlikuma mazināšanas *(residuum-minimization)* un optimizētu lādiņu blīvumu sajaukšanas procedūru [49]. Šī pakete ir uzbūvēta, izmantojot plakano viļņu bāzes funkcijas, kombinētas ar US vai PAW pseidopotenciāliem. *VASP* paketes izstrāde tika sākta 90. gadu sākumā.

3.1. Blīvuma funkcionāļa metodes (DFT) pamati

Par DFT blīvuma teorijas atskaites punktu kļuva Hohenberga–Kona *(Hohenberg-Kohn)* teorēma, kura apgalvo, ka daudzelektronu sistēmas pamatstāvokli var viennozīmīgi aprakstīt ar elektronu blīvuma $\rho(\vec{\mathbf{r}}) = \rho(\vec{\mathbf{r}}, \vec{\mathbf{r}}')$ palīdzību. Sistēmas pilno enerģiju var pierakstīt šādi:

$$E(\rho(\vec{\mathbf{r}})) = \int V(\vec{\mathbf{r}})\rho(\vec{\mathbf{r}})d\vec{\mathbf{r}} + T[\rho(\vec{\mathbf{r}})] + \frac{1}{2}\int \frac{\rho(\vec{\mathbf{r}}')\rho(\vec{\mathbf{r}})}{|\vec{\mathbf{r}} - \vec{\mathbf{r}}'|} d\vec{\mathbf{r}}' d\vec{\mathbf{r}} + E_{xc}[\rho(\vec{\mathbf{r}})], \qquad (3.1.1.)$$

kur labās daļas pirmais loceklis apraksta ārējo potenciālu ietekmi, kas iedarbojas uz sistēmu, piemēram, elektronu pievilkšanās enerģiju pie atomu kodoliem, otrais – kinētisko enerģiju, trešais ir tā sauktais Hartrī *(Hartree)* loceklis, kurš apraksta starpelektronu kulona atgrūšanos, un pēdējais loceklis ir tā sauktais apmaiņas–korelācijas potenciāls, kurā iekļauj visus parējos ieguldījumus, tajā skaitā daudzelektronu mijiedarbību.

Variējot pilnās enerģijas funkcionāli *(vienādojums 3.1.1.)*, var iegūt Kona–Šema vienelektronu vienādojumus (līdzīgus Hartrī–Foka vienādojumiem):

$$(\hat{\mathbf{H}} + \hat{\mathbf{J}} - \hat{\mathbf{V}}_{xc})\varphi_i(\vec{\mathbf{r}}) = \varepsilon_i\varphi_i(\vec{\mathbf{r}}), \qquad (3.1.2.)$$

kur loceklis $\hat{\mathbf{V}}_{XC}[\rho(\vec{\mathbf{r}})] = \frac{\delta E_{xc}[\rho(\vec{\mathbf{r}})]}{\delta\rho(\vec{\mathbf{r}})}$ ir apmaiņas–korelācijas potenciāls [50].

Tā kā Hamiltona un Kulona operatori Kona–Šema vienādojumos $\hat{\mathbf{H}}$ un $\hat{\mathbf{J}}$ ir atkarīgi no blīvuma $\rho(\vec{\mathbf{r}})$, vienādojumi jārisina pašsaskaņotā veidā [50].

Mūsdienu cietvielu DFT aprēķinos ir nepieciešams izdarīt dažas galvenās izvēles: (*i*) izvēlēties apmaiņas–korelācijas funkcionāli, (*ii*) izvēlēties bāzes funkcijas, lai izvirzītu Kona–Šema īpašfunkcijas (plakanie viļņi vai lokalizētās bāzes funkcijas), un izvēlēties, (*iii*) kā raksturot mijiedarbību starp jonu kodoliem un valences elektroniem (pilnā potenciāla pieeja vai pseidopotenciāla pieeja) [52].

3.2. Apmaiņas–korelācijas funkcionāļi

Tā kā precīza apmaiņas–korelācijas funkcionāļa forma nav zināma, milzīgs progress kvantu ķīmijas metodēs tika panākts, izveidojot piemērotus funkcionāļus. Dažādas sarežģītības funkcionāļi tika izveidoti DFT funkcionāļu hierarhijas ietvaros. Vienkāršākais tuvinājums ir lokālā blīvuma tuvinājums (*local density approximation*, LDA), kas balstās

uz precīzu viendabīgas elektronu gāzes apmaiņas enerģiju, kuru var iegūt, pielāgojot korelācijas enerģiju elektronu gāzei [50].

Šajā pētījumā mēs izmantojām vispārināto gradienta tuvinājumu (*Generalized Gradient Approximation*, GGA), kas paredz, ka elektronu blīvums ir sadalīts nevienmērīgi: vislielākais blīvums ir lokalizēts atomu kodolu apkārtnē. Apmaiņas–korelācijas enerģiju var izvirzīt Teilora rindā pēc elektroniskā blīvuma pakāpēm. Ja aprobežojas ar pirmās kārtas locekļiem, tad rezultējošā izteiksme satur elektroniskā blīvuma gradientu $\nabla\rho$ [50, 53].

Reālus funkcionāļus parasti veido, izmantojot pielāgošanas parametrus, kas ļauj ar augstu precizitāti reproducēt dažādu materiālu klašu eksperimentālos datus. Ir ļoti svarīgi atrast tādu funkcionāļa veidu, kuru var lietot daudzu sistēmu aprakstam bez papildu parametru ieviešanas aprēķinu laikā (tieši šajā ziņā šādus aprēķinus sauc par *ab initio* vai aprēķiniem no pirmajiem principiem). Šai pētījumā tika izmantots PW91 apmaiņas–korelācijas funkcionālis [54].

3.3. Pseidopotenciāli

Pseidopotenciālu formālismu plaši izmanto kvantu ķīmijas aprēķinos: elementu ķīmiskās īpašības galvenokārt nosaka valences elektroni, iekšējās čaulas ir ķīmiski inertas, savukārt pusaizpildītām vai pilnībā aizpildītām čaulām piemīt sfēriskā simetrija (tā sauktā Unsolda *(Unsöld)* teorēma [55]). Tas ļauj mums aprakstīt atsevišķi tikai ārējo čaulu elektronus. Savukārt visi iekšējie elektroni var tikt aizstāti ar kopēju efektīvo pseidopotenciālu. Atkarībā no pseidopotenciālā iekļautā elektronu skaita tos var iedalīt lielā serdeņa (*Large Core*, LC) un mazā serdeņa (*Small Core*, SC) RECP pseidopotenciālos.

U atomam, piemēram, ir $1s^2 2s^2 2p^6 3s^2 3p^6 3d^{10} 4s^2 4p^6 4d^{10} 4f^{14} 5s^2 5p^6 5d^{10} 6s^2 6p^6 7s^2 5f^3 6d^1$ elektroniskā struktūra. LC(U) potenciāls iekļauj sevī 78-elektronu serdes potenciālus ($[Xe]4f^{14}5d^{10}$) un 14 valences elektronus ($6s^2 6p^6 7s^2 5f^3 6d^1$), bet SC(U) potenciāls ietver 60-elektronu serdes potenciālus ($[Kr]4d^{10}4f^{14}$) un 32 valences elektronus ($5s^2 5p^6 5d^{10} 6s^2 6p^6 7s^2 5f^3 6d^1$). Atšķirībā no LCAO RECP pseidopotenciāliem, izmantotajiem *CRYSTAL* aprēķinos, RECP pseidopotenciālus PW aprēķiniem nevar tieši reoptimizēt: jauna pseidopotenciāla uzbūve vai tās atkārtotā optimizācija ir ļoti sarežģīts uzdevums, kas var prasīt vairākus mēnešus vai gadus tā atrisināšanai [56]. Galvenais mērķis pašreizējai darbībai, aprakstītai šajās tēzēs, ir pienācīga RECP pseidopotenciāla izmantošana, lai iegūtu ticamus rezultātus, optimāli izvēloties potenciālus no standarta pseidopotenciālu bibliotēkas, kuru nodrošina *VASP* kods (atkarībā no serdeņa struktūras un starpības ar visu elektronu viļņu funkciju). Pseidopotenciāla izvēlei ir jābalstās uz saišu raksturu starp sistēmas joniem [49], ieskaitot testa aprēķinus.

Aprēķiniem, kuri tika veikti pašreizējā PhD pētījumā, mēs izmantojām RECP pseidopotenciālus ar 78 U iekšējiem elektroniem (ar $6s^2 6p^6 6d^2 5f^2 7s^2$ valences čaulu), kā arī ar 2 serdeņa elektroniem gan N, gan O atomiem (attiecīgi ar $2s^2 2p^3$ un $2s^2 2p^4$ valences čaulu).

3.4. Plakano viļņu formālisms

Kona–Šema metode, kas izmanto plakano viļņu bāzes komplektu un pseidopotenciālu aproksimāciju, ir viena no spēcīgākām mūsdienu skaitļošanas materiālzinātnes metodēm. Plakano viļņu bāzes komplekta lietošanai ir vairākas priekšrocības [52]: (*i*) izmantojot ātro Furjē pārveidojumu, ir viegli pāriet no reālās telpas reprezentācijas (kur potenciālajai enerģijai V ir diagonāla reprezentācija) uz apgriezto telpu, kurā kinētiskā enerģija T ir diagonāla; *(ii)* bāzes komplekta konverģences kontrole ir gandrīz triviāla, ir pietiekami kontrolēt īpašvērtības un pilno enerģiju kā funkciju no apgriezuma enerģijas vai, citiem vārdiem, plakano viļņu visaugstāko kinētisko enerģiju izvēlētajā bāzes komplektā; (*iii*) Helmana–Feimana spēkus, kas iedarbojas uz atomiem, un spriedzi elementāršūnā var aprēķināt uzreiz, pamatojoties uz sagaidāmo hamiltoniāna vērtību attiecībā uz jonu koordinātēm; (*iv*) ir apietas superpozīcijas kļūdas, kuras rūpīgi jākontrolē aprēķinos, kas balstās uz lokālajiem bāzes funkciju komplektiem.

Par sākumpunktu Kona–Šema vienādojuma risināšanai ar PW bāzes komplektu parasti lieto Bloha *(Bloch)* teorēmu, kas apraksta elektrona (vai citas daļiņas) viļņu funkciju, novietotu periodiskajā potenciālā [57], vai, citiem vārdiem:

$$\psi_{n\mathbf{k}}(\mathbf{r}+\mathbf{R}) = \psi_{n\mathbf{k}}(\mathbf{r})e^{i\mathbf{kR}} \qquad (3.4.1.)$$

Elementāršūnā viļņu funkcijas periodiskā daļā $u_{n\mathbf{k}}$ tiek ieviesta kā

$$\psi_{n\mathbf{k}}(\mathbf{r}) = u_{n\mathbf{k}}(\mathbf{r})e^{i\mathbf{kr}}, \qquad (3.4.2.)$$

kur $u_{n\mathbf{k}}(\mathbf{R}+\mathbf{r}) = u_{n\mathbf{k}}(\mathbf{r})$. Tas nozīmē, ka visas šūnas periodiskās funkcijas var tikt pierakstītas kā plakano viļņu summa, pārejot uz apgrieztā režģa telpu un veicot Furjē transformāciju:

$u_{\mathbf{k}}(\mathbf{r}) = \sum_{\mathbf{G}} u_{\mathbf{k}}(\mathbf{G})\mathrm{e}^{i\mathbf{Gr}}$ (**G** vektors tiek izvēlēts tā, lai $\mathrm{e}^{i\mathbf{Gr}}$ būtu ar reālās telpas režģa periodiskumu)

$$\psi_{\mathbf{k}}(\mathbf{r}) = (N\Omega_0)^{-1/2}\sum_{\mathbf{G}} u_{\mathbf{k}}(\mathbf{G})\mathrm{e}^{i(k+\mathbf{G})\mathbf{r}}, \qquad (3.4.3.)$$

kur $u_{\mathbf{k}}(\mathbf{G}) = \frac{1}{\Omega_0}\int_{\Omega_0} \mathrm{e}^{-i\mathbf{Gr}}u_{\mathbf{k}}(\mathbf{r})d\mathbf{r}$ (Furjē transformācija).

Faktiski plakano viļņu skaits ir definēts kā funkcija no kinētiskās enerģijas apgriezuma enerģijas, tādējādi veidojot PW sfēru $\frac{(\mathbf{k}+\mathbf{G})^2}{2} < E_{cut}$ apgrieztajā telpā [57].

VASP programmā izmantotā PW formālisma attīstība noveda pie projektora–paplašināto viļņu (PAW) metodes, kuru sākotnēji ieviesa Blohls *(Blöchl)* [44]. Galvenā PAW metodes ideja ir pārveidot fizikāli atbilstošās pilno elektronu (AE) Kona–Šema viļņu funkcijas Ψ_n Hilberta telpā uz jaunajām, aprēķiniem ērtajām pseidoviļņu mīkstajām (*pseudo-wave soft PS*) variacionālajām funkcijām $\tilde{\Psi}_n$ tā saucamā pseido-Hilbertā telpā [58]. PAW formālisma ietvaros AE viļņu funkcijas tiek iegūtas no PS viļņu funkcijām, izmantojot lineāru transformāciju [44]:

$$|\Psi_n\rangle = |\tilde{\Psi}_n\rangle + \sum_i (|\varphi_i\rangle - |\tilde{\varphi}_i\rangle)\langle \tilde{p}_i | \tilde{\Psi}_n \rangle, \qquad (3.4.4.)$$

kur AE parciālie viļņi φ_i tiek iegūti references atomam, savukārt PS parciālie viļņi $\tilde{\varphi}_i$ ir līdzvērtīgi AE parciāliem viļņiem ārpus serdeņa rādiusa r_c^l un atbilst nepārtrauktajiem $\tilde{\varphi}_i$ serdeņa rādiusa iekšpusē (paplašināšanas reģions, līdzīgs linearizēto *muffin-tin* LMTO formālismam); indekss *i* šeit ir atomārās pozīcijas R_i saīsinājums, leņķiskā momenta skaitlis ir *L* = *l*, *m*, turklāt papildu indekss *k* attiecas uz vienelektronu references enerģiju ε_{kl}. Serdeņa rādiuss izvēlēts tā, lai atbilstu pusei no attāluma līdz tuvākajam kaimiņam [58]. Projektora funkcijas $\tilde{p}_i$ ir duālas attiecībā uz PS parciālajiem viļņiem:

$$\langle \tilde{p}_i | \tilde{\varphi}_j \rangle = \delta_{ij} \qquad (Eq.\ 3.4.5)$$

3.5. Aprēķinu parametri *VASP-4* datoru programmā

Iepriekšējā apakšnodaļā mēs esam aprakstījuši vispārējos teorētiskos principus, kas ir iekļauti *VASP* datoru kodā. Šajā apakšnodaļā mēs īsi aprakstīsim galvenos ieejas parametrus mūsu aprēķiniem.

Ievaddati *VASP* aprēķinu veikšanai ietver šādus galvenos failus [49].

I. POSCAR. Šis fails apraksta atoma pozīcijas un ļauj nofiksēt atomu koordinātas, ja tas ir nepieciešams (šo opciju var izmantot, piemēram, lai aprēķinātu starpmezglu pozīcijas, kad ģeometrijas relaksācija noved sistēmu stabilā pamatkonfigurācijā). Visos plātnes aprēķinos mēs veicām daļēju vai pilnīgu struktūras optimizāciju superšūnas robežās ar fiksētiem lineāriem izmēriem, izmantojot pilnās enerģijas minimizācijas kritēriju. Atomu pozīcijas katrai aprēķinātai sistēmai ir noteiktas POSCAR failā saskaņā ar pētāmās struktūras kristalogrāfiskajām īpašībām.

II. POTCAR. Šis fails satur informāciju par tādām īpašībām kā dažādu atomu RECP pseidopotenciāli, atomu masas, enerģijas atomu konfigurācijas, kurām šie pseidopotenciāli tika izveidoti (sīkāka informāciju par pseidopotenciāliem dota 3.3. apakšnodaļā), utt.

Aprēķinu parametrus ir jādefinē divos failos.

III. KPOINTS. Šis fails nosaka *k*-punktu mezglus BZ. Šajā pētījumā mēs ģenerējām k-punktus, izmantojot Monkhorsta–Paka *(Monkhorsts-Pack)* tehniku [59], savukārt elektroniskā apdzīvotība tika noteikta, izmantojot Metfesseļa un Pakstona *(Methfessel and Paxton)* metodi [60], kas ieviesta *VASP* kodā.

Katru aprēķinu sērijai mēs esam atraduši optimālu k-punktu tīklu, kas nodrošina rezultātu konverģenci: 8 × 8 × 8 mezgli tilpuma aprēķiniem, 8 × 8 × 1 lielākajai daļai virsmu aprēķiniem (ideāla UN(001) virsma, vakances uz UN(001) virsmas, skābekļa adsorbcija un migrāciju, kā arī skābekļa iekļaušana jau eksistējošā N vakancē), kā arī 4 × 4 × 1 mezgli molekulārā skābekļa mijiedarbības ar UN(001) virsmu aprēķiniem un visiem UN(110) virsmas aprēķiniem (ieskaitot atomāru adsorbciju, vakances uz UN(110) virsmas un skābekļa iekļaušanu tajos).

IV. INCAR. Šis galvenais *VASP* ievades fails noteic, „ko darīt un kā to darīt". Pilns atslēgvārdu saraksts ir aprakstīts *VASP* rokasgrāmatā [49]. Nākamajās rindkopās mēs aprakstīsim tikai tos parametrus, kuru variācijas ir īpaši svarīgas mūsu aprēķiniem.

IVa. ISPIN. Šī opcija definē spin-polarizētos aprēķinus. Attiecībā uz UN kā uz sistēmu ar magnētiskām īpašībām opcija „jā" tiek lietota vienmēr.

IVb. MAGMOM. Šī opcija nosaka sākotnējo magnētisko momentu katram atomam (aprēķins sākas no noteiktajiem magnētiskajiem momentiem, taču tie tiek mainīti aprēķina laikā). Mēs esam izvēlējušies sākotnējo feromagnētisko stāvokli visiem UN aprēķiniem. Ja jāmeklē feromagnētisks risinājums, to parasti ir drošāk sākt no lielākiem lokālajiem magnētiskajiem momentiem. Tāpēc FM aprēķiniem ar spina relaksāciju mēs esam sākuši no vērtības 2 μ_B uz U atomiem. FM aprēķiniem bez spina relaksācijas mēs esam sākuši no magnētiskajiem momentiem 1 μ_B uz U atomiem.

IVc. NUPDOWN. Šī atslēga nosaka spina momentu visai sistēmai, vienādu ar noteikto vērtību. Aprēķiniem bez spina relaksācijas tika izvēlēts magnētiskais moments 1 μ_B katram U atomam.

IVd. ENCUT. Plakano viļņu atlasi nosaka apgriezuma enerģija E_{cut}. Tika konstatēts, ka optimālā apgriezuma enerģija ir vienāda ar 520 eV.

IVe. ISMEAR. Nosaka, kā katrai viļņa funkcijai tiek noteikta daļēja apdzīvotība. Mūsu aprēķiniem mēs izmantojām Gausa izsmērēšanu.

IVf. SIGMA. Šī atslēga, kas raksturo brīvās un pilnās enerģijas starpību, jāizvēlas pēc iespējas lielāka. Tika atrasts, ka izsmērēšanas rādītājs 0.2 eV ir optimāls saprātīgai konverģencei un dod elektroniskās entropijas ieguldījumu ar 10 meV kārtu.

IVg. NELMDL. Šī opcija definē soļu skaitu bez pašsaskaņošanas aprēķina sākumā: ja inicializē viļņu funkcijas gadījuma veidā, sākotnējās viļņu funkcijas ir tālu no sagaidāmā risinājuma. Šī lādiņu blīvuma atjaunošanas „kavēšanas" atslēgas ieslēgšana ir ļoti svarīga visos gadījumos, kad konverģence ir ļoti slikta [49]. UN aprēķiniem šī vērtība tika palielināta 3–5 reizes, salīdzinot ar noklusējuma izvēles vērtību (palielināta līdz 15–25 soļiem salīdzinājumā ar noklusējuma izvēles 5 soļiem).

IVh. ALGO. Dažādi algoritmi tiek iekļauti *VASP* kodā. Piemēram, var lietot ātru, bet rupju RMM-DIIS algoritmu [49, 61] vai lēnu, bet precīzu Davidsona bloķēto algoritmu [49, 62]. Mūsu pieredze rāda, ka tikai Davidsona algoritma izmantošana ļauj iegūt ticamus rezultātus. Diemžēl datoru resursi vienmēr ir ierobežoti un dažu sistēmu aprēķini ir ļoti laikietilpīgi. Lai atrisinātu problēmu, ko rada īpaši smagi aprēķini, mēs sadalām šos aprēķinus divos posmos. Pirmajā posmā mēs izmantojam RMM-DIIS, lai iegūtu rupji relaksētu ģeometriju un aptuvenu elektronisko blīvumu. Otrajā posmā mēs sākam no ģeometrijas un elektroniskā blīvuma, kas ir iegūti pirmajā posmā, un izmantojam Davidsona algoritmu, lai iegūtu gala rezultātus. Šī pieeja ievērojami samazina skaitļošanas izmaksas daudzām sarežģītām sistēmām.

3.6. Aprēķinu parametri LCAO *CRYSTAL-06* datoru programmā

LCAO aprēķini tika veikti ar *CRYSTAL-06* datoru programmatūras palīdzību [63], kura lieto bāzes komplektiem Gausa tipa funkcijas, centrētas uz atomu kodoliem, lai izvirzītu atomu orbitāļu lineārā kombinācijā (LCAO), kopā ar nelokālu apmaiņas–

korelācijas funkcionāli PBE [64]. Skābekļa bāzes komplekts (BS) 8-411G(1*d*) tika paņemts no ref. [65]. N atomam tika izmantots pilno elektronu BS 6-311G(2*d*) [66]. Visbeidzot, U atomam tika izmantoti trīs potenciāli ar enerģētiski koriģētiem relatīvistiskiem serdeņiem (Štutgartes–Ķelnes grupās pseidopotenciālis SC60 ar 60 elektroniem serdenī [67], kā arī divi Mosjagina–Titova potenciāli: liela serdeņa MT78 un maza serdeņa MT60 ar attiecīgi 60 un 78 elektroniem pseidopotenciāla serdenī [68]). Lai *CRYSTAL* LCAO aprēķinos izvairītos no bāzes komplekta lineārās atkarības, difūzās *s*-, *p*-, *d*- un *f*-Gausa tipa orbitāles ar eksponentēm < 0.2 a.u.$^{-1}$ tika izslēgtas no bāzes komplekta. Citu polarizēto funkciju eksponentes tika pāroptimizētas, lai atjaunotu kopējās enerģijas nepieciešamo precizitāti. Pirms virsmas īpašību pētījuma UN kristāla tilpuma struktūras optimizācija tika paveikta, izmantojot LCAO pieeju. Monkhorsta–Paka shēma [59] ar 8 × 8 × 1 *k*-punktu mezgliem Briljuena zonā (BZ) un Gilata tīkls ar 32 × 32 × 32 k-punktiem [69] tika izmantoti, lai aprēķinātu Fermī enerģiju un blīvuma matricu.

3.7. Plātnes modelis un defektu periodiskums

Aprēķinot PAW virsmu, mēs modelējām UN virsmu, izmantojot simetriskas plātnes, kas satur nepāru atomu slāņu skaitu un tiek atdalītas cita no citas ar 38.9 Å vakuuma spraugu, kas atbilst UN(001) virsmas 16 starpslāņu attālumiem (3.1. att.). Šis attālums ir pietiekami liels, lai novērstu nevēlamo 2D plātņu savstarpējo mijiedarbību 3D modelī. LCAO aprēķiniem nav nepieciešama 2D plātņu mākslīga atkārtošana virsmas normāles virzienā, kā tiek izdarīts PW aprēķinos.

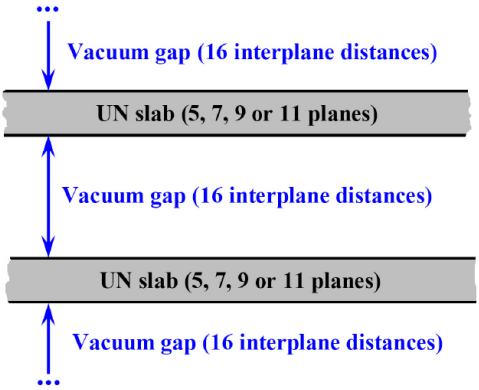

3.1. attēls. UN plātnes 3D modeļa šķērsgriezums

Lai modelētu atsevišķus punktu defektus (N vai U vakances) un skābekļa atomus, adsorbētus uz virsmas vai iekļautus vakancēs, kā arī lai mazinātu laterālo mijiedarbību starp tiem, mēs izmantojām superšūnu pieeju, lietojot primitīvo elementāršūnu ar 2 × 2 vai 3 × 3 paplašinājumu (3.2. att.). Šādas superšūnas satur četrus (2 × 2 superšūna) un deviņus (3 × 3 superšūna) N un U atomu pārus katrā bezdefektu slānī, bet periodiski

sakārtotas virsmas vakances (vai skābekļa atomi / molekulas), pārrēķinot uz virsmas šūnu, atbilst defektu (skābekļa) koncentrācijai, vienādai attiecīgi ar 0.25 un 0.11 no monoslāņa (ML). Lai samazinātu aprēķinu laiku, tika izmantots punktveidu defektu simetrisks divpusējs izvietojums attiecībā pret centrālo (spoguļa) plakni. Piemērota superšūnas izmēra izvēle ir īpaši nozīmīgs jautājums. No vienas puses, modelis ar lielāku superšūnas izmēru ir daudz tuvāks atsevišķa defekta modelim, taču, no otras puses, šādu superšūnu aprēķiniem ir nepieciešami ievērojami lielāki skaitļošanas resursi (piemēram, UN 7-slāņu 3×3 superšūna satur 126 atomus, kas ir 2.25 reizes vairāk, salīdzinot ar 56 atomiem 2×2 UN 7-slāņu superšūnā). Tāpēc mēs analizējām ierobežotas superšūnas izmēra ietekmi, lai novērtētu superšūnas modeļa novirzi no atsevišķa defekta modeļa.

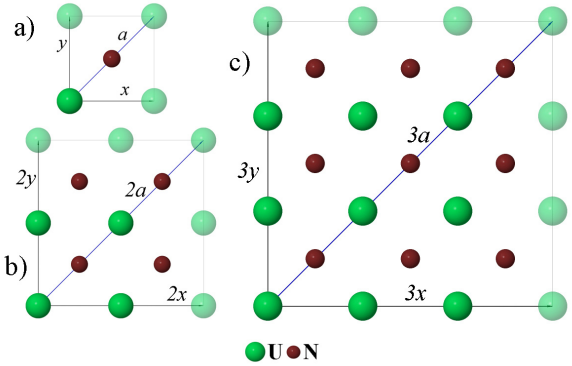

3.2. attēls. Elementāršūnas (a) skats no augšas, kā arī 2×2 (b) un 3×3 (c) superšūnas uz UN(001) virsmas. Šeit x un y asis sakrīt ar virsmas translācijas vektoru virzieniem, savukārt a ir režģa konstante. Puscaurspīdīgie atomi parāda izvēlētās virsmas šūnas robežu

4. UN tilpuma modelēšana

Šā pētījuma vispārējais mērķis ir saprast skābekļa adsorbcijas mehānismu, kā arī urāna nitrīda tālāko oksidēšanās procesu. Pirmais solis UN pētījumos ir izstrādāt metodoloģiju korektam ideāla tilpuma un virsmas īpašību aprakstam. Tas tika veikts publikācijās [P1, P4]. Otrajā solī šo metodoloģiju var lietot, lai pētītu defektīvu virsmu, kā arī skābekļa atomu adsorbciju uz ideālas un defektīvas virsmas. DFT PW tilpuma, ideālas virsmas un atomāra skābekļa adsorbcijas UN aprēķini tika salīdzināti ar atbilstošiem DFT-LCAO rezultātiem, kurus ieguva prof. R. Evarestova grupa (Sanktpēterburgas Valsts universitāte).

Pirms UN aprēķiniem mums jāapskata UN tilpums un jānovērtē tā īpašības. Tilpuma aprēķinu galvenie rezultāti ir apkopoti 4.1. tabulā un liecina par to, ka kohēzijas enerģijas E_c vērtība ir novērtēta par zemu MT78 LCAO aprēķinos un nedaudz pārvērtēta PW aprēķinos. Savukārt E_c vērtība ir tuva eksperimentālai vērtībai LCAO MT60 un SC60 aprēķiniem. Runājot par režģa parametru *a*, tas ir novērtēts par zemu DFT-LCAO aprēķinos (4.78 Å un 4.80 Å), bet maz atšķiras no mūsu un citu autoru iegūtajiem DFT-PW aprēķinu rezultātiem, kas, savukārt, ir ļoti tuvi eksperimentālajām vērtībām. Optimizētā režģa konstante (4.87 Å PAW *VASP* aprēķinos pret. 4.81 Å LCAO *CRYSTAL* aprēķinos) tika izmantota visos mūsu turpmākajos aprēķinos.

4.1. tabula. PW un LCAO UN tilpuma aprēķinu rezultāti: kohēzijas enerģija E_c (eV), režģa konstante a_0 (Å) un elastības modulis *B* (GPa). Eksperimentālās vērtības ir uzrakstītas iekavās pirmajā kolonnā. Spinu blīvums (SD) U atomiem ir dots μ_B mērvienībās

Īpašības (eksperimentālās [1])	**PW *(VASP)***		**PW (citi teorētiskie pētījumi)**		**LCAO (prof. R. Evarestova grupa)**		
	PW91	**PBE**	**PW91 PAW [33]**	**PBE AE-LAPW [20, 25]**	**MT78**	**MT60**	**SC60**
a_0, Å (4.886)	4.868	4.867	4.864	4.886	5.17	4.78	4.80
E_c, eV (13.6)	14.79	14.57	14.7	13.4	9.6	13.4	13.6
B (194)	227	224	226	209	167.2	291.6	276.9
Q_U, *e*	1.69	1.69	1.61	-	1.63	1.55	1.58
SD, μ_B	1.15	1.19	1.05	1.25	3.18	1.18	1.06

Elastības modulis *B* ir pārvērtēts gan PW un LCAO (MT60 un SC60) aprēķinos un novērtēts par zemu MT78 aprēķinos. Aprēķinātais U atoma efektīvais lādiņš (Q_U) it tuvs visiem trim izmantotajiem pseidopotenciāliem un ir salīdzināms ar 1.7 *e* vērtību, kas iegūta PW aprēķinos, izmantojot topoloģisko Badera analīzi.

UN tilpuma zonu struktūras, kas tika aprēķinātas, lietojot divas iepriekš minētās metodes (DFT un LCAO) un piemērojot to pašu PW91 hamiltoniānu, ir attēlotas 4.1. attēlā. Zonu struktūras kvantitatīvā līmenī demonstrē labu korelāciju starp abām metodēm, īpaši zem Fermī līmeņa, un labi saskaņojas gan ar eksperimentu [12], gan arī ar DOS analīzi, kas tika veikta iepriekšējiem PW *VASP* aprēķiniem [30].

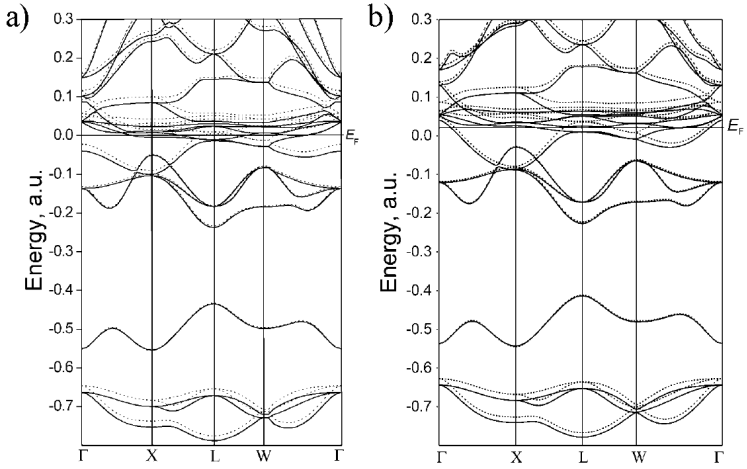

4.1. attēls. UN kristāla enerģijas zonas, kas konstruētas, izmantojot a) PW PW91 (RECP SC78) un b) LCAO PW91 (RECP SC60) hamiltoniānu. Enerģijas ir dotas a. u. mērvienībās, nepārtrauktās un punktveida līnijas atbilst stāvokļiem ar spina orientāciju attiecīgi uz augšu un uz leju

DFT-PW aprēķinos tika iegūta režģa konstante, elastības modulis, kohēzijas enerģija, lādiņu sadales un zonu struktūra UN kristālam. UN tilpuma DFT-PW aprēķinu rezultāti tika salīdzināti ar rezultātiem, kurus savos aprēķinos ieguva prof. R. Evarestova grupa. LCAO (RECP 60) un PW (RECP 78) rezultātu salīdzinājums parāda kvalitatīvu saskaņu īpašību aprēķinos, izmantojot abas metodes, izņemot elastības moduli, kas *CRYSTAL* aprēķinos ir ievērojami pārvērtēts salīdzinājumā ar eksperimentu.

5. UN (001) un (110) virsmas strukturālās īpašības

Sintezētie polikristāliskie UN paraugi satur daļiņas ar dažādi orientētām kristalogrāfiskām skaldnēm [9]. Lai vienkāršotu skābekļa mijiedarbības modelēšanu ar UN virsmu, šajā doktora darbā mēs pētām galvenokārt (001) virsmu, jo saskaņā ar Taskera analīzi [70] šai virsmai ir viszemākā virsmas enerģija. Tomēr reālās UN daļiņas (2.2. att.) satur dažādas kristalografiskās orientācijas skaldnes. Lai palielinātu mūsu rezultātu pamatotību, esam veikuši (110) virsmas papildu aprēķinus. Mēs izvēlējāmies (110) virsmas orientāciju papildu aprēķiniem, jo alternatīvā zemo indeksu (111) virsma satur uzlādētus slāņus un tās aprēķināšanai ir nepieciešamas mākslīgas pieejas. Turklāt, lai stabilizētu polāro (111) virsmu, jānotiek spēcīgai rekonstrukcijai, līdzīgi kā MgO(111) virsmai [71]. UN(110) virsmai, kurai ir mazākais virsmas iepakojuma blīvums, ir mazāks arī starpslāņu attālums z virzienā, salīdzinot ar (001) virsmu (5.1. tab. un 5.1. att.).

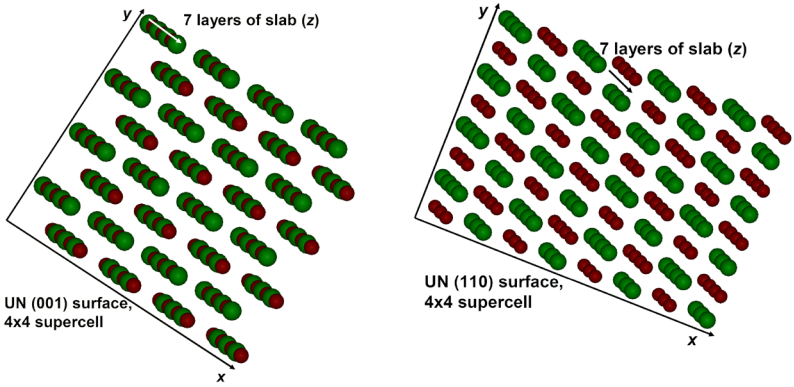

5.1. attēls. Struktūras salīdzinājums plātnēm, kas izmantotas UN (001) (a) un (110) (b) virsmas aprēķinos

Mēs esam modelējuši rekonstrukciju perfektām un defektu saturošām UN(110) virsmām, kā arī atomārā skābekļa adsorbciju, N vakanču veidošanu un skābekļa iekļaušanu tajās. Šie rezultāti ir izklāsti 6.–8. nodaļas attiecīgajās apakšnodaļās.

5.1. tabula. UN (001) un (110) virsmas salīdzinājums (*a* ir režģa konstante kubiskajam *fcc* kristālam)

	(001) virsma	**(110) virsma**
Virsmas šūnas izmērs (Å x Å)	3.44 × 3.44 $(\frac{\sqrt{2}}{2}a \times \frac{\sqrt{2}}{2}a)$ vai $(\frac{1}{2}a \times a)$	4.87 × 3.44 $(a \times \frac{\sqrt{2}}{2}a)$
Attālums starp diviem tuvākajiem U un U (vai N un N) atomiem *xy* plaknē (Å)	3.44 $(\frac{\sqrt{2}}{2}a)$ abos virzienos	4.87 *x* virzienā 3.44 *y* virzienā
Attālums starp tuvākajiem U un N atomiem *xy* plaknē (Å)	2.435 $(\frac{a}{2})$	2.435 $(\frac{a}{2})$ *x* virzienā nav definēts *y* virzienā
Attālums starp kaimiņslāņiem *z* virzienā (Å)	2.435 $(\frac{a}{2})$	1.72 $(a\frac{\sqrt{2}}{4})$
Attālums starp tuvākajiem atomiem *z* virzienā (Å)	2.435 $(\frac{a}{2})$, attālums starp U un N atomiem	3.44 $(\frac{\sqrt{2}}{2}a)$, attālums starp N un N (vai U un U) atomiem

6. UN ideālas virsmas modelēšana

Kā tika jau minēts 2.1. apakšnodaļā, eksperiments rāda, ka UN tilpumā notiek AFM sakārtošanās zem 53 K temperatūras [5]. Mēs veicām aprēķinus gan FM, gan arī AFM stāvoklim. Mūsu testa UN tilpumā PAW aprēķini ir parādījuši, ka FM fāze ir enerģētiski nedaudz izdevīgāka par AFM fāzi. Analoģiskus rezultātus, izmantojot LCAO metodi, ieguva prof. R. Evarestova grupa. Tā kā FM un AFM stāvokļu enerģijas starpība ir neliela (~ 0.001–0.01 eV) un UN virsmas magnētiskā struktūra sarežģīta [31], mūsu UN virsmas aprēķinos tiek apskatīts tikai FM stāvoklis.

6.1. Bezdefektu UN(001) virsmas PW un LCAO aprēķini

Analoģiski ideālā tilpuma aprēķiniem mēs salīdzinām UN(001) virsmas PW un LCAO aprēķinu rezultātus. Neperiodiskais (2D) un periodiskais (3D) modelis, kas ir perpendikulārs plātnes virsmai, tika izmantots LCAO un PW aprēķiniem [51].

Mēs detalizēti apskatījām atomu vertikālās nobīdes (gar *z* asi) gan virsmas, gan arī zemvirsmas slānī salīdzinājumā ar atomu pozīcijām tilpumā (6.1. tab.), efektīvos atomu lādiņus (6.2. tab.), virsmas enerģijas (6.3. tab.), kā arī DOS grafikus, kas iegūti PW aprēķinos (6.2. att.).

Virsmas enerģija *n*-slāņu plātnei tika noteikta, izmantojot standarta pamatattiecību:

$$E_{surf}(n) = \frac{1}{2S}(E_n - nE_b), \qquad \textit{(Eq. 6.1.1)}$$

kur E_n ir plātnes pilnā enerģija, pārrēķināta uz primitīvo virsmas elementāršūnu ar laukumu *S*, savukārt E_b ir primitīvās tilpuma elementāršūnas pilnā enerģija (6.1. att.).

LCAO un PW rezultāti ir labā kvalitatīvā saskaņā strukturālai relaksācijai un atomu efektīvajiem lādiņiem. Pirmkārt, abām metodēm atomi pārvietojas vienādos virzienos: N atomi izvirzās uz ārpusi no virsmas plaknes, savukārt U atomi pārvietojas plāksnes centrālas plaknes virzienā. Tā ir tipiska pārkārtošanās aina oksīdu virsmām. Tika novērots, ka virsmas U nobīdes ir ievērojami lielākas, salīdzinot ar N atomu nobīdēm, savukārt zemvirsmas atomu relaksācijas ir mazākas.

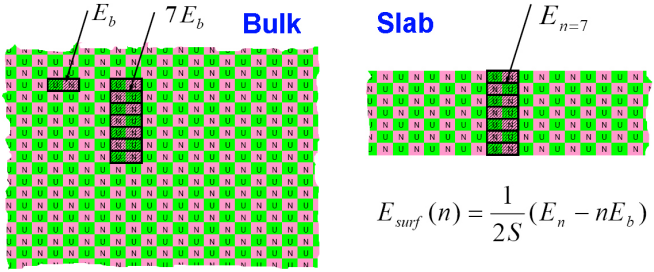

6.1. attēls. Virsmas enerģija, aprēķināta 7-slāņu plātnei. E_n ir kopējā plātnes enerģija primitīvajai virsmas elementāršūnai, E_b ir pilna enerģija vienai primitīvajai tilpuma elementāršūnai, *n* ir slāņu skaits, *S* ir elementāršūnas virsmas laukums

Virsmas enerģijas daļēji stabilizējas plātnēm, kas satur vismaz 5–7 slāņus, savukārt relaksācijas enerģijas ir jutīgākās pret plātnes biezumu (6.3. tab.). Eksperimentālo datu ierobežotības dēļ aprēķinātās virsmas enerģijas var kvalitatīvi salīdzināt tikai ar UO_2 (001) virsmas enerģijas vērtību, kas ir nesen iegūta, izmantojot aprēķinus no pirmajiem principiem [46], un ir vienāda ar 1.2 J/m². Ir paredzams, ka UN virsmu enerģijas ir līdzīgas. Ir novērota kvalitatīva saskaņa starp UN(001) virsmas enerģijām, kas iegūtas gan LCAO, gan PW aprēķinos.

6.1. tabula. Aprēķinātās atomu novirzes Δz (Å) UN(001), ko iegūst dažādiem plātnes biezumiem un ar dažādām metodēm. Pozitīvā zīme nozīmē pārvietošanos no plāksnes centra uz āru

Atoms	Metode	Atomāro slāņu skaits plātnē				
		3	5	7	9	11
Virsmas U	LCAO	-0.085	-0.095	-	-	-
	LCAO (papildu slānis ir pievienots)	-0.026	-0.046	-	-	-
	PW PW91	-0.041	-0.046	-0.050	-0.061	-0.057
Zemvirsmas U	LCAO		-0.011	-	-	-
	LCAO (papildu slānis ir pievienots)		-0.013	-	-	-
	PW PW91		-0.018	-0.016	-0.013	-0.013
Virsmas N	LCAO	0.064	0.058	-	-	-
	LCAO (papildu slānis ir pievienots)	0.049	0.025	-	-	-
	PW PW91	0.030	0.022	0.025	0.033	0.026
Zemvirsmas N	LCAO		-0.002	-	-	-
	LCAO (papildu slānis ir pievienots)		0.014	-	-	-
	PW PW91		0.026	0.028	0.032	0.022

6.2. tabula. Efektīvie atomu lādiņi $q(e)$ UN(001) plātnei

Atoms	Metode	Atomāro slāņu skaits plātnē				
		3	5	7	9	11
Virsmas U	LCAO	1.63	1.63	-	-	-
	LCAO (papildu slānis ir pievienots)	1.64	1.64	-	-	-
	PW PW91	1.65	1.66	1.72	1.67	1.65
Zemvirsmas U	LCAO	-	1.51	-	-	-
	LCAO (papildu slānis ir pievienots)	-	1.55	-	-	-
	PW PW91	-	1.65	1.63	1.63	1.69
U plātnes centrālajā slānī	LCAO	1.45	1.57	-	-	-
	LCAO (papildu slānis ir pievienots)	1.52	1.55	-	-	-
	PW PW91	1.62	1.67	1.72	1.65	1.62
Virsmas N	LCAO	-1.55	-1.55	-	-	-
	LCAO (papildu slānis ir pievienots)	-1.61	-1.60	-	-	-
	PW PW91	-1.64	-1.63	-1.64	-1.63	-1.67
Zemvirsmas N	LCAO	-	-1.59	-	-	-
	LCAO (papildu slānis ir pievienots)	-	-1.57	-	-	-
	PW PW91	-	-1.67	-1.7	-1.64	-1.7
N plātnes centrālajā slānī	LCAO	-1.61	-1.58	-	-	-
	LCAO (papildu slānis ir pievienots)	-1.58	-1.57	-	-	-
	PW PW91	-1.65	-1.7	-1.66	-1.62	-1.64

6.3. tabula. Virsmas enerģijas E_{surf} (Dž · m^{-2}) un relaksācijas enerģijas E_{rel} (eV), kas iegūtas UN(001) virsmas LCAO un PW aprēķinos

Atomāro plakņu skaits plātnē			3	5	7	9	11
Metode	LCAO	E_{surf} (bez relaksācijas)	2.20	2.29	2.28	2.11	-
		E_{surf} (ar relaksāciju)	2.06	2.13	-	-	-
		E_{rel}	0.203	0.230	-	-	-
	LCAO (papildu slānis ir pievienots)	E_{surf} (bez relaksācijas)	1.68	1.45	-	-	-
		E_{surf} (ar relaksāciju)	1.430	1.38	-	-	-
		E_{rel}	0.359	0.121	-	-	-
	Plakanie viļņi PW91	E_{surf} (bez relaksācijas)	1.81	1.87	1.84	1.86	1.90
		E_{surf} (ar relaksāciju)	1.70	1.69	1.70	1.70	1.69
		E_{rel}	0.156	0.258	0.210	0.239	0.305

6.2. attēlā var redzēt FM stāvokļa pilno un projicēto DOSu, kuri iegūti mūsu PW aprēķinos. Nelielā atšķirība joslu formām, kas ir novērota, salīdzinot ar iepriekšējiem UN tilpuma aprēķiniem [34], ir saistīta ar ievērojami lielāku *k*-punktu mezglu skaitu un apgriezuma enerģiju, kas tika izmantoti mūsu pētījumos. U un N atomu DOSa salīdzinājums tilpumam (6.2.a att.) un virsmai (6.2.b att.) parāda galvenokārt neaizņemto līmeņu profila izmaiņas virs Fermī līmeņa. Abos gadījumos U(*5f*) stāvokļiem pie Fermī līmeņa tika novērota jauktā metāliski kovalentā saite, kas apstiprina iepriekšējo eksperimentālo un teorētisko pētījumu rezultātus.

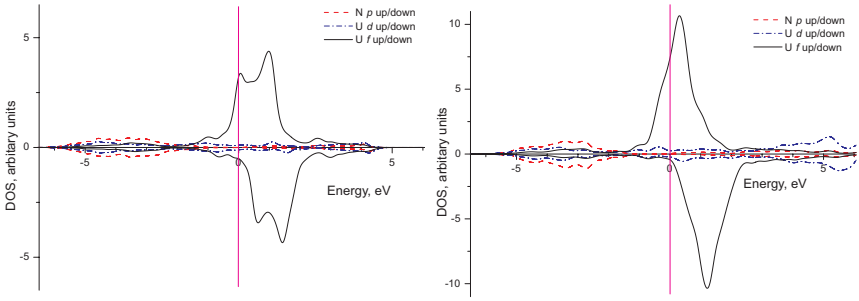

a) b)

6.2. attēls. Projicētais DOS UN tilpumam (a) un 7-slāņu ideālajai UN(001) plātnei (b) FM stāvoklī

6.2. Bezdefektu UN (001) un (110) virsmas PW aprēķini ar spina relaksāciju

Šajā apakšnodaļā tiek apspriesti rezultāti, kas iegūti ideālām UN (001) un (110) virsmām (6.3. att.) spina relaksētajos PW aprēķinos. Efektīvo atomu lādiņu q^{eff}, atomu

novirzes Δr, vidējo U atomu magnētisko momentu μ_{av} un virsmas enerģiju E_{surf} aprēķini plātnēm ar dažādu biezumu tika veikti, lai pārbaudītu, vai šis īpašības ir atkarīgas no atomu spina relaksācijas [P4]. Spina relaksācijas rada ievērojamas E_{surf} izmaiņas atkarībā no slāņu skaitu plātnē (6.4. tab.). Lielākā μ_{av} vērtība tika iegūta U atomiem 5-slāņu plātnēs, un μ_{av} nedaudz (par ~ 0.3 μ_B) samazinās, palielinot plātņu biezumu no 5 līdz 11 slāņiem. Režģa relaksācijas enerģija spina relaksētajos aprēķinos ir ļoti maza, ~ 0.03 eV.

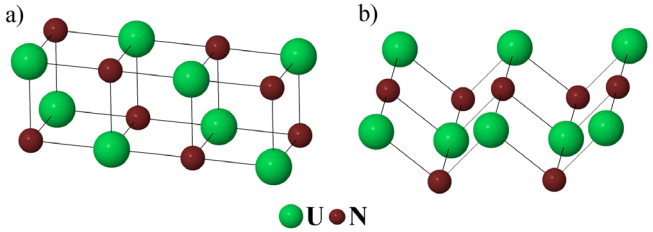

6.3. attēls. 2-slāņu modeļi (001) (a) un (100) (b) virsmai

Atkarībā no plātnes biezuma virsmas enerģija ir par ~ 0,5–0,7 J·m^{-2} lielāka UN (110) virsmai (6.4. tab.). Tas nozīmē, ka UN(001) virsma ir enerģētiski izdevīgāka.

6.4. tabula. Virsmas enerģijas E_{surf} (Dž·m^{-2}), kā arī vidējais U atomu magnētiskais moments (μ_B mērvienībās) bezdefektu UN (001) un UN (110) virsmai. Aprēķiniem ar spina fiksāciju μ tika izvēlēts vienāds ar 1 μ_B

Atomāro slāņu skaits	**E_{surf} (Dž·m^{-2}) (001) plātnei bez spina relaksācijas**	**E_{surf} (Dž·m^{-2}) (001) plātnei ar spina relaksāciju**	**μ_{av}(μ_B) (001)**	**E_{surf} (Dž·m^{-2}) (110) plātnei ar spina relaksāciju**	**μ_{av}(μ_B) (110)**
5	1.69	1.44	1.57	1.977	1.645
7	1.70	1.37	1.44	1.928	1.464
9	1.70	1.29	1.37	1.878	1.417
11	1.69	1.22	1.33	1.830	1.385

Interesanti arī izanalizēt plātnes atomu lādiņu vērtības q^{eff} atkarībā no slāņu skaita plātnē (6.5. tab.). Pirmkārt, šie q^{eff} norāda uz ievērojamu kovalento saiti gan uz virsmas (piemēram, zemvirsmu slānī), gan centrālajā slānī. Otrkārt, UN(001) un UN(110) virsmas atšķirīgo rekonstrukcijas mehānismu dēļ atomu lādiņi arī atšķiras: saites joniskums ir lielāks UN(001) virsmai, un tas noved pie virsmas īpašību zināmām atšķirībām. Treškārt, atomu lādiņi ir atkarīgi gan no spinu relaksācijas, gan no slāņu biezuma (salīdzinot PW aprēķinu rezultātus spina relaksētajiem aprēķiniem un aprēķinus ar fiksētu spinu attiecīgi 6.5. un 6.2. tabulā).

6.5. tabula. Atomu Badera lādiņi bezdefektu UN (001) un (110) virsmai ar spina relaksāciju

	UN(001) atomāro slāņu skaits plātnē				UN(110) atomāro slāņu skaits plātnē			
Atoms	**5**	**7**	**9**	**11**	**5**	**7**	**9**	**11**
Virsmas U	1.68	1.74	1.68	1.72	1.46	1.48	1.49	1.48
Zemvirsmas U	1.67	1.63	1.63	1.67	1.88	1.85	1.83	1.84
U plātnes centrālajā slānī	1.69	1.72	1.65	1.66	1.60	1.74	1.64	1.70
Virsmas N	-1.65	-1.67	-1.67	-1.68	-1.55	-1.55	-1.55	-1.55
Zemvirsmas N	-1.68	-1.70	-1.70	-1.67	-1.75	-1.73	-1.75	-1.73
N plātnes centrālajā slānī	-1.74	-1.65	-1.65	- 1.63	- 1.70	-1.71	-1.75	-1.74

6.6. tabula. Atomu nobīdes Δz(Å)* bezdefektu UN (001) un (110) virsmai

Atomāru slāņu skaits plātnē	U jonu nobīde				N jonu nobīde			
	(001) virsma		(110) virsma		(001) virsma		(110) virsma	
	virsmas	zem-virsmas	virsmas	zem-virsmas	virsmas	zem-virsmas	virsmas	zem-virsmas
5	-0.050	-0.012	-0.053	-0.005	0.023	0.023	-0.279	0.068
7	-0.046	-0.009	-0.038	-0.009	0.024	0.028	-0.272	0.092
9	-0.047	-0.011	-0.042	-0.014	0.024	0.028	-0.279	0.091
11	-0.047	-0.011	-0.015	0.015	0.025	0.031	-0.252	0.118

* Negatīvā zīme norāda uz atomu pārvietošanos plātnes spoguļslāņa virzienā.

Atomu pārvietojumi Δz ievērojami atšķiras U atomiem, kas novietoti ideālā režģī un virsmas un zemvirsmas slāņos (6.6. tab.), un tie ir nedaudz lielāki 5-slāņu plātnei, savukārt slāpekļa atomu pārvietojumi visām plātnēm saglabājas gandrīz nemainīgi. Jāievēro, ka N atomi uz (001) virsmas pārvietojas no plātnes uz āru, savukārt U atomi ir nobīdīti uz iekšu, kas rada virsmas nesakārtotību pat līdz 1.2% no režģa konstantes. Turpretī rekonstruētajai UN(110) virsmai U atomi atrodas augstāk par attiecīgajiem N atomiem, kas labi ilustrē lādiņu un citu iepriekš minēto virsmas īpašību atšķirību.

6.3. Ideālas UN virsmas aprēķini: kopsavilkums

Bezdefektu virsmas modelēšana liecina par UN virsmas izteiktajām metāliskajām īpašībām, kas ir analoģiskas iepriekšējo tilpuma aprēķinu rezultātiem. Salīdzinot DFT PW un LCAO aprēķinu rezultātus, atradām labu korelāciju starp abām pieejām. UN (001) un (110) virsmas salīdzinājums liecina, ka pirmā no tām ir enerģētiski izdevīgāka. Virsmas enerģijas atkarībā no plātnes biezuma ir vienādas ar 1.22–1.44 $J \cdot m^{-2}$ UN(001) virsmai *vs* 1.83–1.98 $J \cdot m^{-2}$ UN(110) virsmai. Šis fakts ļauj mums veikt aprēķinus UN bezdefektu virsmai un skābekļa adsorbcijas aprēķinus galvenokārt (001) virsmai.

7. N un U vakanču modelēšana

7.1. Vakances aprēķini: modelis un veidošanās enerģijas

Lai sīkāk saprastu oksidācijas mehānismu, ir jāņem vērā virsmas defekti un to mijiedarbība ar skābekli. Šim nolūkam mēs pētījām virsmas vakanču pamatīpašības [P4].

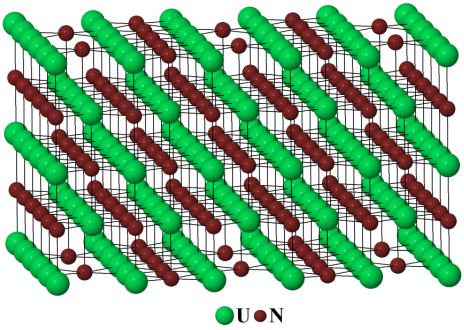

7.1. attēls. 5-slāņu UN(001) plātne, kas satur divpusējas virsmas N vakances, sakārtotas ar 2 × 2 periodiskumu

Mēs aprēķinājām ne tikai virsmas slāņa, bet arī zemvirsmas slāņa un plātnes centrālā slāņa defektus, kā arī apskatījām punktveida defektu izvietojumu uz plātnes abām virsmām, kas ir simetrisks attiecībā pret centrālo spoguļplakni (virsmas N vakanču atomistiskais modelis ar defektu 2 × 2 periodiskumu ir atspoguļots 7.1. attēlā). FM stāvoklis tika izvēlēts visiem mūsu veiktajiem plātnes aprēķiniem ar atomu magnētisko momentu relaksāciju bez spin-orbitālās mijiedarbības iekļaušanas. Esam veikuši sistēmas pilno spina relaksāciju.

Virsmas un zemvirsmas vakancēm punktveida defekta veidošanās enerģija tika aprēķināta šādi:

$$E_{form}^{\mathrm{N(U)}vac} = \frac{1}{2}\left(E^{\mathrm{UN(U/N\_vac)}} + 2E_{ref\_\mathrm{I(II)}}^{\mathrm{N(U)}} - E^{\mathrm{UN}}\right), \qquad (7.1.1a)$$

bet vakancei centrālajā plātnes slānī šādi:

$$E_{form}^{\mathrm{N(U)}vac} = E^{\mathrm{UN(U/N\_vac)}} + E_{ref\_\mathrm{I(II)}}^{\mathrm{N(U)}} - E^{\mathrm{UN}}, \qquad (7.1.1b)$$

Šeit $E^{\mathrm{UN(U/N\_vac)}}$ ir pilnā enerģija pilnīgi relaksētajai plātnei, kas satur N (vai U) vakances, E^{UN} ir tas pats bezdefektu plātnei, savukārt $E_{ref\_\mathrm{I(II)}}^{\mathrm{N(U)}}$ ir atskaites enerģija N (vai U) atomam. Šajā pētījumā defektu veidošanās enerģijas aprēķiniem mēs izmantojām divus U vai N atoma atskaites stāvokļus, kas plaši lietoti literatūrā.

Pirmais stāvoklis N (U) atbilst izolētajam atomam, kas aprēķināts lielā taisnstūra paralēlskaldnī (28.28 × 28.28 × 22 Å^3), tripleta (kvarteta) spina stāvoklī, kuru nosaka $2p^3$ ($5f^3 6d^1$) valences elektronu konfigurācija (turpmāk atskaites stāvoklis I, kā 7.1. tabulā):

$$E^{\mathrm{N(U)}}_{ref\_\mathrm{I}} = E^{\mathrm{N(U)}}_{atom}. \qquad (7.1.2.)$$

Otrais atskaites stāvoklis (turpmāk atskaites stāvoklis II, kā 7.1. tabulā) ir ķīmiskais potenciāls N (U) atomam, kas ir definēts kā funkcija no temperatūras un slāpekļa parciālā spiediena. Neņemot vērā temperatūras un spiediena izmaiņas efektus, N ķīmisko potenciālu var novērtēt kā enerģiju atomam N_2 molekulā. Savukārt U atoma ķīmiskais potenciāls ir puse no pilnās enerģijas elementāršūnai U monokristāla α fāzē zemās temperatūrās ar ortotombisko struktūru [72]. Tādējādi attiecīgo otrā stāvokļa enerģiju var aprēķināt kā

$$E^{\mathrm{N}}_{ref\_\mathrm{II}} = \mu_{\mathrm{N}_2} = \frac{1}{2} E_{tot}\left[\mathrm{N}_2\right], \qquad (7.1.3a)$$

$$E^{\mathrm{U}}_{ref\_\mathrm{II}} = \mu_{\alpha\text{-U}} = \frac{1}{2} E_{tot}\left[\alpha\text{-U}\right], \qquad (7.1.3b)$$

kur $E_{tot}[\mathrm{N}_2]$ ir slāpekļa molekulas kopējā enerģija, bet E_{tot}[α-U] ir kopējā enerģija U tilpuma elementāršūnai, kas satur divus atomus. N un U ķīmiskie potenciāli, kas aprēķināti, izmantojot vienādojumu 7.1.3, reprezentē galējus gadījumus – ar N (U) bagātus nosacījumus *(N(U)-rich conditions)* [73], vai, citiem vārdiem, šo potenciālu minimālās vērtības nav apskatītas šajā pētījumā. N (U) vakanču veidošanās enerģija attiecībā uz N_2 molekulu (vai α-U monokristālu) un N (U) izolēta atoma enerģija ir cieši saistītas: pirmā no tām ir uz pusi lielāka par N_2 molekulas saites enerģiju vai puse no α-U monokristāla kohēzijas enerģijas.

Optimizētie α-U režģa parametri (a = 2.80 Å, b = 5.88 Å, c = 4.91 Å) ir novērtēti nedaudz par zemu, salīdzinot ar iegūtām eksperimentālām vērtībām [72] vai aprēķinātām citur [74, 75], izņemot parametru b, kas labi sakrīt ar eksperimentālo vērtību 5.87 Å [72] (kamēr a = 2.86 Å, c = 4.96 Å [72]). Savstarpējās attiecības c/a, b/a, kā arī parametrs c tika labi verificēti citā plakano viļņu DFT pētījumā [41]. Analoģiski ar izolētu slāpekļa atomu N_2 molekula tika aprēķināta kubiskajā kastē, tikai ar mazāku izmēru (8 × 8 × 8 Å^3). N_2 molekulai raksturīgs 1.12 Å saites garums un 10.63 eV saites enerģija, kas ir labi salīdzināmi ar 1.10 Å un 9.80 eV eksperimentālām vērtībām [76]. Reizinātājs ½ pirms vienādojuma *7.1.1a* rodas sakarā ar divu N (U) vakanču simetrisku sakārtošanos virsmas vai zemvirsmas slāņos attiecībā pret spoguļplakni (7.1. att.).

N un U vakanču veidošanās enerģijas $E^{\mathrm{N(U)}\,vac}_{form}$, kas aprēķinātas, izmantojot vienādojumus *7.1.1–7.1.3* (ar diviem atskaites stāvokļiem), kā funkcijas no plātnes biezuma, ir apkopotas 7.1. tabulā. Tās ir mazākas virsmas slānī un ievērojami palielinās (par ~ 0.6 eV N vakancei un par ~ 1.7 eV U vakancei) zemvirsmas un centrālajā slānī neatkarīgi no atskaites stāvokļa. Tas liecina par tendenci vakancēm uzkrāties uz interfeisiem (uz virmas vai, iespējams, uz kristalītu graudu robežām). Maza $E^{\mathrm{N(U)}\,vac}_{form}$ atkarībā no plātnes biezuma arī ir novērota. $E^{\mathrm{N(U)}\,vac}_{form}$ vērtība stabilizējas 7-slāņu un biezākām plātnēm. Turklāt starpība starp 5-slāņu un 7-slāņu plātņu $E^{\mathrm{N(U)}\,vac}_{form}$ vērtībām virsmas vakancēm ir mazāka nekā analoģiskajām vērtībām centrālajā slānī. Šī atšķirība ir vislielākā U vakancēm centrālajā plaknē (~ 0.16 eV).

7.1. tabula. Vakanču veidošanas enerģijas (eV mērvienībās) diviem atskaites stāvokļiem (detalizētāk sk. tekstu)

Slānis	Slāņu skaits un superšūnas izmērs	Atskaites stāvoklis I, vienādojumi (7.1.1a)–(7.1.2)[a]		Atskaites stāvoklis II, vienādojumi (7.1.1a), (7.1.1b), (7.1.3a) un (7.1.3b)[b]	
		U	N	U	N
Virsmas slānis	5, 2 × 2	8.63	8.84	1.46	3.70
	7, 2 × 2	8.61	8.84	1.44	3.70
	9, 2 × 2	8.61	8.84	1.44	3.71
	11, 2 × 2	8.60	8.85	1.43	3.71
	5, 3 × 3	8.51	8.78	1.34	3.64
	7, 3 × 3	8.47	8.78	1.30	3.65
Zemvirsmas slānis	5, 2 × 2	10.31	9.38	3.14	4.25
	7, 2 × 2	10.29	9.46	3.12	4.33
	9, 2 × 2	10.26	9.46	3.09	4.33
	11, 2 × 2	10.26	9.46	3.09	4.33
	7, 3 × 3	10.18	9.47	3.01	4.34
Centrālais spoguļslānis[c]	5, 2 × 2	10.20	9.48	3.03	4.34
	7, 2 × 2	10.36	9.57	3.19	4.43
	9, 2 × 2	10.34	9.55	3.17	4.42
	11, 2 × 2	10.39	9.56	3.22	4.42
	7, 3 × 3	10.23	9.55	3.06	4.42

[a] I atskaites stāvokļa enerģija ir vienāda ar -4.10 eV U atomam un ar -3.17 eV N atomam,

[b] II atskaites stāvokļa enerģija ar -11.28 eV U atomam un ar -8.30 eV N atomam,

[c] defektu veidošanās enerģija UN tilpumā, izmantojot atskaites stāvokli I ir vienāda ar 9.1–9.7 eV N vakancei un ar 9.4–10.3 U vakancei [34].

II atskaites stāvokļa izmantošana noved pie mazākām $E_{form}^{\mathrm{N(U})\,vac}$ (salīdzinājumā ar tām, kuras dod atskaites stāvoklis I) un parāda divu vakanču veidu būtisku atšķirību. Saskaņā ar atskaites stāvokli II U vakances pie T = 0 K veidojas būtiski vieglāk, salīdzinot ar N vakancēm. Jāievēro, ka O un U atomu ķīmisko potenciālu izmantošana līdzīgiem defektu pētījumiem UO_2 tilpumā neparādīja U vakanču enerģētisko priekšroku [75, 77]. Savstarpējā mijiedarbība starp defektiem nav atbildīga par šo efektu, jo $E_{form}^{\mathrm{N(U})\,vac}$ samazinājās tikai par 0.1 eV, palielinot superšūnu (3 × 3 superšūna 7.1. tabulā). No otras puses, tā kā brīvās N_2 molekulas ķīmiskais potenciāls ir atkarīgs no temperatūras [78], mēs prognozējām N vakances veidošanās enerģijas samazināšanos par ~ 0.8 eV, temperatūrai paaugstinoties no istabas temperatūras līdz 1000 °C. Atšķirībā no II atskaites stāvokļa izmantošanas I atskaites stāvoklis dod līdzīgas veidošanās enerģijas abiem vakanču veidiem. Centrālajā plātnes slānī $E_{form}^{\mathrm{N(U})\,vac}$ vērtības ir līdzīgas tām, kas ir iegūtas tilpumā (7.1. tab.).

7.2. Vakanču radītā virsmas rekonstrukcija

Lokālās atomu nobīdes ap vakancēm ir lielākas vakanču tuvākajiem kaimiņiem. Atomu nobīžu analīze ļauj mums secināt, ka U vakances izkropļo virsmas struktūru daudz spēcīgāk nekā N vakances. Ja N vakance atrodas ārējā slānī, tad tuvākās U atomu nobīdes *z* virzienā sasniedz 0.02–0.05 Å plātnes centrālās plāksnes virzienā. Pie virsmas tuvākām N-vakancēm slāpekļa atomu nobīdes sasniedz 0.05 Å virzienā uz centrālo plakni (*z* virzienā) un 0.01 A virsmas plaknē (*xy*-nobīde). Maksimālās nobīdes centrālajās plaknēs N vakances kaimiņiem ir vienādas ar 0.04–0.07 Å (tuvākie U atomi kaimiņslāņos ir nobīdīti pa *z* asi virzienā uz vakanci) un nepārsniedz 0.025 Å visiem citiem plātnes atomiem.

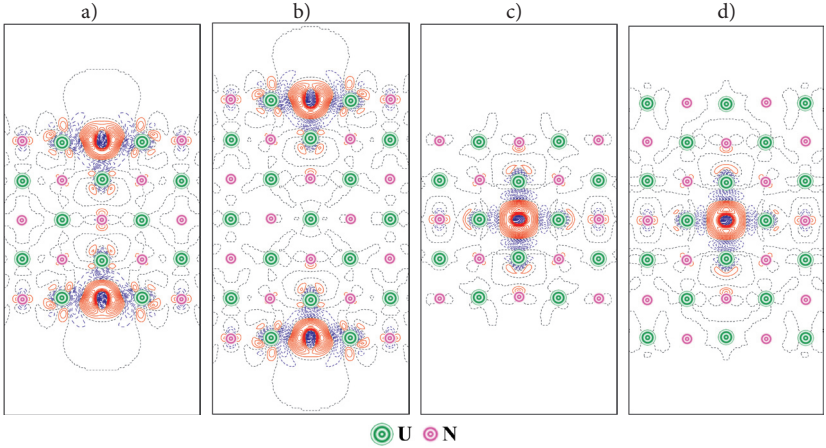

7.2. attēls. 2D šķērsgriezums elektronisko lādiņu pārdalīšanas starpībai ap slāpekļa vakancēm 5-slāņu un 7-slāņu UN(001) plātnēs ar 2×2 superšūnas paplašinājumu: a) N vakance virsmas plaknē, 5-slāņu plātne, b) tas pats, 7-slāņu plātne, c) N vakance centrālajā plāksnē, piecu slāņu plātne, d) tas pats, 7-slāņu plātne. Elektronisko lādiņu pārdalīšanas starpība ir definēta kā pilnais elektroniskais blīvums defektu saturošai virsmai mīnus superpozīcija no ideālās virsmas elektroniskā blīvuma un blīvuma izolētam atomam uz virsmas atbilstošā stāvoklī. Nepārtraukta (sarkana) un pārtraukta (zila) izolīnija atbilst attiecīgi pozitīvam un negatīvam elektroniskam blīvumam (vai attiecīgi elektroniska blīvuma pārpalikumam un trūkumam). Izoblīvumu pieaugums ir vienāds ar 0.25 e a. u.$^{-3}$

Turpretī U vakances izraisa daudz lielākus kaimiņu atomu pārvietojumus neatkarīgi no to pozīcijas. Ja vakances atrodas virsmas slānī, ir novērota tuvāko N atomu nobīde par 0.3–0.32 Å. Ja U vakances atrodas centrālajā slānī, tuvākie N atomi šajā slānī pārvietojas par 0.17 Å, savukārt tuvāko slāņu N atomiem nav nobīdes *xy*-virzienā un tie ir 0.15 Å nobīdīti plātnes virsmas virzienā pa *z* asi. Atomu pārvietojumi ap vakancēm UN tilpumā tika atrasti un bija vienādi attiecīgi ar 0.03 Å N un 0.13 Å U vakancēm [34]. Šīs vērtības ir līdzīgas tām, kas iegūtas, aprēķinot vakances centrālajā plātnes slānī un tādā veidā parādot šo rezultātu tuvumu kristāla tilpumam.

7.3. Elektroniskās īpašības: virsmas šūnas ierobežotā izmēra efekti un superšūnas izmēra izvēle

Ierobežotās plātnes izmēra ietekmi, kuru izraisīja salīdzinoši liela defektu koncentrācija, var ilustrēt, izmantojot elektronisko lādiņu pārdalīšanās starpību $\Delta\rho(\mathbf{r})$. 7.2. attēlā šī pārdalīšanās tika parādīta N vakancēm, novietotām gan ārējā (virsmas) plaknē, gan centrālajā spoguļplaknē 5-slāņu un 7-slāņu plātnēs. Divu simetriski novietotu vakanču klātbūtne 5-slāņu plātnē izraisa to vāju mijiedarbību caur plāksni (7.2a att.), un to ilustrē papildu elektroniska blīvuma parādīšanās ap N atomiem centrālajā plātnes plāksnē. To pašu, traucējot atomus virsmas slānī, izraisa vakance centrālajā plaknē, ja plānā plātne satur tikai 5 slāņus (7.2c att.). Palielinot plātnes biezumu, mēs varam izvairīties no ietekmes, kuru izraisīja ierobežotais plātnes izmērs (7.2b, 7.2d att.). Tas arī izskaidro vakanču veidošanās enerģiju stabilizāciju 7-slāņu un biezāko UN(001) plātņu aprēķiniem (7.1. tab.).

Stāvokļu blīvumi (DOS) gan perfektai, gan defektu saturošai 7-slāņu UN plātnei ir atspoguļoti 7.3. attēlā. Pilnā saskaņā ar iepriekšējiem tilpuma aprēķiniem U(5*f*) elektroni lokalizējas Fermī līmeņa tuvumā (7.3a att.). Šie elektroni joprojām spēcīgi hibridizējas ar N(*2p*) elektroniem. Tas apstiprina kovalento saišu eksistēšanu, kas novērota, analizējot bezdefektu virsmas Badera lādiņus (6.5. tab.). N(2*p*) stāvokļi veido ~ 4 eV platu joslu, kas ir līdzīga tai, kura iegūta tilpumā [P1, 34]. Savukārt U(6*d*) elektronu ieguldījums joprojām nav jutīgs pret vakanču klātbūtni, jo šie stāvokļi ir gandrīz vienmērīgi sadalīti plašā enerģijas diapazonā, ieskaitot vadāmības zonu. Pilno DOS profilu atšķirība perfektajām UN(001) 7-slāņu plātnēm, kas ir redzama 7.3a un 6.2b attēlā, var tikt izskaidrota ar plātņu dažādo ģeometrijas relaksāciju, veicot aprēķinus ar spina relaksāciju un bez tās.

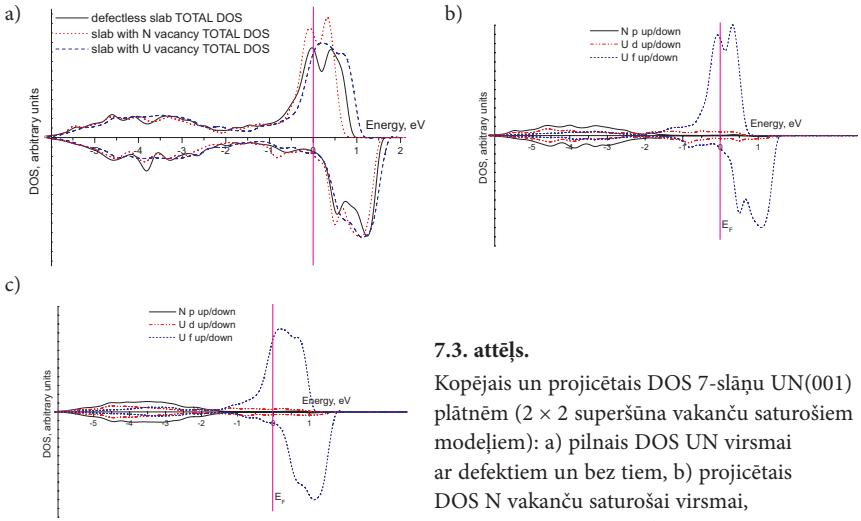

7.3. attēls.
Kopējais un projicētais DOS 7-slāņu UN(001) plātnēm (2 × 2 superšūna vakanču saturošiem modeļiem): a) pilnais DOS UN virsmai ar defektiem un bez tiem, b) projicētais DOS N vakanču saturošai virsmai, c) projicētais DOS U vakanču saturošai virsmai

7.4. Magnētiskās īpašības

Tika veikta arī vidējo U atomu magnētisko momentu analīze (μ_{av}^{U}) defektu saturošām UN plātnēm (7.4. att.). Tie samazinās abu vakanču veidiem kā funkcija no slāņu skaita plātnē, izņemot U vakancēm virsmas slānī, kurām magnētiskie momenti gandrīz nemainās. No otras puses, μ_{av}^{U} ievērojami pieaug, ja U vakances atrodas virsmas vai zemvirsmas slānī. Atšķirībā no U vakanču gadījuma plātnēm ar N vakancēm μ_{av}^{U} ir mazāk jutīgs pret defektu pozīciju un tie ir praktiski identiski N vakancēm virsmas un zemvirsmas slāņos.

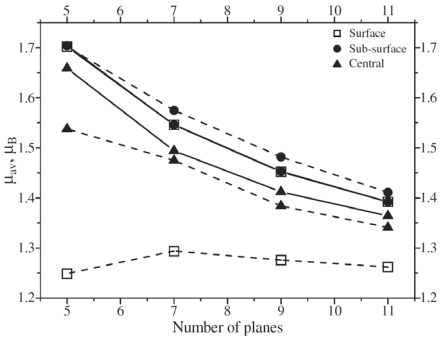

7.4. attēls. Vidējais plātņu U atomu magnētiskais moments μ_{av} (μ_B mērvienībās) atkarībā no slāņu daudzuma plātnē. Svītru līnijas atbilst U vakancēm, savukārt nepārtrauktā līnija apraksta N vakances

7.5. N vakanču aprēķinu rezultātu salīdzinājums UN (001) un (110) virsmai

Lai palielinātu rezultātu ticamību, mēs salīdzinājām N vakanču virsmas UN(001) slāņa aprēķinu rezultātus ar analoģiskiem aprēķiniem (110) virsmai (7.5. att.). (110) virsmai mēs izmantojām 5-, 7-, 9- un 11-slāņu 2 × 2 virsmas superšūnas, kā arī 7-slāņu 3 × 3 superšūnu. Iegūtie rezultāti ir apkopoti 7.2. tabulā. Vakancēm uz (110) virsmas saglabājas visas galvenās tendences. Vidējais magnētiskais moments μ_{av} samazinās abām virsmām kā funkcija no slāņu daudzuma plātnē. No otras puses, vakances veidošanās enerģija ir par ~ 0.7 eV mazāka UN(110) virsmai. Šī atšķirība ir viegli izskaidrojama, jo (110) virsmai piemīt lielāks irdenums, salīdzinot ar (001) virsmu.

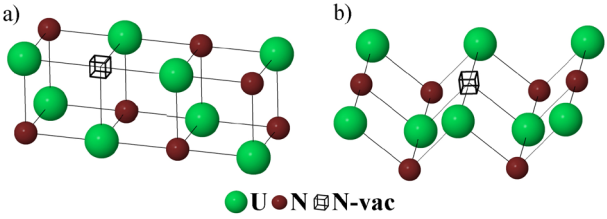

7.5. attēls. 2-slāņu modeļi N vakancēm uz UN (001) (a) un (110) (b) virsmas

7.2. tabula. Skābekļa vakanču veidošanās enerģija (eV mērvienībās), kā arī U atomu vidējais magnētiskais moments μ_{av}, novērtēts UN (001) un (110) virsmai

Slāņu skaits un superšūnas izmērs	N vakances E_{form} uz (001) virsmas	$\mu_{av}(\mu_B)$ (001)	N vakances E_{form} uz (110) virsmas	$\mu_{av}(\mu_B)$ (110)
5, 2 × 2	3.700	1.702	3.075	1.818
7, 2 × 2	3.706	1.548	3.028	1.585
9, 2 × 2	3.708	1.452	3.036	1.512
11, 2 × 2	3.712	1.392	3.026	1.453
7, 3 × 3	3.646	1.487	2.966	1.498

7.6. Vakances aprēķini: kopsavilkums

U un N vakanču veidošanās enerģijas tika noteiktas, izmantojot divus atskaites stāvokļus – izolēto atomu enerģiju, kā arī atomu enerģiju metāliskā α-U fāzē un N_2 molekulā. Vakanču veidošanās enerģijas norāda uz skaidru tendenci vakanču segregācijai uz virsmas (vai, iespējams, uz graudu robežām), jo šīs vērtības virsmas slānim ir ievērojami mazākas, salīdzinot ar analoģiskām vērtībām zemvirsmas un centrālajiem slāņiem (abas pēdējās ir ļoti tuvas). Tomēr magnētiskie momenti zemvirsmas un centrālajā slānī ievērojami atšķiras. Mēs esam parādījuši arī ievērojamu atomu lādiņu vērtību novirzi no formālo lādiņu vērtībām (tās izraisa kovalentais ieguldījums U-N saitē).

8. O adsorbcijas un migrācijas modelēšana uz UN bezdefektu virsmas

8.1. Atomāra skābekļa adsorbcija

8.1.1. Modelis un teorētiskie pamati

Lai modelētu O atoma adsorbciju bez spina relaksācijas, tika izmantotas 5-slāņu plātnes ar 2×2 superšūnām gan PW aprēķiniem, kurus veicām mēs, gan LCAO aprēķiniem, kurus izdarīja prof. R. Evarestova grupa [P2]. 5-slāņu un 7-slāņu 3D plātnes ar 2×2 un 3×3 superšūnām tika lietotas PW aprēķiniem ar spina relaksāciju. Lai samazinātu nepieciešamo skaitļošanas jaudu, esam izmantojuši simetrisko divpusējo skābekļa adatomu izvietojumu (8.1. att.), tāpat kā to darījām vakanču aprēķinos.

Tikai UN feromagnētiskais stāvoklis tika apskatīts šajā pētījumā kā enerģētiski izdevīgāks zemu temperatūru aprēķinos. UN tilpuma aprēķinos tika izmantots magnētiskais moments uz U atomiem, vienāds ar ~ 1 μ_B. *CRYSTAL* visiem aprēķiniem un *VASP* aprēķinu daļai esam veikuši pilnā spina fiksāciju. Tādējādi kopējais magnētiskais moments piecu slāņu plātnei ar 2×2 superšūnu (kas satur 20 U un N atomus) tika nofiksēts uz 20 μ_B.

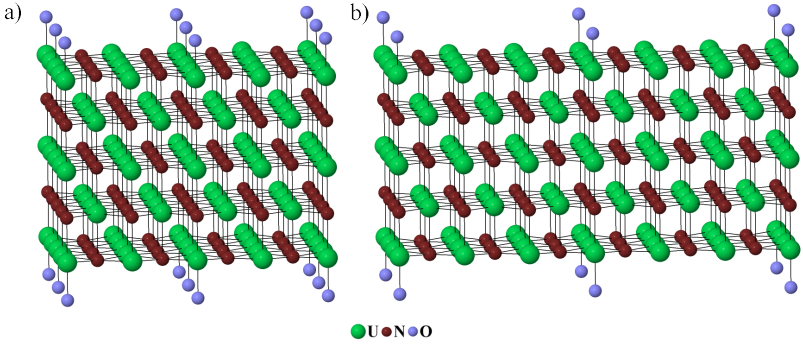

8.1. attēls. O/UN(001) interfeisa modelis: divpusēja periodiska O atomu adsorbcija virs U_{surf} atomiem ar 0.25 ML (a) un 0.11 ML (b) defektu koncentrāciju

Adsorbētā skābekļa atoma (O_{ads}) saites enerģija E_{bind} tika aprēķināta attiecībā pret brīvo O atomu:

$$E_{bind} = \frac{1}{2}\left(E^{\mathrm{UN}} + 2E^{\mathrm{O_{triplet}}} - E^{\mathrm{O/UN}}\right), \qquad (8.1.1.)$$

kur $E^{\mathrm{O/UN}}$ ir pilnā enerģija relaksētajai O/UN(001) plātnei ar O_{ads} novietošanu virs plātnes N vai U ārējā slāņa joniem, E^{UN} ir relaksētās UN plātnes enerģija, un $E^{\mathrm{O_{triplet}}}$ ir O atoma pilnā enerģija pamatstāvoklī (tripleta stāvoklī). Brīvā O atoma PAW aprēķiniem

tika izmantots skābekļa 3D periodiskais izvietojums kubiskajā kastē ar ~ 20 Å šķautni. Reizinātājs ½ pirms iekavām parādās, jo substrāts tiek modelēts, lietojot plātnes modeli, kam ir divas līdzvērtīgas virsmas, un O_{ads} ir novietoti simetriski attiecībā pret virsmām.

8.1.2. *Atomārās adsorbcijas bez spina relaksācijas PW un LCAO aprēķinu salīdzinājums*

VASP un *CRYSTAL* aprēķinu attiecīgie rezultāti, kas balstās uz divām ļoti atšķirīgām pieejām, uzrāda labu kvalitatīvu saskaņu starp O adatoma īpašībām virs virsmas U atomiem (8.2. att.): saites enerģijai (3D plātnes modeļi parasti novērtē šo parametru par zemu, jo blakus polarizētās plātnes atgrūžas), atomu nobīdei un efektīvajiem lādiņiem (kurus aprēķina, izmantojot ļoti atšķirīgas Mallikena (LCAO) un Badera (PAW) procedūras).

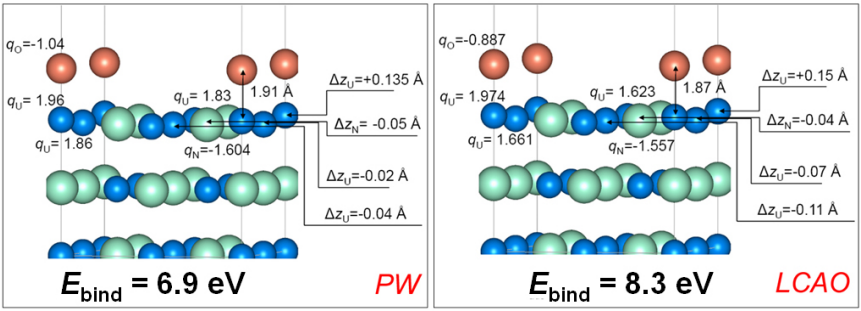

8.2. attēls. Ar PW un LCAO metodi aprēķinātās saites enerģija (E_{bind}), attālums starp O un virsmas U katjonu ($d_{O\text{-}U}$), efektīvais atomu lādiņš (q) un U un N atomu vertikālā (Δz) nobīde no virsmas plaknes situācijā, kad adatoms ir adsorbēts virs virsmas U atoma

8.1.3. *Saites enerģijas, lādiņu un struktūras relaksācijas PW aprēķini*

Tā kā UN savienojuma ķīmiskā saite ir metāliski kovalenta, mēs sagaidām augstu O_{ads} tieksmi pie UN(001) substrāta. O adatomu saites enerģija ir daudz tuvāka pie saites enerģijām regulārajiem O/Al(111) vai O/Al(001) metāliskajiem interfeisiem (~ 10 eV) [79] nekā pie saites enerģijas O/$SrTiO_3$(001) pusvadītāja interfeisam (ar divām iespējamām SrO- vai TiO_2- terminācijām) (~2 eV) [80]. Patiešām, *VASP* aprēķinos mēs ieguvām saites enerģijas, vienādas ar 6.9–7.6 un 5.0–5.7 eV O adatomiem virs virsmas U vai N joniem, kopā ar 0.5–1.2 *e* lādiņu pārnesi no virsmas uz O adatomu (8.1. un 8.2. tab.). Pozitīvi lādētais virsmas U atoms iet uz āru adsorbētā O atoma virzienā (8.4. att.), savukārt konfigurācijai ar O adatomu virs N atoma pēdējais stipri nobīdās no adsorbētā O atoma uz plātnes iekšu, pateicoties N un O savstarpējai atgrūšanai.

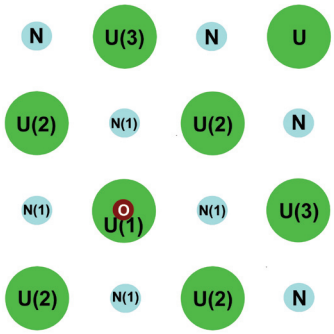

8.3. attēls.
Shematisks modelis: O atoms, kas adsorbēts virs virsmas U atoma. Ar numuriem ir sanumurēti neekvivalentie virsmas atomi, kas aprakstīti 8.1. un 8.2. tabulā

8.1. tabula. Aprēķinātās vērtības saites enerģijai (E_{bind}), attālumam no O līdz U virsmas atomam ($d_{O\text{-}U}$), efektīvajiem atomu lādiņiem uz atomiem (q) un vertikālajiem U un N atomu pārvietojumiem no virsmas plaknes (Δz)[a] O adatoma pozīcijai virs U_{surf}. q vērtības virsmas atomiem, iegūtas 5-slāņu bezdefektu (7-slāņu) plātnēm, bez spina relaksācijas ir vienādas ar +1.66(+1.72) e U_{surf} atomam un −1.63(−1.64) e N_{surf} atomam, savukārt aprēķinos ar spina relaksāciju vērtības ir vienādas ar +1.68 (+1.74) e U_{surf} atomam un −1.65 (−1.67) e N_{surf} atomam [P4]

Modelis	E_{bind}, eV	q_O, e	$q_{U(1)}$, e	$q_{U(2)}$, e	$q_{U(3)}$, e	$q_{N(1)}$, e	$d_{O\text{-}U}$, Å	$\Delta z_{U(1)}$, Å	$\Delta z_{U(2)}$, Å	$\Delta z_{U(3)}$, Å	$\Delta z_{N(1)}$, Å
2 × 2, 5 slāņi ar nerelaksēto spinu	6.9	-1.04	1.96	1.86	1.83	-1.60	1.91	+0.135[a]	-0.02	-0.04	-0.05
2 × 2, 5 slāņi	7.57	-1.08	2.09	1.82	1.84	-1.63	1.88	+0.16	+0.025	+0.003	-0.09
2 × 2, 7 slāņi	7.51	-1.08	2.19	1.78	1.78	-1.64	1.89	+0.17	+0.03	-0.02	-0.09
2×2, 7 slāņi N vakances tuvumā	7.58	-1.08	1.84	1.50	1.48	-1.61* -1.61^	1.88	+0.14	+0.01	-0.02	-0.09* -0.08^
3 × 3, 5 slāņi	7.59	-1.09	2.13	1.80	1.74	-1.62	1.88	+0.16	+0.01	-0.01	-0.10
3 × 3, 7 slāņi	7.57	-1.09	2.13	1.78	1.79	-1.62	1.88	+0.16	+0.01	-0.01	-0.09
3 × 3, 7 slāņi N vakances tuvumā	7.59	-1.09	1.86	1.47*	1.38*	-1.61* -1.61^	1.88	+0.10	-0.025*	-0.06*	-0.12* -0.11^
LCAO[b]	8.3	-0.89	1.97	1.66	1.62	-1.56	1.87	+0.15[b]	-0.07	-0.11	-0.04

[a] plus zīme atbilst atoma nobīdei virzienā no virsmas ārpusi

* ^ O atoma adsorbcija sistēmā, kurā eksistē N vakance, noved pie citu N atomu neekvivalences (8.10a att.),

[b] LCAO aprēķini, kurus veica prof. R. Evarestova grupa, izmantojot *CRYSTAL-2006* programmu.

8.1. un 8.2. tabula skaidri parāda, ka O_{ads}–U_{surf} saites joniskums un efektīvie lādiņi ir nedaudz lielāki spin-polarizētajos aprēķinos (šis efekts ir mazāk izteikts O_{ads}–N_{surf} saitei, kurai esam ieguvuši tikai nelielu pieaugumu $|q_N|$ lielumiem). Struktūras relaksācijas nobīdes ir arī nedaudz lielākas spin-polarizētajos aprēķinos. Saites enerģijas starp adsorbēto O un U/N atomiem ir par ~ 0.6–0.7 eV lielākas aprēķiniem ar spina relaksāciju, salīdzinot ar analoģiskiem aprēķiniem bez spina relaksācijas. Ja mēs novērtējam saites enerģiju O adatomam uz defektīvas virsmas N vakances tuvumā, izmantojot formulu

$$E_{bind} = \frac{1}{2}\left(E^{\mathrm{UN(N\_vac)}} + 2E^{\mathrm{O_{triplet}}} - E^{\mathrm{O/UN(N\_vac)}}\right), \qquad (8.1.2.)$$

kur $E^{\mathrm{UN(N\_vac)}}$ ir pilnā enerģija defektīvajam N vakanču saturošam UN substrātam, savukārt $E^{\mathrm{UN(N\_vac)}}$ ir pilnā enerģija adsorbētajiem skābekļa atomiem virs defektīvā substrāta, tad vērtības, kas ir aprēķinātas, izmantojot vienādojumus (8.1.1. un 8.1.2.), ir gandrīz tādas pašas.

8.2. tabula. Aprēķinātie parametri O atomam, adsorbētam virs N_{surf} atoma[a] (sk. tabulas virsrakstu un zemteksta piezīmes)

Modelis	E_{bind}, eV	q_O, *e*	$q_{N(1)}$, *e*	$q_{N(2)}$, *e*	$q_{N(3)}$, *e*	$q_{U(1)}$, *e*	$d_{O\text{-}N}$, Å	$\Delta z_{N(1)}$, Å	$\Delta z_{N(2)}$, Å	$\Delta z_{N(3)}$, Å	$\Delta z_{U(1)}$, Å
2 × 2, 5 slāņi ar nerelaksēto spinu	5.0	-1.20	-1.44	-1.56	-1.59	1.805	2.19	-0.64	+0.065	+0.06	+0.10
2 × 2, 5 slāņi	5.52	-1.17	-1.48	-1.68	-1.68	1.86	2.19	-0.69	+0.03	+0.05	+0.13
2 × 2, 7 slāņi	5.58	-1.17	-1.48	-1.63	-1.67	1.86	2.21	-0.715	+0.03	+0.03	+0.12
3 × 3, 5 slāņi	5.57	-1.18	-1.51	-1.67	-1.68	1.89	2.20	-0.70	+0.01	+0.01	+0.13
3 × 3, 7 slāņi	5.65	-1.18	-1.51	-1.69	-1.65	1.89	2.22	-0.73	+0.01	+0.02	+0.12

[a] U un N jonu pozīcijas ir samainītas, salīdzinot ar tām, kas ir parādītas 8.3. attēlā.

8.1.4. Elektronisko īpašību analīze

Elektronisko lādiņu blīvuma pārdalīšanās, kas saistīta ar O atoma adsorbciju virs N_{surf} vai U_{surf} atomiem uz UN(001) virsmas, ar spina relaksāciju ir parādīta 8.4. attēlā. Elektronisko lādiņu pārdalīšanās starpības diagramma O_{ads} abām konfigurācijām apstiprina, ka skābekļa adatoms veido spēcīgu saiti ar U_{surf} atomu, kuru var uzskatīt par viencentru adsorbcijas kompleksu (8.4.c, 8.4.d att.).

O adatomam virs N_{surf} atoma veidojas daudzcentru adsorbcijas komplekss, kas ietver četrus virsmas U kaimiņatomus (8.4.a, 8.4.b att.). Kā izriet no 8.2. tabulas, šie virsmas atomi dod lielu ieguldījumu O atoma augstajai saites enerģijai virs N_{surf}. Spēcīgas ķīmiskās saites veidošanās O atomam ar U_{surf} izraisa spēcīgu anizotropu elektronisko lādiņu pārdali, tādējādi norādot uz ievērojamu urāna *f* un *d* elektronu ieguldījumu ķīmiskajā saitē. Elektroniskā blīvuma pārdalīšanās diagrammas liecina par to, ka U_{surf} atomi ekranē kaimiņatomu iedarbību nākamajās koordinācijas sfērās daudz labāk nekā N_{surf} atomi. Lietojot 7-slāņu 3 × 3 superšūnas, mēs varam izvairīties no ierobežota plātnes izmēra efekta ietekmes.

O_{ads} adsorbcija virs virsmas N vai U atomiem UN(001) noved pie specifiskas skābekļa joslas (8.5. att.) parādīšanās stāvokļa blīvuma (DOS) funkcijā, salīdzinot ar DOS grafiku ideālajai UN(001) virsmai (6.2. att.). Skābekļa adsorbcijai virs U_{surf} O(*2p*) stāvokļi pārklājas ar U_{surf}(*6d*) un ar U_{surf}(*5f*) stāvokļu labi izteikto asti N_{surf} (*2p*) stāvokļu valences zonā (-2 līdz -4 eV). Tas vēlreiz norāda uz spēcīgu skābekļa ķīmisko saiti (hemisorbciju) ar U_{surf} atomu, tipisku metāliskajām virsmām. Tomēr, ja O atrodas virs N_{surf}, tad U_{surf}(*5f*) stāvokļu ieguldījums šajā enerģiju diapazonā samazinās, jo N_{surf}(*2p*) stāvokļi ir ievērojami

nobīdīti uz mazāko enerģiju pusi sakarā ar N_{surf} atoma atgrūšanos no negatīvi uzlādēta O adatoma.

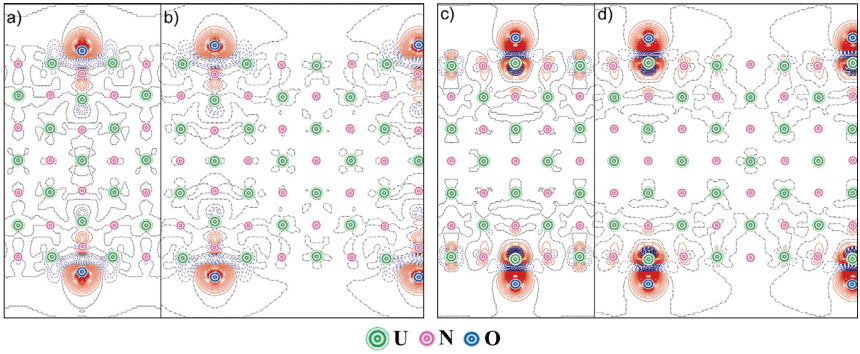

8.4. attēls. 2D šķērsgriezums elektronisko lādiņu blīvuma pārdalīšanai $\Delta\rho$(r) O atomiem, adsorbētiem virs (*i*) N_{surf} atomiem ar 2 × 2 (a) vai 3 × 3 (b) superšūnu, kā arī virs (*ii*) U_{surf} atomiem ar 2 × 2 (c) un 3 × 3 (d) superšūnu 7-slāņu UN(001) plātnēm. Funkcija $\Delta\rho(\mathbf{r})$ ir definēta kā kopējais elektroniskais blīvums interfeisam, kas satur adsorbētus O atomus, mīnus blīvumi pamatnei un adsorbētajiem O atomiem ar ģeometriju, kas sakrīt ar O/UN interfeisa ģeometriju. Nepārtraukta (sarkana) un pārtraukta (zila) izolīnija atbilst attiecīgi pozitīvam un negatīvam elektroniskam blīvumam. Pārtraukta melna līnija atbilst nulles līmenim

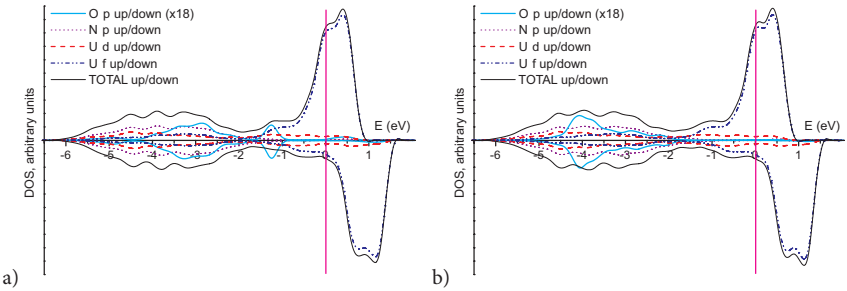

8.5. attēls. Kopējais un projicētais DOS O atomiem, adsorbētiem virs UN(001) substrāta ar 7-slāņu superšūnu un 3 × 3 periodiskumu: a) adsorbcija virs N atoma, b) adsorbcija virs U atoma. Atsevišķu enerģijas līmeņu konvolūcija tika veikta, izmantojot Gausa funkcijas ar pusplatumu, vienādu ar 0.2 eV

8.1.5. Salīdzinājums skābekļa adsorbcijai virs UN(001) un UN(110) virsmas

Mēs arī aprēķinājām saites enerģiju skābekļa adatoma adsorbcijai virs UN(110) virsmas (8.3. tab.). Esam atraduši šiem rezultātiem kvalitatīvu līdzību O adsorbcijai uz (001) virsmas. Abām virsmām skābekļa saites enerģijas virs U atomiem ir lielākas

salīdzinājumā ar adsorbciju virs N atomiem (par ~ 1.9 eV (001) virsmai un par ~ 2.1–2.2 eV (110) virsmai). Turklāt virsmas superšūnas palielināšana no 2 × 2 līdz 3 × 3 noved pie saites enerģijas nelielas palielināšanās. Skābekļa saites enerģijas (110) virsmai ir par ~ 0.1–0.4 eV lielākas, salīdzinot ar vērtībām (001) virsmai. Augstākas E_{bind} vērtības (110) virsmai var izskaidrot ar lielāku attālumu starp virsmas adatomiem uz (110) virsmas, kā rezultātā samazinās adsorbētā skābekļa mijiedarbība ar visiem citiem atomiem, izņemot apakšā novietotos U vai N atomus.

8.3. tabula. Aprēķinātās saites enerģijas ($E_{bind,}$ eV) skābekļa adsorbcijai virs UN (001) un (110) virsmas

Slāņu skaits un superšūnas izmērs		Virs U atoma	Virs N atoma
		Saites enerģija, eV	Saites enerģija, eV
(001)	7, 2 × 2	7.51	5.58
	7, 3 × 3	7.57	5.65
(110)	7, 2 × 2	7.90	5.73
	7, 3 × 3	7.91	5.99

8.1.6. Atomāra skābekļa adsorbcija: kopsavilkums

Tātad rezultāti par atsevišķu skābekļa atomu mijiedarbību ar UN virsmu, prezentēti 8.1. apakšnodaļā, demonstrē stipras UN virsmas hemisorbcijas īpašības, kas ir tipiskas metāliskām virsmām. Lieliskā kvalitatīvā saskaņa starp rezultātiem, kuri iegūti ar divu dažādu pirmo principu metodes palīdzību, palielina UN modelēšanas ticamību. O adatoms virs U_{surf} atoma veido viencentru kompleksu ar apakšnovietotu U_{surf} atomu, savukārt skābekļa adsorbcija virs N_{surf} atoma noved pie virsmas kompleksa veidošanās, un tas sastāv no N_{surf} un četriem kaimiņu U_{surf} atomiem.

8.2. Molekulārā skābekļa adsorbcija

8.2.1. Modelis un teorētiskais pamatojums

Rezultāti, kas tika analizēti 8.1. nodaļā un referencē [P2], skaidri norāda uz UN virsmas metālisko raksturu. Šajā apakšnodaļā mēs apskatījām molekulārā skābekļa mijiedarbību ar ideālo UN(001) virsmu [P3]. Rodas šādi galvenie jautājumi: vai O_2 molekulas disociācija uz virsmas ir enerģētiski iespējama; kāds novietojums ir optimāls molekulas adsorbcijai; un vai disociācija var notikt spontāni, bez enerģijas barjeras, līdzīgi citām metāliskajām virsmām, piemēram, Al [79].

Molekulārās adsorbcijas aprēķini tika veikti, izmantojot nofiksēto pilno spinu, vienādu ar 1 μ_B katram U atomam. Skābekļa molekulas hemisorbcijas modelēšanai mēs izmantojām 5-slāņu superšūnu ar 2 × 2 virsmas vektoru paplašinājumu (kas satur 20 U un 20 N atomus). Periodiska adsorbāta sadalījums atbilst molekulārajam pārklājumam, vienādam ar 0.25 no ML (vai O atomu pārklājumam, vienādam ar 0.5 no ML). Lai samazinātu skaitļošanas pūles, vēlreiz izmantojām simetrisko divpusējo skābekļa molekulu izvietojumu. Saites enerģija E_{bind} uz skābekļa atoma adsorbētā molekulā $(O_2)_{ads}$ tika aprēķināta šādi:

$$E_{bind} = \frac{1}{4}\left(E^{\mathrm{UN}} + 2E^{\mathrm{O_2}} - E^{\mathrm{O_2/UN}}\right), \qquad (8.2.1.)$$

kur $E^{\mathrm{O_2/UN}}$ ir pilnā enerģija pilnīgi relaksētai O_2/UN(001) plātnei ar (O_2) molekulas dažādām pozīcijām virs substrāta (ar molekulas centru virs attiecīgajām virsmas pozīcijām, tas ir parādīts 8.7. attēlā), savukārt $E^{\mathrm{O_2}}$ un E^{UN} ir kopējās enerģijas izolētajai skābekļa molekulai tripleta pamatstāvoklī un relaksētajai UN plātnei. Koeficients 1/4 pirms iekavām, līdzīgi atomārās adsorbcijas aprēķiniem, parādās tādēļ, ka substrāts tiek modelēts, izmantojot plātni, kas satur divas ekvivalentas virsmas ar $(O_2)_{ads}$ molekulām, novietotām simetriski attiecībā pret plātnes virsmām, un katra molekula pirms un pēc disociācijas satur divus O atomus. Modelējot molekulāro adsorbciju, esam analizējuši dažādas O_2 molekulu konfigurācijas tripleta stāvoklī virs UN(001) virsmas. Tika konstatēts, ka skābekļa molekulas vertikālās orientācijas virs virsmām N vai U joniem ir metastabilas attiecībā uz molekulu pārorientēšanos uz horizontālo konfigurāciju, paralēlu virsmai. Mēs novērtējām molekulas saites enerģiju, izmantojot vienādojumu (8.2.1.), un disociācijas enerģiju molekulai (dažās konfigurācijās) vai, citiem vārdiem, starpību plātnei ar O_2 molekulu pirms un pēc disociācijas, kad divi O atomi ir novietoti tripleta stāvoklī virs diviem tuvākajiem U_{surf} atomiem (8.4. tab.).

8.2.2. Spontānā disociācija

Mēs esam atraduši, kā O_2 molekulas disociācija notiek spontāni divos gadījumos: (*i*) ja molekulas centrs atrodas iedobuma pozīcijā starp U atomiem vai (*ii*) virs N atoma ar molekulāro saiti, vērstu uz diviem tuvākajiem U_{surf} atomiem (1. un 5. konfigurācija 8.6. att.). Attiecīgās disociācijas enerģijas E_{diss} ir apkopotas 8.4. tabulā kopā ar citiem sistēmu raksturojošiem parametriem (atomu relaksācija un Badera lādiņu sadalījums). Ģeometrija un lādiņi 1. un 5. konfigurācijai pēc disociācijas (8.4. tab.) ir kvalitatīvi līdzīgi tiem, kas iegūti UN(001) virsmai, pārklātai ar hemisorbētiem O atomiem, piemēram, pēc disociācijas U_{surf} atomi zem skābekļa adatoma tiek nobīdīti uz augšu abām konfigurācijām (8.4. tab.). Tomēr, tā kā koncentrācija O_{ads} šajos aprēķinos ir divreiz lielāka, salīdzinot ar atomāro skābekļa adsorbciju [P2, 8.1. apakšnodaļā], dažas kvantitatīvas atšķirības rezultātiem, kas prezentēti 8.4. un 8.1. tabulā, skābekļa atomu adsorbcijai virs U_{surf} ir neizbēgamas. Piemēram, pēc O_2 disociācijas divu adatomu, kas novietoti virs diviem tuvākajiem U_{surf} atomiem, atgrūšanās enerģija (1. konfigurācija) ir diezgan liela, ~ 0.7 eV.

Mēs atradām divas citas adsorbētā skābekļa molekulas konfigurācijas, kurām disociācija ir enerģētiski iespējama tikai ar enerģijas barjeru: (*i*) virs iedobuma pozīcijas, ja molekulārā saite ir vērsta uz tuvākajiem N_{surf} atomiem (2. konfigurācija 8.6. att.), un (*ii*) virs U_{surf} atoma (jebkādai molekulu orientācijai, piemēram, 3. un 4. konfigurācija 8.6. att.). 2. konfigurācijai mēs novērojām adsorbētās molekulas orientācijas nestabilitāti pret vieglo griešanu, līdz, piemēram, saišu virzībai uz U_{surf} atomiem ar tālāko disociāciju. 3. un 4. konfigurācija apraksta drīzāk metastabilas UO_2 kvazimolekulas, jo starp visiem trim atomiem ir spēcīgas saites (8.7.c att.), un attiecīgie U_{surf} atomi ir ievērojami nobīdīti uz augšu no to sākotnējās pozīcijas uz virsmas (8.4. tab.). $(O_2)_{ads}$ molekulas disociācija 3. konfigurācijā ir enerģētiski iespējama tikai tad, ja tiks pārvarēta aktivācijas enerģijas barjera.

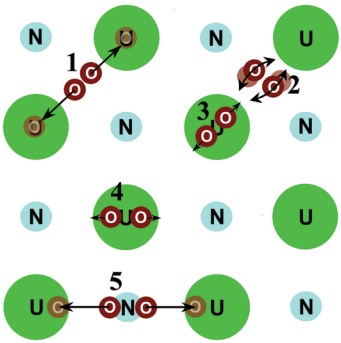

8.6. attēls.
Shematiskais attēls piecām dažādām adsorbētas molekulas horizontālām konfigurācijām uz UN virsmas: 1) virs iedobuma pozīcijas ar saitēm, vērstām uz tuvākajiem U_{surf} atomiem, 2) virs iedobuma pozīcijas ar saitēm, vērstām uz tuvākajiem N_{surf} atomiem, 3) virs U_{surf} atomiem ar saitēm, vērstām uz nākamiem tuvākiem virsmas U_{surf} atomiem, 4) virs U_{surf} atomiem ar saitēm, vērstām uz tuvākajiem N_{surf} atomiem, 5) virs N_{surf} atomiem ar saitēm, vērstām uz tuvākajiem U_{surf} atomiem. Mēs parādījām, ka spontāna molekulas disociācija var notikt, ja O_2 molekula atrodas virs dobuma pozīcijas (1) vai virs N_{surf} atoma (5)

8.4. tabula. Aprēķinātās saites (E_{bind}, vienādojums (8.2.1.)) un disociācijas (E_{diss}) enerģijas, ģeometrija (z, Δz) un Badera lādiņi (q) skābekļa molekulas molekulāras un spontāni disociatīvas hemisorbcijas konfigurācijām uz UN(001) virsmas. Skaitļi iekavās atbilst konfigurācijām, kas ir parādītas 8.6. attēlā. Aprēķinātā saites enerģija brīvajai O_2 molekulai tripleta stāvoklī ir 6.06 eV, un saites garums ir vienāds ar 1.31 Å (salīdziniet ar eksperimentālām vērtībām, vienādām ar 5.12 eV un 1.21 Å) [81]

Pozīcija		E_{bind} **uz O atomu, eV**	z^a, **Å**	E_{diss}, **eV**	q**(O),** e	q**(U1**[b]**),** e	q**(U2**[c]**),** e	q**(N**[d]**),** e	Δz^e**(U1), Å**	Δz^e**(U2), Å**	Δz^e**(N), Å**
iedobuma (1)	molekulārā adsorbcija	3.03	1.893	-	-0.465	1.913	1.762	-1.533	-0.050	-0.050	0.025
	pēc disociācijas	6.04	1.957	3.01	-0.978	2.053	1.978	-1.577	0.075	0.068	-0.133
virs U	ar saiti uz tuvākajiem U atomiem (3)	4.00	2.18	-	-0.5905	2.042	1.836	-1.6065	0.176	-0.048	-0.096
	ar saiti uz tuvākajiem atomiem N (4)	4.18	2.14	-	-0.578	2.0485	1.827	-1.625	0.123	-0.051	-0.106
virs N (5)	molekulārā adsorbcija	2.67	2.020	-	-0.5685	1.8675	1.832	-1.354	-0.050	-0.050	0.025
	pēc disociācijas	5.85	1.955	3.18	-0.979	2.115	1.876	-1.580	0.073	0.021	-0.201

[a] z ir augstums O atomiem virs nerelaksēta UN substrāta,
[b] U1 ir tuvākais virsmas U_{surf} atoms,
[c] U2 ir nākamais tuvākais U_{surf} atoms,
[d] N ir tuvākais N_{surf} atoms,
[e] Δz ir papildu vertikālā nobīde virsmas atomiem attiecībā pret šo atomu pozīcijām bez adsorbētā skābekļa.

8.2.3. Adsorbētās molekulas elektroniskās īpašības

O_2 molekulas adsorbcija (tripleta stāvoklī) ir saistīta ar ~ 1 *e* lādiņu pārnesi katrai molekulai no substrāta (8.4. tab.). 8.7. attēlā mēs analizējām elektronisko lādiņu pārdalīšanas starpību trim horizontāli orientētām $(O_2)_{ads}$ molekulas konfigurācijām uz virsmas: (a) molekulai, kura ir adsorbēta iedobuma pozīcija (1. konfigurācija 8.6. att.), (b) molekulai, kura disociē no iepriekšējās konfigurācijas, un O adatomi atrodas virs tuvākajiem U_{surf} atomiem, (c) molekulai, kas ir adsorbēta virs U_{surf} atomiem (3. konfigurācija).

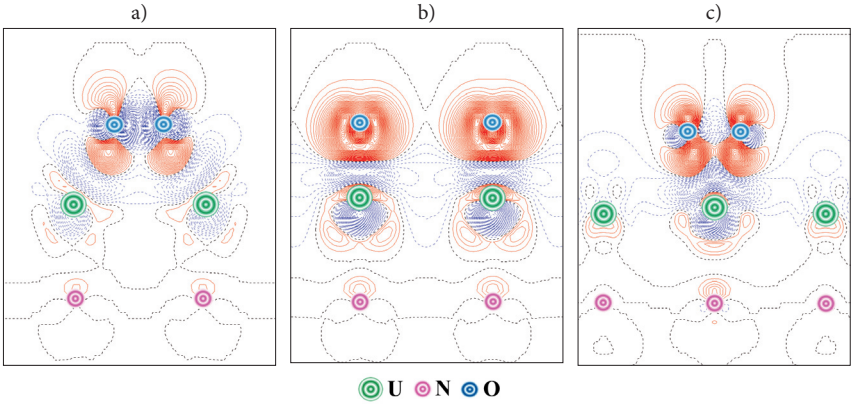

8.7. attēls. 2D šķēlums elektronu blīvuma pārdalījumam $\Delta\rho(r)$ (pilnais interfeisa blīvums mīnus summa pamatnes elektroniskam blīvumam un adsorbata blīvumam ar attiecīgi optimizētu ģeometriju) (a) O_2 molekulai virs dobuma pozīcijas ar saitēm, vērstām uz tuvākajiem U_{surf} atomiem, (b) pēc tās disociācijas 1. konfigurācijā (8.6. att.) ar O atomu virs U_{surf} atomiem un (c) O_2 molekulai virs U_{surf} atoma 3. konfigurācijā (8.6. att.). Nepārtraukta (sarkana) un pārtraukta (zila) izolīnija atbilst attiecīgi pozitīvam un negatīvam elektroniskam blīvumam. Izoblīvumu pieaugums ir vienāds ar 0.003 e a. u.$^{-3}$

Spontāna O_2 disociācija un tādējādi plūdena pāreja no (a) lādiņu pārdalīšanas uz (b) var tikt izskaidrota ar nepārtrauktiem elektroniskā blīvuma apgabaliem (8.7.a att.), kuri ir paralēli virsmai un kurus var uzskatīt par disociācijas kanāliem (analoģiski kanāliem, kurus var redzēt molekulārā skābekļa adsorbcijā Al substrāta blīvuma kartēs [79]). Pēc disociācijas katrs O adatoma lādiņš palielinās par ~1 *e*, pārveidojot O^- jonu tripleta stāvoklī (8.7.b att.). Apskatot 3. molekulāro konfigurāciju, var redzēt, ka šie disociācijas kanāli turpretī pārveidojas par disociācijas barjerām (8.7.c att.). Vienlaikus mēs novērojām ievērojami lielāku elektronisko blīvumu, kas liecina par to, ka veidojas līdzīgs UO_2 molekulas komplekss ar spēcīgu saiti starp O_2 molekulu un virsmas U atomu, virs kura atrodas adsorbētā skābekļa molekula. Tādējādi starpība starp elektroniskā blīvuma kartēm, kas ir atspoguļota 8.7a un 8.7.c attēlā, var tikt izskaidrota ar dažādām disociācijas spējam O_2 1. un 3. molekulas konfigurācijās (8.6. att.).

Tādām pašām adsorbcijas konfigurācijām, kas tika apskatītas iepriekš, mēs esam uzzīmējuši pilno un projicēto elektronisko stāvokļu blīvumu (DOS) (8.8. att.). Molekulārā

adsorbcija šajās konfigurācijās noved pie specifisko skābekļa joslu parādīšanās, salīdzinot ar skābekļa adatomu adsorbciju virs UN virsmas (8.5. att.) un N atomu aizvietošanu ar O atomiem UN tilpumā [82]. Skābekļa adsorbcijai virs iedobuma pozīcijas (8.6.a att.) ir novērots O(2*p*) pīķis pie -1 eV, kas pārklājas ar U(5*f*) un U(6*d*) stāvokļu līmeņiem. Pēc O_2 disociācijas (8.7.b att.) šis pīķis pazūd un tiek aizstāts ar diviem plašajiem maksimumiem N(2*p*) valento stāvokļu zonā (no -2 līdz -5 eV), līdzīgiem DOSu skābekļa adatomu adsorbcijai virs UN(001) substrāta (8.5. att.). Dažas atšķirības ir novērojamas arī starp attiecīgajiem U(5*f*) un U(6*d*) pīķiem diapazonā virs -1 eV (8.8.a–8.8c). Atšķirības varētu izskaidrot gan ar dažādu O un U atomu izkārtojumu šajās konfigurācijās, gan ar U stāvokļu jutīgumu pret skābekļa klātbūtni, kas tādējādi norāda un spēcīgo skābekļa ķīmisko sasaistīšanu (hemisorbciju).

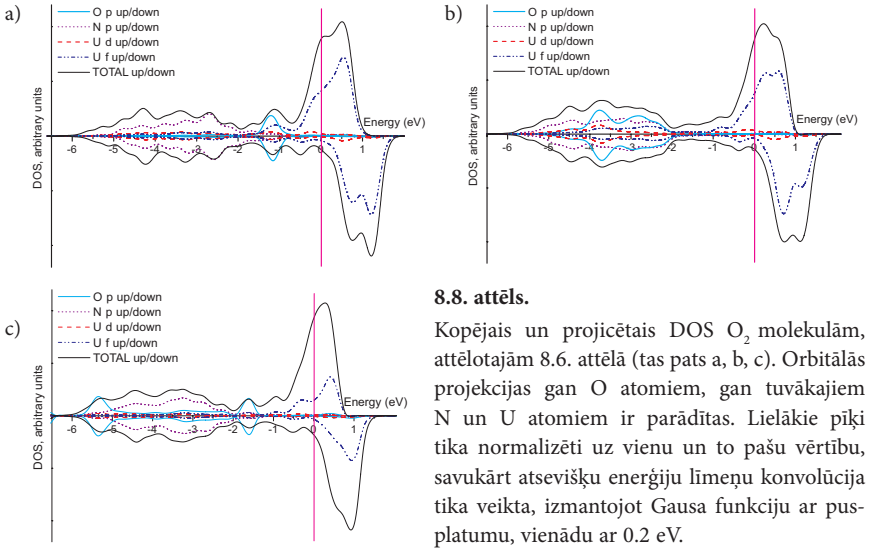

8.8. attēls.

Kopējais un projicētais DOS O_2 molekulām, attēlotajām 8.6. attēlā (tas pats a, b, c). Orbitālās projekcijas gan O atomiem, gan tuvākajiem N un U atomiem ir parādītas. Lielākie pīķi tika normalizēti uz vienu un to pašu vērtību, savukārt atsevišķu enerģiju līmeņu konvolūcija tika veikta, izmantojot Gausa funkciju ar pusplatumu, vienādu ar 0.2 eV.

Ja skābekļa molekula atrodas virs U_{surf} atoma (3. konfigurācija), tad U(5*f*) un U(6*d*) ieguldījumi enerģijas diapazonā virs -1 eV pavājinās, vienlaikus O(2*p*) ieguldījums pieaug, tādējādi palielinot pārklāšanos starp visiem trim stāvokļiem, un norāda uz UO_2 kvazimolekulāras saites veidošanos. Salīdzinot ar skābekļa molekulas adsorbciju virs iedobuma pozīcijas (8.8.a att.), mēs atkal novērojām lielāko O(2*p*) pīķi (pie -1.5 eV) un papildus to pašu O(2*p*) stāvokļa zemāko pīķi (pie -5.5 eV), kas ievērojami pārklājas ar U(5*f*) un U(6*d*) maksimumiem (8.8.c att.). Dažas analoģijas ar šo ainu tika novērotas agrāk projicētās DOS O atomam, kas aizvietoja N atomu UN tilpumā [82]. Visās trīs DOS diagrammās (8.8. att.) būtiski nemainās platā josla, kas satur N*(2p)* projicētos stāvokļus. Tas norāda uz mazu N atomu lomu O_2 molekulas adsorbcijā uz UN(001) virsmas.

Var secināt, ka aprēķinu no pirmajiem principiem rezultāti skābekļa molekulu adsorbcijai uz ideālas UN(001) virsmas skaidri pierāda adsorbētā skābekļa spontānas disociācijas reālu iespēju, analoģisku O_2 disociācijai virs „tradicionālajām" metāla virsmām.

8.3. O adatoma migrācijas trajektoriju modelēšana gar UN(001) virsmu

Mēs esam apskatījuši trīs skābekļa adatoma galvenos migrācijas ceļus pa UN(001) virsmu (8.9. att.): (i) 1. ceļš: starp pozīciju virs U_{surf} atoma uz pozīciju virs tuvākā N_{surf} atoma, (ii) 2. ceļš: starp divām pozīcijām virs U_{surf} kaimiņatomiem, (*iii*) starp divām pozīcijām virs N_{surf} kaimiņatomiem.

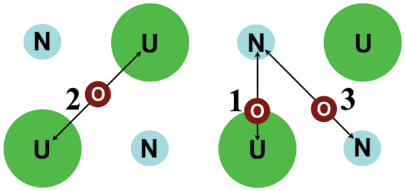

8.9. attēls. Dažādi skābekļa migrācijas ceļi pa UN(001) virsmu (skats no augšas)

8.5. tabula. Adsorbētā skābekļa saites enerģija E_{bind} dažādās pozīcijās virs UN plātnes (8.9. att.)

1. No pozīcijas virs U_{surf} uz pozīciju virs N_{surf} (1. migrācijas ceļš)				
Superšūnas izmērs:	2 × 2		3 × 3	
Atomāro slāņu skaits:	5	7	5	7
virs U_{surf}	7.57	7.51	7.59	7.57
¼ no U-N distances (vai 0.61 Å no U atoma)	7.39	7.39	-	-
½ no U-N distances (vai 1.22 Å no U atoma)	6.97	6.98	-	-
¾ no U-N distances (vai 1.83 Å no U atoma)	5.91	5.93	-	-
virs N_{surf} (vai 2.43 Å no U atoma)	5.52	5.58	5.57	5.65
2. No dobuma pozīcijas (d. p.) uz pozīciju virs U_{surf} (2. migrācijas ceļš)				
Superšūnas izmērs:	2 × 2		3 × 3	
Atomāro slāņu skaits:	5	7	5	7
virs d. p.	7.21	7.245	7.20	7.21
¼ no d. p.-U distances (vai 0.43 Å no d. p.)	7.23	7.255	-	-
½ no d. p.-U distances (vai 0.86 Å no d. p.)	7.32	7.33	-	-
¾ no d. p.-U distances (vai 1.29 Å no d. p.)	7.45	7.45	-	-
virs U_{surf} (vai 1.72 Å no d. p.)	7.57	7.51	7.59	7.57
3. No dobuma pozīcijas (d. p.) uz pozīciju virs N_{surf} (3. migrācijas ceļš)				
Superšūnas izmērs:	2 × 2		3 × 3	
Atomāro slāņu skaits:	5	7	5	7
virs d. p.	7.21	7.25	7.20	7.21
1/4 no d. p.-N distances (vai 0.43 Å no d. p.)	6.61	6.65	-	-
1/2 no d. p.-N distances (vai 0.86 Å no d. p.)	6.32	6.35	-	-
3/4 no d. p.-N distances (vai 1.29 Å no d. p.)	5.54	5.57	-	-
virs N_{surf} (vai 1.72 Å no d. p.)	5.52	5.58	5.57	5.65

Saites enerģija E_{bind} skābekļa atomam, adsorbētam uz UN virsmas, ir definēta 8.1.1. apakšnodaļā. Lai samazinātu skaitļošanas laiku skābekļa adatomu aprēķiniem starppozīcijās, esam relaksējuši tikai plātnes atomu z koordinātas, fiksējot to x un y koordinātas. O atomu adsorbcijai virs N_{surf} un U_{surf} atomiem plātnes kopējās ģeometrijas relaksācija tika veikta, lai kontrolētu simetrijas izmaiņas, kas ir radušās laterālas mijiedarbības dēļ. Rezultāti, kas iegūti visiem adatomu migrācijas ceļiem, plātņu dažādiem biezumiem un superšūnas izmēriem, ir sistematizēti 8.5. tabulā. Šajā tabulā ir apkopotas saites enerģiju vērtības, kas aprēķinātas O adatomu migrācijas trajektorijām gar perfekto UN(001) substrātu (8.9. att.). Mēs aprēķinājām piecas O_{ads} pozīcijas gar migrācijas trajektorijām UN(001) plātnes 2×2 superšūnai un divas pozīcijas 3×3 superšūnai. Abos gadījumos tika optimizēta visizdevīgākā migrācijas trajektorija, kas savieno pozīciju virs tuvākajiem virsmas U atomiem un iedobuma vietām starp tiem (2. trajektorija). Enerģijas barjeras ir vienādas ar 0.36 eV (5-slāņu plātne) un 0.26 eV (7-slāņu plātne). Enerģijas barjeras divām pārējām migrācijas trajektorijām ir ievērojami lielākas (1.93–2.05 eV 1. trajektorijai un 1.31–1.69 eV 3. trajektorijai, 8.9. att.).

Tātad mēs novērojām diezgan lielu O_{ads} atomu kustīgumu pa virsmu salīdzinoši zemo migrācijas barjeru dēļ.

9. O atomu migrācija un iekļaušana UN(001) defektīvā virsmā

9.1. O adatoma zemo barjeru iekļaušana no pozīcijas virs U_{surf} atoma uz N_{surf} vakanci

Lai saprastu sākotnējo adatoma iekļaušanās mehānismu virsējā UN(001) slānī, ir jāprecizē gan enerģētiskās, gan strukturālās iespējas O_{ads} migrācijai gan virs šāda ideālā, gan arī defektīvā substrāta. Lai novērtētu skābekļa adatomu kustīgumu uz UN(001) virsmas, esam veikuši virkni aprēķinu no pirmajiem principiem ar spina relaksāciju.

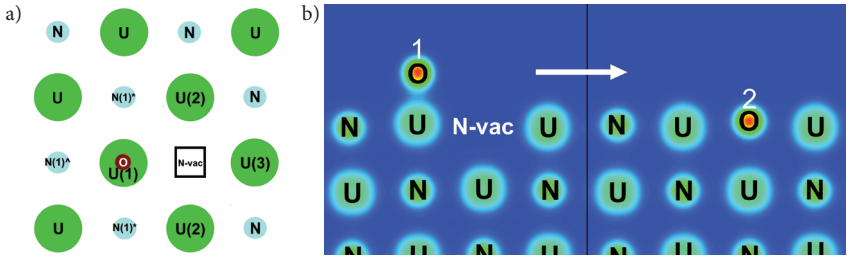

9.1. attēls. Skats no augšas (a) un šķērsgriezums (b) virsmas modelim, kuru izmanto skābekļa atoma zemu barjeru iekļaušanas modelēšanai no sākotnējās pozīcijas (1) virs U_{surf} atoma (pa kreisi) uz tuvāko eksistējošo N_{surf} vakanci (2). Ar dažādiem numuriem tika sanumurēti neekvivalentie virsmas atomi skābekļa adsorbcijas gadījumā N vakances tuvumā (8.3. att.)

Kā izriet no mūsu aprēķiniem, O atoms, adsorbēts virs U_{surf} atoma virsmas N vakances tuvumā, var tikt tajā satverts (9.1. att.) pēc zemas enerģijas barjeras pārvarēšanas (~ 0.5–1 eV). Mēs aprēķinājām enerģijas ieguvumu šādai skābekļa adatoma pārejai, izmantojot formulu

$$\Delta E = \frac{1}{2}\left(E_{tot}^{\mathrm{UN(O\_in\_N\_vac)}} - E_{tot}^{\mathrm{UN(O\_atop\_U)}}\right), \qquad (9.1.1.)$$

kur $E_{tot}^{\mathrm{UN(O\_in\_N\_vac)}}$ ir pilna enerģija superšūnai, kas satur O atomu N vakancē (2. pozīcija, kura ir parādīta 9.1. att.), un $E_{tot}^{\mathrm{UN(O\_atop\_U)}}$ ir pilna enerģija superšūnai ar O atomu, adsorbētu virs U_{surf} atoma, kas ir novietots eksistējošas N vakances tuvumā (1. pozīcija). $E_{tot}^{\mathrm{O/UN(N\_vac)}}$ aprēķiniem mēs nofiksējām x un y skābekļa horizontālās koordinātas, lai novērstu O adatoma migrāciju. Reizinātais ½ vienādojumā (9.1.1.) parādās sakarā ar adsorbēto vai vakancē iekļauto skābekļa atoma simetrisko izvietojumu. Salīdzinot $E_{tot}^{\mathrm{UN(O\_in\_N\_vac)}}$ vērtību (kas ir iegūta adatoma migrācijai no stāvokļa virs U_{surf} atoma uz vakanci) ar $E_{tot}^{\mathrm{UN(O\_in\_N\_vac)}}$, kad O adatoms tieši tiek iekļauts iepriekš eksistējošā vakancē (9.2. apakšnodaļa), mēs atradām, ka starpība nepārsniedz 0.01 eV. Aprēķinātais enerģijas ieguvums (ΔE_g) attiecībā uz pāreju no 1. pozīcijas uz 2. pozīciju (kā parādīts 9.1. att.) ir vienāds ar ~ 2 eV katram skābekļa atomam (1.99 eV 2 × 2 7-slāņu superšūnai un 1.94 eV 3 × 3 7-slāņu superšūnai).

9.2. attēlā elektronisko lādiņu pārdalījumu starpība skābekļa adsorbcijai virs U_{surf} atoma virsmas N vakances tuvumā tiek analizēta. Elektronisko lādiņu pārdalījumi plātnes iekšienē izskatās līdzīgi adsorbcijai virs U_{surf} atoma bez N vakances (8.4.c, d att.). Starp adsorbēto O atomu un eksistējošo N vakanci paralēli virsmai tika novēroti elektrostatiskie kanāli ar elektroniskā blīvuma trūkumu, kas ir vērsti skābekļa adatoma iekļaušanas virzienā uz N vakanci.

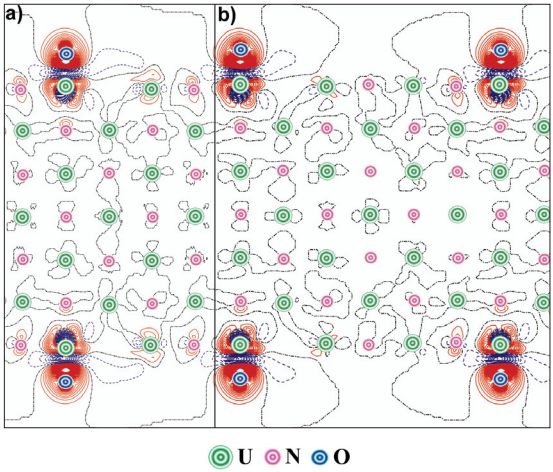

9.2. attēls. 2D šķērsgriezums elektronisko lādiņu blīvuma pārdalījumam $\Delta\rho(r)$ O atomiem, adsorbētajiem virs U_{surf} atomiem virsmas N vakances tuvumā. Cita informācija ir aprakstīta 8.4. attēla parakstā

Tātad, no otras puses, mēs esam parādījuši zemas barjeras skābekļa adatoma iekļaušanas iespēju N vakancē no tuvākās adsorbcijas pozīcijas virs U_{surf} atoma.

9.2. Skābekļa iekļaušana virsmas vakancēs

9.2.1. Modelis un teorētiskais pamatojums

Viens no UN iespējamiem oksidācijas ceļiem ir oksinitrīdu veidošana tuvu UN virsmai [18]. Tādēļ ir ļoti svarīgi aprakstīt skābekļa mijiedarbību ar atsevišķām vakancēm. Kā zināms no literatūras, līdz šim liela uzmanība tika pievērsta primāro defektu (vakances un iekļaušanas piemaisījumi) statiskajām un dinamiskajām īpašībām UN tilpumā [34], tie ietekmē degvielas kvalitāti izmantošanas un pārstrādes laikā. Atsevišķi no tukšo vakanču uzvedības tika apskatīta arī O atomu iekļaušana UN tilpuma vakancēs. Tika konstatēts, ka skābekļa atomu iekļaušana tilpuma N vakancēs ir enerģētiski labvēlīgāka, salīdzinot ar starpmezglu stāvokļiem [82]. Tomēr šķīdināšanas enerģijas rāda pretēju efektu. Lai iegūtu vairāk informācijas par nevēlamo UN oksidēšanās mehānismu, šajā apakšnodaļā

un atsaucē [P5] uzmanība tika pievērsta skābekļa piemaisījumu iekļaušanai N un U vakancēs uz UN(001) virsmas.

Mūsu aprēķini UN virsmai tika veikti, izmantojot superšūnas ar 2 × 2 un 3 × 3 virsmas translācijas vektoru garumiem. N un U vakances, kuras aizņem skābeklis, tika novietotas 2D plātnes virsmās, zemvirsmās un centrālajā slānī. Sakarā ar spoguļslāņa klātbūtni simetriskajā plātnē mēs izmantojām defektu divpusējo simetrisko izvietojumu, izņemot defektu centrālajā plaknē (spoguļplaknē), tādējādi samazinot nepieciešamo skaitļošanas resursu daudzumu. Spina magnētiskais moments tika relaksēts visos aprēķinos. Aprēķini tika veikti no sākumstāvokļa ar FM spinu sakārtojumu urāna apakšrežģī.

9.2.2. Skābekļa iekļaušanas un šķīdināšanas enerģija

Enerģijas bilanci O atoma iekļaušanai vakancē var raksturot ar iekļaušanas enerģiju E_I, kuru ieviesa Graims un Katlovs *(Grimes and Catlow)* [83] čaulu modelī UO_2 kodolšķelšanās produktu aprēķiniem. O atomam, iekļautam N un U vakancēs, centrālajā atomu slānī

$$E_I = E^{\mathrm{UN(O\_}inc\mathrm{)}} - E^{\mathrm{UN(N/U\_vac)}} - E^O \qquad (9.2.1)$$

un N un U vakancēs virsmas vai zemvirsmas slānī

$$E_I = \frac{1}{2}(E^{\mathrm{UN(O\_}inc\mathrm{)}} - E^{\mathrm{UN(N/U\_vac)}} - 2E^O). \qquad (9.2.1b)$$

Šeit $E^{\mathrm{UN(O\_}inc\mathrm{)}}$ ir pilnā enerģija superšūnai, kas satur O atomu N vai U vakancē ($E^{\mathrm{UN(O\_}inc\mathrm{)}} < 0$), $E^{\mathrm{UN(N/U\_vac)}}$ ir enerģija superšūnai ar neaizņemtajām (tukšām) vakancēm, un E^O ir puse no izolētas O_2 molekulas tripleta stāvokļa pilnās enerģijas. To nosaka skābekļa ķīmiskais potenciāls pie 0 K. Šeit E_I vērtība raksturo enerģijas bilanci skābekļa iekļaušanai eksistējošās vakancēs, kur negatīvā enerģija norāda uz izdevīgu iekļaušanas procesu.

Lai ievērotu kopējo enerģijas bilanci, tajā skaitā vakances veidošanās enerģiju E_{form} bezdefektu plātnē, tika definēta šķīdināšanas enerģija [83]:

$$E_S = E_I + E_{form}, \qquad (9.2.2)$$

kur E_{form} ir N vai U vakances veidošanās enerģija plātnē, kas aprēķināta, izmantojot vienādojumu 7.1.1.a vai 7.1.1.b.

Ir vērts pieminēt, ka standarta O pseidopotenciāla izmantošana mūsu *VASP* aprēķinos dod O_2 molekulas labu saites garumu 1.23 Å, tomēr ievērojami pārvērtē saites enerģiju (6.79 eV pret eksperimentālo vērtību 5.12 eV). Zinātniskajā literatūrā tika piedāvātas dažas korekcijas, kā novērst šo nopietno DFT trūkumu [84, 85]. Tādējādi defektu aprēķinātās veidošanās un šķīdināšanas enerģijas var koriģēt par ~ 1 eV (šīs korekcijas ietekme tiek apskatīta turpmāk).

Aprēķinot O adatoma iekļaušanu N vakancē uz UN(001) virsmas, tika konstatēts, ka tā ir enerģētiski izdevīga, jo gan E_I, gan E_S vērtības ir strikti negatīvas (9.1. tab.). Tas sekmē N vakances rašanos un O atoma adsorbciju no gaisa. E_I samazinās par ~ 0.4 eV (kļūst vairāk negatīva) plātnes iekšienē, salīdzinot ar ārējo slāni, savukārt E_S kļūst mazāks N vakancei virsmas slānī. Turpretī aprēķinātās E_I vērtības U vakancēm virsmās un centrālajā slānī ir tuvas nullei. Zemvirsmas slāni raksturo E_I vērtība, kas ir par ~ 1 eV mazāka, salīdzinot ar virsmas un centrālo slāni. Mūsu rezultāti liecina par oksinitrīdu veidošanās svarīgumu. Tomēr E_S ir pozitīva un pieaug O atomiem, iekļautiem U vakancē plāksnes centrālajā slānī. Enerģijas 9.1. tabulā neietver korekcijas, kas tika apspriestas iepriekš O atomiem. Tomēr šādas korekcijas var radīt E_I (vai E_S) palielināšanos par ~ 1 eV un rezultātā dot vairāk pozitīvas E_I vērtības U vakancei. 9.1. tabula arī norāda, ka skābekļa atoma šķīdināšana ir enerģētiski labvēlīgāka virsējos slāņos, nevis plātnes iekšpusē. Superšūnas izmēram palielinoties (3 × 3 paplašinājums 9.1. tabulā), gan E_I, gan E_S vērtības samazinās, savukārt plātnes biezuma ietekme nav tik izteikta. Tomēr izrādās, ka U vakances ir daudz jutīgākas pret superšūnas izmēru, tas ir saistīts ar nevēlamo mijiedarbību starp periodiski atkārtotajiem defektiem. Šajā gadījumā E_I un E_S vērtības var samazināties vidēji par 0.15 eV.

9.1. tabula. Iekļaušanās (E_I) un šķīdināšanas (E_S) enerģija (eV), vidējais U atomu magnētiskais spins μ_{av}^{U} (μ_B), kā arī efektīvais lādiņš skābekļa atomiem (e^-) O iekļaušanai U(001) virsmā. Atskaites stāvokļi iekļaušanas un šķīdināšanas enerģijas aprēķiniem tika izvēlēti kā ķīmiskais potenciāls O, N un U atomiem, kas aprēķināts attiecīgi O_2, N_2 molekulām un α-U fāzei

Slānis	Superšūnas izmērs	Atomāro plakņu skaits plātnē	N vakance				U vakance			
			E_I (eV)	E_S (eV)	μ_{av}^{U} (μ_B)	q_{eff}(e^-)	E_I (eV)	E_S (eV)	μ_{av}^{U} (μ_B)	q_{eff}(e^-)
Virsmas	2 × 2	5	-6.173	-2.473	1.65	-1.36	-0.339	1.120	1.16	-0.98
		7	-6.181	-2.476	1.49	-1.36	-0.855	0.583	1.36	-1.03
		9	-6.188	-2.479	1.41	-1.36	-0.943	0.493	1.31	-1.06
	3 × 3	5	-6.122	-2.481	1.60	-1.37	-0.683	0.654	1.48	-1.05
		7	-6.126	-2.480	1.46	-1.36	-1.073	0.230	1.38	-1.08
Zem-virsmas	2 × 2	5	-6.314	-2.068	1.64	-1.42	-1.856	1.284	1.66	-1.10
		7	-6.419	-2.090	1.49	-1.40	-1.823	1.297	1.45	-1.10
		9	-6.417	-2.091	1.41	-1.40	-1.823	1.271	1.38	-1.10
	3 × 3	7	-6.428	-2.093	1.46	-1.39	-2.012	1.000	1.43	-1.10
Centrālais (spoguļ-slānis)	2 × 2	7	-6.611	-2.180	1.47	-1.42	0.736	3.923	1.44	-0.89
		9	-6.608	-2.192	1.39	-1.38	0.669	3.838	1.38	-0.90
	3 × 3	7	-6.599	-2.182	1.45	-1.42	0.317	3.378	1.47	-0.94

9.2.3. Spinu blīvums un lādiņi pēc Badera

9.1. tabula ļauj mums analizēt arī U atomu vidējo spina blīvumu (μ_{av}^{U}) dažādas morfoloģijas defektīvajām UN(001) virsmām, kurās ir iekļauti O atomi. Analoģiski UN defektīvām virsmām ar tukšām vakancēm [P4] μ_{av}^{U} samazinās plātnēm ar lielāku slāņu daudzumu abiem vakanču veidiem (izņemot O atomu iekļaušanu U vakancē, kas atrodas virsmas slānī). Var arī redzēt, ka virsmas slānī μ_{av}^{U} ir lielāki N vakancei, salīdzinot ar U vakanci. μ_{av}^{U} zemvirsmās un centrālajā slānī ir līdzīgi abu vakanču veidiem. Interesanti, ka efektīvais lādiņš q_{eff} uz O atomiem ir arī augstāks N vakancēm plātnes iekšienē. Savukārt U vakancēm q_{eff} samazinās gandrīz par 0.3 *e*. Tas pats efekts ir novērots arī N kaimiņatomiem: efektīvais lādiņš ir mazāks, salīdzinot ar gadījumu, kad O atoms aizņem U vakanci. Vispārīga aina liecina par to, ka starp dažādiem saites veidiem sistēmā prevalē kovalentā saite.

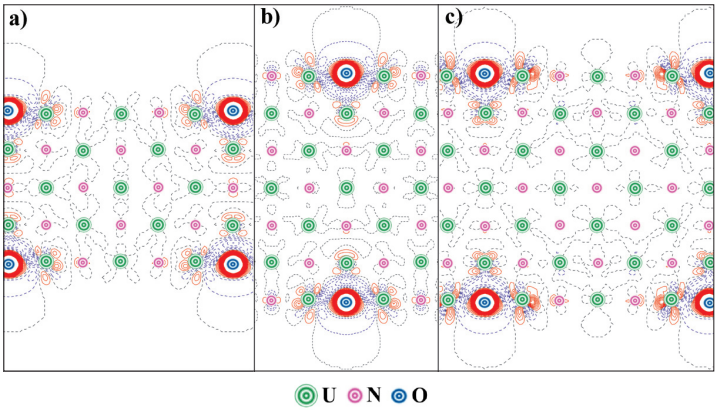

9.3. attēls. 2D šķēlums elektronu blīvuma pārdalījumam Δρ(r) apkārt O atomiem, iekļautiem uz virsmas N vakancēm 5-slāņu un 7-slāņu UN(001) plātnē ar 2 × 2 un 3 × 3 superšūnu paplašinājumiem. Δρ(r) ir definēta kā O saturošās virsmas kopīgais elektroniskais blīvums mīnus blīvums O atomiem attiecīgajās iekļaušanas pozīcijās un blīvums virsmai, kas satur N vakances tajās pašās pozīcijās. a) 5-slāņu plātne ar 3 × 3 skābekļa iekļauto atomu periodiskumu, b) 7-slāņu plātne ar 2 × 2 skābekļa iekļauto atomu periodiskumu, a) Δ 7-slāņu plātne ar 3 × 3 skābekļa iekļauto atomu periodiskumu. Pārējās detaļas ir aprakstītas 8.4. attēla parakstā

9.2.4. Lādiņu pārdalījuma analīze: virsmas šūnas ierobežota izmēra efekti un superšūnas izmēra izvēle

Lielā defektu koncentrācija (25% superšūnas 2 × 2 paplašināšanai 9.1. tabulā) izraisa dažus ierobežota izmēra efektus, kurus var ilustrēt, izmantojot 2D starpību elektroniskā blīvuma pārdalījumu $\Delta\rho(\mathbf{r})$. Šie attēli ir parādīti O atomiem, kas iekļauti N vakancēs virsmas (9.3. att.) un centrālajā slānī (9.4. att.). Divu simetriski novietotu defektu klātbūtne 5-slāņu plātnes iekšā izraisa to savstarpējo mijiedarbību (tas ir redzams

lādiņu pārdalīšanā pāri plātnei 9.3.a att.). Plātnes biezuma palielināšana samazina šo efektu (9.3.c att.). Ja superšūnas izmērs samazinās (2 × 2 paplašinājums 9.3.b att.), ir novērojams papildu elektronu blīvums starp defektiem paralēli virsmas slānim. Līdzīgs efekts ir arī novērots elektroniska blīvuma pārdalījumam ap defektiem spoguļplaknēs (9.4. att.). Superšūnas lieluma ietekme šajā gadījumā ir līdzīga efektam, kas apspriests N vakances gadījumā. Tomēr U virsmas vakances gadījumā, salīdzinot ar N-vakanci, lielāka elektroniska blīvuma koncentrācija ir novērojama starp O atomu un N kaimiņatomiem zemvirsmas slānī. Tādējādi šajā gadījumā plātnes biezuma ietekmi arī nedrīkst novērtēt par zemu.

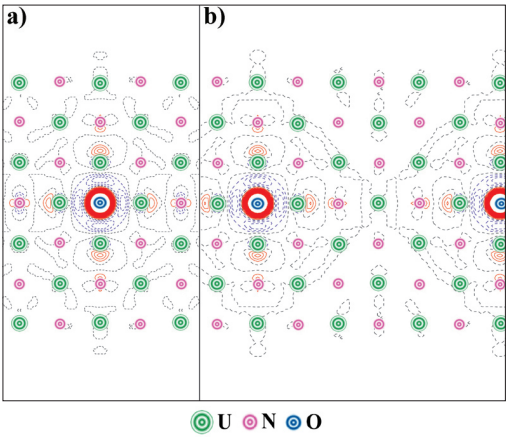

9.4. attēls. 2D šķērsgriezums $\Delta\rho$(r) ap O atomiem, kas iekļauti N vakancēs 7-slāņa UN(001) centrālajā slānī ar (a) 2 × 2 un (b) 3 × 3 superšūnas paplašinājumiem. Cita informācija ir dota 9.3. attēla parakstā

9.2.5. Iekļautā skābekļa elektronisko stāvokļu blīvums (DOS)

9.5. attēlā kopējais un projicētais stāvokļu blīvums ir parādīts UN(001) 7-slāņu virsmai ar O atomiem, iekļautajiem N vakancē. Visos aprēķinos sistēma joprojām saglabā vadīšanas īpašības ar U(5*f*) stāvokļu ievērojamu ieguldījumu uz Fermī līmeņa, līdzīgi ideālas UN(001) plātnes aprēķiniem (6.2. att.). Specifisko O(2*p*) joslu parādīšanās ar enerģijas pīķi pie -6 eV ir novērota. Salīdzinot DOS O atomiem, iekļautajiem N vakancē, novērojama O(2*p*) stāvokļu nobīde (par aptuveni -1.0 eV), un tas ļauj atšķirt virsmas slāni no iekšējiem slāņiem.

Ja vakance atrodas virsmas slānī, šie stāvokļi ievērojami pārklājas ar N(*2p*) joslu, daļēji sajaucoties ar U(5*f*) stāvokļiem (līdzīgie efekti parādās O_2 molekulai virs virsmas U atomiem [P2]). Turpretī O(*2p*) josla joprojām ir gandrīz izolēta no citām joslām (analoģiski ar O atomiem, iekļautajiem N vakancē UN tilpumā [82]). N(*2p*) stāvokļu pozīcija ir nejutīga pret O atomu klātbūtni un atrodas enerģijas diapazonā no -6 līdz -1 eV.

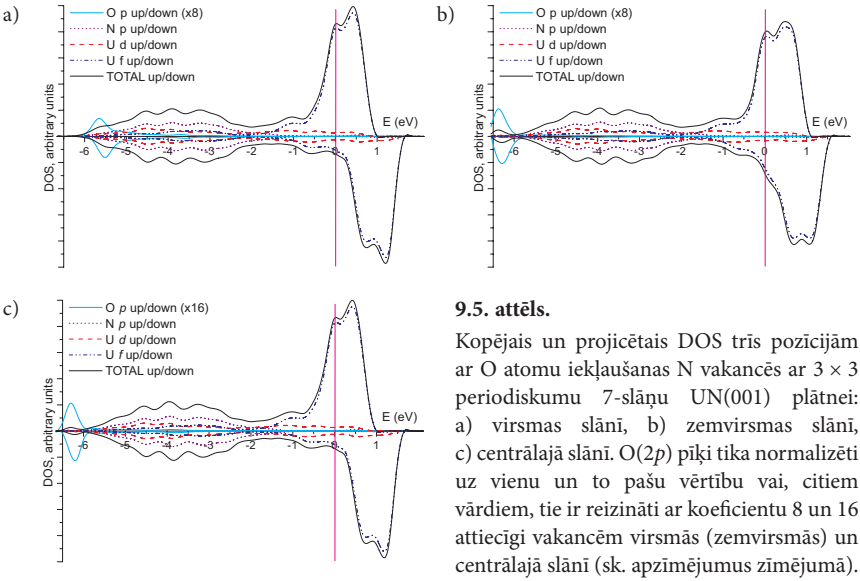

9.5. attēls.

Kopējais un projicētais DOS trīs pozīcijām ar O atomu iekļaušanas N vakancēs ar 3 × 3 periodiskumu 7-slāņu UN(001) plātnei: a) virsmas slānī, b) zemvirsmas slānī, c) centrālajā slānī. O(2*p*) pīķi tika normalizēti uz vienu un to pašu vērtību vai, citiem vārdiem, tie ir reizināti ar koeficientu 8 un 16 attiecīgi vakancēm virsmās (zemvirsmās) un centrālajā slānī (sk. apzīmējumus zīmējumā). Atsevišķo enerģijas līmeņu konvolūcija tika veikta, izmantojot Gausa funkcijas ar pusplatumu, vienādu ar 0.2 eV

9.2.6. Salīdzināšana skābekļa iekļaušanai N vakancē uz UN (001) un (110) virsmas

Līdzīgi kā ideālai UN virsmai, vakanču veidošanai un skābekļa atomu adsorbcijai, interesanti ir salīdzināt iekļaušanas (E_I) un šķīdināšanas (E_S) enerģijas divām virsmām: UN (001) un (110) virsmai (9.6. att.).

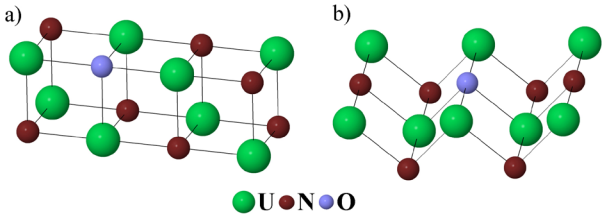

9.6. attēls. 2-slāņu modeļi skābekļa iekļaušanai N vakancē uz (001) (a) un (100) (b) virsmas

9.2. tabula salīdzina šīs enerģijas kā funkciju no plātnes biezuma un superšūnas izmēra. Var redzēt, ka UN(110) virsmai ir raksturīgas vairākas negatīvas šķīdināšanas

enerģijas un enerģiju starpība, kas ir vienāda ar ~ 0.3 eV. No otras puses, iekļaušanas enerģijas ieviešana maina šo tendenci, radot vairāk negatīvas vērtības (001) virsmai. Šādi rezultāti norāda uz E_I aprēķinu svarīgumu, jo mūsu virsma var atrasties arī ekstremālos apstākļos, piemēram, augstās temperatūrās. Tomēr mēs skaidri redzam līdzīgas tendences abām virsmām (9.2. tab.).

9.2. tabula. Iekļaušanas (E_I) un šķīdināšanas (E_S) enerģija (eV), vidējās U atomu spinu magnētiskais μ_{av}^{U} (μ_B) un efektīvais lādiņš O atomiem, iekļautiem uz UN (001) un (110) virsmas. Atskaites stāvokļi iekļaušanas un šķīdināšanas enerģijas aprēķiniem tika izvēlēti kā O un N atomu ķīmiskais potenciāls, kas aprēķināts O_2 un N_2 molekulām (2 × 2 un 3 × 3 superšūnas)

Slāņu skaits	E_I **(eV)**	E_S **(eV)**	μ_{av}^{U} (μ_B)	$q_{eff}(e^-)$	E_I **(eV)**	E_S **(eV)**	μ_{av}^{U} (μ_B)	$q_{eff}(e^-)$
	(001) virsma				(110) virsma			
5, 2 × 2	-6.173	-2.473	1.647	-1.36	-5.853	-2.778	1.736	-1.27
7, 2 × 2	-6.181	-2.476	1.495	-1.36	-5.822	-2.794	1.516	-1.29
9, 2 × 2	-6.186	-2.479	1.412	-1.36	-5.820	-2.784	1.472	-1.29
11, 2 × 2	-6.195	-2.483	1.365	-1.35	-5.817	-2.791	1.416	-1.29
7, 3 × 3	-6.126	-2.480	1.463	-1.36	-5.748	-2.783	1.471	-1.28

9.2.7. Skābekļa iekļaušanas modelēšana: kopsavilkums

Ievērojama enerģētiska priekšroka O atoma iekļaušanai N vakancē, salīdzinot ar U vakanci, norāda uz to, ka novēroto UN oksidāciju nosaka galvenokārt mijiedarbība starp skābekļa atomiem ar N vakancēm virsmas uz zemvirsmas slāņos.

Oksinitrīdu veidošanās, kas ir izraisīta ar skābekļa atomu difūziju starp slāņiem [18], ar tālāko skābekļa satveri slāpekļa vakancēs UN(001) virsmas tuvumā ir sagaidāma, tādējādi izraisot stabilizēšanu un veidojoties ķīmiskām saitēm ar tuvākajiem urāna atomiem. Elektronisko lādiņu sadalījums pierāda perturbācijas blīvuma, kuru izraisa iekļautais O atoms, vietējo raksturu. Stāvokļu blīvumu analīze parāda gan pārklāšanos O(2*p*) stāvokļiem ar N(2*p*) stāvokļiem sākotnējās oksidēšanās posmos (virsmas iekļaušana), gan O(2*p*) stāvokļu atdalīšanu no citiem stāvokļiem, ja skābekļa atomi ir novietoti dziļāk (zemvirsmas penetrācija). Šos analīzes rezultātus var izmantot, interpretējot urāna oksinitrīdu eksperimentālos ultravioletos fotoelektronu spektrus [18].

10. Kopsavilkums

DFT PW metode tika izmantota, lai analizētu galvenās UN tilpuma īpašības, punktu defektu uzvedību uz UN virsmas, kā arī skābekļa mijiedarbību ar UN virsmu. Izmantojot pilnu ģeometrijas relaksāciju, mēs ieguvām rezultātus UN bezdefektu tilpumam un virsmai, slāpekļa un urāna vakancēm, atomārā un molekulārā skābekļa adsorbcijai bezdefektu virsmā, kā arī skābekļa difūzijai uz UN(001) virsmas. Mēs esam novērtējuši virsmas superšūnas izmēru un plātņu biezumu, kas ļauj mums iegūt precīzus rezultātus UN virsmai. Tika konstatēts, ka 7-slāņu plātnes ar 3×3 virsmu paplašinājuma vektoru izmantošana ļauj iegūt rezultātus, kuri ir kvalitatīvi tuvi atsevišķa defekta modelim. Savukārt mazākās 2×2 superšūnās un 5-slāņu plātnēs tika konstatēta ievērojama sānu mijiedarbība starp defektiem. Mēs arī salīdzinājām UN (001) un (110) virsmām enerģijas (*i*) slāpekļa vakances veidošanai, (*ii*) skābekļa atoma adsorbcijai virs U vai N virsmas atomiem, kā arī (*iii*) O atoma iekļaušanai N vakancē.

Neskatoties uz iepriekš minēto, daži jautājumi par UN virsmu joprojām ir atvērti. U vakanču veidošanās enerģiju novērtējumi prasa šo rezultātu papildu verifikāciju, izmantojot citas teorētiskās metodes, kā arī turpmāku attīstību urāna atoma pseidopotenciāliem. Lai iegūtu precīzākus rezultātus skābekļa difūzijai gar UN(001) virsmu, ir jāpiemēro virzītā elastības metode *(Nudged Elastic Band method)* [49]. Šī metode ļauj iegūt reālistiskas atoma migrācijas trajektorijas. Šīs pieejas realizācija ievērojami uzlabota jaunākajā *VASP-5* datora kodu versijā, salīdzinot ar VASP-4 versiju, kura tika izmantota aprēķiniem šajā promocijas darbā. Tas ļaus mums iegūt pietiekamus rezultātus adekvātā procesorlaikā. UN virsmas jaunie eksperimentālie mērījumi (piemēram, EXAFS mērījumi, kuri ļauj apskatīt atomāro apkārtni atsevišķiem atomiem, vai UPS spektru mērījumi oksinitrīdu līdzīgu struktūru identificēšanai) ir nozīmīgi UN oksidēšanās procesu daudzpusīgas ainas izveidošanai. Tas arī ir svarīgi, lai izstrādātu UN paraugu drošu aizsardzību pret agresīvo skābekļa ietekmi.

Kopumā promocijas darbā aprakstītie rezultāti ir nozīmīgs solis aktinīdu savienojumu modelēšanā un veicina UN virsmas oksidēšanās procesu labāku izpratni.

11. Galvenās tēzes

- Rezultāti, kas iegūti, izmantojot divas būtiski atšķirīgas DFT skaitļošanas metodes un balstoties uz plakano viļņu (PW) un atomu orbitāļu lineārās kombinācijas (LCAO) formālismiem, sakrīt kvalitatīvi labi un kalpo arī iegūto rezultātu verifikācijai.
- U un N vakanču veidošanās enerģijas skaidri norāda uz vakanču tendenci akumulēties uz virsmas un, iespējams, graudu robežām.
- Iegūtie rezultāti par O atomu un O_2 molekulu mijiedarbību ar UN virsmām norāda uz stipru hemisorbciju, tipisku metāliskajiem adsorbentiem. Uz perfektas UN(001) virsmas adsorbēto skābekļa molekulu spontānās disociācijas iespēja ir parādīta analoģiski O_2 disociācijai uz metāla virsmām. Pēc molekulārās disociācijas O adatomi veido spēcīgas ķīmiskās saites ar U_{surf} atomiem, tādējādi veidojot viencentru virsmas kompleksu. Savukārt O adatoms virs N_{surf} atomiem veido daudzcentru kompleksu, iesaistot četrus blakus esošos U_{surf} atomus.
- Ir parādīts augstais O_{ads} kustīgums gar virsmu, pateicoties relatīvi zemai migrācijas barjerai (< 0.5 eV). Tika parādīta skābekļa adatoma zemā barjera iekļaušanai eksistējošā N vakancē no tuvākās adsorbcijas pozīcijas virs U_{surf} atoma, kā arī parādīta UN virsmas, kurā iekļauti skābekļa atomi, enerģētiskā stabilitāte.
- Skābeklim, kas ir novietots uz UN(001) virsmas, ir paredzētas šādas reaktivitātes stadijas: *(i)* molekulārā skābekļa hemisorbcija; (*ii*) spontāna O_2 molekulas ķīmiskās saites sabrukšana pēc adsorbcijas uz UN(001) virsmas; (*iii*) divu jaunizveidoto O atomu izvietošana virs virsmas U atomiem; (*iv*) lielu O_{ads} atomu kustīgums gar virsmu; *(v)* skābekļa adatomu zembarjeras iekļaušana no pozīcijas virs U_{surf} atoma uz blakus novietoto N vakanci; *(vi)* O_{ads} atoma stabilizācija N_{surf} vakances iekšienē; (*vii*) *O* atomu iekļaušana zemvirsmas vakancēs iekšējas difūzijas dēļ. Tas skaidro eksperimentāli novēroto UN ātro oksidāciju gaisā.

12. Literatūra

12.1. Autora publicētie darbi par promocijas tēmu

[P1] R.A. Evarestov, A.V. Bandura, M.V. Losev, E.A. Kotomin, Yu.F. Zhukovskii, and D. Bocharov, A first principles DFT study in UN bulk and (001) surface: Comparative LCAO and PW calculations. - J. Comput. Chem., 2008, **29**, p. 2079-2087.

[P2] Yu.F. Zhukovskii, D. Bocharov, E.A. Kotomin, R.A. Evarestov, and A.V. Bandura, First principles calculations of oxygen adsorption on the UN(001) surface. - Surf. Sci., 2009, **603**, p. 50-53.

[P3] Yu.F. Zhukovskii, D. Bocharov, and E.A. Kotomin, Chemisorption of a molecular oxygen on the UN (001) surface: *ab initio* calculations. - J. Nucl. Mater., 2009, **393**, p. 504-507.

[P4] D. Bocharov, D. Gryaznov, Yu.F. Zhukovskii, and E.A. Kotomin, DFT calculations of point defects on UN(001) surface. - Surf. Sci., 2011, **605**, p. 396-400.

[P5] D. Bocharov, D. Gryaznov, Yu.F. Zhukovskii, E.A. Kotomin, *Ab initio* modeling of oxygen impurity atom incorporation into uranium mononitride surface and subsurface vacancies. - J. Nucl. Mater., 2011, **416**, p. 200-204.

12.2. Citi autora publicētie darbi

[O1] D. Bocharov, A. Kuzmin, J. Purans, and Yu.F. Zhukovskii, Quantum chemistry studies of the O *K*-edge X-ray absorption in WO_3 and AWO_3. - SPIE Proceedings, 2008, 71420T (p. 1-9).

[O2] N. Zaporina, O. Doynikova, A. Krumina, D. Bocharov, and J. Grabis, Methods of electron microdiffraction and X-ray analysis in structure study of nanodisperse partially stabilized ZrO_2 powders. - J. Surf. Investigation: X-ray, Synchrotron and Neutron Techniques, 2009, **3**, p. 464-467.

[O3] N. Zaporina, J. Grabis, V.N. Timofeev, and D. Bocharov, Microstructural investigations of multicomponent SiC/Si_3N_4-Al_2O_3-Y_2O_3 nanopowders. - Latv. J. Chem., 2010, No 1, p. 33-38.

12.3. Literatūras saraksts

[1] Hj. Matzke, Science of Advanced LMFBR Fuel, North Holland, Amsterdam, 1986.

[2] The Nuclear Fuel Cycle. P.D. Wilson (Eds.), University Press, Oxford, 1996.

[3] H. Wiame, M. Centeno, S. Pacard, P. Bastian, and P. Grange, Thermal oxidation under oxygen of zirconium nitride studied by XPS, DRIFTS, TG-MS. - J. Eur. Ceram. Soc., 1998, **18**, p. 1293-1299.

[4] M. Walter, Oxidation of inert matrices, JRC-ITU-TN-2005/35 (zinātniskā atskaite).

[5] N. Curry, An investigation of the magnetic structure of uranium nitride by neutron diffraction. - Proc. Phys. Soc., 1965, **86**, p. 1193-1198.

[6] T. Muromura and H. Tagawa, Lattice parameter of uranium mononitride. - J. Nucl. Mater., 1979, **79**, p. 264-266.

[7] P.E. Evans and T.J. Davies, Uranium nitrides. - J. Nucl. Mater., 1963, **10**, p. 43-55.

[8] N.-T.H. Kim-Ngan, A.G. Balogh, L. Havela, and T. Gouder, Ion beam mixing in uranium nitride thin films studied by Rutherford Backscattering Spectroscopy. - Nucl. Instr. Meth. Phys. Res. B, 2010, **268**, p. 1875-1879.

[9] G.W. Chinthaka Silva, Ch.B. Yeamans, L. Ma, G.S. Cerefice, K.R. Czerwinski, and A.P. Sattelberger, Microscopic characterization of uranium nitrides synthesized by oxidative ammonolysis of uranium tetrafluoride. - Chem. Mat., 2008, **20**, p. 3076-3084.

[10] G.C. Allen and N.R. Holmes, The passivation of uranium metal surfaces by nitrogen bombardment - the formation of uranium nitride. - J. Nucl. Mater., 1988, **152**, p. 187-193.

[11] P.R. Norton, R.L. Tapping, D.K. Creber, and W.J.L. Buyers, Nature of the 5*f* electrons in uranium nitride: A photoelectron spectroscopic study of UN, U, UO_2, ThN, and Th. - Phys. Rev. B, 1980, **21**, p. 2572-2577.

[12] T. Ito, H. Kumigashira, S. Souma, T. Tahakashi, and T. Suzuki, High-resolution angle-resolved photoemission study of UN and USb; Dual character of 5*f* electrons. - J. Magn. Magn. Mater., 2001, **226-230**, p. 68-69.

[13] M. Marutzky, U. Barkow, J. Schoenes, and R. Troć, Optical and magneto-optical properties of single crystalline uranium nitride. - J. Magn. Magn. Mater., 2006, **299**, p. 225-230.

[14] B. Reihl, G. Hollinger, and F.J. Himpsel, Itinerant 5*f*-electron antiferromagnetism in uranium nitride: A temperature-dependent angle-resolved photoemission study. - Phys. Rev. B, 1983, **28**, p. 1490-1494.

[15] M. Paljević and Z. Despotović, Oxidation of uranium mononitride. - J. Nucl. Mater., 1975, **57**, p. 253-257.

[16] Y. Arai, M. Morihira, and T. Ohmichi, The effect of oxygen impurity on the characteristics of uranium and uranium-plutonium mixed nitride fuels. - J. Nucl. Mater., 1993, **202**, p. 70-78.

[17] L. Black, F. Miserque, T. Gouder, L. Havela, J. Rebizant, and F. Wastin, Preparation and photoelectron spectroscopy study of UN_x thin films. - J. Alloys Comp., 2001, **315**, p. 36-41.

[18] M. Eckle, and T. Gouder, Photoemission study of UN_xO_y and UC_xO_y in thin films. - J. Alloys Comp., 2004, **374**, p. 261-264.

[19] S. Sunder and N.H. Miller, XPS and XRD studies of corrosion of uranium nitride by water. - J. Alloys Comp., 1998, **271-273**, p. 568-572.

[20] D. Sedmidubsky, R.J.M. Konings, and P. Novak, Calculation of enthalpies of formation of actinide nitrides. - J. Nucl. Mater., 2005, **344**, p. 40-44.

[21] P. Weinberger, C.P. Mallett, R. Podloucky, and A. Neckel, The electronic structure of HfN, TaN and UN. - J. Phys. C: Solid St. Phys., **13**, 1980, p. 173-187.

[22] M.S. Brooks and D. Glötzel, Some aspects of the electronic structure of uranium pnictides and chalcogenides. - Physica B, 1980, **102**, p. 51-58.

[23] M.S. Brooks, Electronic structure of NaCl-type compounds of the light actinides. I. UN, UC, and UO. - J. Phys. F: Met. Phys., 1984, **14**, 639-652.

[24] G.K. Johnson and E.H.P. Cordfunke, The enthalpies of formation of uranium mononitride and α- and β-uranium sesquinitride by fluorine bomb calorimetry. - J. Chem. Thermodyn., 1981, **13**, p. 273-282.

[25] R. Atta-Fynn and A.K. Ray, Density functional study of the actinide nitrides. - Phys. Rev. B, 2007, **76**, 115101 (p. 1-12).

[26] P.F. Weck, E. Kim, N. Balakrishnan, F. Poineau, C.B. Yeamans, and K.R. Czerwinski, First-principles study of single-crystal uranium mono- and dinitride. - Chem. Phys. Lett., 2007, **443**, p. 82-86.

[27] Y. Lu, B.-T. Wang, R.-W. Li, H. Shi, and P. Zhang, Structural, electronic, and thermodynamic properties of UN: Systematic density functional calculations. - J. Nucl. Mater., 2010, **406,** p. 218-222.

[28] B. Dorado, B. Amadon, M. Freyss, and M. Bertolus, DFT+*U* calculations of the ground state and metastable states of uranium dioxide. - Phys. Rev. B, 2010, **79**, 235125 (p. 1-8).

[29] B. Dorado, G. Jomard, M. Freyss, and M. Bertolus, Stability of oxygen point defects in UO_2 by first-principles DFT+*U* calculations: Occupation matrix control and Jahn-Teller distortion. - Phys. Rev. B, 2010, **82**, 035114 (p. 1-11).

[30] D. Gryaznov, E. Heifets and E.A. Kotomin, *Ab initio* DFT+*U* study of He atom incorporation into UO_2 crystals. - Phys. Chem. & Chem. Phys., 2009, **11**, p. 7241-7247

[31] D. Rafaja, L. Havela, R. Kuel, F. Wastin, E. Colineau, and T. Gouder, Real structure and magnetic properties of UN thin films. - 2005, **386,** p. 87-95.

[32] Z. Yongbin, M. Daqiao, Z. Zhenghe, and M. Meizhong, Pseudopotential plane-wave study of the uranium metals and uranium compounds. - Chin. J. Chem. Phys., 2005, **18**, p. 735-739.

[33] E.A. Kotomin, Yu.A. Mastrikov, Yu.F. Zhukovskii, P. Van Uffelen, and V.V. Rondinella, First-principles modelling of defects in advanced nuclear fuels. - Phys. Stat. Sol. (c), 2007, **4**, p. 1193-1196.

[34] E.A. Kotomin, R.W. Grimes, Yu.A. Mastrikov, and N.J. Ashley, Atomic scale DFT simulations of point defects in uranium nitride. - J. Phys.: Cond. Mat, 2007, **19**, 106208 (p. 1-9).

[35] E.A. Kotomin, D. Gryaznov, R.W. Grimes, D. Parfitt, Yu.F. Zhukovskii, Yu.A. Mastrikov, P. Van Uffelen, V.V. Rondinella, and R.J.M. Konings, First-principles modelling of radiation defects in advanced nuclear fuels. - Nucl. Instr. Meth. Phys. Res. B, 2008, **266**, p. 2671-2675.

[36] R.A. Evarestov, M.V. Losev, A.I. Panin, N.S. Mosyagin, and A.V. Titov, Electronic structure of crystalline uranium nitride: LCAO DFT calculations. - Phys. Stat. Solidi (b), 2008, **245**, p. 114 -122.

[37] R.A. Evarestov, A.I. Panin, A.V. Bandura, and M.V. Losev, Electronic structure of crystalline uranium nitrides UN, U_2N_3 and UN_2: LCAO calculations with the basis set optimization. - J. Phys.: Conf. Ser., 2008, **117**, 012015 (p. 1-8).

[38] K.N. Kudin, G. E. Scuseria, and R.L. Martin, Hybrid Density-Functional Theory and the insulating gap of UO_2. - Phys. Rev. Lett. 2002, **89**, 266402 (p. 1-4).

[39] S.L. Dudarev, G.A. Botton, S.Y. Savrasov, C.J. Humphreys, and A.P. Sutton, Electron-energy-loss spectra and the structural stability of nickel oxide: An LSDA+*U* study. - Phys. Rev. B, 1998, **57**, p. 1505-1509.

[40] F. Gupta, G. Brillant, and A. Pasturel, Correlation effects and energetics of point defects in uranium dioxide: a first principle investigation. - Phil. Mag., 2007, **87**, p. 2561-2569.

[41] M. Freyss, First-principles study of uranium carbide: Accommodation of point defects and of helium, xenon, and oxygen impurities. - Phys. Rev. B, 2010, **81**, 014101 (p. 1-16).

[42] H. Shibata, T. Tsuru, M. Hirata, and Y. Kaji, First principles study on elastic properties and phase transition of NpN - J. Nucl. Mater., 2010, **401**, p. 113-117.

[43] C.D. Taylor, Evaluation of first-principles techniques for obtaining materials parameters of α-uranium and the (001) α-uranium surface. - Phys. Rev. B, 2008, **77**, 094119 (p. 1-9).

[44] P.E. Bloechl, Projector augmented-wave method. - Phys. Rev. B, 1994, **50**, p. 17953-17979.

[45] A.H.H. Tan, M. Abramowski, R.W. Grimes, and S. Owens, Surface defect configurations on the (100) dipolar surface of UO_2. - Phys. Rev. B, 2005, **72,** p. 035457 (p. 1-6).

[46] F.N. Skomurski, R.C. Ewing, A.L. Rohl, J.D. Gale, and U. Becker, Quantum mechanical *vs.* empirical potential modeling of uranium dioxide (UO_2) surfaces: (111), (110), and (100). - Amer. Mineral., 2006, **91,** p. 1761-1772.

[47] M.N. Huda and A.K. Ray, Electronic structures and bonding of oxygen on plutonium layers. - Eur. Phys. J. B, 2004, **40**, p. 337-346.

[48] R. Atta-Fynn and A. K. Ray, *Ab initio* full-potential fully relativistic study of atomic carbon, nitrogen, and oxygen chemisorption on the (111) surface of δ-Pu. - Phys. Rev. B, 2007, **75**, 195112 (p. 1-13).

[49] G. Kresse and J. Furthmüller, *VASP* the Guide, University of Vienna, 2009; *http://cms.mpi.univie.ac.at/vasp/*

[50] А.В. Бандура и Р.А. Эварестов, Неэмпирические расчеты кристаллов в атомном базисе. Изд-во С.-Петерб. ун-та, Санкт Петербург, 2004 (krievu valodā).

[51] R.A. Evarestov, Quantum Chemistry of Solids: The LCAO First Principles Treatment of Crystals. Springer Series in Solid State Science, Springer-Verlag, Berlin, 2007.

[52] J. Hafner, *Ab initio* simulations of materials using *VASP*: Density-Functional Theory and beyond. - J. Comput. Chem., 2008, **29**, p. 2044-2078.

[53] L.N. Kantorovich, Quantum Theory of the Solid State: an Introduction. Springer-Verlag, Berlin, 2004.

[54] J.P. Perdew, J.A. Chevary, S.H. Vosko, K.A. Jackson, M.R. Pederson, D.J. Singh, and C. Fiolhais, -Phys. Rev. B, 1992, **46**, p. 6671-6687.

[55] A. Unsöld, Beiträge zur Quantenmechanik des Atoms. - Ann. Phys., 1927, **82**, p. 355-393 (vācu valodā); *http://demonstrations.wolfram.com/UnsoeldsTheorem/*

[56] M. Krack, Pseudopotentials for H to Kr optimized for gradient-corrected exchange-correlation functionals. - Theor. Chem. Acc., 2005, **114**, p. 145-152.

[57] N.W. Ashcroft and N.D. Mermin, Solid State Physics. Saunders College Press, Philadelphia, 1976.

[58] G. Kresse and D. Joubert, From ultrasoft pseudopotentials to the projector augmented-wave method. - Phys. Rev. B, 1999, **59**, p. 1758-1775.

[59] H.J. Monkhorst and J.D. Pack, Special points for Brillouin-zone integrations. - Phys. Rev. B, 1976, **13**, p. 5188-5192.

[60] M. Methfessel and A.T. Paxton, High-precision sampling for Brillouin-zone integration in metals. - Phys. Rev. B, 1989, **40**, p. 3616-3621.

[61] G. Kresse and J. Furthmüller, Efficient iterative schemes for *ab initio* total-energy calculations using a plane-wave basis set. - Phys. Rev. B, 1996. **54**, p. 11169-11186.

[62] A. Stathopoulos and C.F. Fischer, A Davidson program for finding a few selected extreme eigenpairs of a large, sparse, real, symmetric matrix. - Comput. Phys. Comm., 1994, **79**, p. 268-290.

[63] R. Dovesi, V.R. Saunders, C. Roetti, R. Orlando, C.M. Zicovich-Wilson, F. Pascale, B. Civalleri, K. Doll, N.M. Harrison, I.J. Bush, Ph. D'Arco and M. Llunell, *CRYSTAL*2006 User's Manual, Università di Torino, Turin, 2006; *http://www.crystal.unito.it/*

[64] J.P. Perdew, K. Burke, and M. Ernzerhof, Generalized gradient approximation made simple. - Phys. Rev. Lett., 1996, **77**, p. 3865-3868.

[65] S. Piskunov, E. Heifets, R.I. Eglitis, and G. Borstel, Bulk properties of $SrTiO_3$, $BaTiO_3$ and $PbTiO_3$ perovskites: An *ab initio* HF/DFT study. - Comput. Mater. Sci., 2004, **29**, p. 165-178.

[66] M.J. Frisch, J.A. Pople, and J.S. Binkley, Self-consistent molecular orbital methods 25. Supplementary functions for Gaussian basis sets. - J. Chem. Phys., 1984, **80**, p. 3265-3269.

[67] W. Kuchle, M. Dolg, H. Stoll, and H. Preuss, Energy-adjusted pseudopotentials for the actinides. Parameter sets and test calculations for thorium and thorium monoxide. - J. Chem. Phys., 1994, **100**, p. 7535-7544.

[68] A.V. Titov and N.S. Mosyagin, Generalized relativistic effective core potential: Theoretical grounds. - Int. J. Quant. Chem., 1999, 71, p. 359-401.

[69] G. Gilat, General analytic method of zone integration for joint densities of states in metals. - Phys. Rev. B, 1982, **26**, p. 2243-2246.

[70] P.W. Tasker, The stability of ionic crystal surfaces. - J. Phys. C: Solid State Phys., 1979, **12**, p. 4977-4984.

[71] A. Subramanian, L.D. Marks, O. Warschkow, and D.E. Ellis, Direct observation of charge transfer at a MgO (111) surface. - Phys. Rev. Lett., 2004, **92**, 026101 (p. 1-4).

[72] J. Akella, S. Weir, J. M. Wills, and P. Söderlind, Structural stability in uranium. - J. Phys.: Condens. Matter, 1997, **9**, L549 (p. 1-7).

[73] C.G. Van de Walle and J. Neugebauer, First-principles calculations for defects and impurities: Applications to III-nitrides. - J. Appl. Phys., 2004, **95**, p. 3851-3879.

[74] P. Söderlind, First-principles elastic and structural properties of uranium metal. - Phys. Rev. B, 2002, **66,** 085113 (p. 1-7).

[75] B. Dorado, M. Freyss, and G. Martin, GGA+*U* study of the incorporation of iodine in uranium dioxide. - Eur. Phys. J. B, 2009, **69,** p. 203-210.

[76] D.R. Lide (ed.), CRC Handbook of Chemistry and Physics, 88th Edition, CRC Press (2007-2008).

[77] M. Iwasawa, Y. Chen, Y. Kaneta, T. Ohnuma, H. Y. Geng, and M. Kinoshita, First-principles calculation of point defects in uranium dioxide. - *Mat. Trans*, 2006, **47,** p. 2651-2657.

[78] NIST Chemistry Web-book (2010); *http://www.webbook.nist.gov/chemistry/*

[79] Yu.F. Zhukovskii, P.W.M. Jacobs, and M. Causà, On the mechanism of the interaction between oxygen and close-packed single-crystal aluminum surfaces. - J. Phys. Chem. Solids, 2003, **64**, p. 1317-1331.

[80] S. Piskunov, Yu.F. Zhukovskii, E.A. Kotomin, E. Heifets, and D.E. Ellis, Adsorption of atomic and molecular oxygen on the $SrTiO_3$(001) surfaces: Predictions by means of hybrid density functional calculations. - MRS Proc., 2006, **894**, LL08-05 (p. 1-6).

[81] R. Weast, CRC Handbook of Chemistry and Physics. CRC Press Inc., Boca Baton (FL), 1985.

[82] E.A. Kotomin and Yu.A. Mastrikov, First-principles modelling of oxygen impurities in UN nuclear fuels. - J. Nucl. Mater., 2008, **377**, p. 492-495.

[83] R.W. Grimes and C.R.A. Catlow, The stability of fission products in uranium dioxide. - Phil. Trans. Roy. Soc. A, 1991, **335**, p. 609-634.

[84] Y.-L. Lee, J. Kleis, J. Rossmeisl, and D. Morgan, *Ab initio* energetics of $LaBO_3$ (001) (B = Mn, Fe, Co, and Ni) for solid oxide fuel cell cathodes. - Phys. Rev. B, 2009, **80**, 224101 (p. 1-20).

[85] Yu.A. Mastrikov, R. Merkle, E. Heifets, E.A. Kotomin, and J. Maier, Pathways for oxygen incorporation in mixed conducting perovskites: a DFT-based mechanistic analysis for (La, Sr)$MnO_{3-\delta}$. - J. Phys. Chem. C, 2010, **114**, p. 3017-3027.

13. Dalība zinātniskās konferencēs

1. ***LU Cietvielu fizikas institūta 23. zinātniskā konference (Rīga, Latvija, februāris, 2007).*** D. Bočarovs, J. Žukovskis, J. Kotomins. Skābekļa adsorbcijas modelēšana no pirmajiem principiem uz UN(001) ideālas un defektīvas virsmas. Kopsavilkums, 17. lpp.
2. ***The 5th International Conference „Information Technologies and Management", IT&M'2007 (Rīga, Latvija, aprīlis, 2007).*** Yu. F. Zhukovskii, D. Bocharov, and E. A. Kotomin. Oxygen chemisorption on the UN(001) surface: periodic DFT simulation. Kopsavilkums, 9.-10. lpp.
3. ***LU Cietvielu fizikas institūta 24. zinātniskā konference (Rīga, Latvija, februāris, 2008).*** D. Bočarovs, J. Žukovskis, D. Grjaznovs, R. Evarestovs un J. Kotomins**.** UN kodolu degvielas struktūra un īpašības: kvantu ķīmijas pieeja. Kopsavilkums, 6. lpp.
4. ***International Baltic Sea Region conference „Functional materials and nanotechnologies 2008" (Rīga, Latvija, aprīlis, 2008).*** D. Bocharov, Yu. Zhukovskii, R. A. Evarestov, E. A. Kotomin, and A. Bandura. Atomic and molecular oxygen adsorption on the UN (001) surface. Kopsavilkums, 87. lpp.
5. ***7th International Workshop „Materials Models and Simulations for Nuclear Fuels" (Karlsrūe, Vācija, septembris, 2008).*** D. Bocharov, Yu. F. Zhukovskii, and E. A. Kotomin. Interaction of the oxygen molecule with the UN(001) surface: *Ab initio* modeling.
6. ***LU Cietvielu fizikas institūta 25. zinātniskā konference (Rīga, Latvija, februāris, 2009).*** D. Bočarovs, J. Žukovskis, E. Kotomins. Molekulāra skābekļa hemosorbcija uz urāna nitrīda (001) virsmas. Kopsavilkums, 54. lpp.
7. ***International conference „Functional materials and nanotechnologies" FM&NT-2009 (Rīga, Latvija, aprīlis, 2009).*** D. Bocharov, D. Gryaznov, Yu. F. Zhukovskii, and E. A. Kotomin. Perfect and defective (001) surface of uranium nitride: *ab initio* calculations. Kopsavilkums, 100. lpp.
8. ***The 7th International Conference „Information Technologies and Management", IT&M'2009 (Rīga, Latvija, aprīlis, 2009).*** D. Bocharov, D. Gryaznov, Yu. F. Zhukovskii, and E. A. Kotomin. *Ab initio* calculations on the atomic and electronic structure of defective UN(001) surface. Kopsavilkums, 32.-33. lpp.
9. ***International Workshop „DFT modelling of actinide solid solutions with the emphasis to bulk properties and Helium behaviour" (Karlsrūe, Vācija, septembris, 2009).*** Yu. F. Zhukovskii, E. A. Kotomin, D. Bocharov, and V. N. Kuzovkov. The DFT+U calculations on defects in PuO_2 and MOX.
10. ***LU Cietvielu fizikas institūta 26. zinātniskā konference (Rīga, Latvija, februāris, 2010).*** D. Bočarovs, D. Grjaznovs, J. Žukovskis, E. Kotomins. Virsmas un zemvirsmas vakances urāna nitrīdā: aprēķini no pirmajiem principiem. Kopsavilkums, 31. lpp.
11. ***International conference „Functional materials and nanotechnologies" FM&NT-2010 (Rīga, Latvija, marts, 2010).*** D. Bocharov, D. Gryaznov, Yu. F. Zhukovskii and E. A. Kotomin. First principles calculations on oxygen impurities incorporated in the vacancies of UN(001) substrate. Kopsavilkums, 37. lpp.
12. ***The 8th International Conference „Information Technologies and Management", IT&M'2010 (Rīga, Latvija, aprīlis, 2010).*** D. Bocharov, D. Gryaznov, Yu. F. Zhukovskii, and E. A. Kotomin. *Ab initio* calculations on pure and oxygen-occupied vacancies upon the UN(001) surface. Kopsavilkums, 38.-39. lpp.
13. ***Spring European Materials Research Society (E-MRS) Meeting (Strasbūra, Francija, jūnijs, 2010).*** D. Bocharov, D. Gryaznov, Yu. F. Zhukovskii, and E. A. Kotomin. Ab initio

modeling of oxygen impurities incorporated within UN(001) surface and subsurface vacancies. Kopsavilkums, NPVI-23.

14. ***F-BRIDGE School on Ceramic Nuclear Fuel and Cladding Materials (Karlsrūe, Vācija, septembris-oktobris, 2010).*** D. Bocharov, D. Gryaznov, Yu. F. Zhukovskii, and E. A. Kotomin. First principles calculations of surface and subsurface vacancies as well as oxygen impurity atoms on UN(001) substrate.
15. ***LU Cietvielu fizikas institūta 27. zinātniskā konference (Rīga, Latvija, februāris, 2011).*** D. Bočarovs, J. Žukovskis, D. Grjaznovs, J. Kotomins. Skābekļa difūzijas procesi uz UN(001) virsmas. Kopsavilkums, 23. lpp.
16. ***45th Russian School on Condensed State Physics (Sanktpēterburga, Krievija, marts, 2011).*** D. Bocharov, D. Gryaznov, Yu. F. Zhukovskii, and E. A. Kotomin. Quantum-chemical modeling of oxidation processes on surface of nitride nuclear fuel. Kopsavilkums, 27. lpp.
17. ***International conference „Functional materials and nanotechnologies" FM&NT-2011 (Rīga, Latvija, aprīlis, 2011).*** Yu. F. Zhukovskii, D. Bocharov, D. Gryaznov, and E. A. Kotomin. First-principles simulations on initial stage of uranium nitride surface oxidation. Kopsavilkums, 20. lpp.
18. ***International conference „Functional materials and nanotechnologies" FM&NT-2011 (Rīga, Latvija, aprīlis, 2011).*** D. Bocharov, Yu. F. Zhukovskii, D. Gryaznov, and E. A. Kotomin. UN(110) surface properties: ab initio calculations. Kopsavilkums, 166. lpp.
19. ***Spring European Materials Research Society (E-MRS) Meeting (Nica, Francija, maijs, 2011).*** D. Bocharov, Yu. F. Zhukovskii, D. Gryaznov, and E. A. Kotomin. First-principles simulations on initial stages of UN(001) surface oxidation. Kopsavilkums, V4-17.

Pateicības

Autors izsaka pateicību Eiropas Sociālā fonda projektam Nr. 2009/0216/1DP/1.1.1.2.0/09/APIA/VIAA/044 un šī fonda doktorantūras studiju atbalsta programmai. Autors sirsnīgi pateicas J. Čepkasovai, R. Evarestovam, D. Grjaznovam, V. Kaščejevam, J. Kotominam, A. Kuzminam, J. Mastrikovam, P. Nazarovam, S. Piskunovam, J. Timošenko, P. van Ufelenam un G. Zvejniekam par vērtīgiem ierosinājumiem un daudzām stimulējošām diskusijām. Ārkārtīgi vērtīga bija arī A. Gopejenko un A. Guseva tehniskā palīdzība. Īpašu pateicību autors izsaka zinātniskam vadītājam J. Žukovskim, kurš pastāvīgi atbalstīja zinātnisko darbu visā doktora studiju laikā un šo tēžu sagatavošanas laikā, kā arī manai ķīmijas skolotājai J. Zaikinai, fizikas skolotājai M. Samucevičai un maniem vecākiem.

UNIVERSITY OF LATVIA
FACULTY OF PHYSICS AND MATHEMATICS

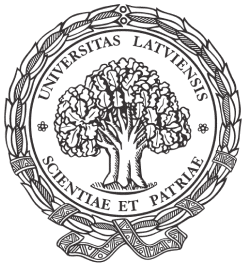

Dmitry Bocharov

FIRST PRINCIPLES SIMULATIONS ON SURFACE PROPERTIES AND REACTIVITY OF SUSTAINABLE NITRIDE NUCLEAR FUELS

Summary of Doctoral Thesis

Promotion to the Degree of Doctor of Physics
Subbranch: Solid State Physics

Scientific advisor: Dr. Chem. Yuri Zhukovskii

Riga 2012

This work was performed at the Institute of Solid State Physics, University of Latvia, beginning with October 2006 until August 2011.

Type of thesis: scientific papers

This work has been supported by the European Social Fund within the project „Datorzinātnes pielietojumi un tās saiknes ar kvantu fiziku" (Employment of computer sciences and its connection with quantum physics)
Līguma Nr. 2009/0216/1DP/1.1.1.2.0/09/APIA/VIAA/044

Scientific advisor: *Dr. Chem.* **Yuri Zhukovskii,** Senior Researcher, Institute of Solid State Physics, University of Latvia.

Reviewers of
Doctoral Thesis:

Dr. Lecturer **Girts Barinovs,** University of Latvia, Faculty of Physics and Mathematics.

Dr. Prof. **Roberto Caciuffo,** Institute for Transuranium Elements, Joint Research Centre, European Commission.

Dr. habil. Leading Researcher **Linards Skuja,** Institute of Solid State Physics, University of Latvia.

The defense of these Doctoral Thesis will take place in open session of the Physics, Astronomy and Mechanics Promotion Council of the University of Latvia to be held on January 24, 2012 at 15:00 in conference room of the Institute of Solid State Physics at Kengaraga Street 8, Riga, Latvia.

The full text of Thesis and its summary are available at Library of the University of Latvia (Kalpaka Blvd. 4, Riga, Latvia) and at the Latvian Academic Library (Rupniecibas Str. 10, Riga, Latvia).

LU Physics, Astronomy and Mechanics chairperson of Specialized Promotion Council: *Dr. Habil. Phys*., **Ivars Tāle**

ISBN 978-9984-45-437-5

Contents

Abstract 5

List of abbreviations 6

1. Introduction 7
   - 1.1. Motivation 7
   - 1.2. Author's contribution 7
   - 1.3. Scientific novelty 9
2. Literature review 10
   - 2.1. Experimental study of UN properties 10
   - 2.2. Interaction of uranium nitride with oxygen 12
   - 2.3. Previous theoretical simulations on UN and related actinide compounds 14
3. Theoretical background 18
   - 3.1. DFT method basics 18
   - 3.2. Exchange-correlation functionals 18
   - 3.3. The pseudopotentials 19
   - 3.4. The plane wave formalism 20
   - 3.5. Computational parameters in the *VASP-4* computer code 21
   - 3.6. Computational parameters in LCAO *CRYSTAL-06* code 23
   - 3.7. Slab model and defect periodicity 23
4. Modeling of UN bulk 25
5. Structural properties of UN (001) and (110) surfaces 27
6. Modeling of perfect UN surface 29
   - 6.1. Spin-frozen PW and LCAO calculations on defectless UN(001) surface 29
   - 6.2. Spin-relaxed PW calculations of defectless UN (001) and (110) surfaces 32
   - 6.3. Perfect UN surface calculations: summary 33
7. Modeling of single N and U vacancies 34
   - 7.1. Vacancy calculations: model and formation energies 34
   - 7.2. Surface reconstruction induced by vacancies 36
   - 7.3. Electronic properties: Finite-size effects and choice of supercell size 37
   - 7.4. Magnetic properties 38
   - 7.5. Comparison of results for N vacancies on UN (001) and (110) surfaces 39
   - 7.6. Vacancy calculations: summary 40

8. Modeling of O adsorption and migration on perfect UN surface 41
8.1. Atomic oxygen adsorption 41
8.1.1. Model and theoretical background 41
8.1.2. Comparison of spin-frozen PW and LCAO calculations on atomic adsorbtion 42
8.1.3. PW calculations on binding energies, charges and structure relaxation 42
8.1.4. Analysis of electronic properties 44
8.1.5. Comparison of oxygen adsorbtion upon UN(001) and UN(110) surfaces 45
8.1.6. Atomic oxygen adsorption: Summary 46
8.2. Molecular oxygen adsorption 46
8.2.1. Model and theoretical background 46
8.2.2. Spontaneous dissociation 47
8.2.3. Electronic properties of adsorbed molecule 48
8.3. Simulation of migration path for O adatom along the UN(001) surface 51
9. O atom migration and incorporation into defective UN(001) slab 53
9.1. Low-barrier incorporation of O adatom from site atop U_{surf} atom to N_{surf} vacancy 53
9.2. Oxygen incorporation into surface vacancies 54
9.2.1. Model and computational details 54
9.2.2. Oxygen incorporation and solution energies 55
9.2.3. Spin densities and Bader charges 56
9.2.4. Charge redistribution analysis: Finite-size effects and choice of supercell size 57
9.2.5. Electronic densities of states (DOS) for incorporated oxygen 59
9.2.6. Comparison of oxygen incorporation into N vacancy on the UN(001) and (110) surfaces 59
9.2.7. Modeling of O adatom incorporation: summary 60
10. Summary 61
11. Main theses 62
12. Literature 63
12.1. Author's publications related to this work 63
12.2. Other author's publications 63
12.3. References 63
13. Contributions at scientific conferences 68
Acknowledgements 70

Abstract

The uranium mononitride UN is a material considered as promising candidate for Generation-IV nuclear reactors. Due to considerable amount of aggressive oxygen impurities in UN samples, it is necessary to understand the mechanism of O adsorption and further oxidation of UN.

The first detailed study of UN surface, including its interaction with oxygen, have been performed using DFT PAW method as implemented in the *VASP* computer code. The formation energies of U and N vacancies as well as binding energies of O atoms and molecules adsorbed atop the UN surface are discussed together with the charge redistributions, densities of states, and O atom migration trajectories. Calculations allow us to propose energetically feasible mechanism for the partial saturation of UN(001) surface by oxygen which can lead to easy UN oxidation observed in air.

Keywords: Quantum chemistry, Density Functional Theory calculations, uranium mononitride, surface defects, oxygen adsorption

List of abbreviations

2D: Two-dimensional

3D: Three-dimensional

AE: All-electron

AFM: Antiferromagnetic state

BS: Basis set

BZ: Brillouin zone

CASTEP: Commercial and academic software package within formalism of PW and pseudopotentials

CRYSTAL: General-purpose computer code for *ab initio* LCAO study of periodic systems and molecules

DC: Direct current

DFT: Density functional theory

DOS: Density of states

EC FP-7: Seventh Framework Programme of the European Commission

EXAFS: Extended X-ray absorption fine structure

fcc: face centered cubic structure

FM: Ferromagnetic state

GAUSSIAN: General-purpose computer code, to enable *ab initio* LCAO electronic structure calculations

GGA: Generalized gradient approximation

ISSP: Institute of Solid State Physics, University of Latvia

KKR-GF: Korringa-Kohn-Rostoker Green's function

LAPW: Linearized augmented-plane wave

LC: Large core pseudopotentials

LCAO: Linear combination of atomic orbitals

LDA: Local density approximation

LMTO: Linear muffin-tin orbitals

ML: Monolayer

MT60: Mosyagin-Titov's small-core pseudopotential for atom containing 60 electrons in core

MT78: Mosyagin-Titov's large-core pseudopotential for atom containing 78 electrons in core

PAW: Projector augmented-waves

PBE: Perdew-Burke-Ernzerhof exchange-correlation functional-

ppm: particles *per* million

PS: Pseudo-wave soft function

PW: Plane waves

PW91: Perdew-Wang-91 exchange-correlation functional

RBS: Rutherford backscattering spectroscopy

RECP: Relativistic effective core pseudopotetntial

RMM-DIIS: Residual minimization method in the direct inversion of iterative subspace

SC: Small core pseudopotentials

SC60: Stuttgart-Cologne group pseudopotential for atom containing 60 electrons in core

SEM: Scanning electron microscopy

UPS: Ultraviolet photoelectron spectroscopy

US-PP: Ultra-soft pseudopotential

UV: Ultra-violet

VASP: Vienna *ab initio* simulation package within formalism of PW and pseudopotentials

wt%: weight percents

XPS: X-ray photoelectron spectroscopy

XRD: X-ray diffraction

1. Introduction

1.1. Motivation

Uranium mononitride (UN) is an advanced material for the non-oxide nuclear fuel considered as a promising candidate for the use in Generation-IV fast nuclear reactors to be in operation for the next 20-30 years [1, 2]. UN reveals several advantages over a traditional UO_2–type fuel (*e.g.*, higher thermal conductivity and metal density as well as high solubility in nitric acid in the case of fuel reprocessing [2]). However, one of important problems with actinide nitrides is their effective oxidation in oxygen-containing atmosphere (even at low partial pressure) which can affect nuclear fuel performance [3, 4]. Thus, it is important to understand the mechanism of the initial stage of UN oxidation and to find proper solutions, in order ways to improve the quality of nuclear fuel in the future.

The main objective of this PhD Thesis is to acquire reliable information on the atomic and electronic structure of both perfect and defective UN surfaces as well as to understand the mechanism of early stages of surface oxidation. This must be achieved through the solution of the following tasks:

- Modeling of an UN bulk for proper choice of parameters for surface calculations.
- Modeling of perfect UN surface with a focus on the surface anisotropic relaxation and reconstruction.
- Modeling of single N and U vacancies and calculations on formation energies of surface defects.
- Modeling of both molecular and atomic oxygen adsorption upon perfect UN surfaces.
- Modeling of oxygen migration upon both perfect and defective UN (001) surface.
- Modeling of O adatom incorporation inside existing surface vacancy.
- Comparison of results obtained for UN (001) and (110) surfaces.
- Development of an atomistic model for oxidation of UN surface.

The current study is performed within the collaboration between Institute of Solid State Physics, Riga, and Institute for Transuranium Elements, Karlsruhe, Germany, (Contract No 205343-2006-07 F1ED KAR LV) and as one of tasks included in the EC FP-7 project: Basic Research for Innovative Fuel Design for Generation-IV systems (F-BRIDGE).

1.2. Author's contribution

Main results of our calculations considered and analyzed in this PhD Thesis were described in 5 papers published in high-ranking International scientific journals [P1-P5] as well as presented at International and Local conferences as posters and oral reports (see conference list in Section 13). The author substantially contributed to preparation and

writing of papers and conference presentations, he was also selected as the corresponding author for Refs. [P2-P5].

Major part of considered results were obtained by author using PW calculations (*VASP* code) (almost all calculations presented in the papers [P1-P5] excluding calculations on N_2 molecule and alpha-uranium crystal [P4, P5]), although LCAO calculations (*CRYSTAL* code) were performed too [P1, P2] (in cooperation with St. Petersburg State University, Russia), to compare both *ab initio* approaches used for simulations on UN substrate and its chemical reactivity. The author installed computer codes in single and parallel regime at both Latvian Supercluster (LASC, ISSP, Riga) and Computational Facilities of Research Center Garching (Germany). Moreover, the author optimized both input parameters and key sets for *VASP* code (see Section 3 for details), performed careful analysis of output files and extracted results for further treatment and interpretation, as well as wrote several scripts, to operate this code and to perform analysis of obtained results (for example, to plot DOS from *VASP* output file, to construct bulk structure, to calculate magnetic moments and bulk modulus as well as to distribute resources in parallel calculations).

Due to a restricted number of theoretical and experimental data available in literature so far, very important question was a proper verification of the calculated results presented in this PhD Thesis. The author chose the following verification methods:

1. *Comparison of obtained results with existing experimental or theoretical data.*

For example, as known from literature [1], the UN lattice constant $a_0 = 4.886$ Å, the bulk modulus $B = 194$ GPa and the cohesive energy $E_0 = 13.6$ eV. These parameters were used for comparison with values obtained in theoretical calculations performed in this study.

2. *Simultaneous application and comparision of different theoretical methods.*

The results of our PW calculations on UN bulk and perfect (001) surface as well as atomic oxygen adsorption on this substrate were compared with the corresponding LCAO results calculated by group of Prof. R.A. Evarestov (*St. Petersburg State University*) [P1, P2]. Qualitative accordance of results obtained using the two different first-principles methods greatly increases the reliability of obtained results.

3. *Finding of internal criteria for convergence.*

For example, in calculations on vacancy-containing UN slab, the control of spin distribution is very important. Averaged magnetic moment μ_{av} *per* U atom in spin-relaxed calculations must be larger than 1 μ_B, otherwise we cannot achieve a convergence of formation energies for defects depending on thickness of UN slab [P4]. This effect appears due to a presence of local energy minima for considered slab configurations. Global energy minimum corresponds to spin redistribution with $\mu_{av} > 1$, while for other redistributions, we failed in localization of global minima, *i.e.*, reliability of obtained results is rather doubtful.

4. *Comparison of results obtained for the same system with varied computational parameters.*

For example, we compared vacancy formation energy for the same defect periodicity (2×2 or 3×3) but for different number of atomic layers; we also found criteria for cut-off energy divergence (see Section 3 for details) [P4].

1.3. Scientific novelty

Theoretical simulations of uranium compounds are especially complicated due to a relativistic character of an electron motion inside the U atomic core. Moreover, UN is characterized by a mixed metal-covalent chemical bonding: physical and chemical properties of light actinides are determined by partly localized *5f* electrons, requiring time-consuming calculations. In this study, we *firstly* present DFT calculations on UN surface and propose the UN surface oxidation mechanism. These results convincingly illustrate possibilities of quantum-chemistry simulations on actinides and their surfaces. Obtained results can be used for verification of alternative theoretical calculations on uranium nitrides and related actinide compounds (for example, uranium monocarbide UC). Moreover, the results of DOS analysis presented in this work can be used for qualitative interpretation of the experimental ultra-violet photoelectron spectra (UPS) for uranium oxynitrides which will be synthesized in the future.

2. Literature review

2.1. Experimental study of UN properties

Uranium mononitride is a compound with metallic lustre and low electrical resistivity ($1.6 \cdot 10^{-4}$ cm) [5], possessing *fcc* structure (space group $Fm\bar{3}m$, Fig. 2.1) over a wide temperature range [1]. The UN lattice constant is sensitive to carbon impurities [1] being insensitive to small oxygen impurities [6]. High melting point (~2780±25 K) [1], high fissile atom density (14.32 g/cm^2 vs 10.96 g/cm^2 for UO_2 [7]) and high thermal conductivity (13 W/mK) [8] make UN fuel a prospective material for nuclear reactors [1].

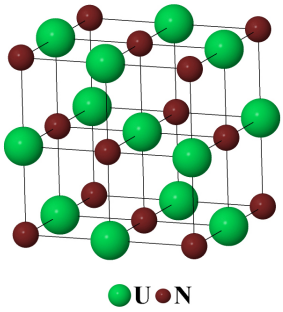

Figure 2.1. *fcc* structure of uranium mononitride

Various fabrication methods were used so far to produce UN. Samples of uranium nitrides were produced beginning with 19th century by annealing either UCl_4 salt in NH_3 atmosphere or uranium bicarbide (UC_2) in nitrogen at 1100 °C [1]. Nowadays, the most widespread UN fabrication methods are:

- Nitration of uranium in N_2 or NH_3 atmosphere at ~800-900 °C. Frequently, U_2N_3 is used as an intermediate product which subsequently is decomposed, to obtain UN powder with a low concentration of oxygen impurity [1].
- Carbothermic reduction. Formation of UN in the carbothermic reduction/nitrification process is possible, starting with pressed mixtures of UO_2 + C, following the reaction $UO_2 + 2C + 1/2N_2 \rightarrow UN + 2CO$ that are held at 1700 °C in N_2, N_2/H_2 or NH_3 atmosphere. However, such products contain a large amount of O_2, typically 0.1 wt% [1, 9].
- Nitration of melting U in N_2 gas by voltaic arc at pressure of 3-5 bar. If tungsten electrodes are used, a pollution of resulting UN material with W impurities is unavoidable. This is why U electrodes at higher N_2 pressure (20 bar) were also used [1]. The products, however, are also inhomogeneous.
- Hydride route. This method results in formation of a good quality powder with particle size ~1 μm. When using such a method, UH_3 is produced by reacting U

with H_2 at 200-300 °C. It is subsequently decomposed ($UH_3 \rightarrow U + 3/2H_2$) to a U powder in inert gas atmosphere or in vacuo at temperature 400-600 °C. U powder reacts with N_2 at 800 °C, to yield UN_{1+x}, which can be decomposed to UN, as above, by heating at temperatures between 1100 and 1300 °C in vacuo. A direct reaction between UH_3 and N_2 was used too [1].

- Alternative processes of UN fabrication, starting with the halides UF_4 or $UC1_4$, are less important for commercial production [1]. Notice, that for scientific researches, just specific alternative methods are frequently used. For example, UN surface could also be produced by bombardment of an U metal surface by activated nitrogen [10].

Fascinating and often enigmatic array of UN magnetic and electronic properties is induced by U(5*f*) electrons which are found to be intermediate between the highly localized 4*f* electrons of the lanthanides and the strongly delocalized *d* valence electrons in the transition metals [11]. The UN was found to be antiferromagnetic at temperatures lower than a Neel temperature (T_N ~ 53 K), which was detected in the heat capacity measurements [1]. Investigation of the magnetic structure of uranium nitride was performed in 60s using methods of neutron diffraction [5]. The magnetic structure known as ordering of the first kind, where ferromagnetic sheets parallel to the (001) planes are antiferromagnetically coupled, was deducted [5]. The value of 0.75 μ_B found for the magnetic moment at low temperatures appears to be surprisingly small (the lowest amongst the uranium monopnictides UX, where X = P, As, Sb) [5] which requires a careful analysis of results for UN surface obtained using the DFT calculations and their comparison with the corresponding experimental data.

Photoelectron spectroscopy also confirmed the complexity of UN. A very high density of states in proximity of the Fermi level was observed, which gives an evidence that the U(5*f*) electrons participate in bonding being strongly hybridized with the U(6*d*) electrons. The occupation of the conduction U(5*f*) band is 2.2 ± 0.5 *e*, of which ~1.8 *e* resides near the Fermi level [11]. In [12], the band structure of UN at 25 K was constructed taking into account the second derivative of high-resolution angle-resolved photoemission spectra. A highly dispersive band was observed for UN near the Fermi level centered at Γ(X) point, whose bottom is located at about 2 eV. First magneto-optical Kerr measurements on UN also shows narrow U(5*f*) band formation around the Fermi level as well as increased hybridization of the U(5*f*) states with U(6*d*) and N(2*p*) states as compared to similar data for heavier uranium monopnictides [13]. On the other hand, uranium nitride has the smallest U-U distance amongst the UX compounds (X=N, P, As, Sb, S, Se, and Te) which is equal to 3.46 Å being close to the critical 3.4 Å value given by Hill diagrams separating non-magnetic from magnetic compounds, so that delocalization of U(5*f*) states should be expected [14].

Extraction of the data for diffusion of nitride atoms or vacancies is also non-trivial for UN. Unfortunately, a radioactive isotope suitable for diffusion measurements does not exist for nitrogen. Therefore, either mass-spectrometric measurements with ^{15}N or a nuclear reaction induced in the UN specimen following the annealing are needed, to measure nitrogen diffusion coefficients [1]. On the other hand, thermally created and radiation-induced point defects can be studied by measuring a physical quantity sensitive to their presence. For example, the electrical resistivity ρ for actinide compounds can be

used for this purpose: the changes of ρ depending on vacancy concentration are found to be very large (for example, 12 μΩ·cm for 1% of C vacancies in UC) [1]. By studying the thermal recovery of these defects during isochronal annealing, or also by applying the "change-of-slope method" during isothermal annealing with suddenly increased temperature, the defect migration energy can be determined. Unfortunately, these methods do not identify the defect or even the type of atom involved (*e.g.,* C, O or N), unlike the diffusion studies with radioactive tracers [1].

2.2. Interaction of uranium nitride with oxygen

Initially, the oxidation of uranium mononitride in an oxygen atmosphere was systematically studied in [15]. The two main types of UN samples were used for those experiments: powdered UN and smoothly polished UN pieces. Following a weight change of the UN powder sample during the oxidation process at elevated temperatures, a strong exothermic reaction was identified at 250 °C characterized by rapid oxygen absorption. The weight was increased by 11.5%. X-ray diffraction patterns of the intermediate product at temperatures 250-260 °C showed both weak diffraction lines corresponding to UN and very pronounced line broadening corresponding to UO_2. Smoothly polished UN pieces were used for kinetic study of UN oxidation. Measurements showed that reaction rate is proportional to the area covered by the oxide or the oxidized volume. Analysis of both kinetic studies and X-ray diffraction data suggested that the isothermal oxidation of UN proceeds from the beginning of lateral spreading of the oxide, $UO_2(N)$, accompanied by a slight N_2 release and by the formation of $U_2N_3(O)$ during the reaction between UN and released nitrogen.

In [16], such characteristics as the chemical composition, phases, lattice parameter, sinterability, grain growth and thermal conductivity of the samples are investigated using chemical, X-ray and ceramographic analyses for pellets of uranium nitride powder containing certain amounts of oxygen (~0.3, ~0.6 and ~1.0 wt%) which are products of carbothermic reduction. Note, that conductivity of UN samples was found to be gradually decreased under oxidation [16]. The principal results are that the average UN grain size of matrix phase decreases with increase of oxygen content. Moreover, thermal conductivity of the pellets containing about 1 wt% oxygen is lower than that of usual nitride pellets (containing 1000-2000 ppm oxygen) by 9-10% and 12-13% at 1000 and 1500 K, respectively.

In [9], direct ammonolysis of UF_4 was used, to synthesize UN_2 sample which was heated to 1100 °C for 30 min inside the inert atmosphere producing these UN powder samples with UO_2 inclusions saturated at 5.0 wt%. The methods of X-ray diffraction (XRD) and scanning electronic microscopy (SEM) were used for morphology analysis of these samples. The SEM images show that UN particles are primarily irregular grains with incompletely crystallized faces (Fig. 2.2). The observed characteristic length distribution of particles ranges from 0.1 to 6 μm. The measured UN surface area was equal to 0.23 m^2/g. Both the electron microprobes and X-ray diffraction analysis showed that there are considerable amount of oxygen impurities in UN samples consisting of the primary UN phase and the secondary UO_2 impurity phase. This supports the conclusion that oxide impurities are likely to be formed by a diffusive process from the chemical environment

and, thus, they are also likely to be formed along the particle surface. Concentration of oxygen impurities increases upon exposure to air: UN sample exposed for 3 months shows the growth of oxide contamination. The quantitative analysis performed for the XRD patterns showed that the UO_2 concentration increases from 5.0 wt% to 14.8 wt% over this time period [9].

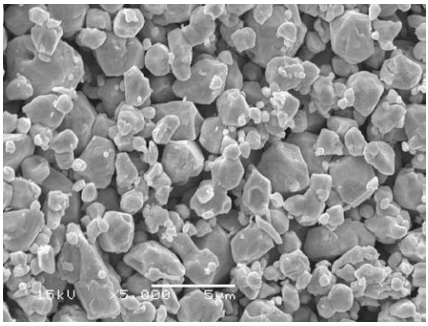

Figure 2.2. SEM image of UN sample [9].

UPS measurements performed for thin layers of UO_2, UN, UO_xN_y and UO_xC_y using He-II 40.81 eV excitation radiation produced by a UV rare-gas discharge source were described in [17, 18]. These layers were prepared *in situ* by reactive DC sputtering in an Ar atmosphere. Fig. 2.3 shows that U(5*f*) states form a peak close to the Fermi level (0 eV), which proves their itinerant character. The valence band spectrum of UO_xN_y shows a broad band interpreted as superposition of the narrow O(2*p*) and N(2*p*) bands. The maximum at 6 eV binding energy clearly comes from the O(2*p*) state contribution while the smaller shoulder at 3 eV coincides with the N(2*p*) signal in UN sample.

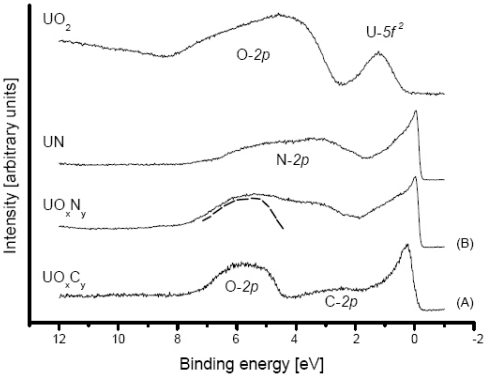

Figure 2.3. He-II valence band spectra of UO_xC_y, UO_xN_y, UN and UO_2 spectra are given as reference [18].

In [19], XPS and XRD methods as well as the measurement of ammonia concentration in the aqueous phase at the end of each experiment were used, in order to study corrosion of UN in water. UO_2 film arising during the surface reaction with water was detected using XPS for the surface of freshly polished UN pellet. The high corrosion rates of UN in water (at 928 °C) indicated that UN is not stable inside the hot aqueous environment. Corrosion rate for UN is much lower than that for U metal but higher that of uranium silicide.

Thickness, composition, concentration depth profile and ion irradiation effects on uranium nitride thin films deposited upon fused silica were investigated in [8] using Rutherford Backscattering Spectroscopy (RBS) for 2 MeV He^+ ions. Deposition at -200 °C provided formation of thick stoichiometric UN film. This film was found to be stable for exposure to air. The surface oxidation is much more enhanced and the oxidized surface layer becomes gradually thicker in films deposited at higher temperature (+25 °C and +300 °C). A large influence of the ion irradiation on the film structure and layer composition was observed. This study also showed possibility to produce stoichiometric UN film with the required uranium content of 50% and to obtain the required film thickness by ion irradiation.

Finally, experimental studies also clearly showed that oxygen contacting to the surface of uranium mononitride can result in growth of the oxide compound and, at initial stages, can lead to the formation of surface layer structurally similar to oxynitrides UO_xN_y [14].

2.3. Previous theoretical simulations on UN and related actinide compounds

Due to increasing interest to the fast breeder reactors and to the issues of transmutation of uranium, plutonium and minor actinides, first-principles and other theoretical calculations on actinide nitride compounds attract great attention nowadays. However, previous theoretical studies were performed mainly on UN bulk. Beginning with 80s [21-23], for its *ab initio* calculations, the methods based on the DFT were mainly used.

In first relativistic calculations on UN single crystal, there were used methods of full-potential Korringa-Kohn-Rostoker (KKR) Green's function [21] and Linear Muffin-Tin Orbitals (LMTO) [22, 23] focused mainly on the atomic and electronic structure. The calculated lattice parameters were found within 3% of experimental value, whereas the bulk modulus was reproduced worse when comparing with experimental data: by 23% higher [22] or within 10% [23]. DOS analysis showed that no gap exists between the valence and conduction bands in UN. The valence bands, found to be ~5-6 eV wide, appeared below the Fermi level by ~2 eV. The main peak was located below the Fermi level by 1 eV [23].

Recently, a number of first-principles DFT calculations on UN bulk were performed. In particular, the all-electron calculations within the Linear Augmented Plane Wave (LAPW) approach were performed, using the PBE (Perdew-Burke-Ernzerhof) exchange-correlation functionals (with and without incorporation of the spin-orbital coupling) as implemented in the *WIEN-2k* program package, for a series of actinide nitrides

(AcN, ThN, PaN, UN, NpN, PuN, AmN) [20]. The enthalpies of their formation, which main contribution arises from the ground state cohesive energies, were evaluated. The obtained enthalpies of formation were found to be in excellent agreement with the experimental data (in the case UN, the best correlation was achieved with results of calorimetric measurements: theoretical value of -291.0 kJ·mol^{-1} *vs.* experimental value of -290.5±1.4 kJ·mol^{-1} [24]). Certain discrepancies with experimental data observed for PuN and ThN still need to be clarified.

In [25], the same LAPW formalism within the GGA approximation was used to study the structural, electronic, and magnetic properties of the actinide compounds. The observed chemical bonding between the actinides and nitrogen was characterized by a significant ionic character. The calculated cohesive energies were found to be close to the experimental values (14.3 eV *vs.* 13.6 eV, respectively). Although lattice constants were calculated in a good agreement with the experiment (within ~0.4%), the UN, AmN, PuN, and NpN were found to be ferromagnetic (FM) that contradict to experimental results for these compounds (antiferromagnetic structures were experimentally observed at low temperatures). The calculated spin density for UN in FM state was equal to 0.96 μ_B. On the other hand, the calculated ferromagnetic structure of NpN and the non-magnetic structure of ThN agreed well with the corresponding experimental measurements.

In [26], the all-electron relativistic spin-polarized DFT calculations were performed, to evaluate the total energies, optimized geometries, as well as electronic and thermodynamic properties of perfect stoichiometric UN and UN_2 single crystals. For this purpose, the GGA PW91 exchange-correlation functional was used, and the numerical double-ξ basis sets with *d*-type polarization functions were added to atoms heavier than hydrogen. Structural properties recently measured using EXAFS and XRD methods were successfully reproduced in theoretical calculations (within error of 0.03 Å). Calculated DOSs showed hybridization of the U(*6d*), U(*5f*) and N(*2p*) states as well as domination of the U(*5f*) state in the conduction band. Novelty of that paper consisted in a calculation of the phonon frequencies and heat capacities. The authors suggested an important role of itinerant U(*5f*) states in thermodynamic properties.

The lattice parameters, electronic structure, as well as the thermodynamic properties of UN using LDA+*U* and GGA+*U* semi-empirical schemes included Hubbard potential *U* were presented in [27]. The total energy dependences on *U*-parameter for UN bulk in FM and AFM states obtained in those calculations show that FM state is preferable for the range of *U*-parameter between 0 and 2 eV while AFM state could be favorable for *U*-parameter larger than 2 eV. Nevertheless, even though the AFM state of UN bulk is reproduced, the ground state in hardly obtainable when using the DFT+*U* method [28]. This may produce large errors when calculating defect formation energies [29, 30]. We avoid application of this method in the present study due to ferromagnetic nature of UN surface [31], reproducible by standart DFT functionals.

The PW approach was applied for UN atomic structure calculations beginning with [32]. In that study, where the Ultra-Soft (US) pseudopotentials and PBE exchange-correlation functional were used, the experimental UN and U_2N_3 lattice constants were reproduced within 3% error while the difference of their atomic coordination can be described within 5% error.

In more detailed PW calculations on UN bulk, the *VASP* and *CASTEP* codes were employed using the Perdew-Wang (PW91) non-local GGA exchange-correlation functional combined with either US or PAW pseudopotentials, respectively [33, 34]. Both series of calculations agree well on the mixed metallic-covalent nature of UN chemical bonds qualitatively reproducing the lattice constants, bulk moduli and cohesive energies.

Then the PW approach combined with a supercell model was used for the calculations on defective UN crystal, containing single point defects as well as Frenkel and Schottky defect pairs. In [34], it was shown that N vacancies practically have no influence on the UN lattice constant, even for concentrations higher than 25%. The formation energies of U or N vacancy in UN bulk were obtained equal to 9.1-9.7 eV for N vacancy and 9.4-10.3 for U vacancy. The calculated activation energy of the interstitial N atom migration along the (001) axis was estimated as rather low, 2.73 eV [33]. This fact confirms the suggestion that the interstitial migration might be a predominant mechanism of N diffusion in UN fuel [1]. Apart the behavior of empty vacancies, the O atom incorporation into vacancies in bulk UN was considered too [35]. Its incorporation into the N vacancies was found to be energetically more favorable as compared to the interstitial sites. However, the calculated values of solution energy showed an opposite effect. The calculated migration energy of the interstitial O atoms is very similar (2.84 eV). This fact confirms that O atoms can easily substitute the host N atoms in UN structure.

Recent LCAO calculations on UN bulk [36, 37] were performed using the *GAUSSIAN-03* computer code with the PW91 exchange-correlation functional. The values of cohesive energy calculated using the Relativistic Effective Core Potentials RECP78 and RECP60 considerably differ (9.86 eV and 12.8 eV, respectively), thus indicating an importance of variation for the U outer shell. Group-theoretical analysis performed for interpretation of the UN band structure showed that both the bottom of the conducting band and the top of the valence band are formed by U(*5f*) states which result in the metallic nature of UN [36, 37] unlike UO_2 which is a semiconductor [38]. The Mulliken effective atomic charges of ±(1.5-2.0) *e* calculated using the *GAUSSIAN-03* code confirmed the mixed nature of the UN chemical bonding, being in agreement with the Bader topological charges of ±1.6 *e* obtained in PW calculations [34].

A number of studies on related actinide compounds were also published in last years. In [29], formation energies of oxygen vacancy in UO_2 compound were calculated using the Dudarev's DFT+*U* approach [39]. The formation energy of oxygen vacancy in UO_2 bulk was found to be 3.5-5.67 eV. In [40], formation energies of O and U vacancies were calculated using GGA approximation. Those calculations showed small difference between the FM and AFM states (4.0 eV for U vacancy formation in FM state *vs.* 4.4 eV for AFM state as well as 6.1 eV in both cases for O vacancy). In [41], point defects in uranium monocarbide bulk were studied using the PAW method combined with the PBE functional. The formation energy of uranium vacancy was found to be 4.54-4.55 eV while the same energy for carbon vacancy was equal to 0.8-0.83 eV. The mechanical properties of NpN were studied using the same GGA PBE functional [42]. The calculated bulk modulus for NpN ranged within interval 147-227 GPa depending on the magnetic state (AFM, FM or non-magnetic).

The first electronic structure simulations on actinide surfaces and their reactivity towards the molecular and atomic oxygen were performed only recently. It is, however, not surprising since actinide surfaces cannot be easily calculated using the DFT methods, due to a large number of electrons *per* unit cell. Nevertheless, some results on simulations performed for α-U, δ-Pu and UO_2 surfaces are available in the literature. In particular, Taylor [43] showed that the PAW method [44], used also in the present study, is fitting for reliable calculations on the (001) surface of α-U.

Tan *et al.* obtained UO_2 surface energies, using the atomic-scale computer simulation within the approach of interatomic potentials, which systematically classifies the 153 unique planar surface configurations that can be generated within 2×2 supercells [45]. The calculated surface energies ranged between 2.28 and 3.12 eV for UO_2(001) surface and 1.27-1.54 eV for UO_2(111) surface. The PW91 functional has been used for simulations on (111), (110), and (100) surfaces of UO_2 [46]. The calculations showed that the (111) surface has the lowest surface energy (0.461 J/m^2), followed by the (110) surface (0.846 J/m^2), and the (100) surface (1.194 J/m^2).

The calculations performed by Atta-Fynn and Ray [47, 48] also confirm the effectiveness of DFT methods for calculations on O, C and N ion chemisorption upon the δ-Pu(111) surface. The calculations were performed using the GGA PBE exchange-correlation functional. A 50% surface coverage by adatoms was considered. Calculations were performed at two levels: with and without spin-orbit coupling. Inclusion of spin-orbit coupling lowers the chemisorption energy by 0.05–0.27 eV, on the other hand, it negligibly influences on chemisorption geometries. Analysis of effective charges for each atom indicates that chemisorption primarily occurs on the surface layer. Pu-adatom hybridizations is dominated by Pu(6*d*) and adatom 2*p* states, with a significant reduction in the first peak of the projected Pu(5*f*) DOS, indicating the delocalization of some Pu(5*f*) electrons.

In any case, for the moment, no results of UN surface calculations are found to be published in the literature, excluding the current study performed within this PhD Thesis [P1-P5].

3. Theoretical background

For UN modeling, we use the *VASP-4* computer code, the commercial complex package based on density functional theory (DFT) and included an iterative solution of Kohn-Sham equations, based on residuum-minimization and optimized charge-density mixing routines [49], employing a plane-wave basis set combined with either US or PAW pseudopotentials. Elaboration of *VASP* package was began at early 90s.

3.1. DFT method basics

The cornerstone of DFT was laid by Hohenberg–Kohn (HK) theorem, which suggests that ground state properties of a many-electron system should be uniquely determined by an electron density $\rho(\vec{\mathbf{r}}) = \rho(\vec{\mathbf{r}}, \vec{\mathbf{r}}')$. The total energy of system in this case can be written as

$$E(\rho(\vec{\mathbf{r}})) = \int V(\vec{\mathbf{r}})\rho(\vec{\mathbf{r}})d\vec{\mathbf{r}} + T[\rho(\vec{\mathbf{r}})] + \frac{1}{2}\int \frac{\rho(\vec{\mathbf{r}}')\rho(\vec{\mathbf{r}})}{|\vec{\mathbf{r}} - \vec{\mathbf{r}}'|} d\vec{\mathbf{r}}' d\vec{\mathbf{r}} + E_{xc}[\rho(\vec{\mathbf{r}})], \qquad \textit{(Eq. 3.1.1)}$$

where the first term on right hand side describes the external potential influencing on the interacting system, for example, attraction of electrons to atomic nucleus, the second term describes the kinetic energy of electrons, the third term denotes the so-called Hartree term describing the electron–electron Coulomb repulsion, while the last term is called the exchange-correlation potential and includes all other contributions, in particularly the many-electron interactions [50, 51].

Varying the full energy functional (*Eq. 3.1.1)*, the Kohn-Sham one-electron equations (similar to Hartri-Fock equations) may be derived:

$$(\hat{\mathbf{H}} + \hat{\mathbf{J}} - \hat{\mathbf{V}}_{xc})\varphi_i(\vec{\mathbf{r}}) = \varepsilon_i \varphi_i(\vec{\mathbf{r}}), \qquad \textit{(Eq. 3.1.2)}$$

where the term $\hat{\mathbf{V}}_{XC}[\rho(\vec{\mathbf{r}})] = \frac{\delta E_{xc}[\rho(\vec{\mathbf{r}})]}{\delta\rho(\vec{\mathbf{r}})}$ is the exchange-correlation potential [50].

Due to dependence of Hamilton and Coulomb operators $\hat{\mathbf{H}}$ and $\hat{\mathbf{J}}$ in Kohn-Sham equations on electronic density $\rho(\vec{\mathbf{r}})$, these equations should be solved using self-consistence method [50].

Contemporary DFT calculations on solids are determined by several key options: (*i*) the choice of exchange-correlation functional, (*ii*) the choice of a basis set to expand the Kohn-Sham eigenfunctions (plane waves or localized basis functions), and (*iii*) the choice of a way to describe interactions between the ionic core and the valence electrons (full-potential approach or pseudopotential approach) [52].

3.2. Exchange-correlation functionals

Since the exact form of exchange-correlation functional is not known, tremendous progress in quantum chemistry methods is achieved by creation of proper functionals. Functionals of different complexity were developed within the hierarchy of DFT

functionals. The simplest approximation is the local-density approximation (LDA) based on the exact exchange energy for a uniform electron gas which can be obtained from fits to the correlation energy for a uniform electron gas [50].

In the present study, we use the Generalized Gradient Approximation (GGA) functionals, which foresee that the electronic density is unevenly distributed: the highest density of electronic density is located around the atom nucleus. The exchange-correlation energy may be expanded in the Taylor Series depending on the electronic density degrees. If only the first order of expansion is taken into account the resulting expression contains an electronic density gradient $\nabla\rho$ [50, 53].

Real functional is typically formed involving the fitting parameters which can reproduce the experimental data for different classes of materials with a high accuracy. It is very important to find such a functional, which can be used for description of large number of systems without additional parameters involved during calculation (In this sense, such calculations are called as *ab initio* or first principles calculations). In our study, the PW91 exchange-correlation functional has been used [54].

3.3. The pseudopotentials

Formalism of the pseudopotentials uses the widespread quantum-chemical approaches: the chemical properties are mostly determined by the valence electrons, the inner shells are chemically rather inert, while shells half-filled or completely filled with electrons possess the spherical symmetry (so-called Unsold's Theorem [55]). It allows us to describe separately only the outer shells' electrons. In turn, all inner electrons can be substituted by a joint effective pseudopotential. Depending on number of included electrons the pseudopotentials can be separated as Large Core (LC) and Small Core (SC) RECP pseudopotentials.

For example, U atom possesses the $1s^2 2s^2 2p^6 3s^2 3p^6 3d^{10} 4s^2 4p^6 4d^{10} 4f^{14} 5s^2 5p^6 5d^{10} 6s^2 6p^6 7s^2 5f^3 6d^1$ electronic structure. The LC(U) potential includes 78-electron core potential ($[Xe]4f^{14}5d^{10}$) and 14 valence electrons ($6s^2 6p^6 7s^2 5f^3 6d^1$) while the SC(U) potential includes 60-electron core potential ($[Kr]4d^{10}4f^{14}$) and 32 valence electrons ($5s^2 5p^6 5d^{10} 6s^2 6p^6 7s^2 5f^3 6d^1$). Unlike the LCAO RECP pseudopotentials applied for *CRYSTAL* calculations, the RECP pseudopotentials for PW calculations cannot be directly re-optimized: creation of a new pseudopotential or its re-optimization is very complicated task requesting up to several months or years for its solution [56]. Main aim of the current PhD activity in respect to a proper applicaton of RECP pseudopotentials for reliable calculations is their optimal choice from the library of standard pseudopotentials supplying the *VASP* code (depending on both structure of the core and diference with the all-electron wave function). Choice of pseudopotential for the calculated system must be based on the character of bonding between the ions in the system [49] including its test calculations.

For calculations performed within the current PhD study, we have applied RECP pseudopotential for 78 U internal electrons (with $6s^2 6p^6 6d^2 5f^2 7s^2$ valence shell), as well as 2 core electrons for both N and O atoms (with $2s^2 2p^3$ and $2s^2 2p^4$ valence shells, respectively).

3.4. The plane wave formalism

The Kohn-Sham method employing a plane-wave basis set and the pseudopotential approximation is one of powerful techniques in contemporary computational material science. The use of a plane-wave basis has several immediate advantages [52]: (*i*) it is easy to change from a real-space representation (where the potential energy *V* has a diagonal representation) *via* a Fast Fourier Transform to momentum-space where the kinetic energy *T* is diagonal; (*ii*) the control of basis-set convergence is almost trivial; it is sufficient to monitor the eigenvalues and total energies as a function of the *cut-off* energy, *i.e.*, the highest kinetic energy of a plane-wave within the chosen basis set; (*iii*) the Hellmann-Feynman forces acting on the atoms and the stresses on the unit cell may be calculated straightforwardly in terms of the expectation value of the Hamiltonian with respect to the ionic coordinates; (*iv*) basis-set superposition errors that have to be carefully controlled in calculations based on local basis sets are avoided.

As a starting-point to solve Kohn-Shame equations in PW basis set, the Bloch theorem usually serves, which describes wave function of electron (or other particle) placed in a periodic potential [57], *i.e.*,

$$\psi_{n\mathbf{k}}(\mathbf{r}+\mathbf{R}) = \psi_{n\mathbf{k}}(\mathbf{r})e^{i\mathbf{kR}} \qquad \textit{(Eq. 3.4.1)}$$

The unit cell periodic part $u_{n\mathbf{k}}$ of the wave functions is introduced as

$$\psi_{n\mathbf{k}}(\mathbf{r}) = u_{n\mathbf{k}}(\mathbf{r})e^{i\mathbf{kr}}, \qquad \textit{(Eq. 3.4.2)}$$

where $u_{n\mathbf{k}}(\mathbf{R}+\mathbf{r}) = u_{n\mathbf{k}}(\mathbf{r})$. It means that all cell periodic functions can be written as a sum of plane waves, going to reciprocal space lattice and performing Fourier transform:

$u_{\mathbf{k}}(\mathbf{r}) = \sum_{\mathbf{G}} u_{\mathbf{k}}(\mathbf{G})\mathrm{e}^{i\mathbf{Gr}}$ ($\mathbf{G}$ is chosen by such a way that $\mathrm{e}^{i\mathbf{Gr}}$ has the periodicity of the real space lattice)

$$\psi_{\mathbf{k}}(\mathbf{r}) = (N\Omega_0)^{-1/2}\sum_{\mathbf{G}} u_{\mathbf{k}}(\mathbf{G})\mathrm{e}^{i(k+\mathbf{G})\mathbf{r}}, \qquad \textit{(Eq. 3.4.3)}$$

where $u_{\mathbf{k}}(\mathbf{G}) = \frac{1}{\Omega_0}\int_{\Omega_0} \mathrm{e}^{-i\mathbf{Gr}}u_{\mathbf{k}}(\mathbf{r})d\mathbf{r}$ (Fourier transform).

In fact, the number of plane waves can be determined as a function of the kinetic energy cut-off, thus forming the PW sphere $\frac{(\mathbf{k}+\mathbf{G})^2}{2} < E_{cut}$ in reciprocal space [57].

Development of PW formalism as used in *VASP* computer code resulted in implementation of the *projector-augmented wave* (PAW) *method* originally introduced by Blöchl [44]. The main idea of PAW method is to transform the physically relevant full all-electron (AE) Kohn-Sham wave functions Ψ_n of this Hilbert space into a new computationally convenient pseudo-wave soft (PS) variational functions $\tilde{\Psi}_n$ in so-called

pseudo-Hilbert space [58]. Within the PAW formalism the AE wave function is derived from the PS wave function by means of a linear transformation [44]:

$$|\Psi_n\rangle = |\tilde{\Psi}_n\rangle + \sum_i (|\varphi_i\rangle - |\tilde{\varphi}_i\rangle)\langle \tilde{p}_i | \tilde{\Psi}_n \rangle \qquad \textit{(Eq. 3.4.4)}$$

where the AE partial waves φ_i are obtained for a reference atom whereas the PS partial waves $\tilde{\varphi}_i$ are equivalent to the AE partial waves outside a core radius r_c^l and match continuously onto $\tilde{\varphi}_i$ inside the core radius (the augmentation region, similar to linearized muffin-tin LMTO formalism); the index i is a shorthand for the atomic site R_i, the angular momentum numbers $L = l$, m, and an additional index k referring to the one-electron reference energy ε_{kl}. The core radius is chosen approximately about half the nearest-neighbor distance [58]. The projector functions $\tilde{p}_i$ are dual to the PS partial waves:

$$\langle \tilde{p}_i | \tilde{\varphi}_j \rangle = \delta_{ij} \qquad \textit{(Eq. 3.4.5)}$$

3.5. Computational parameters in the *VASP-4* computer code

In previous subsections, we have desribed general theoretical principles which are included in *VASP* computer code. In this subsection we shortly describe the key input parameters for our calculations.

Input for performing *VASP* calculations contains the following main files [49]:

I. POSCAR. This file describes atom positions and allows fixing of atomic coordinates if necessary (it can be used, for example, to calculate interstitial positions when geometry relaxation leads to the system of stable basic configuration). In all slab calculations, we perform partial or complete structure optimization within the supercell of fixed linear dimensions using criterion of the total energy minimization. Atom positions for each calculated system are defined in POSCAR file, according to crystallographic properties of studied structure.

II. POTCAR. This file contains information about such properties of different atoms as the RECP pseudopotentials, atomic masses, the energy of reference atomic configuration, which the pseudopotential was created for (more detailed information about pseudopotentials is contained in Subsection 3.3), *etc*.

Computational parameters must be defined in following two files:

III. KPOINTS. This file determines the *k*-point mesh in the BZ. In this study, we have generated *k*-points using the Monkhorst-Pack's technique [59] whereas the electron populations were determined following the method of Methfessel and Paxton [60] as implemented in the *VASP* code.

For each series of calculations, we have found the optimal *k*-point mesh that would provide the convergence of results: the $8 \times 8 \times 8$ mesh for bulk calculations, the $8 \times 8 \times 1$ mesh for major part of surface calculations (perfect UN surface, vacancies on the UN(001) surface, oxygen adsorption and migration, as well as oxygen incorporation into pre-existing N vacancies), as well as the $4 \times 4 \times 1$ mesh for calculations of

molecular oxygen interaction with UN(001) surface and for all UN(110) surface calculations (including molecular adsorption, vacancies on UN(110) surface, and oxygen incorporation).

IV. INCAR. This main *VASP* input file determines "what to do and how to do it". Complete list of keywords is enumerated in the *VASP* manual [49]. In following paragraphs we describe only those parameters which variation has been especially important for our calculations.

IVa. ISPIN. This option defines the spin-polarized calculations. For UN, as a system with magnetic properties, the key "yes" has been used always.

IVb. MAGMOM. This option defines the initial magnetic moment on each atom (the calculation begins from the defined magnetic moments, however, they are changed during this calculation). We have chosen initial ferromagnetic state for all UN calculations. If one is searching for a ferromagnetic solution, it is usually safest to start from the larger local magnetic moments. This is why for spin-relaxed FM calculations, we have started from the value of 2 μ_B *per* U atom. For spin-frozen FM calculations, we have started from the magnetic moment 1 μ_B *per* U atom.

IVc. NUPDOWN. This key fixes the spin moment of the whole system to specified value. For spin-frozen calculations, we suggest the magnetic moment 1 μ_B *per* U atom.

IVd. ENCUT. Selection of plane waves is determined by the cut-off energy E_{cut}. The optimal cut-off energy has been found to be equal to 520 eV.

IVe. ISMEAR. Determines how the partial occupancies are defined for each wavefunction.We use Gaussian smearing for our calculations.

IVf. SIGMA. This key, describing the difference between the free energy and the total energy, must be chosen as large as possible. The smearing parameter of 0.2 eV has been found to be optimal for reasonable convergence suggesting the electronic entropy contribution of the order of 10 meV.

IVg. NELMDL. This key gives the number of *non*-self-consistent steps at the beginning: if one initializes the wave functions randomly, the initial wave functions are far from anything reasonable. Choice of key "delay" for starting the charge density update becomes essential in all cases where the convergence is very poor [49]. In UN calculations, this value has been increased 3-5 times as compared to the default value (15-25 steps *vs.* 5 default steps).

IVh. ALGO. Different algorithms are implemented into *VASP* code. For example, fast but rough RMM-DIIS algorithm [49, 61] *vs.* slow but accurate Davidson blocked algorithm [49, 62]. Our experience shows that only application of the Davidson algorithm leads to reliable results. Unfortunately, computer recourses are always limited and calculations for some systems are very time-consuming. To resolve this problem for especially hard calculations, we have splitted calculations within two stages. At first stage, we have used RMM-DIIS to obtain roughly-relaxed geometry and approximate electronic density. At second stage, we have started from geometry and electronic density relaxed at first stage, using Davidson algorithm to obtain final results. This approach significantly decreases computational expenses for many complicated systems.

3.6. Computational parameters in LCAO *CRYSTAL-06* code

For LCAO calculations, the *CRYSTAL-06* code have been used [63], which applies the Gaussian-type functions centered on the atomic nuclei as the basis sets for expansion of the linear combination of atomic orbitals (LCAO) combined with the non-local exchange-correlation functional PBE [64]. The oxygen basis set (BS) 8-411G(1*d*) has been taken from Ref. [65]. For the N atom, the all-electron BS 6-311G(2*d*) has been used [66]. Finally, for the U atom, the three energy-adjusted relativistic core effective potentials have been used (the pseudopotential of Stuttgart-Cologne group, SC60, with 60 electrons in the core [67] as well as the two Mosyagin-Titov large-core (MT78) and small-core (MT60) pseudopotentials with 60 and 78 electrons in the core, respectively [68]) To avoid linear dependence of basis set in the *CRYSTAL* LCAO calculations, the diffuse *s*-, *p*-, *d*- and *f*- Gaussian-type orbitals with exponents < 0.2 a.u.$^{-1}$ have been removed from the basis sets. The exponents of other polarization functions have been reoptimized, to restore the required precision in the total energy. Prior to a study of surface properties, the bulk structure optimization of UN crystal has been performed using the LCAO approach. The Monkhorst-Pack scheme with 16 × 16 × 16 *k*-point mesh for the BZ sampling [59] and 32 × 32 × 32 *k*-point Gilat net for the calculation of the Fermi energy and density matrix [69] have been used for this purpose.

3.7. Slab model and defect periodicity

When performing PAW surface calculations, we simulate the UN surface using the symmetrical slabs containing odd number of atomic layers and separated by the vacuum gap of 38.9 Å which corresponds to 16 inter-layers for UN(001) surface (Fig. 3.1). These vacuum gaps are large enough, to exclude the direct interaction between the neighboring 2D slabs within 3D slab model. LCAO calculations do not require artificial repetition of 2D slab along the normal to the surface direction as it is realized in PW calculations.

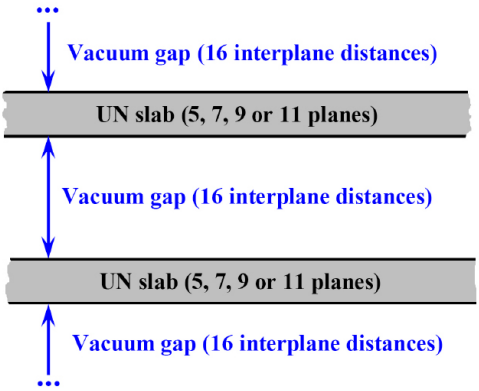

Figure 3.1. Cross-section of 3D model for UN slab.

To simulate single point defects (either N or U vacancies) and oxygen atom adsorbed on surface or incorporated into pre-existing vacancy as well as to reduce lateral interactions between them, we have applied a supercell approach, using 2 × 2 and 3 × 3 extensions of primitive unit cell (Fig. 3.2). These supercells contain four (2 × 2 supercell) and nine (3 × 3 supercell) pairs of N and U atoms in each defectless layer while periodically distributed surface vacancies (or oxygen atoms/molecules) *per* surface cell correspond to defect (oxygen) concentrations of 0.25 and 0.11 monolayers (ML), respectively. To reduce computational efforts, we have often considered the two-sided arrangement of the point defects which is symmetrical with respect to the central (mirror) plane. The suitable choice of supercell size is especially significant question. From one side, larger supersell is much closer to the model of isolated defect, on the other hand, this supercell requires considerably larger computational resourses (for example, 3 × 3 UN 7-layer supercell contains 126 atoms, *i.e.*, 2.25 times larger as compared to 56 atoms in 2 × 2 UN 7-layer supercell). In present study, we perform analysis of the finite-size effects in supercells of different sizes, to estimate deviation from the model of isolated defect.

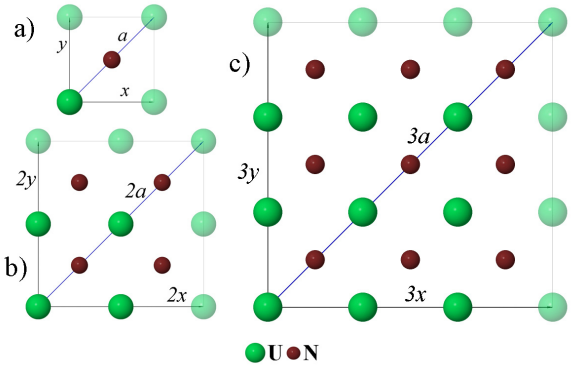

Figure 3.2. Atop views of primitive cell (a) as well as 2 × 2 (b) and 3 × 3 (c) supercells upon UN(001) surface. Here *x* and *y* axes coincide with directions of surface translation vectors while *a* is lattice constant. Half-shaded atoms show borders of chosen surface cells.

4. Modeling of UN bulk

The global aim of this stydy is to understand the mechanism of oxygen adsorption as well as further oxidation of uranium nitride. The first step of the current theoretical study is to develop methodology for correct description of ideal bulk and surface properties as performed in Refs. [P1, P4]. At a second step, this methodology can be applied to study defective surfaces as well as adsorption of oxygen atoms and molecules on perfect or defective surface. The results of DFT-PW calculations on UN bulk, perfrect surface and atomic oxygen adsorption upon it were compared with the corresponding DFT-LCAO results obtained by group of Prof. R.A. Evarestov (*St. Petersburg State University*).

Before calculations on UN surface, we must consider UN bulk and estimate its bulk properties. The main results obtained in bulk calculations are collected in Table 4.1, which shows that the cohesion energy E_c is essentially underestimated in LCAO MT78 calculations and slightly underestimated in PW calculations. The value of E_c is close to the experimental value in while in LCAO MT60 and SC60 calculations. As to the lattice parameter *a*, its DFT-LCAO values are underestimated (4.78 Å and 4.80 Å) but they do not differ too much from those obtained in DFT-PW calculations performed by us and other authors, being very close to experimental value. The optimized lattice constant (4.87 Å for PAW *VASP vs.* 4.81 Å for LCAO *CRYSTAL* calculations) has been used in all our further calculations.

Table 4.1. The results of calculations on UN bulk: the cohesive energy E_c (eV), the lattice constant a_0 (Å) and the bulk modulus B (GPa). The experimental values are given in brackets in the first column. The spin density (SD) for U atom is given in μ_B.

Property (experimental [1])	PW (*VASP*)		PW (other theoretical studies)		LCAO (Prof. R. Evarestov group)		
	PW91	PBE	PW91 PAW [33]	PBE AE-LAPW [20, 25]	MT78	MT60	SC60
a_0, Å (4.886)	4.868	4.867	4.864	4.886	5.17	4.78	4.80
E_c, eV (13.6)	14.79	14.57	14.7	13.4	9.6	13.4	13.6
B (194)	227	224	226	209	167.2	291.6	276.9
Q_U, *e*	1.69	1.69	1.61	-	1.63	1.55	1.58
SD, μ_B	1.15	1.19	1.05	1.25	3.18	1.18	1.06

The bulk modulus *B* is overestimated in both PW and LCAO (MT60 and SC60) calculations and underestimated in MT78 calculations. The calculated effective charge of U atom (Q_U) in UN is close to 1.6 *e* for all three LCAO RECP pseudopotentials used and comparable to 1.7 *e* for PW calculations using the topological Bader analysis. A comparison of LCAO (RECP 60) and the PW (RECP 78) results demonstrates a qualitative correlation of properties calculated using both methods, except for bulk modulus which is noticeably overestimated in the *CRYSTAL* calculations as compared to the experimental value.

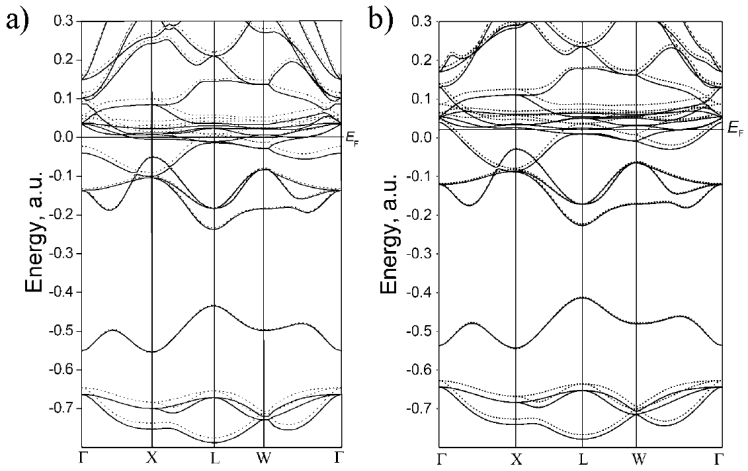

Figure 4.1. The energy bands of UN crystal constructed using: a) PW PW91 (RECP SC78) and b) LCAO PW91 (RECP SC60) Hamiltonians. The energies are given in a.u., solid and dotted lines correspond to the states with spin up and spin down, respectively.

The band structures for UN bulk calculated using the two above-mentioned methods (DFT and LCAO), when applying the same PW91 Hamiltonian, are presented in Fig. 4.1. Band structures demonstrate good correlation between both approaches, even at quantitative level, especially below the Fermi level, being in agreement with the experiment [12] and the DOS analysis performed in previous PW *VASP* calculations [34].

The results of DFT-PW calculations on the lattice constant, bulk modulus, cohesive energy, charge distribution and band structure for UN single crystal are obtained. The results of DFT-PW calculations on UN bulk were compared with the corresponding DFT-LCAO results obtained by group of Prof. R.A. Evarestov. The results of PW and LCAO calculations on UN bulk demonstrate a good qualitative agreement between them.

5. Structural properties of UN (001) and (110) surfaces

Synthesized specimens of polycrystalline UN contains particles with differently oriented crystallographic facets [9]. To simplify modeling of the oxygen interaction with UN surface, we study in this PhD work mainly the (001) surface since according to Tasker analysis [70] it has the lowest surface energy. Nevertheless, real UN particles (Fig. 2.2) contain facets with different crystallographic orientation. To increase validity of our results, we have additionally performed (110) surface calculations. We chose (110) surface orientation for additional calculations since alternative low-indiced (111) surface contains charged planes and its calculation requires artificial approaches. Moreover, strong reconstruction must occur, in order to stabilize polar (111) surface, similarly to MgO(111) [71]. Less densely-packed UN(110) surface is characterized by smaller interlayer distance in *z* direction as compared to (001) surface (Table 5.1 and Fig. 5.1).

Table 5.1. Comparison between the UN(001) and UN(110) surfaces (*a* is a lattice constant of cubic *fcc* crystal).

	(001) surface	**(110) surface**
Size of surface unit cell (Å x Å)	3.44 × 3.44 $(\frac{\sqrt{2}}{2}a \times \frac{\sqrt{2}}{2}a)$ or $(\frac{1}{2}a \times a)$	4.87 × 3.44 $(a \times \frac{\sqrt{2}}{2}a)$
Distance between two nearest U and U (or N and N) atoms in *xy* plane (Å)	3.44 $(\frac{\sqrt{2}}{2}a)$ in both directions	4.87 in *x* direction 3.44 in *y* direction
Distance between nearest U and N atoms in *xy* plane (Å)	2.435 $(\frac{a}{2})$	2.435 $(\frac{a}{2})$ in *x* direction not defined in *y* direction
Distance between neighbor layers in z direction (Å)	2.435 $(\frac{a}{2})$	1.72 $(a\frac{\sqrt{2}}{4})$
Distance between nearest atoms in *z* direction (Å)	2.435 $(\frac{a}{2})$, distance between U and N atoms	3.44 $(\frac{\sqrt{2}}{2}a)$, distance between N and N (or U and U) atoms

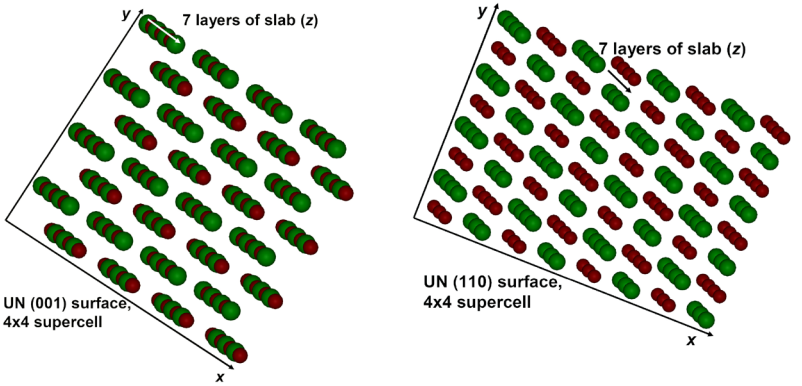

Figure 5.1. Structural comparison of slabs used for simulation of (001) (a) and (110) (b) UN surfaces.

We simulated reconstruction of perfect and defective UN(110) surface as well as atomic oxygen adsorption, formation of N vacancies and oxygen incorporation into them. These results are distributed in the corresponding subsections of Sections 6-8.

6. Modeling of perfect UN surface

As has been mentioned in Section 2.1, experiment shows that UN bulk undergoes the AFM ordering below 53 K [5]. We have performed the calculations on both FM and AFM states. Our PAW test calculations on UN bulk have shown that the FM phase is energetically slightly more favorable than AFM phase. Analogous results were obtained using LCAO method as applied by group of Prof. R.A. Evarestov. Due to a small diference between the energies in FM and AFM states (~0.001-0.01 eV) and due to a complicated magnetic structure of UN surface [31], only FM state has been considered in our UN surface calculations.

6.1. Spin-frozen PW and LCAO calculations on defectless UN(001) surface

Analogously to perfect bulk calculations, we compare results of PW and LCAO calculations on UN(001) surface. Aperiodic (2D) and periodic (3D) models in regards to the direction normal to the slab have been used for LCAO and PW calculations, respectively [51].

We have analyzed in detail the vertical displacements (along *z* axis) of both surface and subsurface atoms from their host lattice sites in UN bulk (Table 6.1), effective atomic charges (Table 6.2), the surface energies (Table 6.3) as well as DOS obtained in the PW calculations (Fig. 6.2).

Surface energy of an *n*-layer slab has been estimated from the standard basic relationship:

$$E_{surf}(n) = \frac{1}{2S}(E_n - nE_b) \qquad \textit{(Eq. 6.1.1)}$$

where E_n is the total slab energy *per* primitive surface unit cell and *S* its area, while E_b the total energy *per* primitive bulk unit cell (Fig. 6.1).

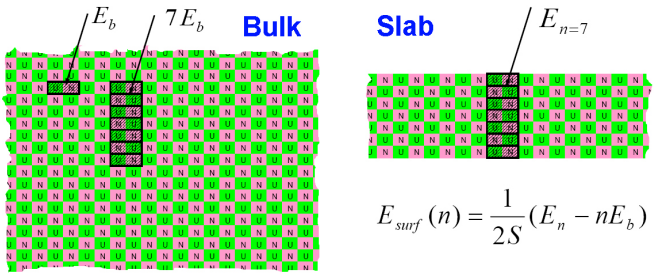

Figure 6.1. Surface energy calculated for 7-layer slab. E_n is the total slab energy *per* primitive surface unit cell, E_b is the total energy *per* primitive bulk unit cell, n is number of layers, S is unit cell surface area.

There is a good qualitative agreement between structural relaxations and effective atomic charges for the LCAO and PW data. First of all, in both methods atomic displacements have the same directions: N atoms go outside the surface whereas U atoms relax towards the slab center. This is a pattern typical for the rumpling observed on oxide surfaces. There have been also observed substantially larger magnitudes of surface U displacements as compared to N atoms, whereas subsurface atom relaxations are smaller.

Table 6.1. The calculated atomic displacements Δz (Å) on UN(001) obtained for different slabs and methods. Positive sign means an outward displacement from the slab center.

Atom	Method	Number of atomic layers in slab				
		3	5	7	9	11
surface U	LCAO	-0.085	-0.095	-	-	-
	LCAO (extra layer added)	-0.026	-0.046	-	-	-
	PW PW91	-0.041	-0.046	-0.050	-0.061	-0.057
subsurface U	LCAO		-0.011	-	-	-
	LCAO (extra layer added)		-0.013	-	-	-
	PW PW91		-0.018	-0.016	-0.013	-0.013
surface N	LCAO	0.064	0.058	-	-	-
	LCAO (extra layer added)	0.049	0.025	-	-	-
	PW PW91	0.030	0.022	0.025	0.033	0.026
subsurface N	LCAO		-0.002	-	-	-
	LCAO (extra layer added)		0.014	-	-	-
	PW PW91		0.026	0.028	0.032	0.022

Table 6.2. The effective atomic charges $q(e)$ on UN(001) slab

Atom	Method	Number of atomic layers in slab				
		3	5	7	9	11
surface U	LCAO	1.63	1.63	-	-	-
	LCAO (extra layer added)	1.64	1.64	-	-	-
	PW PW91	1.65	1.66	1.72	1.67	1.65
subsurface U	LCAO	-	1.51	-	-	-
	LCAO (extra layer added)	-	1.55	-	-	-
	PW PW91	-	1.65	1.63	1.63	1.69
middle U (mirror plane of slab)	LCAO	1.45	1.57	-	-	-
	LCAO (extra layer added)	1.52	1.55	-	-	-
	PW PW91	1.62	1.67	1.72	1.65	1.62
surface N	LCAO	-1.55	-1.55	-	-	-
	LCAO (extra layer added)	-1.61	-1.60	-	-	-
	PW PW91	-1.64	-1.63	-1.64	-1.63	-1.67
subsurface N	LCAO	-	-1.59	-	-	-
	LCAO (extra layer added)	-	-1.57	-	-	-
	PW PW91	-	-1.67	-1.7	-1.64	-1.7
middle N (mirror plane of slab)	LCAO	-1.61	-1.58	-	-	-
	LCAO (extra layer added)	-1.58	-1.57	-	-	-
	PW PW91	-1.65	-1.7	-1.66	-1.62	-1.64

The surface energies are partly stabilized for slabs containing at least 5-7 layers whereas the relaxation energy is more sensitive to the thickness (Table 6.3). Due to scarceness of experimental results, the calculated values of surface energy could be qualitatively compared only with 1.2 J/m^2 obtained recently for UO_2(001) surface energy using the first-priciples calculations [46]. As one can see, the surface energies of these surfaces are predicted to be similar. A qualitative agreement is observed between the UN(001) surface energies obtained using both LCAO and PW calculations.

Table 6.3. Surface energies E_{surf} (J · m^{-2}) and relaxation energies E_{rel} (eV) obtained for UN(001) surface in LCAO and PW calculations

Number of atomic layers in slab			3	5	7	9	11
Method	LCAO	E_{surf} (unrelaxed)	2.20	2.29	2.28	2.11	-
		E_{surf} (relaxed)	2.06	2.13	-	-	-
		E_{rel}	0.203	0.230	-	-	-
	LCAO (extra layer added)	E_{surf} (unrelaxed)	1.68	1.45	-	-	-
		E_{surf} (relaxed)	1.430	1.38	-	-	-
		E_{rel}	0.359	0.121	-	-	-
	Plane waves PW91	E_{surf} (unrelaxed)	1.81	1.87	1.84	1.86	1.90
		E_{surf} (relaxed)	1.70	1.69	1.70	1.70	1.69
		E_{rel}	0.156	0.258	0.210	0.239	0.305

The total and projected DOSs in the FM state obtained in our PAW calculations are present in Fig. 6.2. There is a small difference in band shapes as compared to previous UN bulk calculations [34], due to noticeably higher *k*-point mesh and cut-off energy used in our studies. A comparison of the bulk DOS (Fig. 6.2a) with that for the projections of the surface U and N atoms (Fig. 6.2b) shows mainly changes in the shape of unoccupied states above the Fermi level. In both cases, the mixed metallic-covalent bonding is observed for U(*5f*) states at the Fermi level which confirms results of previous experimental and theoretical studies.

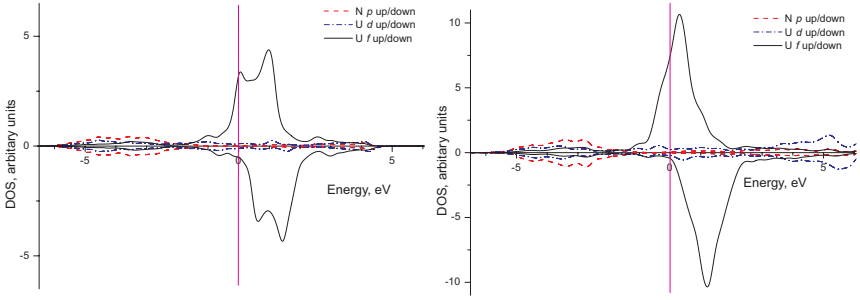

Figure 6.2. The projected DOS for UN bulk (a) and for perfect 7-layer UN(001) slab (b) in FM states.

6.2. Spin-relaxed PW calculations of defectless UN (001) and (110) surfaces

The results obtained in spin-relaxed PAW calculations on perfect UN (001) and (110) surfaces (Fig. 6.3) are discussed. The calculations of the effective atomic charges q^{eff}, atomic displacements Δr, average magnetic moments μ_{av} of U atoms, and surface energies E_{surf} for defect-free slabs of different thicknesses (Tables 6.4 and 6.5) have been performed, in order to check how these properties depend on atomic spin relaxation [P4]. The spin relaxation leads to considerable change of the E_{surf} depending on the number of layers in a slab (Table 6.4). The largest μ_{av} value was obtained for U atoms in the 5-layer slab, *i.e.*, μ_{av} slightly decreases with the thickness suggesting difference of 0.3 μ_B between the 5- and 11-layer slabs. The lattice relaxation energies in spin-relaxed calculations turn out to be quite small, *i.e.*, ~0.03 eV.

Depending on slab thickness, the surface energies are ~0.5-0.7 J·m^{-2} larger for UN(110) surface (Table 6.4). It means that the UN(001) surface is energetically more favorable.

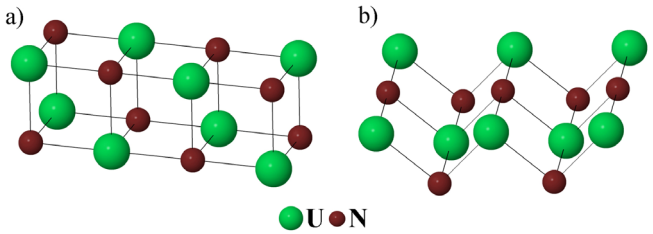

Figure 6.3. 2-layer models of UN(001) (a) and UN(110) (b) surfaces.

Table 6.4. Surface energies E_{surf} (J·m^{-2}) as well as averaged magnetic moment (in μ_B) of U atom for the defectless UN(001) and UN(110) surfaces. In spin-frozen calculations, μ was chosen to be 1 μ_B

Number of atomic layers	E_{surf} (J·m^{-2}) spin-frozen slab (001)	E_{surf} (J·m^{-2}) spin-relaxed slab (001)	μ_{av}(μ_B) (001)	E_{surf} (J·m^{-2}) spin-relaxed slab (110)	μ_{av}(μ_B) (110)
5	1.69	1.44	1.57	1.977	1.645
7	1.70	1.37	1.44	1.928	1.464
9	1.70	1.29	1.37	1.878	1.417
11	1.69	1.22	1.33	1.830	1.385

It is also interesting to analyze q^{eff} values for atoms across the slab as a function of the number of layers in a slab (Table 6.5). First, these q^{eff} show considerable covalent bonding both on the surface (*e.g.*, sub-surface) and on the central plane since the values. Second, due to different reconstruction mechanisms of UN(001) and UN(110) surfaces, the atomic charges are different too: ionicity of bonds at (001) surface is higher, thus leading to certain difference in surface properties. Third, the atomic charges depend on

both the spin relaxation and the number of layers (*cf.* results of spin-relaxed calculations and spin-frozen PW calculations presented in Tables 6.5 and 6.2, respectively).

Table 6.5. Atomic Bader charges for the defectless spin-relaxed UN (001) and (110) surfaces.

	Number of UN(001) slab atomic layers				Number of UN(110) slab atomic layers			
Atom	**5**	**7**	**9**	**11**	**5**	**7**	**9**	**11**
Surface U	1.68	1.74	1.68	1.72	1.46	1.48	1.49	1.48
Sub-surface U	1.67	1.63	1.63	1.67	1.88	1.85	1.83	1.84
U in central (mirror) plane	1.69	1.72	1.65	1.66	1.60	1.74	1.64	1.70
Surface N	-1.65	-1.67	-1.67	-1.68	-1.55	-1.55	-1.55	-1.55
Sub-surface N	-1.68	-1.70	-1.70	-1.67	-1.75	-1.73	-1.75	-1.73
N in central (mirror) plane	-1.74	-1.65	-1.65	- 1.63	- 1.70	-1.71	-1.75	-1.74

Table 6.6. Atomic displacements Δz(Å)* for defectless UN (001) and (110) surfaces.

Number of atomic layers	U atom displacements				N atom displacements			
	(001) surface		(110) surface		(001) surface		(110) surface	
	Surface	**Sub-surface**	**Surface**	**Sub-surface**	**Surface**	**Sub-surface**	**Surface**	**Sub-surface**
5	-0.050	-0.012	-0.053	-0.005	0.023	0.023	-0.279	0.068
7	-0.046	-0.009	-0.038	-0.009	0.024	0.028	-0.272	0.092
9	-0.047	-0.011	-0.042	-0.014	0.024	0.028	-0.279	0.091
11	-0.047	-0.011	-0.015	0.015	0.025	0.031	-0.252	0.118

* negative sign means an inward atomic displacement towards the mirror plane of slab

The atomic displacements Δz from perfect lattice sites differ significantly for U atoms positioned at the surface and sub-surface layers (Table 6.6) being somewhat larger for the 5-layer slab while displacements of nitrogen atoms for all the slabs remain almost unchanged. Note that N atoms on (001) surface are displaced up whereas U atoms are shifted inwards the slab center which results in the surface rumpling up to 1.2% of the lattice constant. In contrary, the surface U atoms of rumpled UN(110) surface lie higher than the corresponding N atoms which well illustrates the difference of charges and other surface properties mentioned above.

6.3. Perfect UN surface calculations: summary

Our defectless surface modeling shows metallic properties of UN surface, analogously to previous bulk calculations. We compared results for DFT PW and LCAO calculations and found a good corellation between both approaches. Comparison of UN(001) and UN(110) surfaces shows that the former is energetically more favorable. The surface energies depending of slab thickness are equal to 1.22-1.44 $J \cdot m^{-2}$ for UN(001) *vs.* 1.83-1.98 $J \cdot m^{-2}$ for UN(110) surface. This fact allow us to perform both calculations on defectless UN surface and oxygen adsorbtion upon the (001) surface mainly.

7. Modeling of single N and U vacancies

7.1. Vacancy calculations: model and formation energies

To understand the oxidation mechanism in more detail, one has to take into account *surface defects* and their interaction with oxygen. For this reason, we studied basic properties of *surface* vacancies [P4]. We have calculated not only the outermost surface defects, but also the sub-surface defects as well as those positioned at the central layer of the slab. We have considered the two-sided arrangement of the point defects which is symmetrical with respect to the central (mirror) plane (the atomistic model of surface N vacancies with the 2 × 2 periodicity of defects is shown in Fig. 7.1). The FM state has been chosen for all our slab calculations performed for the self-consistent (relaxed) atomic magnetic moments with no spin-orbit interactions included. We have performed the total spin relaxation in the system.

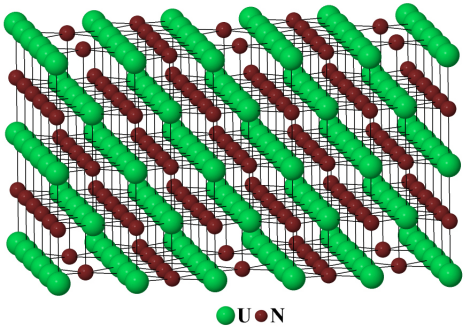

Figure 7.1. 5-layer UN(001) slab containing the two-sided surface N vacancies distributed with a 2 × 2 periodicity.

The formation energy of point defect is calculated either as

$$E_{form}^{\mathrm{N(U)}vac} = \frac{1}{2}\left(E^{\mathrm{UN(U/N\_vac)}} + 2E_{ref\_\mathrm{I(II)}}^{\mathrm{N(U)}} - E^{\mathrm{UN}}\right), \qquad \textit{(Eq. 7.1.1a)}$$

for surface and sub-surface vacancies, or

$$E_{form}^{\mathrm{N(U)}vac} = E^{\mathrm{UN(U/N\_vac)}} + E_{ref\_\mathrm{I(II)}}^{\mathrm{N(U)}} - E^{\mathrm{UN}}, \qquad \textit{(Eq. 7.1.1b)}$$

for a vacancy in the central layer of the slab. Here $E^{\mathrm{UN(U/N\_vac)}}$ is the total energy of fully relaxed slab containing N (or U) vacancies, E^{UN} the same for a defect-free slab, while $E_{ref\_\mathrm{I(II)}}^{\mathrm{N(U)}}$ is reference energy for N (or U) atom. In the present study, we have considered the two reference states for calculations of the defect formation energy, both are widely used in the literature.

The first reference corresponds to N (U) isolated atom in triplet (quartet) spin states determined by $2p^3$ ($5f^36d^1$) valence electron configurations (hereafter, reference I as in Table 7.1) calculated in a large rectangular parallelepiped box (28.28 × 28.28 × 22 Å^3), *i.e.*:

$$E^{\mathrm{N(U)}}_{ref\_\mathrm{I}} = E^{\mathrm{N(U)}}_{atom}. \qquad \textit{(Eq.7.1.2)}$$

The second reference state (hereafter, reference II as in Table 7.1) represents the chemical potential of N (U) atom which is defined as a function of temperature and partial nitrogen pressure. By neglecting these effects, the N chemical potential can be treated as the energy of atom in the molecule N_2. Consequently, the chemical potential of U atom is given by the one-half total energy (*per* unit cell) of U single crystal in its low-temperature α-phase having the orthorhombic structure [72]. Thus, the corresponding second reference energies can be estimated as:

$$E^{\mathrm{N}}_{ref\_\mathrm{II}} = \mu_{\mathrm{N}_2} = \frac{1}{2} E_{tot}\left[\mathrm{N}_2\right], \qquad \textit{(Eq.7.1.3a)}$$

$$E^{\mathrm{U}}_{ref\_\mathrm{II}} = \mu_{\alpha\text{-U}} = \frac{1}{2} E_{tot}\left[\alpha\text{-U}\right], \qquad \textit{(Eq.7.1.3b)}$$

where $E_{tot}[N_2]$ is the total energy of nitrogen molecule while E_{tot}[α-U] the total energy of U bulk unit cell containing two atoms. The chemical potentials of N and U, as calculated according to *Eq. 7.1.3*, represent extreme cases of N(U)-rich conditions [73], *i.e.*, their minimum values have not been considered in the present study. The formation energy of N (U) vacancy with respect to the N_2 molecule (or α-U single crystal) and the energy of N (U) isolated atom are closely related: the former being larger than the latter by half the binding energy of the N_2 molecule or half the cohesive energy of α-U single crystal.

The optimized lattice parameters of α-U (a = 2.80 Å, b = 5.88 Å, c = 4.91 Å) have been slightly underestimated as compared to values obtained experimentally [72] and calculated elsewhere [74, 75], except for the parameter b which is in a good agreement with experimental value of 5.87 Å [72] (while a = 2.86 Å, c = 4.96 Å [72]). Also, the ratios c/a, b/a as well as the parameter c are well verified by another plane-wave DFT study [41]. Analogously to an isolated nitrogen atom, the N_2 molecule has been calculated in the cubic box but of a smaller size ($8 \times 8 \times 8$ Å^3). The molecule N_2 is characterized by the bond length of 1.12 Å and the binding energy of 10.63 eV being well comparable with the experimental values of 1.10 Å and 9.80 eV [76], respectively. The pre-factor of ½ in *Eq. 7.1.1a* arises due to a mirror arrangement of two N(U) vacancies on the surface and sub-surface layers (Fig. 7.1).

The formation energies of N and U vacancies ($E^{\mathrm{N(U)}\,vac}_{form}$) calculated using *Eqs. 7.1.1-7.1.3* (with the two reference states) as functions of the slab thickness are collected in Table 7.1. These are smallest for the surface layer and considerably increase (by ~0.6 eV for the N vacancy and by ~1.7 eV for the U vacancy) in the sub-surface and central layers, independently of the reference state. This indicates the trend for vacancy segregation at the interfaces (surface or crystalline grain boundaries). A weak dependence of $E^{\mathrm{N(U)}\,vac}_{form}$ on the slab thickness is also observed. The value of $E^{\mathrm{N(U)}\,vac}_{form}$ is saturated with the slab thicknesses of seven atomic layers and more. Moreover, the difference between values of $E^{\mathrm{N(U)}\,vac}_{form}$ for the 5- and 7-layer slabs is less for the surface vacancies than for those in the central layer. This difference is the largest for the U vacancy in the central plane (~0.16 eV).

The reference state II leads to smaller $E_{form}^{N(U)\,vac}$ (as compared to those found for the reference state I) and demonstrates a significant difference for two types of vacancies. According to reference II, the U vacancy could be substantially easier formed at T = 0 K than the N vacancy. Notice that the chemical potentials of O and U atoms used in similar defect studies on UO_2 bulk did not reveal the energetic preference for U vacancy [75, 77]. The defect-defect interaction is not responsible for this effect as $E_{form}^{N(U)\,vac}$ decreased by 0.1 eV only with the larger supercell size (3 × 3 in Table 7.1). On the other hand, due to the temperature dependence of the chemical potential of a free N_2 molecule [78], we predict reduction of the formation energy of the N vacancy by ~0.8 eV as the temperature increases from room temperature up to 1000 °C. Unlike the reference state II, the reference I results in similar formation energies for both types of the vacancies. In the central slab layer, values of $E_{form}^{N(U)\,vac}$ are similar to those in the bulk (Table 7.1).

Table 7.1. The vacancy formation energies (in eV) for the two reference states (see the text for details).

Layer	Number of layers and supercell size	Reference I, Eqs. (7.1.1a)–(7.1.2)[a]		Reference II, Eqs. (7.1.1a), (7.1.1b), (7.1.3a) and (7.1.3b)[b]	
		U	N	U	N
Surface layer	5, 2 × 2	8.63	8.84	1.46	3.70
	7, 2 × 2	8.61	8.84	1.44	3.70
	9, 2 × 2	8.61	8.84	1.44	3.71
	11, 2 × 2	8.60	8.85	1.43	3.71
	5, 3 × 3	8.51	8.78	1.34	3.64
	7, 3 × 3	8.47	8.78	1.30	3.65
Sub-surface layer	5, 2 × 2	10.31	9.38	3.14	4.25
	7, 2 × 2	10.29	9.46	3.12	4.33
	9, 2 × 2	10.26	9.46	3.09	4.33
	11, 2 × 2	10.26	9.46	3.09	4.33
	7, 3 × 3	10.18	9.47	3.01	4.34
Central (mirror) layer[c]	5, 2 × 2	10.20	9.48	3.03	4.34
	7, 2 × 2	10.36	9.57	3.19	4.43
	9, 2 × 2	10.34	9.55	3.17	4.42
	11, 2 × 2	10.39	9.56	3.22	4.42
	7, 3 × 3	10.23	9.55	3.06	4.42

[a] reference energies I equal to -4.10 eV for U atom and -3.17 eV for N atom,
[b] reference energies II equal to -11.28 eV for U atom and -8.30 eV for N atom,
[c] defect formation energies for UN bulk using reference state I are 9.1-9.7 eV for N vacancy and 9.4-10.3 for U vacancy [34]

7.2. Surface reconstruction induced by vacancies

The local atomic displacements around the vacancies are largest for the nearest neighbors of vacancies. The analysis of atomic displacements allows us to suggest that the U vacancy disturbs the structure of the surface stronger than the N vacancy. If the N vacancy lies in the surface layer, displacements of the nearest U atoms in *z*-direction achieve 0.02-0.05 Å towards the central plane of slab. The displacements of N atom nearest

to surface N vacancy achieve 0.05 Å towards the central plane (*z*-direction) and 0.01 Å in the surface plane (*xy*-displacement). Maximum displacements of neighbor atoms around the N vacancy in the central plane have been found to be 0.04-0.07 Å (nearest U atoms from the neighboring layers are shifted in *z*-direction towards the vacancy) not exceeding 0.025 Å for all the other atoms in the slab.

In contrary, the U vacancy results in much larger displacements of neighboring atoms, irrespectively of its position. If this vacancy lies in the surface layer, the displacements of 0.3-0.32 Å for the nearest N atoms are observed. If the U vacancy lies in the central layer, the nearest N atoms from this layer are displaced by 0.17 Å while the N atoms from the nearest layers are not shifted in *xy*-direction, being shifted by 0.15 Å towards the slab surface in the *z*-direction. The atomic displacements around the vacancies in the UN bulk have been found to be –0.03 Å and 0.13 Å for N and U vacancies, respectively [34]. These values are close to those found in the present calculations for the vacancies in the central slab layer, which mimics the crystal bulk.

7.3. Electronic properties: Finite-size effects and choice of supercell size

The finite slab-size effects caused by relatively large concentration of defects could be illustrated using the difference electron density redistribution $\Delta\rho(\mathbf{r})$. In Fig. 7.2, these redistributions are shown for N vacancies positioned at both the outer (surface) and the central (mirror) planes of 5- and 7-layer slabs.

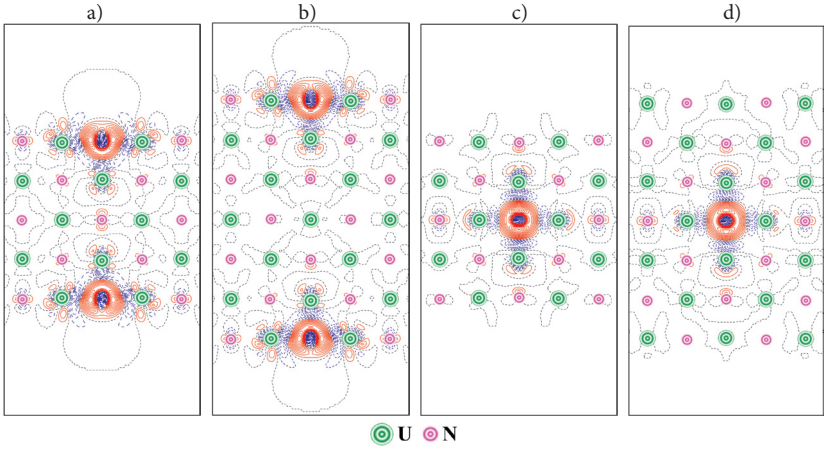

Figure 7.2. 2D sections of the electron density redistributions around the nitrogen vacancies in five- and seven-layer UN(001) slabs with 2 × 2 supercell extension defined as the total electron density of defected surface minus a superposition of the electron densities for both perfect surface and isolated atom in the regular position on the surface: a) N vacancy in a surface plane, five-layer slab, b) the same, 7-layer slab, c) N vacancy in a central plane, five-layer slab, d) the same, 7-layer slab. Solid (red) and dashed (blue) isolines correspond to positive (excess) and negative (deficiency) electron density, respectively. Isodensity increment is 0.25 e a.u.$^{-3}$.

Presence of two symmetrically positioned vacancies in the 5-layer slab induces their weak interaction across the slab (Fig. 7.2a) illustrated by appearance of an additional electron density around the N atoms in the central plane of the slab. Similarly, the vacancy in the mirror plane disturbs the atoms in the surface plane if thin slab contains only 5 layers (Fig. 7.2c). By increasing the slab thickness, we can avoid the effect of finite-slab size (Figs. 7.2b,d) which explains the stabilization of formation energies calculated for the 7-layer and thicker UN(001) slabs (Table 7.1).

The densities of states (DOS) are presented in Fig. 7.3. for both perfect and defective 7-layer UN slab. In accordance with previous bulk calculations, the U(5*f*) electrons are localized close to the Fermi level (Fig. 7.3a). These electrons are still strongly hybridized with the N(*2p*) electrons. It confirms the existence of covalent bonding observed in the analysis of Bader charges for defectless surface (Table 6.5). The N(2*p*) states form a band of the width ~4 eV, similar to that obtained in the bulk [P1, 34]. In contrast, the contribution of U(6*d*) electrons remains insensitive to the presence of vacancies since the corresponding levels are almost homogeneously distributed over a wide energy range including the conduction band. The visible difference of total DOS profiles in Fig. 7.3a and Fig. 6.2b for perfect 7-layer UN(001) slab can be explained by different slab geometry relaxation when performing spin-relaxed and spin-frozen calculations, respectively.

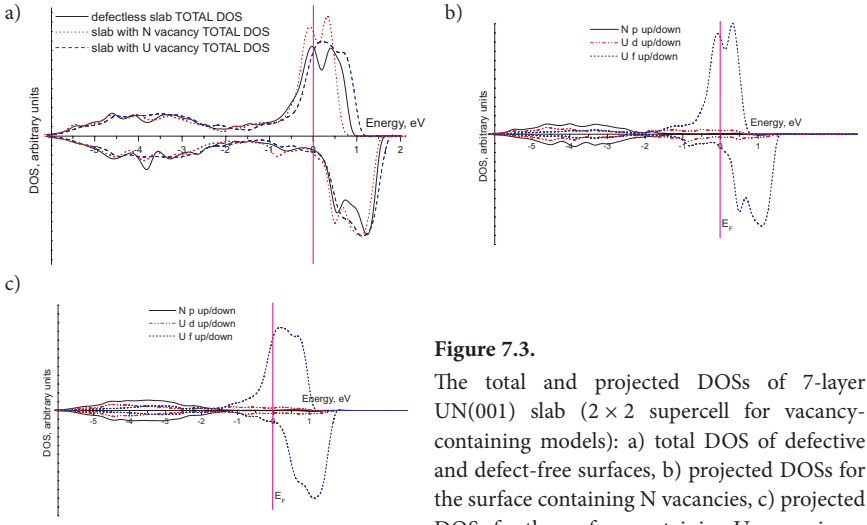

Figure 7.3.
The total and projected DOSs of 7-layer UN(001) slab (2 × 2 supercell for vacancy-containing models): a) total DOS of defective and defect-free surfaces, b) projected DOSs for the surface containing N vacancies, c) projected DOSs for the surface containing U vacancies.

7.4. Magnetic properties

The analysis of the averaged magnetic moment of U atoms (μ_{av}^{U}) in the defective UN slabs is done too (Fig. 7.4). It decreases for both types of vacancies as a function of a number of layers in the slab, except for the U vacancy in the surface layer which remains

almost unchanged. On the other hand, μ_{av}^{U} increases significantly when the U vacancy is located in the subsurface and surface layers. In contrast to the U vacancies, μ_{av}^{U} for the slabs with the N vacancies are less sensitive to the position of defect, they are practically identical for the slabs with the N vacancies in the surface and subsurface planes.

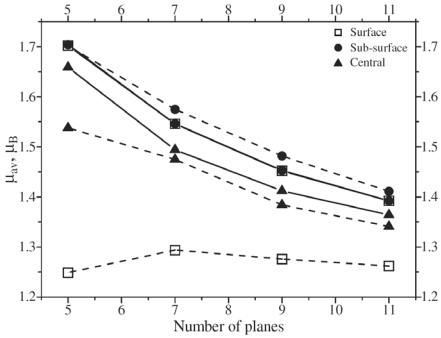

Figure 7.4. The averaged U magnetic moment μ_{av} (in μ_B) in the slab as a function of a number of planes. The dashed curves correspond to U vacancy whereas the solid curves describe the N vacancy.

7.5. Comparison of results for N vacancies on UN (001) and (110) surfaces

To increase the reliability of the results we also compare the results of calculations on N vacancies in surface layer upon UN(001) with analogous calculations on (110) surface (Fig. 7.5). For (110) surface, we have used 5-, 7-, 9- and 11-layer 2 × 2 surface supercells as well as 7-layer 3 × 3 supercell. Obtained results are presented in Table 7.2. All basic tendencies remain similar for vacancies on (110) surface. Averaged magnetic moment μ_{av} decreases as a function of a number of layers in the slab for both surfaces. On the other hand, vacancy formation energies are by ~0.7 eV smaller for UN(110) surface. This distinction is easy explainable due to a larger friability of the (110) surface as compared to the (001) surface.

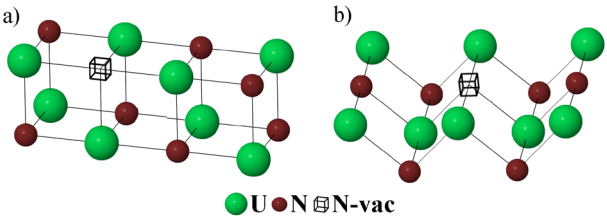

Figure 7.5. 2-layer models of N vacancy on UN (001) (a) and (110) (b) surface.

Table 7.2. Nitrogen vacancy formation energies (in eV) as well as averaged magnetic moment μ_{av} of U atom evaluated for UN (001) and (110) surfaces.

Number of layers and supercell size	N vacancy E_{form} on (001) surface	$\mu_{av}(\mu_B)$ (001)	N vacancy E_{form} on (110) surface	$\mu_{av}(\mu_B)$ (110)
5, 2 × 2	3.700	1.702	3.075	1.818
7, 2 × 2	3.706	1.548	3.028	1.585
9, 2 × 2	3.708	1.452	3.036	1.512
11, 2 × 2	3.712	1.392	3.026	1.453
7, 3 × 3	3.646	1.487	2.966	1.498

7.6. Vacancy calculations: summary

The formation energies for U and N vacancies have been determined using the two reference states, which include the energies of isolated atoms as well as atoms in the metallic α-U phase and N_2 molecule, respectively. The formation energies have indicated a clear trend for segregation towards the surface (and probably, grain boundaries) as these energies for surface layer are noticeably smaller than those for sub-surface and central layers (although both latter are very close). However, the magnetic moments in the subsurface and central layers differ significantly. We have demonstrated also a considerable deviation of effective atomic charges from formal charges (caused by a covalent contribution to the U-N bond).

8. Modeling of O adsorption and migration on perfect UN surface

8.1. Atomic oxygen adsorption

8.1.1. Model and theoretical background

To simulate the O atom adsorption, the 5-layer slabs with 2 × 2 supercell have been used for our PW calculations and spin-frozen LCAO calculations performed by group of Prof. R.A. Evarestov [P2]. The 5- and 7-layer 3D slabs with 2 × 2 and 3 × 3 supercells were used for our spin-relaxed PW calculations. To reduce computational efforts, we have considered symmetric two-sided arrangement of oxygen adatom (Fig. 8.1) similarly to calculations on vacancies.

Only ferromagnetic UN ground state has been considered in this study as the energetically most preferable state for low-temperature calculations. The calculations of UN bulk structure suggest the magnetic moment on the U atom ~1 μ_B. For *CRYSTAL* calculations and selected *VASP* calculations, we have fixed the total spin of the system. Thus, for five-layer slab the total magnetic moment of a 2 × 2 supercell (containing 20 U and 20 N atoms) in spin-frozen calculations was fixed at 20 μ_B.

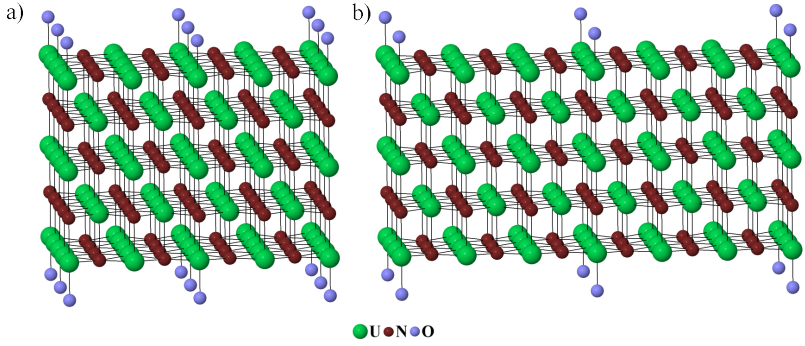

Figure 8.1. Model of O/UN(001) interface: two-sided adsorption of O atoms regularly distributed atop U_{surf} atoms with 2 × 2 (a) and 3 × 3 (b) periodicity.

The binding energy E_{bind} of adsorbed oxygen atom (O_{ads}) was calculated with respect to a free O atom:

$$E_{bind} = \frac{1}{2}\left(E^{UN} + 2E^{O_{triplet}} - E^{O/UN}\right), \qquad \textit{(Eq. 8.1.1)}$$

where $E^{O/UN}$ is the total energy of relaxed O/UN(001) slab for O_{ads} positions atop either the N or U surface ions, $E^{O_{triplet}}$ and E^{UN} the energies of an isolated O atom in the ground (triplet) state and of a relaxed UN slab. In PAW calculations, of free O atom, the

cubic box with edge ~20 Å has been used. The factor ½ before brackets appears since the substrate is modeled by slab with the two equivalent surfaces and O_{ads} is positioned symmetrically with respect to the surfaces.

8.1.2. *Comparison of spin-frozen PW and LCAO calculations on atomic adsorbtion*

The corresponding results of *VASP* and *CRYSTAL* calculations based on the two very different methods demonstrate a good qualitative agreement for O adatom properties atop the surface U atom (Fig. 8.2): the binding energies (3D slab models usually underestimate this parameter, due to a weak repulsion between the adjacent polarized slabs), atomic displacements and effective charges (which are calculated using the very different Mulliken (LCAO) and Bader (PAW) procedures).

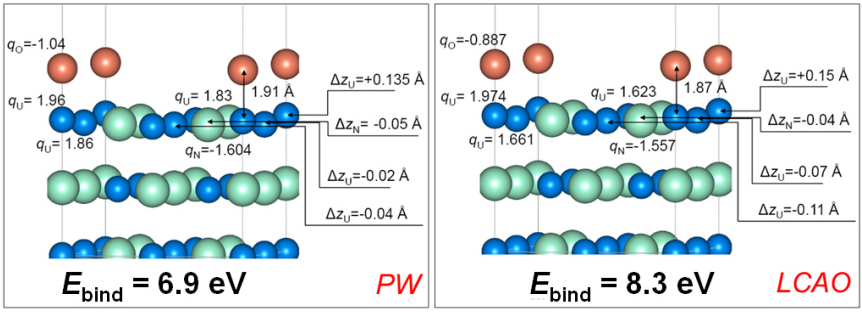

Figure 8.2. The calculated binding energy (E_{bind}), the distance between O and surface U cation ($d_{O\text{-}U}$), the effective atomic charges (q), and vertical (Δz) displacements of U and N atoms from the surface plane for adatom position atop the surface U atom calculated with PW and LCAO methods.

8.1.3. *PW calculations on binding energies, charges and structure relaxation*

Due to a mixed metallic-covalent nature of the chemical bonding in UN, we expect a high affinity of O_{ads} towards the UN(001) substrate. The binding energy *per* O adatom is expected to be closer to that on a regular O/Al(111) or O/Al(001) metallic interfaces (~10 eV) [79] than on semiconducting O/$SrTiO_3$(001) interfaces (with two possible SrO- or TiO_2-terminations) (~2 eV) [80]. Indeed, we have obtained in the *VASP* calculations the binding energies of 6.9-7.6 and 5.0-5.7 eV *per* O adatom atop the surface U or N ions, respectively, accompanied with 0.5-1.2 *e* charge transfer from the surface towards the O adatom (Tables 8.1 and 8.2). The positively charged surface U atom goes outwards, to the adsorbed O atom (Fig. 8.4), whereas in the O configuration atop the N atom, the latter is strongly displaced from the adsorbed O atom inwards the slab, due to a mutual repulsion between N and O.

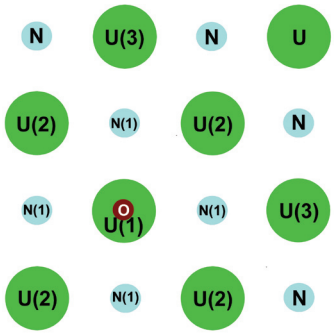

Figure 8.3.
Schematic view of O atoms adsorbed atop the surface U atom. Numbers enumerate non-equivalent surface atoms described in Tables 8.1 and 8.2.

Table 8.1. The calculated values of the binding energy (E_{bind}), the distance between O and surface U atom ($d_{O\text{-}U}$), the effective atomic charges on atoms (q), and vertical U and N displacements (Δz)[a] from the surface plane for adatom position atop the U_{surf}. Values of q for surface atoms on the perfect surface equal to +1.66 (+1.72) e for U_{surf} and −1.63 (−1.64) e for N_{surf} obtained in PAW 5-layer (7-layer) slab spin-frozen calculations [P1] *vs.* +1.68 (+1.74) e for U_{surf} and −1.65 (−1.67) e for N_{surf} obtained in analogous spin-polarized calculations [P4].

Model of system	E_{bind}, eV	q_O, e	$q_{U(1)}$, e	$q_{U(2)}$, e	$q_{U(3)}$, e	$q_{N(1)}$, e	$d_{O\text{-}U}$, Å	$\Delta z_{U(1)}$, Å	$\Delta z_{U(2)}$, Å	$\Delta z_{U(3)}$, Å	$\Delta z_{N(1)}$, Å
2 × 2, 5-layers, with frozen spin	6.9	-1.04	1.96	1.86	1.83	-1.60	1.91	+0.135[a]	-0.02	-0.04	-0.05
2 × 2, 5-layers	7.57	-1.08	2.09	1.82	1.84	-1.63	1.88	+0.16	+0.025	+0.003	-0.09
2 × 2, 7-layers	7.51	-1.08	2.19	1.78	1.78	-1.64	1.89	+0.17	+0.03	-0.02	-0.09
2 × 2, 7-layers, in proximity of N vacancy	7.58	-1.08	1.84	1.50	1.48	-1.61* -1.61^	1.88	+0.14	+0.01	-0.02	-0.09* -0.08^
3 × 3, 5-layers	7.59	-1.09	2.13	1.80	1.74	-1.62	1.88	+0.16	+0.01	-0.01	-0.10
3 × 3, 7-layers	7.57	-1.09	2.13	1.78	1.79	-1.62	1.88	+0.16	+0.01	-0.01	-0.09
3 × 3, 7-layers, in proximity of N vacancy	7.59	-1.09	1.86	1.47*	1.38*	-1.61* -1.61^	1.88	+0.10	-0.025*	-0.06*	-0.12* -0.11^
LCAO[b]	8.3	-0.89	1.97	1.66	1.62	-1.56	1.87	+0.15[b]	-0.07	-0.11	-0.04

[a] positive sign corresponds to atom displacement outward the substrate;
*, ^ adsorbed O atom in presence of non-equivalent N atomic neighbors for system containing N vacancy (Fig. 8.10a);
[b] LCAO calculations performed using *CRYSTAL-2006* code by group Prof. Evarestov.

Tables 8.1 and 8.2 clearly show that ionicity of O_{ads}–U_{surf} bond and effective atomic charges are slightly larger in spin-polarized calculations (this effect is less pronounced for O_{ads}–N_{surf}, we have obtained only slight increase of $|q_N|$). Relaxation shifts are also slightly larger in spin-relaxed calculations. The binding energy between adsorbed O and U/N

atoms is ~0.6-0.7 eV larger for spin-relaxed calculations as compared to the analogous spin-frozen calculations. If we estimate the binding energy of O adatom with defective surface in the proximity of N vacancy according to formula

$$E_{bind} = \frac{1}{2}\left(E^{\mathrm{UN(N\_vac)}} + 2E^{\mathrm{O_{triplet}}} - E^{\mathrm{O/UN(N\_vac)}}\right), \qquad \textit{(Eq. 8.1.2)}$$

where $E^{\mathrm{UN(N\_vac)}}$ is a total energy of defective UN substrate containing N vacancies while $E^{\mathrm{UN(N\_vac)}}$ the total energy of adsorbed oxygen atoms atop the defective substrate, the values calculated using Eqs. (*8.1.1* and *8.1.2*) are almost the same.

Table 8.2. The calculated parameters for O atom adsorbed atop the N_{surf} atom[a] (see caption and footnotes of Table 8.1 for explanation).

Model of system	E_{bind}, eV	q_O, *e*	$q_{N(1)}$, *e*	$q_{N(2)}$, *e*	$q_{N(3)}$, *e*	$q_{U(1)}$, *e*	$d_{O\text{-}N}$, Å	$\Delta z_{N(1)}$, Å	$\Delta z_{N(2)}$, Å	$\Delta z_{N(3)}$, Å	$\Delta z_{U(1)}$, Å
2 × 2, 5-layers, with frozen spin	5.0	-1.20	-1.44	-1.56	-1.59	1.805	2.19	-0.64	+0.065	+0.06	+0.10
2 × 2, 5-layers	5.52	-1.17	-1.48	-1.68	-1.68	1.86	2.19	-0.69	+0.03	+0.05	+0.13
2 × 2, 7-layers	5.58	-1.17	-1.48	-1.63	-1.67	1.86	2.21	-0.715	+0.03	+0.03	+0.12
3 × 3, 5-layers	5.57	-1.18	-1.51	-1.67	-1.68	1.89	2.20	-0.70	+0.01	+0.01	+0.13
3 × 3, 7-layers	5.65	-1.18	-1.51	-1.69	-1.65	1.89	2.22	-0.73	+0.01	+0.02	+0.12

[a] atomic positions of U and N ions are reversed as compared to those shown in Fig. 8.3.

8.1.4. Analysis of electronic properties

Electron density redistributions caused by the absorption of O atom atop N_{surf} or U_{surf} atoms on UN(001) surface in spin-relaxed case are shown in Fig. 8.4. An analysis of the difference density plots for both configurations of O_{ads} confirms that the oxygen adatom forms a strong bonding with the U_{surf} atom which can be considered as one-center adsorption complex (Fig. 8.4c, 8.4d). In the case of O adatom atop the N_{surf} atom, this is rather multi-center adsorption complex involving four adjacent surface U atoms (Fig. 8.4a, 8.4b). As follows from Table 8.2., these surface atoms mostly contribute to the high O binding energy atop the N_{surf}. Formation of the strong chemical bonding of O atom with the U_{surf} results in a strong anisotropic redistribution of the electronic charges, thus, indicating considerable contribution of uranium *f* and *d* electrons to chemical bonding. Plots of electron density redistributions clearly show that U_{surf} atoms shield influence of neighbor atoms on the next coordination spheres much better than N_{surf} atoms. When using 7-layers 3 × 3 supercells, we can avoid the effect of finite-slab size.

Adsorption of O_{ads} atop the surface N or U atoms on the UN(001) surface leads to appearance of the specific oxygen bands in the density of states (DOS) (Fig. 8.5) as compared to DOS for a pure UN(001) surface (Fig. 6.2). For oxygen atop the U_{surf}, O(*2p*) states overlap with the U_{surf}(*6d*) and with a well-pronounced tail of U_{surf}(*5f*) states in the region of the N_{surf} (*2p*) valence band (-2 to -4 eV). This indicates once more a strong oxygen chemical bonding (chemisorption) with U_{surf} typical for metal surfaces. However,

when O is located atop N_{surf}, the contribution from $U_{surf}(5f)$ state in this energy region diminishes whereas $N_{surf}(2p)$ states are noticeably pushed down to smaller energies, due to N_{surf} atom repulsion from negatively charged O adatom.

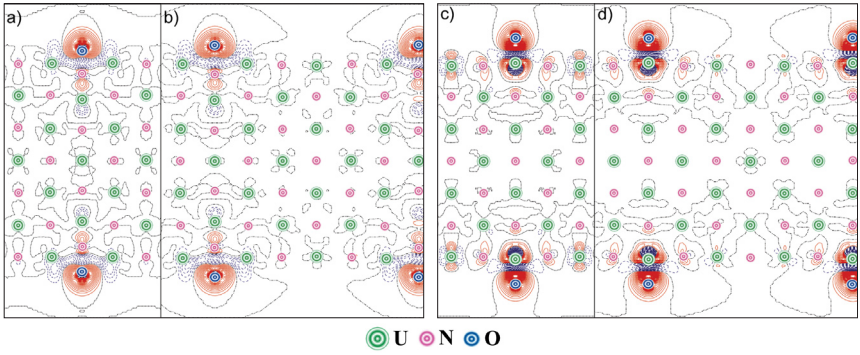

Figure 8.4. The 2D sections of the electron charge density re-distributions $\Delta\rho(\mathbf{r})$ for O atoms adsorbed atop (*i*) N_{surf} atom for 2 × 2 (a) and 3 × 3 (b) supercells as well as (*ii*) U_{surf} atom for 2 × 2 (c) and 3 × 3 (d) supercells upon the seven-layer UN(001) slab. Function $\Delta\rho(\mathbf{r})$ is defined as the total electron density of the interface containing adsorbed O atom minus the densities of substrate and adsorbate with optimized interfacial geometry. Solid (red) and dashed (blue) isolines correspond to positive and negative electron densities, respectively. Dot-dashed black isolines correspond to the zero-level.

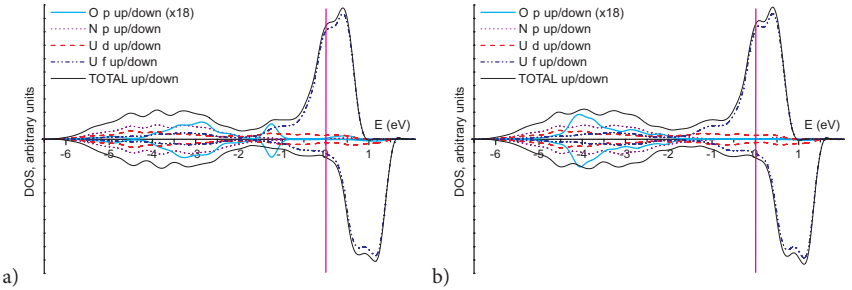

Figure 8.5. The total and projected DOS for O atoms distributed with 3 × 3 periodicity atop 7–layer UN(001) slab: a) adsorpion atop N atom, b) adsorpion atop U atom. A convolution of individual energy levels has been plotted using the Gaussian functions with a half-width of 0.2 eV.

8.1.5. Comparison of oxygen adsorbtion upon UN(001) and UN(110) surfaces

We have also estimated the binding energies of oxygen adatom with UN(110) surface (Table 8.3). We have found these results qualitatively similar to those for O adsorption

on (001) surface. For both surfaces, oxygen binding energy with U atom is larger as compared to that with N atom (~1.9 eV for (001) and ~2.1–2.2 eV for (110) surface). Moreover, increase of the surface supercell from 2 × 2 to 3 × 3 leads to slight growth of binding energy. Oxygen binding energies on (110) surface are ~0.1-0.4 eV larger as compared to (001) surface. Higher E_{bind} values for (110) surface can be explained by larger distances between surface adatoms upon (110) surface resulting in decreased interactions between adsorbed oxygen and all other atoms, excluding underlying U or N atom.

Table 8.3. The calculated binding energies ($E_{bind,}$ eV) for oxygen adsorption atop UN (001) and (110) surfaces.

Number of layers and supercell size		Atop U	Atop N
		Binding energy, eV	Binding energy, eV
(001)	7, 2 × 2	7.51	5.58
	7, 3 × 3	7.57	5.65
(110)	7, 2 × 2	7.90	5.73
	7, 3 × 3	7.91	5.99

8.1.6. Atomic oxygen adsorption: Summary

Summing up, the results presented in subsection 8.1 for single oxygen atom interaction with UN surfaces demonstrate strong chemisorption typical for metallic surfaces. The excellent qualitative agreement of the results obtained using the two different first principles methods supports their reliability for simulations on O/UN interface. O adatom atop U_{surf} atom forms the one-center complex with underlying U_{surf} atom, while oxygen adsorption atop N_{surf} leads to formation of complex containing the four adjacent U_{surf} atoms.

8.2. Molecular oxygen adsorption

8.2.1. Model and theoretical background

The results analyzed in Section 8.1 and Ref. [P2] clearly demonstrate the metallic nature of UN surface. In this subsection, we simulate the interaction of *molecular* oxygen with the perfect UN(001) surface [P3]. The key questions arisen here are: whether the O_2 dissociation upon the surface is energetically possible, which adsorption sites are optimal for this, and whether it can occur spontaneously, without energy barrier, similarly to other metallic surfaces, for example Al [79].

Calculations on molecular adsorption have been performed using the fixed total spin equals to 1 μ_B on each U atom. For simulation on the chemisorption of oxygen molecule, we have used the 5-layer 2 × 2 extended surface supercell (containing 20 U and 20 N atoms). The periodic adsorbate distribution corresponds to the molecular coverage of 0.25 ML (or atomic O coverage of 0.5 ML). To reduce computational efforts, we have used a symmetric two-sided arrangement of oxygen molecules again. The binding energy E_{bind} *per* oxygen atom in the adsorbed molecule $(O_2)_{ads}$ was calculated as:

$$E_{bind} = \frac{1}{4}\left(E^{\mathrm{UN}} + 2E^{\mathrm{O_2}} - E^{\mathrm{O_2/UN}}\right), \qquad \textit{Eq. (8.2.1)}$$

where $E^{\mathrm{O_2/UN}}$ is the total energy of a fully relaxed O_2/UN(001) slab for several configurations of (O_2) upon the substrate (with a center of molecule atop the corresponding surface site as shown in Fig. 8.7), $E^{\mathrm{O_2}}$ and E^{UN} the total energies of an isolated oxygen molecule in the ground (triplet) state and of a relaxed UN slab, respectively. The factor 1/4 before brackets, similar to atomic adsorbtion calculations, appears since the substrate is modeled by a slab containing the two equivalent surfaces with $(O_2)_{ads}$ positioned symmetrically relatively to slab surfaces whereas each molecule before and after dissociation contains two O atoms. When modeling the molecular adsorption, we have analyzed different configurations of O_2 molecule in the triplet state on the UN(001) substrate. *Vertical* orientations of the molecule atop the surface N or U ions have been found to be metastable with respect to molecule reorientation to the *horizontal* configuration, parallel to the surface. We have estimated both the binding energy of a molecule, using Eq. (8.2.1), and the dissociation energy of molecule (for some configurations), *i.e.,* the difference of the total energies of a slab with an O_2 molecule before and after dissociation, when the two O atoms in the triplet state are positioned atop the two nearest U_{surf} atoms (Table 8.4).

8.2.2. Spontaneous dissociation

We have found that a spontaneous, barrierless O_2 dissociation takes place in the two cases: when the molecular center is atop either (*i*) a hollow site or (*ii*) N_{surf} atom, with the molecular bond directed towards the two nearest U_{surf} atoms (the configurations 1 and 5 in Fig. 8.6, respectively). The relevant dissociation energies E_{diss} are given in Table 8.4, along with other parameters characterizing the atomic relaxation and the Bader charge distribution. Geometry and charges for the configurations 1 and 5 after dissociation (Table 8.4) are qualitatively similar to those obtained for UN(001) substrate covered by chemisorbed O atoms, *e.g.*, U_{surf} atoms beneath the oxygen adatom after dissociation are shifted up in both configurations (Table 8.4). However, since concentration of O_{ads} in these calculations is twice as larger as compared to that for atomic oxygen adsorbtion [P2, subsection 8.1], some quantitative differences of the results presented in Tables 8.4 and 8.1 for oxygen atom adsorbtion atop U_{surf} atom are unavoidable. For example, the *repulsion* energy between the two adatoms after O_2 dissociation, which are positioned atop the two nearest U_{surf} atoms (the configuration 1) is quite noticeable, ~0.7 eV.

We have also identified two other configurations of adsorbed oxygen molecules where the dissociation is energetically possible with energy barrier: (*i*) atop the hollow site when a molecular bond is oriented towards the nearest N_{surf} atoms (the configuration 2 in Fig. 8.6) and (*ii*) atop the U_{surf} atom (for any molecular orientation, *e.g.*, the configurations 3 and 4 in Fig. 8.6). For the configuration 2, we have observed the orientation instability of the adsorbed molecule which easily rotates, *e.g.*, towards the U_{surf} atom with further dissociation. The configurations 3 and 4 rather describe metastable UO_2 *quasi-molecules*, due to a strong bonding between all three atoms (Fig. 8.7c) and since the corresponding U_{surf} atom is noticeably shifted up from its initial positions on surface (Table 8.4). The dissociation of $(O_2)_{ads}$ molecule in configuration 3 is energetically possible but only after overcoming the activation energy barrier.

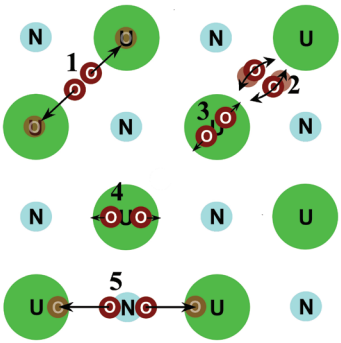

Figure 8.6.
Schematic view of five different horizontal configurations for the O_2 molecule adsorption on UN surface: 1) atop the hollow site oriented towards the nearest U_{surf} atoms, 2) atop the hollow site oriented towards the nearest N_{surf} atoms, 3) atop the U_{surf} atoms oriented towards the next-nearest surface U_{surf} atoms, 4) atop the U_{surf} atoms oriented towards the nearest N_{surf} atoms, 5) atop the N_{surf} atoms oriented towards the nearest U_{surf} atoms. We show that spontaneous dissociation of molecule can occur when O_2 is located either atop the hollow site (1) or atop the N_{surf} atom (5).

Table 8.4. The calculated values of binding (E_{bind}, Eq. (8.2.1)) and dissociation (E_{diss}) energies, geometry (z, Δz) and Bader charges (q) for configurations of molecular and spontaneous dissociative chemisorption of oxygen molecule upon the UN(001) substrate. Numbers in brackets correspond to the configurations shown in Fig. 8.6. The calculated binding energy for a free O_2 molecule in the triplet state is 6.06 eV and a bond length is 1.31 Å (*cf.* with experimental values of 5.12 eV and 1.21 Å, respectively) [81].

Position		E_{bind} per O atom, eV	z[a], Å	E_{diss}, eV	q(O), e	q(U1[b]), e	q(U2[c]), e	q(N[d]), e	Δz[e](U1), Å	Δz[e](U2), Å	Δz[e](N), Å
hollow (1)	molecular adsorption	3.03	1.893	-	-0.465	1.913	1.762	-1.533	-0.050	-0.050	0.025
	after dissociation	6.04	1.957	3.01	-0.978	2.053	1.978	-1.577	0.075	0.068	-0.133
atop U	towards next-nearest U (3)	4.00	2.18	-	-0.5905	2.042	1.836	-1.6065	0.176	-0.048	-0.096
	towards nearest N (4)	4.18	2.14	-	-0.578	2.0485	1.827	-1.625	0.123	-0.051	-0.106
atop N (5)	molecular adsorption	2.67	2.020	-	-0.5685	1.8675	1.832	-1.354	-0.050	-0.050	0.025
	after dissociation	5.85	1.955	3.18	-0.979	2.115	1.876	-1.580	0.073	0.021	-0.201

[a] z is the height of O atoms respectively the non-relaxed UN substrate,
[b] U1 the nearest surface U_{surf} atom,
[c] U2 the next-nearest U_{surf} atom,
[d] N the nearest N_{surf} atom,
[e] Δz the additional vertical shifts of the same surface atoms from their positions in absence of adsorbed oxygen.

8.2.3. Electronic properties of adsorbed molecule

Adsorption of an O_2 molecule (in the triplet state) is accompanied by the charge transfer of ~1 e (*per* molecule) from the substrate (Table 8.4). In Fig. 8.7, we analyze the difference electron charge redistributions for three configurations of horizontally

oriented $(O_2)_{ads}$ molecules upon the surface: (*a*) molecule adsorbed upon the hollow site (the configuration 1, Fig. 8.6), (*b*) molecule dissociated from this configuration with O adatoms located atop the nearest U_{surf} atoms, and (*c*) molecule adsorbed upon the U_{surf} atom (at configuration 3). Spontaneous O_2 dissociation and, thus, a smooth transition from the charge distribution (a) to (b) can be explained by continuous areas of the electron density (Fig. 8.7a) parallel to the surface which may be considered as *dissociation channels*, analogously to the density plot for a molecular oxygen upon the Al substrate [79].

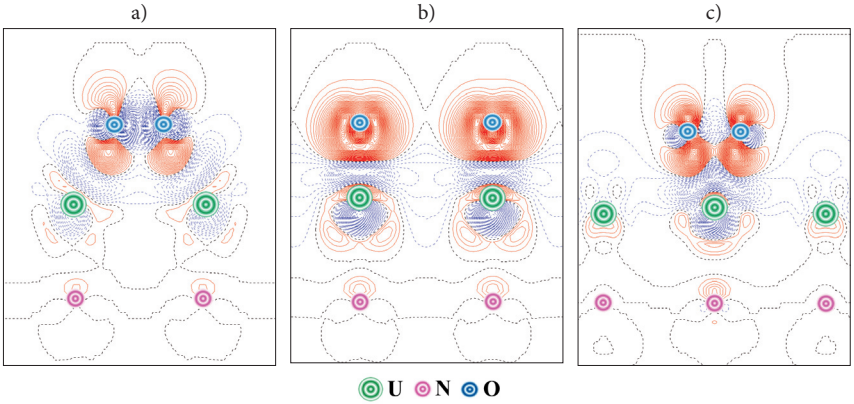

Figure 8.7. The difference electron density maps $\Delta\rho(\mathbf{r})$ (the total density of the interface minus the sum of densities of substrate and adsorbate with optimized interfacial geometry) (a) for the O_2 molecule upon the hollow position oriented to the nearest U_{surf} atoms, (b) after its dissociation in the configuration 1 (Fig. 8.6) with O atoms atop the U_{surf} atoms and (c) for the O_2 molecule atop the U_{surf} atom in the configuration 3 (Fig. 8.6). Solid (red) and dashed (blue) isolines correspond to positive and negative electron density, respectively. Isodensity increment is 0.003 e Å^{-3}.

After dissociation, each O adatom contains an extra charge of ~1 *e*, *i.e.,* transforms into O^- ion in the triplet state (Fig. 8.7b). In contrast, when considering the molecular configuration 3, these *dissociation channels* are transformed into *dissociation barriers* (Fig. 8.7c). Simultaneously, we observe considerably higher electron density, indicating a kind of UO_2 quasi-molecule with a strong bonding between the O_2 molecule and surface U atom beneath. Thus, difference between the electron density plots presented in Figs. 8.7a and 8.7c can explain different dissociation abilities of O_2 molecule in the configurations 1 and 3 (Fig. 8.6).

For the same adsorbate configurations considered above, we have constructed the total and projected densities of states (DOS) (Fig. 8.8). Molecular adsorption in these configurations leads to appearance of the specific *oxygen bands* as compared to those for oxygen adatoms upon UN surface (Fig. 8.5) and O atom substituted for a host N atom in UN bulk [82]. For a molecular oxygen atop the hollow position (Fig. 8.6a), O(*2p*) peak

is observed at -1 eV overlapping with the U(*5f*) and U(*6d*) bands. After O_2 dissociation (Fig. 8.7b) this peak disappears being replaced by the broad two-peak band in the region of the N(*2p*) valence band (from -2 to -5 eV), similarly to the DOS for oxygen adatoms on UN(001) substrate (Fig.8.5). Some differences are also noticeable between the corresponding U *5f* and *6d* peaks in the spectral range above -1 eV (Figs. 8.8a-8.8c) which can be caused by both different arrangement of O and U atoms in these configurations and sensitivity of U states to the presence of oxygen, thus indicating a strong oxygen chemical bonding (chemisorption). When oxygen molecule is located atop the U_{surf} atom (the configuration 3), the U(5*f*) and U(6*d*) contributions in the energy range above -1 eV are diminished, simultaneously the O(*2p*) contribution grows, thus increasing an overlap between all three states and indicating UO_2 quasi-molecular bond formation. As compared to the adsorption of oxygen molecule upon the hollow site (Fig. 8.8a), we again observe a higher O(*2p*) peak (at -1.5 eV) and an additional lower peak of the same O(*2p*) (at -5.5 eV) which noticeably overlaps with the U(*5f*) and U(*6d*) subpeaks (Fig. 8.8c). Some analogue of the latter pattern was observed earlier for the projected DOS of O atom substituted for N atom in UN bulk [82]. In all three DOSs (Fig. 8.8), a broad band containing the N(*2p*) projected states is not changed drastically which means a weak influence of N atoms on the O_2 molecule adsorption upon the UN(001) surface.

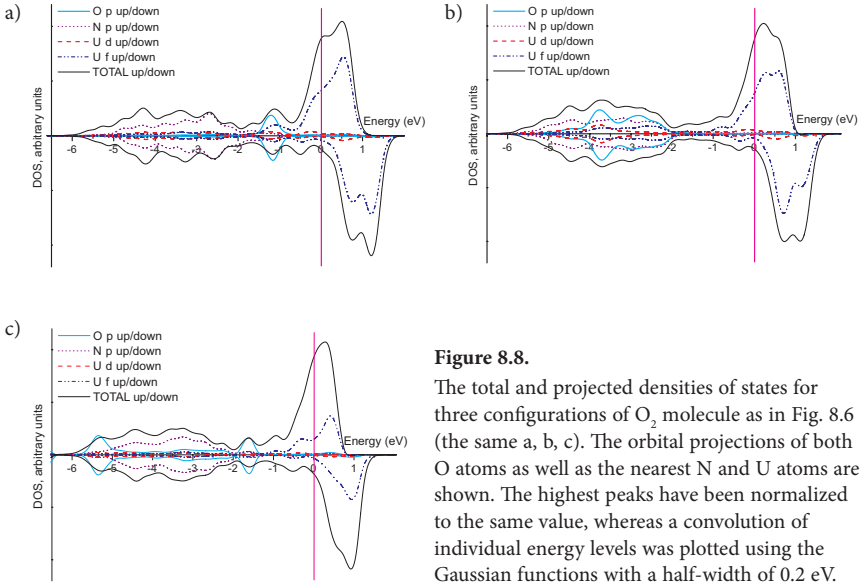

Figure 8.8.
The total and projected densities of states for three configurations of O_2 molecule as in Fig. 8.6 (the same a, b, c). The orbital projections of both O atoms as well as the nearest N and U atoms are shown. The highest peaks have been normalized to the same value, whereas a convolution of individual energy levels was plotted using the Gaussian functions with a half-width of 0.2 eV.

Summing up, the results of *ab initio* calculations on adsorption of oxygen molecule upon the perfect UN(001) surface clearly demonstrate a real possibility for spontaneous dissociation of the adsorbed oxygen, analogously to the O_2 dissociation on "traditional" metallic surfaces.

8.3. Simulation of migration path for O adatom along the UN(001) surface

We have considered three main migration paths of oxygen adatom upon the UN(001) surface (Fig. 8.9): (*i*) path 1: between the sites atop U_{surf} atom and the nearest N_{surf} atom, (*ii*) path 2: between the sites atop the two neighboring U_{surf} atoms, (*iii*) path 3: between the sites atop the two neighboring N_{surf} atoms:

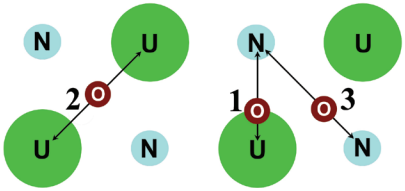

Figure 8.9. Different oxygen migration paths upon the UN(001) surface (atop view).

Table 8.5. Binding energies E_{bind} of adsorbed oxygen in different positions atop UN slab (Fig. 8.9).

1. From site atop U_{surf} to site atop N_{surf} (migration path 1)				
Supercell size:	2 × 2		3 × 3	
Number of atomic layers:	5	7	5	7
atop U_{surf}	7.57	7.51	7.59	7.57
¼ of distance U-N (or 0.61 Å from U atom)	7.39	7.39	-	-
½ of distance U-N (or 1.22 Å from U atom)	6.97	6.98	-	-
¾ of distance U-N (or 1.83 Å from U atom)	5.91	5.93	-	-
atop N_{surf} (or 2.43 Å from U atom)	5.52	5.58	5.57	5.65
2. From hollow position (h.p.) to site atop U_{surf} (migration path 2)				
Supercell size:	2 × 2		3 × 3	
Number of atomic layers:	5	7	5	7
atop h.p.	7.21	7.245	7.20	7.21
¼ of distance h.p.-U (or 0.43 Å from h.p.)	7.23	7.255	-	-
½ of distance h.p.-U (or 0.86 Å from h.p.)	7.32	7.33	-	-
¾ of distance h.p.-U (or 1.29 Å from h.p.)	7.45	7.45	-	-
atop U_{surf} (or 1.72 Å from h.p.)	7.57	7.51	7.59	7.57
3. From hollow position (h.p.) to site atop N_{surf} (migration path 3)				
Supercell size:	2 × 2		3 × 3	
Number of atomic layers:	5	7	5	7
atop h.p.	7.21	7.25	7.20	7.21
1/4 of distance h.p.-N (or 0.43 Å from h.p.)	6.61	6.65	-	-
1/2 of distance h.p.-N(or 0.86 Å from h.p.)	6.32	6.35	-	-
3/4 of distance h.p.-N(or 1.29 Å from h.p.)	5.54	5.57	-	-
atop N_{surf} (or 1.72 Å from h.p.)	5.52	5.58	5.57	5.65

The binding energy E_{bind} of oxygen atom adsorbed upon the UN surface has been defined in subsection 8.1.1. To reduce the computational time for calculations on oxygen adatom in interstitial positions, we have relaxed only z coordinates of slab atoms fixing their x and y coordinates. For adsorption of O atoms atop the N_{surf} or U_{surf} atoms, the total slab geometry relaxation has been performed, to control changes of symmetry arisen due to lateral interaction. The results obtained for all migration paths of adatom for different slab thicknesses and supercell extensions are systematized in Table 8.5. This Table presents the values of binding energies calculated for migration paths of O adatoms upon the perfect UN(001) substrate shown in Fig. 8.9. We have fixed five sites along the O_{ads} migration trajectories for 2×2 supercells of UN(001) slab and two sites for 3×3 supercells. In both cases, the most favorable migration trajectory has been optimized to be the line joining the sites atop the nearest surface U atoms and the hollow sites between them (trajectory 2). The corresponding energy barriers found to be 0.36 eV (5-layer slab) and 0.26 eV (7-layer slab) indicates on a high mobility of O_{ads} atoms upon UN. The energy barriers along other two migration trajectories are substantially larger (1.93-2.05 eV and 1.31-1.69 eV for trajectories 1 and 3, Fig. 8.9).

Thus, we observe quite high mobility of atoms along the surface, due to relatively low migration barriers.

9. O atom migration and incorporation into defective UN(001) slab

9.1. Low-barrier incorporation of O adatom from site atop U_{surf} atom to N_{surf} vacancy

To understand the initial mechanism of adatom incorporation into the surface layer of UN(001), it is necessary to clarify both energetic and structural possibilities of O_{ads} migration along this substrate, both perfect and defective. To estimate oxygen adatom mobility upon the UN(001) surface, we have performed a series of *ab initio* spin-polarized calculations.

According to our calculations, O atom adsorbed atop the U_{surf} atom in the proximity of the surface N vacancy can be captured by the latter (Fig. 9.1) when overcoming a low energy barrier (~0.5-1 eV). We have estimated the energy gain for such a transition of oxygen adatom using the formula:

$$\Delta E = \frac{1}{2}\left(E_{tot}^{\mathrm{UN(O\_in\_N\_vac)}} - E_{tot}^{\mathrm{UN(O\_atop\_U)}}\right), \qquad \textit{Eq. (9.1.1)}$$

where $E_{tot}^{\mathrm{UN(O\_in\_N\_vac)}}$ is the total energy of the supercell containing the O atom in the N vacancy (position 2 as shown in Fig. 9.1), and $E_{tot}^{\mathrm{UN(O\_atop\_U)}}$ the total energy of the supercell with O atom adsorbed atop U_{surf} atom positioned in the proximity of existing N vacancy (position 1). For calculations on $E_{tot}^{\mathrm{O/UN(N\_vac)}}$, we have fixed horizontal *x* and *y* oxygen coordinates, to prevent O adatom migration. Multiplier ½ in Eq. (9.1.1) appears due to the symmetric arrangement of adsorbed or incorporated O atoms. When comparing $E_{tot}^{\mathrm{UN(O\_in\_N\_vac)}}$ value (obtained as a result of adatom migration from position atop U_{surf} atom into vacancy) with $E_{tot}^{\mathrm{UN(O\_in\_N\_vac)}}$ where O adatom is directly incorporated into pre-existing vacancy (Section 9.2) the corresponding difference does not exceed 0.01 eV. The calculated energy gain (ΔE_g) for the transition from position 1 to position 2 (as shown in Fig. 9.1) equals to ~2 eV *per* oxygen adatom (1.99 eV for 2 × 2 7-layer supercell and 1.94 eV for 3 × 3 7-layer supersell).

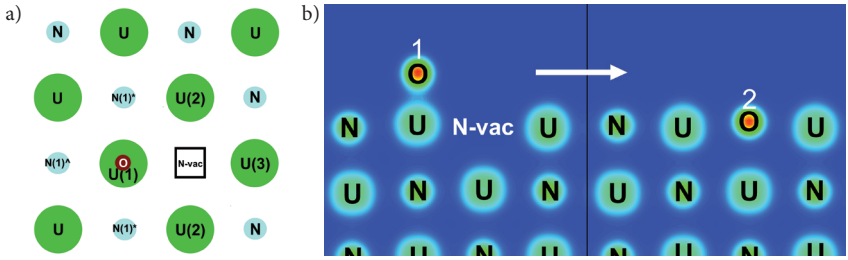

Figure 9.1. Atop (a) and across (b) views of surface model used for simulation of oxygen atom low-barrier incorporation from the initial position (1) atop U_{surf} atom (left) into the nearest existing N_{surf} vacancy (2). Numbers enumerate non-equivalent surface atoms for oxygen adsortion in proximity of N_{surf} vacancy (see caption of Fig. 8.3).

In Fig. 9.2, the diference of electron charge redistributions for oxygen adsorpion atop U_{surf} atom in the proximity of the surface N vacancy is analyzed. The electron charge redistributions in the slab look similarly to adsobtion atop U_{surf} atom without adjacent N vacancy (Fig. 8.4c,d). Parallel to the surface between adsorbed O atom and existing N vacancy the electrostatic channels with electronic density shortage can be observed which are directed towards the oxygen adatom incorporation into the N vacancy.

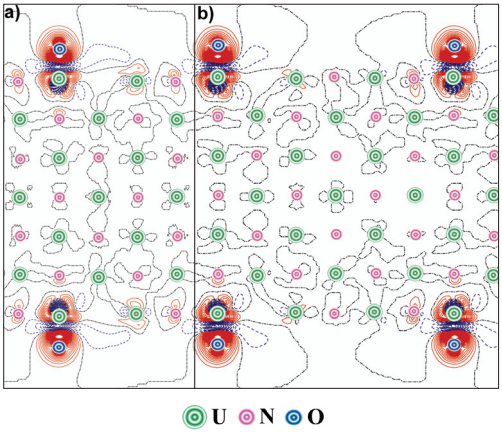

Figure 9.2. The 2D sections of the electron charge density re-distributions $\Delta\rho(\mathbf{r})$ for O atoms adsorbed atop U_{surf} atom near the surface N vacancy. Other details are given in caption of Figure 8.4.

Thus, we have showed the possibility of low-barrier oxygen adatom incorporation into existing N vacancy from the nearest adsorption site atop U_{surf} atom.

9.2. Oxygen incorporation into surface vacancies

9.2.1. Model and computational details

One of possible ways for UN surface oxidation is the formation of oxynitrides near the UN surface [18]. Hence, it is very impotant to describe the oxygen interaction with the single vacancies. As known from literature, considerable attention was paid so far for the static and dynamic properties of primary defects (vacancies and incorporated impurities) in UN *bulk* [34] which affect the fuel performance during operation and its reprocessing. Apart the behavior of empty vacancies, the O atom incorporation into vacancies in bulk UN has been considered too. Incorporation of oxygen atom into the N vacancy in bulk has been found to be energetically more favorable as compared to the interstitial sites [82]. However, the solution energy shows an opposite effect. In order to shed more light on the mechanism of unwanted UN oxidation, the incorporation of oxygen impurities into the N- and U- vacancies on the UN(001) surface is focused in this subsection and Ref. [P5].

Our calculations have been performed for the supercells with 2×2 and 3×3 extensions of translation vector upon the UN surface. Oxygen-occupied N and U vacancies have been disposed in the surface, subsurface and central layers of 2D slab. Due to the presence of mirror layers in the symmetric slabs, one can consider the two-sided symmetric arrangement of defects, except for the central mirror plane, thus, minimizing the computational expenses. The spin magnetic moment was allowed to relax in all the calculations for the FM spin arrangements on the uranium sublattice.

9.2.2. Oxygen incorporation and solution energies

The energy balance for the incorporation of an O atom into a vacancy can be characterized by *the incorporation energy* E_I suggested by Grimes and Catlow [83] in the shell model calculations on fission products in UO_2:

$$E_I = E^{\mathrm{UN(O\_}inc\mathrm{)}} - E^{\mathrm{UN(N/U\_vac)}} - E^O, \qquad \textit{Eq. (9.2.1a)}$$

for the O atom incorporated into the N- and U vacancy disposed in the central atomic layer and

$$E_I = \frac{1}{2}(E^{\mathrm{UN(O\_}inc\mathrm{)}} - E^{\mathrm{UN(N/U\_vac)}} - 2E^O), \qquad \textit{Eq. (9.2.1b)}$$

for the same incorporation in the surface or sub-surface layers. Here $E^{\mathrm{UN(O\_}inc\mathrm{)}}$ is the total energy of the supercell containing the O atom at either the N- or U vacancy ($E^{\mathrm{UN(O\_}inc\mathrm{)}} < 0$), $E^{\mathrm{UN(N/U\_vac)}}$ the energy of the supercell containing an unoccupied (empty) vacancy, and E^O half the total energy of isolated O_2 molecule in the triplet state. It is defined by the oxygen chemical potential at 0 K. Since the value of E_I describes the energy balance for the incorporation into pre-existing vacancies, it has to be negative for energetically favorable incorporation processes.

To take into account the total energy balance, including the vacancy formation energy E_{form} in the defect-free slab, the solution energy [83] has been defined as:

$$E_S = E_I + E_{form}, \qquad \textit{Eq. (9.2.2)}$$

where E_{form} is the formation energy of N- or U vacancy in the slab calculated using *Eq.7.1.1a* or *7.1.1b.*

It is worth mentioning, however, that use of the standard O pseudopotential in our *VASP* calculations gave good bond length of 1.23 Å for the O_2 molecule but considerable overestimated its binding energy (6.79 eV *vs.* the experimental value of 5.12 eV). Several corrections were suggested in the literature how to take into account this serious DFT shortcoming [84, 85]. Thus, the calculated formation and solution energies of defect may be corrected by ~1 eV (its impact is discussed below).

Table 9.1. Incorporation (E_I) and solution (E_S) energies (eV), average spin magnetic moments of U atoms μ_{av}^{U} (μ_B) as well as effective charge of oxygen atoms (e^-) for O incorporation into the UN(001) surface. The reference states for calculation of the incorporation and solution energies have been chosen as the chemical potentials of O, N and U calculated for O_2, N_2 molecules and α-U, respectively.

Layer	Supercell size	Number of atomic layers in slab	N vacancy				U vacancy			
			E_I (eV)	E_S (eV)	μ_{av}^{U} (μ_B)	$q_{eff}(e^-)$	E_I (eV)	E_S (eV)	μ_{av}^{U} (μ_B)	$q_{eff}(e^-)$
Surface	2 × 2	5	-6.173	-2.473	1.65	-1.36	-0.339	1.120	1.16	-0.98
		7	-6.181	-2.476	1.49	-1.36	-0.855	0.583	1.36	-1.03
		9	-6.188	-2.479	1.41	-1.36	-0.943	0.493	1.31	-1.06
	3 × 3	5	-6.122	-2.481	1.60	-1.37	-0.683	0.654	1.48	-1.05
		7	-6.126	-2.480	1.46	-1.36	-1.073	0.230	1.38	-1.08
Subsurface	2 × 2	5	-6.314	-2.068	1.64	-1.42	-1.856	1.284	1.66	-1.10
		7	-6.419	-2.090	1.49	-1.40	-1.823	1.297	1.45	-1.10
		9	-6.417	-2.091	1.41	-1.40	-1.823	1.271	1.38	-1.10
	3 × 3	7	-6.428	-2.093	1.46	-1.39	-2.012	1.000	1.43	-1.10
Central (mirror)	2 × 2	7	-6.611	-2.180	1.47	-1.42	0.736	3.923	1.44	-0.89
		9	-6.608	-2.192	1.39	-1.38	0.669	3.838	1.38	-0.90
	3 × 3	7	-6.599	-2.182	1.45	-1.42	0.317	3.378	1.47	-0.94

The calculated O adatom incorporation into the N vacancy at the UN(001) surface has been found to be energetically favorable since both values of E_I and E_S are strictly negative (Table 9.1). This is in favor of both creation of the N vacancy and adsorption of the O atom from air. Also, E_I decreases by ~0.4 eV (becomes more negative) within the slab as compared to the surface layer, whereas E_S is smallest for the N vacancy just on the surface layer. In contrary, in the case of U vacancies, the values of E_I calculated for the surface and central layers have been found to be close to zero. The sub-surface layer is characterized by E_I which is ~1 eV smaller than that for the surface and central layers. Our results indicate importance of oxynitride formation. However, E_S is positive and increases for O atoms in the the U vacancy and the slab center. The energies in Table 9.1 do not include the corrections discussed above for the O atoms. However, such corrections may lead to E_I (or E_S) increased by ~1 eV and, as a result, more positive E_I for the U vacancy. Table 9.1 also indicates that solution of the oxygen atoms is energetically more favorable at the surface layers than inside the slab. As the supercell size increases (the 3 × 3 extension in Table 9.1), both E_I and E_S values decrease whereas influence of the slab thickness is not so clear. Nevertheless, the U vacancy appeared to be most sensitive to the supercell size related to spurious interactions between the periodically repeated defects. The E_I as well as E_S values may be reduced by 0.15 eV at the average in this case.

9.2.3. Spin densities and Bader charges

Table 9.1 allows us to analyze also the averaged spin density of U atoms (μ_{av}^{U}) for different morphologies of defective UN(001) surfaces with incorporated O atoms. Analogously to defective UN surface with empty vacancies [P4], μ_{av}^{U} decreases with

a number of layers in the slab for both types of the vacancies (except for the O atom incorporated into the U vacancy in the surface layer). It is also seen that μ_{av}^{U} is higher in the surface layer for the N vacancy than for the U vacancy. The sub-surface and central layers are characterized by similar μ_{av}^{U} for both types of vacancies. Interestingly, the effective charge q_{eff} on O atoms is also higher for the N vacancy and inside the slab. However, in the case of U vacancy, q_{eff} decreases by almost 0.3 *e*. The same effect has been also observed for adjacent N atoms: their effective charge is smaller when the O atom occupies the U vacancy. The overall picture suggests prevalence of the covalent bonding between different species in the system.

9.2.4. Charge redistribution analysis: Finite-size effects and choice of supercell size

Large concentrations of defects (25% for the 2 × 2 extension in Table 9.1) causes certain finite-size effects which can be illustrated using the 2D difference electron density redistributions $\Delta\rho(\mathbf{r})$. These plots are shown for the O atoms incorporated into the N vacancies at the surface (Fig. 9.3) and central layers (Fig. 9.4). Inside the 5-layer slab, a presence of the two symmetrically positioned defects induces their interaction (visible in charge redistribution across a slab in Fig. 9.3a). An increase of the slab thickness reduces this effect (Fig. 9.3c). If the supercell size is decreased (the 2 × 2 extension, Fig. 9.3b) an additional electron density parallel to the surface layer is observed between the defects. Similar effects are also observed for redistributions of the electron density around defects in the mirror planes (Fig. 9.4). The effect of supercell size in this case is similar to that discussed for the N vacancy.

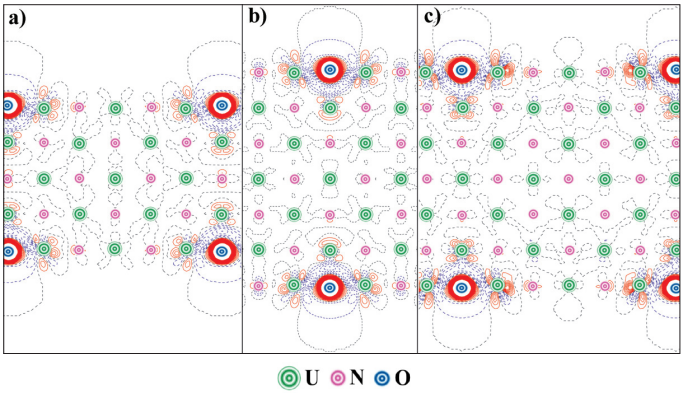

Figure 9.3. The 2D sections of the electron charge density re-distributions $\Delta\rho(\mathbf{r})$ around the O atoms incorporated into the surface N vacancies of the 5- and 7-layer UN(001) slabs with 2 × 2 and 3 × 3 supercell extensions. $\Delta\rho(\mathbf{r})$ are defined as the total electron density of the O-containing defected surface minus a superposition of the electron densities of the surface containing the N vacancies and the O atom in the regular positions on the surface. a) 3 × 3 periodicity of the O atoms upon the five-layer slab, b) 2 × 2 periodicity of the O atoms upon the seven-layer slab, c) 3 × 3 periodicity of the O atoms upon the seven-layer slab. Other details are given in caption of Figure 8.4.

The effect of supercell size in this case is similar to that discussed for the N vacancy. However, in the case of surface U vacancy, a larger concentration of electron density was seen between the O atom and neighbouring N atoms in the sub-surface layer, in a comparison to the N vacancy. Thus, the effect of slab thickness also may not be underestimated in this case.

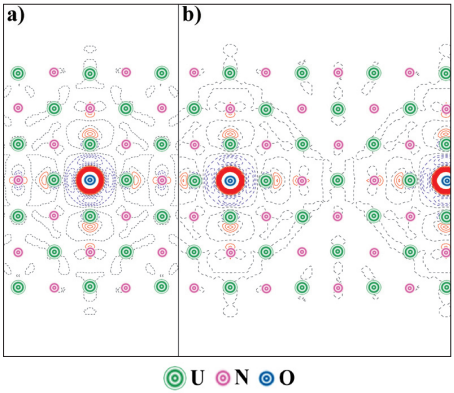

Figure 9.4. The 2D sections of $\Delta\rho(\mathbf{r})$ around the O atoms incorporated into the N vacancies in central layer of 7-layer UN(001) slabs with (a) 2 × 2 and (b) 3 × 3 supercell extensions. Other details are given in caption of Figure 9.3.

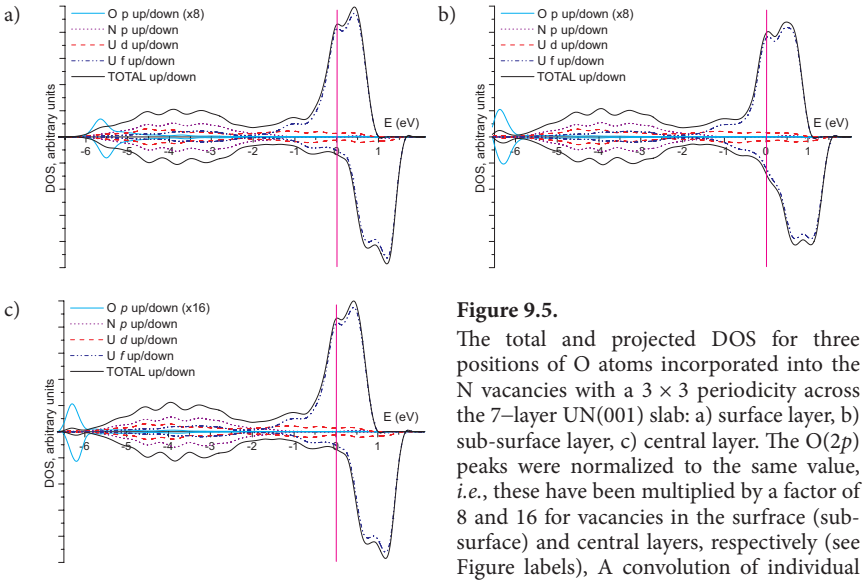

Figure 9.5.
The total and projected DOS for three positions of O atoms incorporated into the N vacancies with a 3 × 3 periodicity across the 7–layer UN(001) slab: a) surface layer, b) sub-surface layer, c) central layer. The O(2*p*) peaks were normalized to the same value, *i.e.*, these have been multiplied by a factor of 8 and 16 for vacancies in the surfrace (sub-surface) and central layers, respectively (see Figure labels), A convolution of individual energy levels was plotted using the Gaussian functions with a half-width of 0.2 eV.

9.2.5. *Electronic densities of states (DOS) for incorporated oxygen*

In Figure 9.5, the total and projected densities of states are shown for the 7-layer defective UN(001) surface with the O atom incorporated into the N vacancy. The system remains conducting throughout all the calculations with the significant contribution from the U(*5f*) states at the Fermi level similar to perfect UN(001) slab (Fig. 6.2). The appearance of specific O(2*p*) band with the energy peak at –6 eV is observed. When comparing the DOS for the O atoms incorporated into the N vacancies, a noticeable shift of the O(*2p*) band (by about -1.0 eV) allows one to distinguish the surface layer from the internal layers.

Moreover, in the case of surface layer, this band considerably overlaps with the N(*2p*) band, partly mixed with the U(*5f*) states (similar effects occur with the O_2 molecule atop the surface U atom [P2]). In contrary, the O(*2p*) band remains quasi-isolated from the other bands (analogously to the O atom incorporated into the N vacancy in UN bulk [82]). Position of the N(*2p*) band is insensitive to presence of O atoms and lies within energy range of -6 and -1 eV.

9.2.6. *Comparison of oxygen incorporation into N vacancy on the UN(001) and (110) surfaces*

Similarly to results for perfect UN surface as well as vacancy formation and atomic oxygen adsorbtion, it could be interesting further to compare incorporation (E_I) and solution (E_S) energies for two surfaces, *i.e.* UN (001) and (110) (Fig. 9.6). Table 9.2 compares these energies as function of slab thickness and supercell size. One can see that the UN(110) surface is characterized by more negative solution energy, eVen though the difference between their solution energies is ~0.3. eV. On the other hand, the incorporation energy changes this trend suggesting more negative values for the (001) surface. Moreover, the difference between incorporation energies approaches to 0.4 eV. Such results demonstrate importance of E_I calculations as our surface might function under extreme conditions like high temperatures. Nevertheless, we clearly see similar tendencies for both surfaces (Table 9.2).

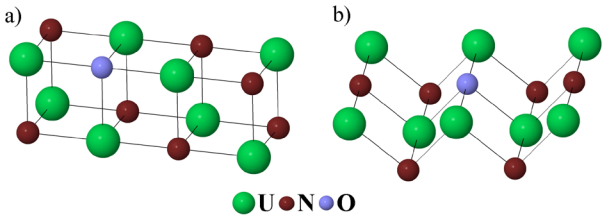

Figure 9.6. 2-layer models of oxygen incorporation into surface N vacancy on UN (001) (a) and (110) (b) surface

Table 9.2. Incorporation (E_I) and solution (E_S) energies, average spin magnetic moments of U atoms and effective charge on O atoms for oxygen incorporated into N vacancy on UN (001) and (110) surfaces. The reference states for calculations on the incorporation and solution energies are the chemical potentials of O and N calculated for O_2 and N_2 molecules, respectively (2 × 2 and 3 × 3 supercells).

Number of layers and supercell size	E_I (eV)	E_S (eV)	μ_{av}^{U} (μ_B)	q_{eff}(e^-)	E_I (eV)	E_S (eV)	μ_{av}^{U} (μ_B)	q_{eff}(e^-)
	(001) surface				(110) surface			
5, 2 × 2	-6.173	-2.473	1.647	-1.36	-5.853	-2.778	1.736	-1.27
7, 2 × 2	-6.181	-2.476	1.495	-1.36	-5.822	-2.794	1.516	-1.29
9, 2 × 2	-6.186	-2.479	1.412	-1.36	-5.820	-2.784	1.472	-1.29
11, 2 × 2	-6.195	-2.483	1.365	-1.35	-5.817	-2.791	1.416	-1.29
7, 3 × 3	-6.126	-2.480	1.463	-1.36	-5.748	-2.783	1.471	-1.28

9.2.7. Modeling of O adatom incorporation: summary

Considerable energetic preference of O atom incorporation into the N vacancy as compared to U vacancy indicates that the observed oxidation of UN is determined mainly by the interaction of oxygen atoms with the surface and sub-surface N vacancies.

The formation of oxynitrides [18] near the UN(001) surface is proposed, which can be caused by diffusion of the oxygen atoms within the interlayers of uranium nitride with further capture by nitrogen vacancies, thus, resulting in their stabilization due to formation of the chemical bonds with the nearest uranium atoms. The electronic charge redistributions demonstrate quite local nature of the density perturbation caused by the incorporated O atoms. The analysis of density of states shows both overlapping of the O(2*p*) states with the N(2*p*) states at initial stages of oxidation (*surface incorporation*) and separation of the O(2*p*) states from other bands in the case of deeper positioned oxygen atoms (*sub-surface penetration*). The results of this analysis could be used for the interpretation of the experimental ultraviolet photoelectron spectra for uranium oxynitrides [18].

10. Summary

The PAW method is used to analyze basic UN bulk properties, point defects behavior on UN surface as well as oxygen interaction with UN surface. We obtain results of such calculations for pure UN bulk an surface, nitride and uranium vacancies on the surface, atomic and molecular adsorbtion as well as oxygen diffusion on UN(001) surface which hase been performed with complete relaxation. We estimate surface supercell size and slab thickness which allow us to obtain accurate results for UN surface. It has been found that use of 7-layer slab with 3×3 surface extension vectors gives results that are qualitatively close to single defect model. However, in the case of smaller 2×2 supercells and 5-layers slabs one can observe noticeable lateral interaction between the defects. We have also compared energies of (*i*) nitrogen vacancy formation, (*ii*) oxygen atom adsorption upon U or N surface atom as well (*iii*) O atom incorporation into N vacancy evaluated for both UN (001) and (110) surfaces.

In spite of aforesaid, some questions about UN surface are still opened. evaluations of formation energies for U vacancies performed so far demand additional verifications of these results using other theoretical methods as well as further development of uranium atom pseudopotentials. To obtain more precise results for oxygen diffusion along the UN(001) surface, the Nudged Elastic Band method [49] must be applied which allows one to obtain more realistic trajectories of atom migration. The performance of this approach will be significantly improved when using the latest release of *VASP-5* computer code as compared to *VASP-4* version used for calculations within this PhD Thesis. It will allow us to obtain reasonable results during the reasonable CPU time. The new experimental measuruments on UN surface (for example, EXAFS measurments, which allow one to observe atomic environment around separate atoms or UPS spectra for identification of oxynitride-like structures) will be also significant for versatile pucture construction of UN oxidation process. This is also important for elaboration of reliable protection of UN samples against aggressive influence of oxygen.

On the whole, the results described in the PhD Thesis represent the significant step for modeling of actinide compounds and promote to better understanding of UN surface oxidation.

11. Main theses

- The results obtained using the two substantially different DFT computational methods based on formalisms of Plane-Waves (PW) and Linear Combination of Atomc Orbitals (LCAO) demonstrate their good qualitative agreement, *i.e.* serve as a reliable verification of obtained results.
- The formation energies for U and N vacancies indicate a clear trend for segregation of vacancies towards the surface (and probably, grain boundaries).
- Results obtained for interaction of O atoms and O_2 molecules with UN surfaces demonstrate a strong chemisorption, typical for metallic adsorbents. The possibility for spontaneous dissociation of the adsorbed oxygen molecules upon the perfect UN(001) surface, analogously to the O_2 dissociation on metallic surfaces, has been demonstrated. After molecular dissociation, O adatom forms a strong chemical bond with the U_{surf} atom beneath which can be considered as one-center surface complex. In the case of O adatom positioned atop the N_{surf} atom, this complex is rather multi-center which involves 4 adjacent U_{surf} atoms.
- High mobility of O_{ads} atoms along the surface due to relatively low migration barriers (<0.5 eV) has been demonstrated. The possibility of low-barrier (~0.5-1 eV) oxygen adatom incorporation into existing N vacancy from the nearest adsorption site atop U_{surf} atom has been proved too as well as energetical stability of UN surface containing incorporated oxygen atoms.
- The following stages for reactivity of oxygen positioned atop the UN surface could be suggested: (*i*) chemisorption of molecular oxygen, (*ii*) spontaneous breaking of the O_2 chemical bond after molecular adsorption, (*iii*) location of the two newly formed O adatoms atop the adjacent surface U atoms, (*iv*) high mobility of O_{ads} atoms along the surface, (*v*) low-barrier incorporation of oxygen adatoms from the positions atop U_{surf} atoms into the nearest N vacancies, *(vi)* stabilization of O_{ads} atom inside N_{surf} vacancy, (*vii*) incorporation of O atoms in existing subsurface N vacancies as a result of inter-lattice diffusion. This explains an easy UN oxidation observed in air.

12. Literature

12.1. Author's publications related to this work

[P1] R.A. Evarestov, A.V. Bandura, M.V. Losev, E.A. Kotomin, Yu.F. Zhukovskii, and D. Bocharov, A first principles DFT study in UN bulk and (001) surface: Comparative LCAO and PW calculations. - J. Comput. Chem., 2008, **29**, p. 2079-2087.

[P2] Yu.F. Zhukovskii, D. Bocharov, E.A. Kotomin, R.A. Evarestov, and A.V. Bandura, First principles calculations of oxygen adsorption on the UN(001) surface. - Surf. Sci., 2009, **603**, p. 50-53.

[P3] Yu.F. Zhukovskii, D. Bocharov, and E.A. Kotomin, Chemisorption of a molecular oxygen on the UN(001) surface: *ab initio* calculations. - J. Nucl. Mater., 2009, **393**, p. 504-507.

[P4] D. Bocharov, D. Gryaznov, Yu.F. Zhukovskii, and E.A. Kotomin, DFT calculations of point defects on UN(001) surface. - Surf. Sci., 2011, **605**, p. 396-400.

[P5] D. Bocharov, D. Gryaznov, Yu.F. Zhukovskii, E.A. Kotomin, *Ab initio* modeling of oxygen impurity atom incorporation into uranium mononitride surface and subsurface vacancies. - J. Nucl. Mater., 2011, **416,** p. 200-204.

12.2. Other author's publications

[O1] D. Bocharov, A. Kuzmin, J. Purans, and Yu.F. Zhukovskii, Quantum chemistry studies of the O *K*-edge X-ray absorption in WO_3 and AWO_3. - SPIE Proceedings, 2008, 71420T (p. 1-9).

[O2] N. Zaporina, O. Doynikova, A. Krumina, D. Bocharov, and J. Grabis, Methods of electron microdiffraction and X-ray analysis in structure study of nanodisperse partially stabilized ZrO_2 powders. - J. Surf. Investigation: X-ray, Synchrotron and Neutron Techniques, 2009, **3**, p. 464-467.

[O3] N. Zaporina, J. Grabis, V.N. Timofeev, and D. Bocharov**,** Microstructural investigations of multicomponent SiC/Si_3N_4-Al_2O_3-Y_2O_3 nanopowders. - Latv. J. Chem., 2010, No 1, p. 33-38.

12.3. References

[1] Hj. Matzke, Science of Advanced LMFBR Fuel, North Holland, Amsterdam, 1986.

[2] The Nuclear Fuel Cycle. P.D. Wilson (Eds.), University Press, Oxford, 1996.

[3] H. Wiame, M. Centeno, S. Pacard, P. Bastian, and P. Grange, Thermal oxidation under oxygen of zirconium nitride studied by XPS, DRIFTS, TG-MS. - J. Eur. Ceram. Soc., 1998, **18**, p. 1293-1299.

[4] M. Walter, Oxidation of inert matrices, JRC-ITU-TN-2005/35 (Research report).

[5] N. Curry, An investigation of the magnetic structure of uranium nitride by neutron diffraction. - Proc. Phys. Soc., 1965, **86**, p. 1193-1198.

[6] T. Muromura and H. Tagawa, Lattice parameter of uranium mononitride. - J. Nucl. Mater., 1979, **79**, p. 264-266.

[7] P.E. Evans and T.J. Davies, Uranium nitrides. - J. Nucl. Mater., 1963, **10**, p. 43-55.

[8] N.-T.H. Kim-Ngan, A.G. Balogh, L. Havela, and T. Gouder, Ion beam mixing in uranium nitride thin films studied by Rutherford Backscattering Spectroscopy. - Nucl. Instr. Meth. Phys. Res. B, 2010, **268**, p. 1875–1879.

[9] G.W. Chinthaka Silva, Ch.B. Yeamans, L. Ma, G.S. Cerefice, K.R. Czerwinski, and A.P. Sattelberger, Microscopic characterization of uranium nitrides synthesized by oxidative ammonolysis of uranium tetrafluoride. - Chem. Mat., 2008, **20**, p. 3076-3084.

[10] G.C. Allen and N.R. Holmes, The passivation of uranium metal surfaces by nitrogen bombardment - the formation of uranium nitride. - J. Nucl. Mater., 1988, **152**, p. 187-193.

[11] P.R. Norton, R.L. Tapping, D.K. Creber, and W.J.L. Buyers, Nature of the 5*f* electrons in uranium nitride: A photoelectron spectroscopic study of UN, U, UO_2, ThN, and Th. - Phys. Rev. B, 1980, **21**, p. 2572-2577.

[12] T. Ito, H. Kumigashira, S. Souma, T. Tahakashi, and T. Suzuki, High-resolution angle-resolved photoemission study of UN and USb; Dual character of 5*f* electrons. - J. Magn. Magn. Mater., 2001, **226-230**, p. 68-69.

[13] M. Marutzky, U. Barkow, J. Schoenes, and R. Troć, Optical and magneto-optical properties of single crystalline uranium nitride. - J. Magn. Magn. Mater., 2006, **299**, p. 225–230.

[14] B. Reihl, G. Hollinger, and F.J. Himpsel, Itinerant 5*f*-electron antiferromagnetism in uranium nitride: A temperature-dependent angle-resolved photoemission study. - Phys. Rev. B, 1983, **28**, p. 1490–1494.

[15] M. Paljević and Z. Despotović, Oxidation of uranium mononitride. - J. Nucl. Mater., 1975, **57**, p. 253-257.

[16] Y. Arai, M. Morihira, and T. Ohmichi, The effect of oxygen impurity on the characteristics of uranium and uranium-plutonium mixed nitride fuels. - J. Nucl. Mater., 1993, **202**, p. 70-78.

[17] L. Black, F. Miserque, T. Gouder, L. Havela, J. Rebizant, and F. Wastin, Preparation and photoelectron spectroscopy study of UN_x thin films. - J. Alloys Comp., 2001, **315**, p. 36–41.

[18] M. Eckle, and T. Gouder, Photoemission study of UN_xO_y and UC_xO_y in thin films. - J. Alloys Comp., 2004, **374**, p. 261–264.

[19] S. Sunder and N.H. Miller, XPS and XRD studies of corrosion of uranium nitride by water. - J. Alloys Comp., 1998, **271–273**, p. 568–572.

[20] D. Sedmidubsky, R.J.M. Konings, and P. Novak, Calculation of enthalpies of formation of actinide nitrides. - J. Nucl. Mater., 2005, **344**, p. 40–44.

[21] P. Weinberger, C.P. Mallett, R. Podloucky, and A. Neckel, The electronic structure of HfN, TaN and UN. - J. Phys. C: Solid St. Phys., **13**, 1980, p. 173-187.

[22] M.S. Brooks and D. Glötzel, Some aspects of the electronic structure of uranium pnictides and chalcogenides. - Physica B, 1980, **102**, p. 51-58.

[23] M.S. Brooks, Electronic structure of NaCl-type compounds of the light actinides. I. UN, UC, and UO. - J. Phys. F: Met. Phys., 1984, **14**, 639-652.

[24] G.K. Johnson and E.H.P. Cordfunke, The enthalpies of formation of uranium mononitride and α- and β-uranium sesquinitride by fluorine bomb calorimetry. - J. Chem. Thermodyn., 1981, **13**, p. 273-282.

[25] R. Atta-Fynn and A.K. Ray, Density functional study of the actinide nitrides. - Phys. Rev. B, 2007, **76**, 115101 (p. 1-12).

[26] P.F. Weck, E. Kim, N. Balakrishnan, F. Poineau, C.B. Yeamans, and K.R. Czerwinski, First-principles study of single-crystal uranium mono- and dinitride. - Chem. Phys. Lett., 2007, **443**, p. 82–86.

[27] Y. Lu, B.-T. Wang, R.-W. Li, H. Shi, and P. Zhang, Structural, electronic, and thermodynamic properties of UN: Systematic density functional calculations. - J. Nucl. Mater., 2010, **406,** p. 218–222.

[28] B. Dorado, B. Amadon, M. Freyss, and M. Bertolus, DFT+*U* calculations of the ground state and metastable states of uranium dioxide. - Phys. Rev. B, 2010, **79**, 235125 (p. 1-8)

[29] B. Dorado, G. Jomard, M. Freyss, and M. Bertolus, Stability of oxygen point defects in UO_2 by first-principles DFT+*U* calculations: Occupation matrix control and Jahn-Teller distortion. - Phys. Rev. B, 2010, **82**, 035114 (p. 1-11).

[30] D. Gryaznov, E. Heifets and E.A. Kotomin, *Ab initio* DFT+*U* study of He atom incorporation into UO_2 crystals. - Phys. Chem. & Chem. Phys., 2009, **11**, p. 7241-7247

[31] D. Rafaja, L. Havela, R. Kuel, F. Wastin, E. Colineau, and T. Gouder, Real structure and magnetic properties of UN thin films. – 2005, **386,** p. 87-95.

[32] Z. Yongbin, M. Daqiao, Z. Zhenghe, and M. Meizhong, Pseudopotential plane-wave study of the uranium metals and uranium compounds. – Chin. J. Chem. Phys., 2005, **18**, p. 735-739.

[33] E.A. Kotomin, Yu.A. Mastrikov, Yu.F. Zhukovskii, P. Van Uffelen, and V.V. Rondinella, First-principles modelling of defects in advanced nuclear fuels. - Phys. Stat. Sol. (c), 2007, **4**, p. 1193-1196.

[34] E.A. Kotomin, R.W. Grimes, Yu.A. Mastrikov, and N.J. Ashley, Atomic scale DFT simulations of point defects in uranium nitride. - J. Phys.: Cond. Mat, 2007, **19**, 106208 (p. 1-9).

[35] E.A. Kotomin, D. Gryaznov, R.W. Grimes, D. Parfitt, Yu.F. Zhukovskii, Yu.A. Mastrikov, P. Van Uffelen, V.V. Rondinella, and R.J.M. Konings, First-principles modelling of radiation defects in advanced nuclear fuels. - Nucl. Instr. Meth. Phys. Res. B, 2008, **266**, p. 2671–2675.

[36] R.A. Evarestov, M.V. Losev, A.I. Panin, N.S. Mosyagin, and A.V. Titov, Electronic structure of crystalline uranium nitride: LCAO DFT calculations. - Phys. Stat. Solidi (b), 2008, **245**, p. 114 -122.

[37] R.A. Evarestov, A.I. Panin, A.V. Bandura, and M.V. Losev, Electronic structure of crystalline uranium nitrides UN, U_2N_3 and UN_2: LCAO calculations with the basis set optimization. – J. Phys.: Conf. Ser., 2008, **117**, 012015 (p. 1-8).

[38] K.N. Kudin, G. E. Scuseria, and R.L. Martin, Hybrid Density-Functional Theory and the insulating gap of UO_2. - Phys. Rev. Lett. 2002, **89**, 266402 (p. 1-4).

[39] S.L. Dudarev, G.A. Botton, S.Y. Savrasov, C.J. Humphreys, and A.P. Sutton, Electron-energy-loss spectra and the structural stability of nickel oxide: An LSDA+*U* study. - Phys. Rev. B, 1998, **57**, p. 1505–1509.

[40] F. Gupta, G. Brillant, and A. Pasturel, Correlation effects and energetics of point defects in uranium dioxide: a first principle investigation. - Phil. Mag., 2007, **87**, p. 2561–2569.

[41] M. Freyss, First-principles study of uranium carbide: Accommodation of point defects and of helium, xenon, and oxygen impurities. - Phys. Rev. B, 2010, **81**, 014101 (p. 1-16).

[42] H. Shibata, T. Tsuru, M. Hirata, and Y. Kaji, First principles study on elastic properties and phase transition of NpN - J. Nucl. Mater., 2010, **401**, p. 113–117.

[43] C.D. Taylor, Evaluation of first-principles techniques for obtaining materials parameters of α-uranium and the (001) α-uranium surface. - Phys. Rev. B, 2008, **77**, 094119 (p. 1-9).

[44] P.E. Bloechl, Projector augmented-wave method. - Phys. Rev. B, 1994, **50**, p. 17953-17979.

[45] A.H.H. Tan, M. Abramowski, R.W. Grimes, and S. Owens, Surface defect configurations on the (100) dipolar surface of UO_2. - Phys. Rev. B, 2005, **72,** p. 035457 (p. 1-6).

[46] F.N. Skomurski, R.C. Ewing, A.L. Rohl, J.D. Gale, and U. Becker, Quantum mechanical *vs.* empirical potential modeling of uranium dioxide (UO_2) surfaces: (111), (110), and (100). - Amer. Mineral., 2006, **91,** p. 1761-1772.

[47] M.N. Huda and A.K. Ray, Electronic structures and bonding of oxygen on plutonium layers. - Eur. Phys. J. B, 2004, **40**, p. 337–346.

[48] R. Atta-Fynn and A. K. Ray, *Ab initio* full-potential fully relativistic study of atomic carbon, nitrogen, and oxygen chemisorption on the (111) surface of δ-Pu. - Phys. Rev. B, 2007, **75**, 195112 (p. 1-13).

[49] G. Kresse and J. Furthmüller, *VASP* the Guide, University of Vienna, 2009; *http://cms.mpi.univie.ac.at/vasp/*

[50] А.В. Бандура и Р.А. Эварестов, Неэмпирические расчеты кристаллов в атомном базисе. Изд-во С.-Петерб. ун-та, Санкт Петербург, 2004 (In Russian).

[51] R.A. Evarestov, Quantum Chemistry of Solids: The LCAO First Principles Treatment of Crystals. Springer Series in Solid State Science, Springer-Verlag, Berlin, 2007.

[52] J. Hafner, *Ab initio* simulations of materials using *VASP*: Density-Functional Theory and beyond. - J. Comput. Chem., 2008, **29**, p. 2044–2078.

[53] L.N. Kantorovich, Quantum Theory of the Solid State: an Introduction. Springer-Verlag, Berlin, 2004.

[54] J.P. Perdew, J.A. Chevary, S.H. Vosko, K.A. Jackson, M.R. Pederson, D.J. Singh, and C. Fiolhais, -Phys. Rev. B, 1992, **46**, p. 6671–6687.

[55] A. Unsöld, Beiträge zur Quantenmechanik des Atoms. - Ann. Phys., 1927, **82**, p. 355-393 (In German); *http://demonstrations.wolfram.com/UnsoeldsTheorem/*

[56] M. Krack, Pseudopotentials for H to Kr optimized for gradient-corrected exchange-correlation functionals. - Theor. Chem. Acc., 2005, **114**, p. 145-152.

[57] N.W. Ashcroft and N.D. Mermin, Solid State Physics. Saunders College Press, Philadelphia, 1976.

[58] G. Kresse and D. Joubert, From ultrasoft pseudopotentials to the projector augmented-wave method. - Phys. Rev. B, 1999, **59**, p. 1758-1775.

[59] H.J. Monkhorst and J.D. Pack, Special points for Brillouin-zone integrations. - Phys. Rev. B, 1976, **13**, p. 5188-5192.

[60] M. Methfessel and A.T. Paxton, High-precision sampling for Brillouin-zone integration in metals. - Phys. Rev. B, 1989, **40**, p. 3616–3621.

[61] G. Kresse and J. Furthmüller, Efficient iterative schemes for *ab initio* total-energy calculations using a plane-wave basis set. - Phys. Rev. B, 1996. **54**, p. 11169-11186.

[62] A. Stathopoulos and C.F. Fischer, A Davidson program for finding a few selected extreme eigenpairs of a large, sparse, real, symmetric matrix. - Comput. Phys. Comm., 1994, **79**, p. 268–290.

[63] R. Dovesi, V.R. Saunders, C. Roetti, R. Orlando, C.M. Zicovich-Wilson, F. Pascale, B. Civalleri, K. Doll, N.M. Harrison, I.J. Bush, Ph. D'Arco and M. Llunell, *CRYSTAL*2006 User's Manual, Università di Torino, Turin, 2006; *http://www.crystal.unito.it/*

[64] J.P. Perdew, K. Burke, and M. Ernzerhof, Generalized gradient approximation made simple. - Phys. Rev. Lett., 1996, **77**, p. 3865-3868.

[65] S. Piskunov, E. Heifets, R.I. Eglitis, and G. Borstel, Bulk properties of $SrTiO_3$, $BaTiO_3$ and $PbTiO_3$ perovskites: An *ab initio* HF/DFT study. - Comput. Mater. Sci., 2004, **29**, p. 165-178.

[66] M.J. Frisch, J.A. Pople, and J.S. Binkley, Self-consistent molecular orbital methods 25. Supplementary functions for Gaussian basis sets. - J. Chem. Phys., 1984, **80**, p. 3265-3269.

[67] W. Kuchle, M. Dolg, H. Stoll, and H. Preuss, Energy-adjusted pseudopotentials for the actinides. Parameter sets and test calculations for thorium and thorium monoxide. - J. Chem. Phys., 1994, **100**, p. 7535- 7544.

[68] A.V. Titov and N.S. Mosyagin, Generalized relativistic effective core potential: Theoretical grounds. - Int. J. Quant. Chem., 1999, 71, p. 359–401.

[69] G. Gilat, General analytic method of zone integration for joint densities of states in metals. - Phys. Rev. B, 1982, **26**, p. 2243–2246.

[70] P.W. Tasker, The stability of ionic crystal surfaces. - J. Phys. C: Solid State Phys., 1979, **12**, p. 4977-4984.

[71] A. Subramanian, L.D. Marks, O. Warschkow, and D.E. Ellis, Direct observation of charge transfer at a MgO (111) surface. - Phys. Rev. Lett., 2004, **92**, 026101 (p. 1-4).

[72] J. Akella, S. Weir, J. M. Wills, and P. Söderlind, Structural stability in uranium. - J. Phys.: Condens. Matter, 1997, **9**, L549 (p. 1-7).

[73] C.G. Van de Walle and J. Neugebauer, First-principles calculations for defects and impurities: Applications to III-nitrides. - J. Appl. Phys., 2004, **95**, p. 3851-3879.

[74] P. Söderlind, First-principles elastic and structural properties of uranium metal. - Phys. Rev. B, 2002, **66.** 085113 (p. 1-7).

[75] B. Dorado, M. Freyss, and G. Martin, GGA+*U* study of the incorporation of iodine in uranium dioxide. - Eur. Phys. J. B, 2009, **69,** p. 203-210.

[76] D.R. Lide (ed.), CRC Handbook of Chemistry and Physics, 88th Edition, CRC Press (2007-2008).

[77] M. Iwasawa, Y. Chen, Y. Kaneta, T. Ohnuma, H. Y. Geng, and M. Kinoshita, First-principles calculation of point defects in uranium dioxide. - *Mat. Trans*, 2006, **47,** p. 2651-2657.

[78] NIST Chemistry Web-book (2010); *http://www.webbook.nist.gov/chemistry/*

[79] Yu.F. Zhukovskii, P.W.M. Jacobs, and M. Causà, On the mechanism of the interaction between oxygen and close-packed single-crystal aluminum surfaces. - J. Phys. Chem. Solids, 2003, **64**, p. 1317-1331.

[80] S. Piskunov, Yu.F. Zhukovskii, E.A. Kotomin, E. Heifets, and D.E. Ellis, Adsorption of atomic and molecular oxygen on the $SrTiO_3$(001) surfaces: Predictions by means of hybrid density functional calculations. - MRS Proc., 2006, **894**, LL08-05 (p. 1-6).

[81] R. Weast, CRC Handbook of Chemistry and Physics. CRC Press Inc., Boca Baton (FL), 1985.

[82] E.A. Kotomin and Yu.A. Mastrikov, First-principles modelling of oxygen impurities in UN nuclear fuels. - J. Nucl. Mater., 2008, **377**, p. 492-495.

[83] R.W. Grimes and C.R.A. Catlow, The stability of fission products in uranium dioxide. - Phil. Trans. Roy. Soc. A, 1991, **335**, p. 609-634.

[84] Y.-L. Lee, J. Kleis, J. Rossmeisl, and D. Morgan, *Ab initio* energetics of $LaBO_3$ (001) (B = Mn, Fe, Co, and Ni) for solid oxide fuel cell cathodes. - Phys. Rev. B, 2009, **80**, 224101 (p. 1-20).

[85] Yu.A. Mastrikov, R. Merkle, E. Heifets, E.A. Kotomin, and J. Maier, Pathways for oxygen incorporation in mixed conducting perovskites: a DFT-based mechanistic analysis for (La, Sr)$MnO_{3-\delta}$. - J. Phys. Chem. C, 2010, **114**, p. 3017-3027.

13. Contributions at scientific conferences

1. ***23rd ISSP Conference (Riga, Latvia, February, 2007).*** D. Bocharov, Yu.F. Zhukovskii, and E.A. Kotomin, "First-principles simulations of oxygen adsorption on perfect and defective UN(001) surface". Abstracts: p. 17.
2. ***The 5th International Conference "Information Technologies and Management", IT&M'2007 (Riga, Latvia, April, 2007).*** Yu.F. Zhukovskii, D. Bocharov, and E.A. Kotomin, "Oxygen chemisorption on the UN(001) surface: periodic DFT simulation". Abstracts: p. 9-10.
3. ***24th Institute of Solid State Physics Conference (Riga, Latvia, February, 2008).*** D. Bocharov, Yu.F. Zhukovskii, D. Gryaznov, R.A. Evarestov, and E.A. Kotomin, "Structure and properties of UN nuclear fuels: quantum chemistry approach". Abstracts: p. 6.
4. ***International Baltic Sea Region conference "Functional materials and nanotechnologies 2008" (Riga, Latvia, April, 2008).*** D. Bocharov, Yu. Zhukovskii, R.A. Evarestov, E.A. Kotomin, and A. Bandura, "Atomic and molecular oxygen adsorption on the UN(001) surface". Abstracts: p. 87.
5. ***7th International Workshop "Materials Models and Simulations for Nuclear Fuels" (Karlsruhe, Germany, September, 2008).*** D. Bocharov, Yu.F. Zhukovskii, and E.A. Kotomin, "Interaction of the oxygen molecule with the UN(001) surface: *Ab initio* modeling".
6. ***25th ISSP Conference (Riga, Latvia, February, 2009).*** D. Bocharov, Yu.F. Zhukovskii, and E.A. Kotomin, "Chemisorption of a molecular oxygen on the UN(001) surface". Abstracts: p. 54.
7. ***International conference "Functional materials and nanotechnologies" FM&NT-2009 (Riga, Latvia, April, 2009).*** D. Bocharov, D. Gryaznov, Yu.F. Zhukovskii, and E.A. Kotomin, "Perfect and defective (001) surface of uranium nitride: *ab initio* calculations". Abstracts: p. 100.
8. ***The 7th International Conference "Information Technologies and Management", IT&M'2009 (Riga, Latvia, April, 2009).*** D. Bocharov, D. Gryaznov, Yu.F. Zhukovskii, and E.A. Kotomin, "*Ab initio* calculations on the atomic and electronic structure of defective UN(001) surface". Abstracts: p. 32-33.
9. ***International Workshop "DFT modelling of actinide solid solutions with the emphasis to bulk properties and Helium behaviour" (Karlsruhe, Germany, September, 2009).*** Yu.F. Zhukovskii, E.A. Kotomin, D. Bocharov, and V.N. Kuzovkov, "The DFT+U calculations on defects in PuO_2 and MOX".
10. ***26th ISSP Conference (Riga, Latvia, February, 2010).*** D. Bocharov, D. Gryaznov, Yu.F. Zhukovskii and E.A. Kotomin, "Surface and subsurface vacancies in uranium nitride: first principles calculations". Abstracts: p. 31.
11. ***International conference "Functional materials and nanotechnologies" FM&NT-2010 (Riga, Latvia, March, 2010).*** D. Bocharov, D. Gryaznov, Yu.F. Zhukovskii and E.A. Kotomin, "First principles calculations on oxygen impurities incorporated in the vacancies of UN(001) substrate". Abstracts: p. 37.
12. ***The 8th International Conference "Information Technologies and Management", IT&M'2010 (Riga, Latvia, April, 2010).*** D. Bocharov, D. Gryaznov, Yu.F. Zhukovskii, and E.A. Kotomin, "*Ab initio* calculations on pure and oxygen-occupied vacancies upon the UN(001) surface". Abstracts: p. 38-39.

13. ***Spring European Materials Research Society (E-MRS) Meeting (Strasbourg, France, June, 2010).*** D. Bocharov, D. Gryaznov, Yu.F. Zhukovskii, and E.A. Kotomin, „Ab initio modeling of oxygen impurities incorporated within UN(001) surface and subsurface vacancies". Abstracts: NPVI-23.
14. ***F-BRIDGE School on Ceramic Nuclear Fuel and Cladding Materials (Karlsruhe, Germany, September-October, 2010).*** D. Bocharov, D. Gryaznov, Yu.F. Zhukovskii, and E.A. Kotomin, "First principles calculations of surface and subsurface vacancies as well as oxygen impurity atoms on UN(001) substrate".
15. ***27th ISSP Conference (Riga, Latvia, February, 2011).*** D. Bocharov, Yu.F. Zhukovskii, D. Gryaznov, and E.A. Kotomin, "Oxygen diffusion processes on UN(001) surface". Abstracts: p. 23.
16. ***45th Russian School on Condensed State Physics (St. Petersburg, Russia, March, 2011).*** D. Bocharov, D. Gryaznov, Yu.F. Zhukovskii, and E.A. Kotomin, „Quantum-chemical modeling of oxidation processes on surface of nitride nuclear fuel". Abstracts: p. 27.
17. ***International conference "Functional materials and nanotechnologies" FM&NT-2011 (Riga, Latvia, April, 2011).*** Yu.F. Zhukovskii, D. Bocharov, D. Gryaznov, and E.A. Kotomin, "First-principles simulations on initial stage of uranium nitride surface oxidation". Abstracts: p. 20.
18. ***International conference "Functional materials and nanotechnologies" FM&NT-2011 (Riga, Latvia, April, 2011).*** D. Bocharov, Yu.F. Zhukovskii, D. Gryaznov, and E.A. Kotomin, "UN(110) surface properties: ab initio calculations". Abstracts: p. 166.
19. ***Spring European Materials Research Society (E-MRS) Meeting (Nice, France, May, 2011).*** D. Bocharov, Yu.F. Zhukovskii, D. Gryaznov, and E.A. Kotomin, "First-principles simulations on initial stages of UN(001) surface oxidation". Abstracts: V4-17.

Acknowledgements

The author gratefully acknowledges the doctoral studies support by the European Social Fund and European Social Fund project No. 2009/0216/1DP/1.1.1.2.0/09/APIA/VIAA/044. The author sincerely thanks J. Chepkasova, R.A. Evarestov, D. Gryaznov, V. Kashcheyevs, E.A. Kotomin, A. Kuzmin, Yu.A. Mastrikov, P. Nazarov, S. Piskunov, J. Timoshenko, P. Van Uffelen, and G. Zvejnieks for valuable suggestions and many stimulating discussions. The technical assistance of A. Gopejenko and A. Gusev is the most valuable. Special gratitute is expressed to my scientific advisor Yu.F. Zhukovskii for permanent support of scientific work during the whole period of PhD studentship, including Thesis preparation as well as to my teacher of chemistry J. Zaikina, teacher of physics M. Samucevicha and to my parents.

LATVIJAS UNIVERSITĀTE
FIZIKAS UN MATEMĀTIKAS FAKULTĀTE

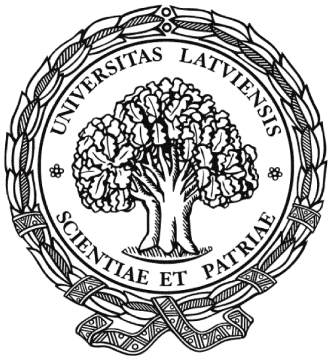

Dmitrijs Bočarovs

VIRSMAS ĪPAŠĪBU UN REAKCIJAS SPĒJU MODELĒŠANA NO PIRMAJIEM PRINCIPIEM NITRĪDU KODOLU DEGVIELAI

Promocijas darbs

Doktora zinātniskā grāda iegūšanai fizikā

Apakšnozare: cietvielu fizika

Promocijas darba vadītājs: *Dr. chem.* **Jurijs Žukovskis**

Rīga, 2012

Promocijas darbs izstrādāts no 2006. gada oktobra līdz 2011. gada augustam
Latvijas Universitātes Cietvielu fizikas institūtā.

Darba forma: publikāciju kopa.

Šis darbs izstrādāts ar Eiropas Sociālā fonda atbalstu projekta „Datorzinatnes pielietojumi un tās saiknes ar kvantu fiziku".
Līguma Nr. 2009/0216/1DP/1.1.1.2.0/09/APIA/VIAA/044

IEGULDĪJUMS TAVĀ NĀKOTNĒ

Promocijas darba vadītājs:
Dr. chem. LU Cietvielu fizikas institūta vadošais petnieks **Jurijs Žukovskis**

Promocijas darba recenzenti:
Dr. lektors **Ģirts Barinovs,** Latvijas Universitātes Fizikas un matemātikas fakultāte
Dr. prof. **Roberto Kačufo** *(Roberto Caciuffo),* Eiropas Komisijas Transurāna elementu institūts
Dr. habil. vadošais pētnieks **Linards Skuja,** Latvijas Universitātes Cietvielu fizikas institūts

Promocijas darbs tiks aizstāvēts atklātā sesijā
LU Fizikas, astronomijas un mehānikas specializētajā promocijas padomes sēdē 2012. gada 24. janvārī. plkst. 15.00 Cietvielu fizikas institūtā Ķengaraga ielā 8, Rīgā.

Ar darbu un tā kopsavilkumu var iepazīties Latvijas Universitātes Bibliotēkā Rīgā, Kalpaka bulv. 4, un Latvijas Akadēmiskajā bibliotēkā Rīgā, Rūpniecības ielā 10.

LU Fizikas un astronomijas zinātnes nozares specializētās promocijas padomes priekšsēdētājs: *Dr. habil. phys.* **Ivars Tāle**

Anotācija

Urāna mononitrīds UN ir viens no materiāliem, kuru var izmantot kā perspektīvu degvielu IV paaudzes kodolu reaktoriem. Tā kā UN paraugos vienmēr atrodas ievērojams daudzums skābekļa piemaisījumu, nepieciešams izprast O adsorbcijas mehānismu, kā arī tam sekojošo UN oksidēšanos.

Mēs pirmo reizi veicām UN virsmas un tās mijiedarbības ar skābekli detalizētu pētījumu, izmantojot DFT PAW metodi *VASP* programmas ietvaros. U un N vakances veidošanās enerģijas, kā arī saites enerģijas virs UN virsmas adsorbētajiem skābekļa atomiem un molekulām tika apskatītas kopā ar lādiņu pārdalīšanos, elektronisko stāvokļu blīvumu un O atomu migrācijas trajektorijām. Veiktie aprēķini ļauj piedāvāt enerģētiski iespējamo mehānismu UN(001) virsmas daļējai piesātināšanai ar skābekli. Tas izskaidro eksperimentāli novērojamo vieglo UN oksidāciju gaisā.

Atslēgvārdi: kvantu ķīmija, blīvuma funkcionāļa teorijas aprēķini, urāna mono- nitrīds, virsmas defekti, skābekļa adsorbcija.

Abstract

The uranium mononitride UN is a material considered as promising candidate for Generation-IV nuclear reactors. Due to considerable amount of aggressive oxygen impurities in UN samples, it is necessary to understand the mechanism of O adsorption and further oxidation of UN.

The first detailed study of UN surface, including its interaction with oxygen, have been performed using DFT PAW method as implemented in the *VASP* computer code. The formation energies of U and N vacancies as well as binding energies of O atoms and molecules adsorbed atop the UN surface are discussed together with the charge redistributions, densities of states, and O atom migration trajectories. Calculations allow us to propose energetically feasible mechanism for the partial saturation of UN(001) surface by oxygen which can lead to easy UN oxidation observed in air.

Keywords: Quantum chemistry, Density Functional Theory calculations, uranium mononitride, surface defects, oxygen adsorption

Autora publicētie darbi par promocijas tēmu

[P1] R.A. Evarestov, A.V. Bandura, M.V. Losev, E.A. Kotomin, Yu.F. Zhukovskii, and D. Bocharov, A first principles DFT study in UN bulk and (001) surface: Comparative LCAO and PW calculations. - J. Comput. Chem., 2008, **29**, p. 2079-2087.

[P2] Yu.F. Zhukovskii, D. Bocharov, E.A. Kotomin, R.A. Evarestov, and A.V. Bandura, First principles calculations of oxygen adsorption on the UN(001) surface. - Surf. Sci., 2009, **603**, p. 50-53.

[P3] Yu.F. Zhukovskii, D. Bocharov, and E.A. Kotomin, Chemisorption of a molecular oxygen on the UN (001) surface: *ab initio* calculations. - J. Nucl. Mater., 2009, **393**, p. 504-507.

[P4] D. Bocharov, D. Gryaznov, Yu.F. Zhukovskii, and E.A. Kotomin, DFT calculations of point defects on UN(001) surface. - Surf. Sci., 2011, **605**, p. 396-400.

[P5] D. Bocharov, D. Gryaznov, Yu.F. Zhukovskii, E.A. Kotomin, *Ab initio* modeling of oxygen impurity atom incorporation into uranium mononitride surface and subsurface vacancies. - J. Nucl. Mater., 2011, **416**, p. 200-204.

A First-Principles DFT Study of UN Bulk and (001) Surface: Comparative LCAO and PW Calculations

R. A. EVARESTOV,[1] A. V. BANDURA,[1] M. V. LOSEV,[1] E. A. KOTOMIN,[2] Yu. F. ZHUKOVSKII,[2] D. BOCHAROV[2]
[1]*Department of Quantum Chemistry, St. Petersburg State University, 198504 St. Peterhof, University Prospect 26, Russia*
[2]*Institute for Solid State Physics, University of Latvia, 8 Kengaraga Str., Riga, LV-1063, Latvia*

Received 13 January 2008; Revised 10 April 2008; Accepted 11 April 2008
DOI 10.1002/jcc.21023
Published online 21 May 2008 in Wiley InterScience (www.interscience.wiley.com).

Abstract: LCAO and PW DFT calculations of the lattice constant, bulk modulus, cohesive energy, charge distribution, band structure, and DOS for UN single crystal are analyzed. It is demonstrated that a choice of the uranium atom relativistic effective core potentials considerably affects the band structure and magnetic structure at low temperatures. All calculations indicate mixed metallic-covalent chemical bonding in UN crystal with U5*f* states near the Fermi level. On the basis of the experience accumulated in UN bulk simulations, we compare the atomic and electronic structure as well as the formation energy for UN(001) surface calculated on slabs of different thickness using both DFT approaches.

 J Comput Chem 29: 2079–2087, 2008

Key words: first-principles calculations; actinides; uranium nitride

Introduction

Uranium mononitride and carbide (UN, UC) attract a considerable attention as promising nuclear fuel materials for novel Generation IV reactors.[1] In particular, nitrides and carbides exhibit higher thermal conductivity, melting temperature, and metal density when compared with uranium dioxide that is commonly used nowadays. To predict nuclear fuel performance under different operating conditions and then a prolonged time in repository for used fuel, it is necessary to understand and predict material physicochemical properties. Of special importance are surface properties because commercial fuels are used as powders and UN, UC are effectively oxidized in air. The more so, numerous grain boundaries considerably affect material properties.

Theoretical studies of uranium compounds are difficult due to a relativistic character of electron motion in the U atom core and strong electron–electron correlation. Moreover, UN is a rather complicated system because it is characterized by a mixed metal-covalent chemical bonding. The metallic part (U5*f* states near the Fermi level) is better described by a delocalized basis of the Plane Waves (PW), whereas the covalent part (U5*f*-N2*p* hybridization) by a Linear Combination of Atomic Orbital (LCAO) basis set. This is why in this article we compare results of both approaches.

In Section "Previous *ab initio* simulations on UN bulk," the comparison is made for the bulk properties (studied earlier experimentally), with a detailed analysis of relativistic pseudopotentials in Section "Current DFT LCAO and PW calculations on UN bulk." In "DFT LCAO and PW calculations on UN(001) surface" section, we discuss—for the first time—the (001) surface properties (so far, the atomistic simulations on U compound substrates were performed only for densely packed UO_2 surfaces[2]).

Previous *Ab Initio* Simulations on UN Bulk

UN single crystal possesses *fcc* (face-centered cubic) structure with two atoms per unit cell: the lattice constant $a_0 = 4.886$ Å, the bulk modulus $B = 194$ GPa, and the cohesive energy $E_0 = 13.6$ eV.[1] These properties could be used as the test for theoretical calculations. Below 53 K UN undergoes the antiferromagnetic (AFM) ordering with the doubled unit cell and the spin density (SD) of 0.75 μ_B per U ion (at 4.2 K). Above this temperature, it reveals paramagnetic properties with the effective magnetic moment in the Curie-Weiss law of $\sim$3.1 μ_B. UN shows a metallic conductivity.

So far, most of calculations were performed for the high temperature phase (a primitive unit cell) relevant for fuel applications. The first relativistic KKR[3] and LMTO[4] calculations were performed already in 80s focusing mostly on the atomic and band structure of UN crystal. The calculated lattice parameters were within 3% of the experimental value, whereas the bulk

Correspondence to: R. A. Evarestov; e-mail: re1973@re1973.spb.edu

Table 1. Calculated Properties of UN Bulk Crystal.[a]

Property	PBE-AE-LAPW[5,6 b]	PBE-US[9]	PW91-PAW[10 c]	PW91-US[11 d]	PW91-AE[12]	PW91-LCAO[13 e]
a_0, Å	4.886	4.820	4.864	4.954	4.90	Fixed expt.
B, GPa	209		226	182		
E_c, eV	13.4		14.7	12.3		9.9–12.8
SD, μ_B	1.25		1.05			3.02–3.20

Lattice constant a_0, bulk modulus B, cohesive energy E_c and spin density SD per unit cell. AE, all electrons; US, ultrasoft pseudopotentials.
[a]In the LCAO approach, the value of E_c is calculated with respect to the free N and U atoms, whereas in the PW approach it was estimated with respect to the same atoms placed in cubic supercells with large (10 Å) translation vectors.
[b]WIEN-2k code.
[c]VASP code.
[d]CASTEP code.
[e]GAUSSIAN code.

modulus was reproduced worse, within 11%. Only recently these first principles calculations were continued (Table 1). In particular, the all-electron (AE) LAPW calculations (refs. 5, 6; Sedmidubsky et al., unpublished, 2005) were performed using the GGA-PBE (Perdew-Burke-Ernzerhof) exchange correlation functionals with and without incorporation of the spin-orbital interaction (WIEN-2k computer code) for a series of actinide nitrides. The calculated cohesive energy and the lattice constant are close to the experimental values. Incorporation of the spin-orbital coupling leads to a large (8.2 eV) splitting of U*6p* semicore into $6p_{1/2}$ and $6p_{3/2}$ as well as slight reduction of the magnetic moment from 1.25 down to 1.16 μ_B. The hybridization of N*2p*, U*5f*, and U*6d* states was observed in the Brillouin zone (BZ) due to their overlap: the N*2p* energy levels lie in the region of -6 to -1 eV whereas the U*5f* states dominate near and at the Fermi level. The calculated band structure around the Fermi level is in qualitative agreement with the experimental UPS spectra.[7,8]

In ref. 6 the WIEN-2k calculations were complemented by a study of the AFM phase. The lattice constant is in a good agreement with the experiment (~0.4%), but—unlike the experiment—the ferromagnetic structure is found to be lower in energy, with the SD = 0.96 μ_B. It should be pointed out that this is presumably a failing of the PBE functional. Notice, that due to use of muffin-tin spheres, the attribution of the electronic and spin density to individual ions is not uniquely defined.

Systematic DFT-PW calculations were also performed, starting with a study[9] focused on the UN and UC atomic structure. Using the ultra-soft (US) pseudopotentials and PBE96 exchange-correlation functional, the experimental UN and U_2N_3 lattice constants were reproduced within 3% error. In the more detailed UN, UN_2, and U_2N_3 DFT PW calculations, the VASP[10] and CASTEP[11] codes using the Perdew-Wang (PW91) nonlocal GGA exchange-correlation functional[14] were employed and combined with either the US or PAW pseudopotentials, respectively. Both methods agree on complicated mixed metallic-covalent nature of the UN chemical bonding and reproduce well the lattice constants, bulk moduli, and cohesive energies. Analogously to previous calculations for the primitive unit cell, they suggest the magnetic moment on U ion close to unity. The DFT PW approach combined with a supercell model was further used in the calculations of defective UN crystal, containing single point defects and Frenkel and Schottky defect pairs.[10,11] A study of defect properties is of key importance for the prediction of fuel behavior under operational conditions and in further centuries-long depository.

One more first-principles all-electron relativistic DFT study with GGA PW91 exchange correlation functional and numerical double ξ basis set was performed recently for UN and UN_2[12]; the results are compared with the experimental EXAFS and X-ray diffraction data. New element in that article is a calculation of the phonon frequencies and heat capacities, which are important for the fuel behavior prediction. Authors provide additional evidence for an important role of itinerant U*5f* states in thermodynamic properties.

To understand better the UN fuel performance, careful study of the chemical bonding in crystalline bulk and its surface properties is a necessary step. The LCAO approach is a natural way for such a study as it extends for the periodic systems the chemical bonding analysis developed in quantum chemistry of molecules,[15] and it is free of muffin-tin approximation problems. In particular, recent first principles DFT and hybrid HF-DFT LCAO calculations of UO_2 crystal[16] provided the structural, electronic, and magnetic properties in a good agreement with the experimental data.

The ground state valence electronic configurations of U and N atoms are $5f^3 6d^1 7s^2$ and $2s^2 2p^3$, respectively. In a crude ionic bonding picture, the U*6d* and *7s* electrons fill the N*2p* states and the three U*5f* electrons form the highest occupied molecular orbital (HOMO).[17] The LCAO calculations allow one to study this qualitative picture in more detail, analyzing the changes of the free atom electronic structure due to the chemical bonding formation, and to connect the energy bands of a solid with the atomic states. However, the first LCAO electronic structure calculations of crystalline UN have been only recently performed.[13] In that article, several different Relativistic Effective Core Potentials (RECP) containing 60, 78, and 81 electrons in a U ion core, which are discussed in more detail in the next RECP Formalism, were used and compared. In particular, for the RECP78, there exist 14 outermost uranium atom electrons

included into the valence shell ($6s^26p^66d^15f^37s^2$). The results obtained were compared with those for RECP60, where 32 outermost uranium atom electrons are included in the valence shell (the configuration $5s^25p^65d^{10}6s^26p^66d^15f^37s^2$). Lastly, in the RECP81 U5*f* electrons are included into the atomic core.

Recent LCAO calculations on UN bulk[13] have been performed using the GAUSSIAN-03 computer code with the PW91 exchange-correlation functional and periodic boundary conditions. Unlike previous PW calculations, the LCAO (RECP78) suggests the ground state with the three unpaired electrons ($S_z = 3/2$, i.e., $SD \approx 3\ \mu_B$) whereas the $S_z = 1/2$ state lies slightly higher in energy (~0.5 eV). The latter is close to that experimentally observed. The values of cohesive energy calculated for RECP78 and RECP60 considerably differ (9.86 and 12.8 eV, respectively, last column in Table 1), thus indicating an importance of the U outer shell relaxation.

Group-theoretical analysis performed for interpretation of the UN band structure demonstrates that threefold degenerate (at Γ point) U5*f* t_{2u} state is split at X and W points of the BZ due to hybridization with the N2*p* states, which produces a narrow band near the Fermi level (~2 eV). This band is occupied with 3 spin-up electrons. The U5*f* t_{1u} state is allowed by symmetry to mix up with N2*p* state at the Γ point and form a broad band to the lower-energy side. Lastly, the nondegenerate U5*f* a_{2u} state is empty; it forms the bottom of the conduction band (CB). In other words, both bottom of the CB and the top of the valence band (VB) are formed by U5*f* states which leads to the metallic nature of this compound[13] (unlike UO_2 which is a semiconductor[16]). The Mulliken effective atomic charges of ±(1.5–2.0) *e* calculated using the GAUSSIAN-03 code confirm the mixed nature of the UN chemical bonding and are in agreement with the Bader topological charges of ±1.6 *e* obtained in PW calculations.[11]

Current DFT LCAO and PW Calculations on UN Bulk

RECP Formalism

As mentioned above, the proper choice of relativistic core pseudopotentials is important for reliable DFT calculations. The different methods for construction of RECP have been suggested so far.[15] To the best of our knowledge, the small core (SC) pseudopotentials of U atom (60 core electrons, with 5*s*, 5*p*, and 5*d* electrons referred to the valence shell) were generated only for LCAO calculations. Unreliability of the large core (LC) pseudopotentials RECP78 for U was known in calculations of uranyl UO_2^{+2} ion[18] as well as molecules of uranium fluorides UF_5 and UF_6.[19] In particular, the most famous molecular failure was that for the uranyl ion, predicted to be bent using the LC RECP, whereas the correct linear structure was recovered only with the SC pseudopotential.

We use here the energy-adjusted small core (SC) pseudopotential by Stuttgart-Cologne group (SC60).[20] Its parameters are fitted to the excitation and ionization energies obtained in the relativistic all-electron calculations performed using a numerical finite difference approach. The RECP generation method based on numerical Dirac-Hartree-Fock wave function, allows one the computation of averaged (over $(l-1/2)$ and $(l+1/2)$ components) relativistic effective potentials (AREP) and includes also the effective spin-orbit potential (ESOP) operators. Use of the energy-adjusted pseudopotentials SC60 in the complete form (with ESOP) requires use of a two-component spinor (spin-orbital) formalism in molecular or crystalline calculations. In our scalar-relativistic calculations only the AREP part of RECP has been employed.

The accuracy of the calculations with the energy-adjusted RECPs is essentially limited by the demand that only the radially local (semilocal) RECP operator is used. A more strict treatment of the outermost core electrons (for example, U6*s* and 6*p* electrons) demands to treat them explicitly. Since effective potentials are somewhat different for the outermost core and valence electrons with the same orbital and total moment, new terms with projectors on the outermost core pseudoorbitals were added to the conventional core pseudopotential operator in the Generalized RECP (GRECP) method (see ref. 21 and references herein). The importance of additional nonlocal terms in the expression GRECP operator is demonstrated in U atom calculations.[22] In the present calculations we have used for U atom the only radially local AREP version by the Mosyagin-Titov LC (MT78) and SC (MT60) pseudopotentials.[13]

The radially local AREP form used in LCAO calculations is a sum of a Coulomb term *C*, a local term V_{loc} and a semilocal term V_{sl} usually presented analytically as

$$V_{PS}(\mathbf{r}) = C + V_{loc} + V_{sl} = -\frac{Z_N}{r} + \sum_{k=1}^{M} r^{n_k-2} C_k \exp(-\alpha_k r^2) + \sum_{l=0}^{3}\left[\sum_{k=1}^{M_l} r^{n_{kl}-2} C_{kl} \exp(-\alpha_{kl} r^2)\right]\hat{P}_l \quad (1)$$

where Z_N in a Coulomb term is the effective nuclear charge (total nuclear charge minus the number of electrons represented by RECP); n_k, n_{kl} = 0, 1, 2 and C_k, C_{kl}, α_k, α_{kl} are fitting parameters. The local term is a sum of products of polynomial and Gaussian radial functions whereas a semilocal term contains a sum of products of polynomial radial functions, Gaussian radial functions and angular momentum projection operators $\hat{P}_l$. Therefore, to specify the semilocal RECP, one needs to include a set of triplets (coefficient, power of *r* and exponent) for each term in each angular momentum of RECP. The contraction coefficients C_k, C_{kl}, exponents α_k, α_{kl} and powers n_k, n_{kl} are found by fitting the numerical AREP to expansions in Gaussian type functions (GTF) for the different RECP versions.

For each AREP the corresponding numerical atomic orbitals are approximated by the GTFs linear combinations, including both contracted and primitive GTOs. In particular, the contracted part of a U basis set (12*s*11*p*10*d*8*f*)/(8*s*7*p*6*d*4*f*) corresponding to the RECP SC60 in the segmented contraction scheme, defines three *s*-type (5*s*, 6*s*, 7*s*), two *p*-type (5*p*, 6*p*), two *d*-type (5*d*, 6*d*) and one *f*-type (5*f*) orbitals, occupied by the valence electrons in the ground state of U atom. The rest (primitive) GTOs are polarizing and diffuse orbitals necessary to properly describe the tails of the free-atom wave functions. The basis sets 11*s*5*p*6*d*5*f* and 6*s*3*p*4*d*4*f* have been used in our MT60 and MT78 RECP calculations, respectively. Table 2 presents the diffuse primitive Gaus-

Table 2. Diffuse Primitive Gaussian Exponents in the Basis Set of a Free U Atom Corresponding to the Stuttgart-Cologne Pseudopotential SC60.[18]

	Shell type			
GTO	*s*	*p*	*d*	*f*
1	0.071170	0.005000	0.073273	0.181420
2	0.030539		0.005000	0.005000
3	0.005000			

sian exponents in the basis set of a free U atom corresponding to the SC60 pseudopotential.

It is well known that for LCAO bulk calculations the basis set (BS) of free atom has to be modified as the diffuse functions cause numerical problems because of the large overlap with the core functions of the neighboring atoms in a dense-packed crystal.[15] This is why in the bulk calculations the diffuse exponents are either removed (as done in our calculations) or optimized, in order to minimize the total energy per unit cell. For example, the detailed BS optimization performed for Hartree-Fock (HF) and DFT LCAO calculations on $ATiO_3$ perovskites (A = Sr, Ba, Pb)[15] resulted in a good correlation with available experimental data (lattice parameters, bulk moduli and optical band gaps). Although there exist different algorithms for minimization of many-variables functions,[23,24] no analysis of their efficiency for the BS optimization in crystals was done so far.

In our PW calculations presented here the VASP code[25] was applied with the projector-augmented-wave (PAW) pseudopotentials for U and N atoms. The PAW method by Blöchl[26] uses the transformation operator between pseudo-orbitals and original orbitals combining the pseudopotential approach and LAPW method. The U PAW78 pseudopotential with a large U core (LC) RECP (78 core electrons, 14 valence electrons) is the same as in previous VASP calculations on UN[10,11] containing the closed shell configuration $6s^26p^65f^26d^27s^2$ while the U ground state possesses an open shell configuration known as $6s^26p^65f^36d^17s^2$.[25] Unlike those calculations, we have used here two different exchange-correlation functionals and very high accuracy in both *k*-point mesh and cut-off energy. Both LCAO and PW spin-polarized (FM) bulk calculations have been performed for the cubic crystalline structure of UN.

LCAO and PW Calculations on UN Bulk

Previous LCAO calculations clearly demonstrated that the chemical bonding in UN crystal has a metallic-covalent character.[13,17] The partly covalent bonds are formed by the interaction of U5*f* and 6*d* states with the N2*p* states. It was shown that the inclusion of 5*f* electrons in the atomic core (RECP81[13]) introduces small changes in the calculated cohesive energy of UN crystal and electron charge distribution. However, the inclusion of 5*s*, 5*p*, and 5*d* electrons in the valence shell results in a better agreement with values of both calculated and experimentally measured cohesion energy.

In the present and former[13] LCAO studies of UN bulk, we have used the two computer codes: the GAUSSIAN-03[27] and the CRYSTAL-06[28] suited for periodic systems. Both these codes give close results if the direct lattice summation is made up to 50 a.u. in the GAUSSIAN-03 and the tolerances 8 8 8 16 are used in CRYSTAL-06 for the Coulomb and exchange integrals calculations. The Monkhorst-Pack scheme[29] for 16 × 16 × 16 *k*-point mesh in the BZ was applied in both cases. For the N atom, the all-electron basis set 6-311++G(2*d*,2*p*)[30] was used, while the diffuse Gaussian function with the orbital exponent 0.0639 $a.u^{-1}$ was removed from the crystal calculation. As to BS of U atom, all diffuse orbitals (with orbital exponents less than 0.1 $a.u^{-1}$) were removed from the bulk calculations but retained in the free atom calculations.

The results of DFT-LCAO calculations on UN bulk using PW91 exchange and correlation functionals are presented in Table 3 for three different RECPs described above in RECP Formalism. Table 3 shows that the E_c is essentially underestimated in MT78 calculations, but is close to the experimental value in MT60 and SC60 calculations. As to the lattice parameter a_0, our LCAO DFT values (4.78 and 4.80 Å) do not differ much from those obtained in other DFT calculations (Table 1). The bulk modulus B is underestimated in MT78 calculations and overestimated both in MT60 and SC60 calculations. The calculated effective charge of U atom in UN (Q_U) is close to 1.6 *e* for all three RECP used and comparable to 1.7 *e* found in PW PAW78 calculations[10] using the topological Bader analysis.

Table 3 shows also that the populations of 6*d* and 5*f* orbitals on U atom are sensitive to the RECP choice. The AO populations allow us to analyze a role of different U atomic orbitals in the U-N chemical bonding using the RECP SC60 for a valence configuration $5s^25p^65d^{10}6s^26p^66d^15f^37s^2$. The conclusion could be drawn from the Table 3 that the sum of 5*s* and 6*s* orbital populations is close to 4 *e* thus demonstrating their small participation in the U-N chemical bonding. From the UPS and XPS investigations of the core and valence levels of UN, the popula-

Table 3. The Results of Current LCAO Calculations for UN Bulk.

Property		MT78	MT60	SC60
a_0 (4.89)		5.17	4.78	4.80
E_{tot}		−106.5218	−531.0228	−531.9898
E_U		−51.5970	−475.9572	−476.9186
E_c (13.6)		9.6	13.4	13.6
B (194)		167.2	291.6	276.9
Q_U		1.63	1.55	1.58
SD		3.18	1.18	1.06
Populations, *e*				
U	*s*	2.05	4.20	4.04
	p	5.98	12.03	12.15
	d	1.11	11.96	11.96
	f	3.23	2.26	2.27
N	*s*	3.89	3.87	3.87
	p	4.72	4.58	4.64
	d	0.02	0.10	0.07

The energy *per* unit cell E_{tot} and the U atom energy E_U (given in a.u.), the cohesive energy E_c (eV), the lattice constant a_0 (Å), and the bulk modulus *B* (GPa). The experimental values are given in brackets in the first column. The U atom spin density (SD) is given in μ_B.

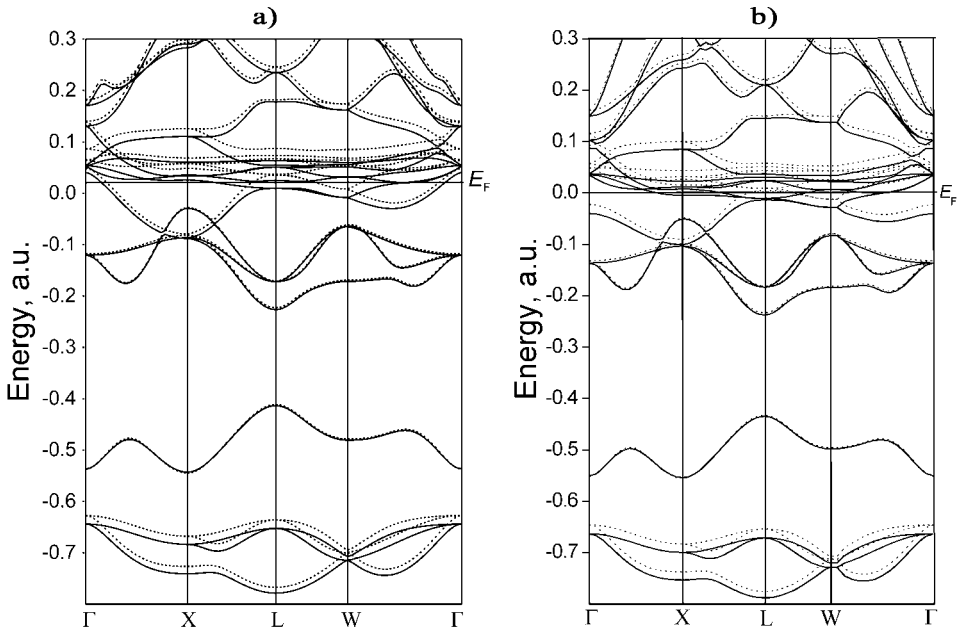

Figure 1. The energy bands of UN crystal constructed for: (a) LCAO PW91 (RECP 60) and (b) PW PW91 (RECP 78) Hamiltonians. The energies are given in a.u., solid and dotted lines correspond to the states with spin up and spin down, respectively.

tion of 2.2 ± 0.5 *e* in the U5*f* band near the Fermi level has been estimated.[17] This result is in good agreement with our DFT-LCAO (2.27 *e*, see Table 3) and FP LAPW (2.17 *e* [6]) values for U5*f* populations. As to U6*d* orbitals, their participation in the chemical bonding is seen from Table 3: for the RECP MT78, 6*d* population is 1.11 *e*, but for both RECPs-60 it is 1.96 *e*. It is also seen that the covalent part of bonding is defined mainly by N2*p* orbitals.

As follows from Table 3, the SD value in the ground state of metallic UN crystals is close to unity in the calculations with the RECP 60. The calculated spin-density of 1.06 μ_B (SC60) is the most close to the experimental value of 0.75 μ_B.[1] This result differs from that found in article[11,13] for different RECP 78 when the ground state with the spin projection 3/2 appeared to be more favorable (the three U5*f* electrons with parallel spins occupying the t_{2u} states near the Fermi level).

Figure 1a shows the upper part of the valence and the lower part of the conduction energy bands obtained in the LCAO DFT-PW91 calculations with the RECP SC60 for the total spin projection $S_z = 1/2$. The lowest in energy threefold degenerates subband and next nondegenerate subband are formed by U6*p* and U6*s*+N2*s* states, respectively. The next threefold subband centered at −0.10 a.u is formed by the hybridized U5*f* + N2*p* states. The highest subbands up to the Fermi level are formed mainly by U5*f* states. The more detailed analysis of the crystalline orbitals at the BZ shows, in particular, that the nondegenerate a_{2u} level is occupied by two (spin-up and spin-down) 5*f* electrons; the third 5*f* unpaired spin-up electron occupies three-fold degenerate t_{2g} level formed by U6*d* states. The relative position of different U5*f* subbands near the Fermi level depends on the RECP chosen. As it follows from ref. [13], the RECP78 calculations change the order of bands in such a way that three spin-up electrons occupy the states of three-fold band near the Fermi level. Thus, the spin density calculated depends on the RECP chosen (∼3 *e* for RECP78 and ∼1 *e* for the RECP60, see Table 3). The choice of the RECP SC60 is preferable, as it gives the best agreement with the experimentally known UN properties. Therefore, in our LCAO surface calculations to be analyzed in next section we used the RECP SC60 for the core electrons.

Computational procedure of the VASP code[25] used for our current DFT-PW calculations applies a standard iterative solution of the Kohn-Sham equations based on residuum-minimization and optimized charge-density mixing routines.[31] They include the calculations of the Hellmann-Feynman forces acting on the atoms and the stresses on the unit cell.[32] The total energy is optimized with respect to the positions of the atoms within the unit cell or supercell. For UN bulk PW calculations, we have applied the same 16 × 16 × 16 *k*-point mesh in the BZ in the framework of Monkhorst-Pack scheme[29] as used in LCAO calculations described above. The cut-off energy was chosen to be 520 eV for the PW91 and PBE Hamiltonians compared here. Main results of these calculations are presented in Table 4 and Figure 1b.

The conclusion could be drawn from the Table 4 that the two DFT functionals used give similar results close to the previous VASP calculations[10,11] performed with a smaller *k*-point mesh and the cut-off energy. A comparison of Tables 3 and 4 demonstrates a qualitative correlation of properties calculated using the LCAO (RECP 60) and the PW (RECP 78) methods, except for bulk modulus which is noticeably overestimated in the CRYSTAL calculations as compared with the experimental value.

The analysis of band structures for UN bulk presented in Figure 1 calculated by LCAO and PW methods using the same

Table 4. The Results of Current PW Calculations for UN Bulk and Their Comparison with Previously Published Data.

Property	PW91	PBE	PW91-PAW[10]	PBE-AE-LAPW[5,6]
a_0 (4.886)	4.868	4.867	4.864	4.886
E_c (13.6)	14.79	14.57	14.7	13.4
B (194)	227	224	226	209
Q_U	1.69	1.69	1.61	–
SD	1.15	1.19	1.05	1.25

See Table 3 footnote for explanation.

PW91 Hamiltonian demonstrates even good quantitative correlation in details especially below the Fermi level, in agreement with the experiment[7] and the previous DOS analysis performed in earlier PW VASP calculations.[11]

DFT LCAO and PW Calculations on UN(001) Surface

Single (2D) and Repeated (3D) Slab Models of a Surface

The single (2D) and repeated (3D) slab models are used in LCAO and PW surface calculations, respectively.[15] The LCAO calculations do not require artificial repeating of slab along the normal to the surface direction as it is made in PW calculations to restore 3D periodicity. However, use of atom-centered Gaussian BS faces in LCAO calculations a rather serious problem known as the basis-set superposition error (BSSE). The problem is that in a system comprising interacting fragments A and B, the fact that the basis sets on A and B are practically always incomplete means that the fragment energy of A has necessarily to be improved by the basis functions on B, irrespective there is any genuine binding interaction in the AB system or not. The improvement in the fragment energies lowers the energy of the combined AB system. The BSSE is an ever-present phenomenon and accurate calculations should always include the BSSE analysis. The examples when one should be particularly concerned include the binding energy of molecules adsorbed on surfaces or calculation of defect formation energies.[15] The approach most commonly used to estimate the BSSE effect is the *counterpoise correction*[33]: the separated fragment energies are computed not in the individual fragment basis sets, but the total basis set for the system including "ghost basis functions" for the fragment that is not present. These energies are then used to define the counterpoise-corrected (CPC) interaction energy.

In the bulk crystal the AO basis of a given atom is extended by AOs centered on atoms in the neighboring unit cells. However, in the slab calculations this is not true for surface atoms. This may lead to underestimate of the slab energy and as a consequence, to overestimate of the surface energy. Moreover, the AO used in the crystal and slab calculation may not be sufficiently diffused to reproduce correctly the electronic density distribution tail in the vacuum outside the surface. Corresponding corrections are similar to those arising for bulk solids and molecules. The simple and physically reasonable way to introduce the CPC interaction for the slab model of a surface (bare, reduced, relaxed) was suggested in ref. [34] and includes the addition of one and two extra layers of ghost atoms on both slab surfaces. The fixed ghost atoms are placed at their bulk positions, thus forming the crystallographic planes next to the surface atomic planes. The additional Gaussians are centered on the ghost atoms and called the extra layer basis set (ELBS). This approach was applied in ref. 34 in a study of water adsorption on $SrTiO_3$ (001) surface. The geometric structure of slabs was reoptimized, fixing the positions of the ghost atoms. It was found that addition of the first ELBS introduces noticeable changes in the calculated properties, whereas the second ELBS has no further effect. In particular, the BSSE correction reduces the surface energy of cubic semiconducting perovskites and decreases the water adsorption energy. For metallic UN crystal the large electron delocalization may increase the influence of the BSSE on the calculated surface energies and surface relaxation. This is demonstrated in the following section.

For DFT-PW surface calculations, we use 3D symmetric slabs consisting of 3–11 atomic layers separated by vacuum gaps up to 15 empty layers (see Fig. 2). This inter-slab distance is large enough to exclude interaction between the neighboring 2D slabs and to allow one the comparison of 2D LCAO and 3D PW results.

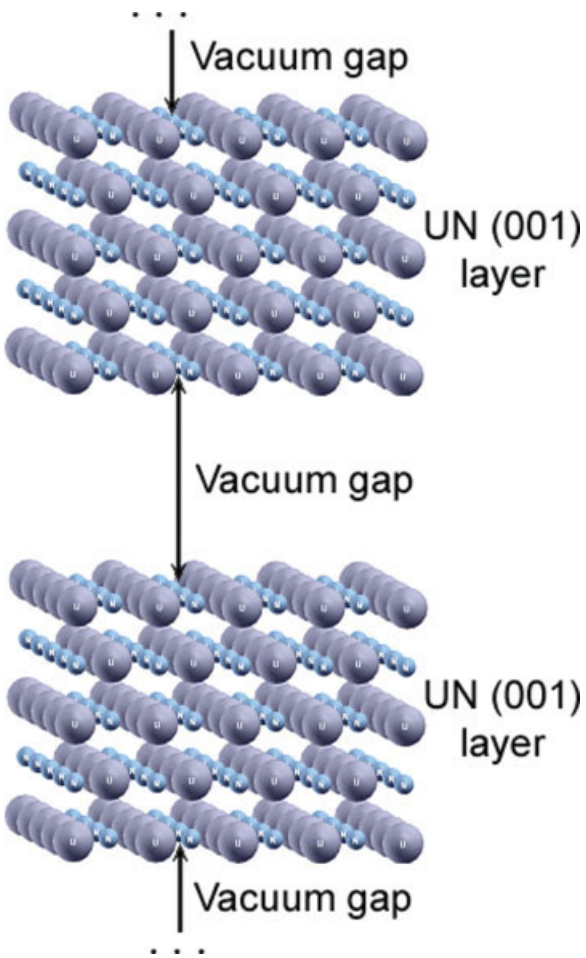

Figure 2. Side view of five-layer 3D slab model of the UN(001) surface.

Table 5. The Calculated Atomic Displacements Δz (Å) on UN (001) obtained for Different Slabs and Methods.

Atom	Method	Number of atomic planes in slab				
		3	5	7	9	11
Surface U	LCAO	−0.085	−0.095	–	–	–
	LCAO (extra layer added)	−0.026	−0.046	–	–	–
	PW PW91	−0.041	−0.020	−0.050	−0.061	−0.057
Subsurface U	LCAO		−0.011	–	–	–
	LCAO (extra layer added)		−0.001	–	–	–
	PW PW91		−0.018	−0.016	−0.013	−0.013
Surface N	LCAO	0.064	0.058	–	–	–
	LCAO (extra layer added)	0.049	0.048	–	–	–
	PW PW91	0.030	0.022	0.025	0.033	0.026
Subsurface N	LCAO		−0.002	–	–	–
	LCAO (extra layer added)		0.027	–	–	–
	PW PW91		0.026	0.028	0.032	0.022

Positive sign means an outward displacement from the slab center and *vice versa*.

In the PW surface calculations, we have used the PW91 Hamiltonian only, since a comparison between results of the PW91 and PBE calculations on UN bulk (Table 4) do not show any noticeable differences. We have applied the same Monkhorst-Pack scheme for the 8 × 8×1 *k*-point mesh. The cut-off energy was chosen 520 eV, similar to the bulk. All calculations were performed for the spin-polarized (FM) surface states.

Comparison of LCAO and PW Results for Unrelaxed and Relaxed Surface

We have analyzed in detail the vertical displacements along the *z* axis of both surface and subsurface atoms from their host lattice sites in UN bulk (Table 5), effective atomic charges (Table 6), the surface energies (Table 7) as well as DOS obtained in the PW calculations (see Fig. 3). The surface energy of an *n*-layer slab was estimated from the standard basic relationship:

$$E_{surf}(n) = \frac{1}{2S}(E_n - nE_b) \quad (2)$$

where E_n is the total slab energy per primitive surface unit cell and S its area, while E_b is the total energy per primitive bulk unit cell.

There is a good qualitative agreement between structural relaxations and effective atomic charges for the LCAO with the

Table 6. The Effective Atomic Charges $q(e)$ on the UN (001) Slab.

Atom	Method	Number of atomic planes in slab				
		3	5	7	9	11
Surface U	LCAO	1.63	1.63	–	–	–
	LCAO (extra layer added)	1.64	1.64	–	–	–
	PW PW91	1.65	1.66	1.72	1.67	1.65
Subsurface U	LCAO	–	1.51	–	–	–
	LCAO (extra layer added)	–	1.55	–	–	–
	PW PW91	–	1.65	1.63	1.63	1.69
Middle U (mirror plane of slab)	LCAO	1.45	1.57	–	–	–
	LCAO (extra layer added)	1.52	1.55	–	–	–
	PW PW91	1.62	1.67	1.72	1.65	1.62
Surface N	LCAO	−1.55	−1.55	–	–	–
	LCAO (extra layer added)	−1.61	−1.60	–	–	–
	PW PW91	−1.64	−1.63	−1.64	−1.63	−1.67
Subsurface N	LCAO	–	−1.59	–	–	–
	LCAO (extra layer added)	–	−1.57	–	–	–
	PW PW91	–	−1.67	−1.7	−1.64	−1.7
Middle N (mirror plane of slab)	LCAO	−1.61	−1.58	–	–	–
	LCAO (extra layer added)	−1.58	−1.57	–	–	–
	PW PW91	−1.65	−1.7	−1.66	−1.62	−1.64

Table 7. Surface Energies E_{surf} (J m^{-2}) and Relaxation Energies E_{rel} (eV) obtained for UN(001) Surface in LCAO and Plane Wave Calculations.

Number of atomic planes in slab			3	5	7	9	11
Method	LCAO	E_{surf} (unrelaxed)	2.20	2.29	2.28	2.11	–
		E_{surf} (relaxed)	2.06	2.13	–	–	–
		E_{rel}	0.203	0.230	–	–	–
	LCAO (extra layer added)	E_{surf} (unrelaxed)	1.68	1.45	–	–	–
		E_{surf} (relaxed)	1.430	1.38	–	–	–
		E_{rel}	0.359	0.121	–	–	–
	Plane waves PW91	E_{surf} (unrelaxed)	1.81	1.87	1.84	1.86	1.90
		E_{surf} (relaxed)	1.70	1.69	1.70	1.70	1.69
		E_{rel}	0.156	0.258	0.210	0.239	0.305

extra-layer and the corresponding PW data (Table 5). First of all, in both methods atomic displacements have the same directions: N atoms go outwards from the surface whereas U atoms relax inwards, to the slab center. This is a pattern typical for the rumpling observed on oxide surfaces but the rumpling in UN is considerably larger. One observes also substantially larger magnitudes of surface U displacements than N atoms, whereas subsurface atom relaxations are smaller.

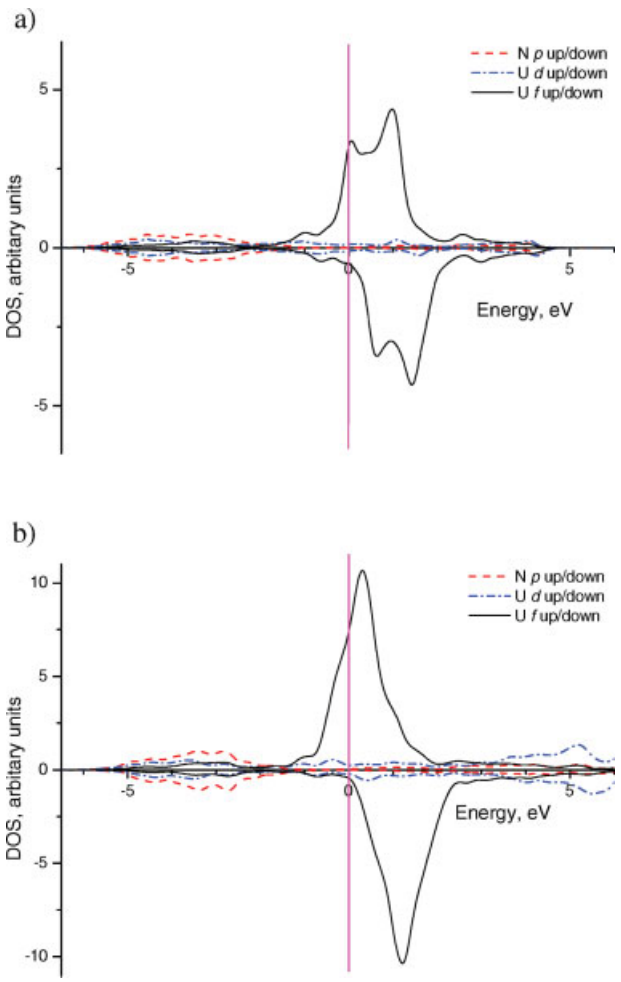

Figure 3. The projected DOS for the bulk (a) and the perfect UN(001) surface (b) in FM states.

There is also a good agreement of the effective atomic charges calculated in the LCAO and PW using two very different methods (Table 6). These charges indicate a considerable U-N bond covalency in both UN bulk and on the surface. Asymmetrical electron charge redistribution on U and N atoms is likely caused by atomic displacements from a crystalline 2D plane.

The surface energies are stabilized for slab thicknesses around 5–7 layers whereas the relaxation energy is more sensitive to the thickness (Table 7). Because of lack of experimental results, the calculated values of surface energy could be qualitatively compared only with 1.0–1.2 J/m^2 obtained recently for UO_2(001) surface energy using the quantum mechanical calculations.[2] As one can see, the surface energies of UN(001) and UO_2(001) are predicted to be similar. A qualitative agreement is observed between the UN(001) surface energies obtained in the LCAO calculations using extra-layer and the PW calculations. Increase of the number of atomic layers in the UN(001) slab stabilizes the energy of relaxed surface.

The total and projected DOS in the FM state obtained in our PW calculations is present in Figure 3. There is a small difference in band shapes from previous UN bulk calculation,[11] due to the much higher *k*-point mesh and cut-off energy used here. A comparison of the bulk DOS (Fig. 3a) with that for the projection of the surface U and N atoms (Fig. 3b) shows mainly changes in the shape of unoccupied states above the Fermi level. In both cases the mixed metallic-covalent chemical occurs with U5*f* states at the Fermi level, which is in line with previous experimental and theoretical studies[1,4–6,8].

Conclusions

In this article, we demonstrated an importance of choice of the proper effective core potentials in actinide (U) compound calculations which can considerably change the results obtained (e.g., the magnetic structure). We have also shown that the reliable LCAO calculations of the surface properties needs introduction

of an extra layer of the ghost functions simulating correct electronic density decay into vacuum from the surface. All this allowed us to perform first detailed study on properties of the densely packed UN(001) surface.

The results obtained by means of two substantially different DFT methods—LCAO and PW—demonstrate good agreement. We observed considerable relaxation of surface atoms which affects the surface energy. These results will be used in further study of surface defects and processes, first of all, UN surface oxidation which is important practical problem for its use as advanced nuclear fuel.

Acknowledgments

Authors are indebted to A. V. Titov, N. S. Mosyagin, P. Weck, A. Ray, D. Sedmidubsky, E. Heifets, Yu. Mastrikov, D. Gryaznov, and P. van Uffelen for fruitful discussions (DG, YM also for a technical assistance). D. B. gratefully acknowledges funding from the European Social Fund (ESF). This study was partly supported by the EC Framework 7 EURATOM.

References

1. Matzke, H. Science of Advanced LMFBR Fuels; North Holland: Amsterdam, 1986.
2. Skomurski, F. N.; Ewing, R. C.; Rohl, A. L.; Gale, J. D.; Becker, U. Am Mineral 2006, 91, 1761.
3. Weinberger, P.; Mallett, C. P.; Podloucky, R.; Neckel, A. J Phys C: Solid State Phys 1980, 13, 173.
4. (a) Brooks, M. S.; Glotzer, D. Phys B 1980, 102, 51; (b) Brooks, M. S. J Phys F: Met Phys 1984, 14, 639.
5. Sedmidubsky, D.; Konings, R. J. M.; Novak, P. J Nucl Mat 2005, 344, 40.
6. Atta-Fynn, R.; Ray, A. K. Phys Rev B 2007, 76, 115101.
7. Ito, T.; Kumigashira, H.; Souma, S.; Tahakashi, T.; Suzuki, T. J Magn Magn Mater 2001, 68, 226.
8. (a) Black, L.; Miserque, F.; Gouder, T.; Havela, L.; Rebizant, J.; Wastin, F. J Alloys Compd 2001, 315, 36; (b) Rafaja, D.; Havela, L.; Kuzel, R.; Wastin, F.; Colineau, E.; Gouder, T. J Alloys Compd 2005, 386, 87.
9. Yongbin, Z.; Daqiao, M.; Zhenghe, Z.; Meizhong, M. Chin J Chem Phys 2005, 18, 735.
10. Kotomin, E. A.; Mastrikov, Yu.; Zhukovskii, Yu. F.; Van Ufflen, P.; Rondinella, V. V. Phys Status Solidi C 2007, 4, 1193.
11. Kotomin, E. A.; Grimes, R. W.; Mastrikov, Yu.; Ashley, N. J. J Phys: Condens Matter 2007, 19, 106208.
12. Weck, P. F.; Kim, E.; Balakrishnan, N.; Poineau, F.; Yeamans, C. B.; Czerwinski, K. R. Chem Phys Lett 2007, 443, 82.
13. Evarestov, R. A.; Losev, M. V.; Panin, A. I.; Mosyagin, N. S.; Titov, A. V. Phys Status Solidi C 2008, 245, 114.
14. Perdew, J. P.; Wang, Y. Phys Rev B 1992, 45, 13244.
15. Evarestov, R. A. Quantum Chemistry of Solids. The LCAO First Principles Treatment of Crystals, Springer Series in Solid State Sciences, Vol. 153; Springer: Berlin, 2007.
16. Kudin, K. N.; Scuseria, G. E.; Martin, R. L. Phys Rev Lett 2002, 89, 266402.
17. Marutzky, M.; Barkow, U.; Schoenes, J.; Troc, R. J Magn Magn Mater 2006, 299, 225.
18. De Jong, W. A.; Harrison, R. J.; Nichols, J. A.; Dixon, D. A. Theor Chem Acc 2001, 107, 22.
19. Batista, E. R.; Martin, R. L.; Hay, P. J.; Peralta, J. E.; Scuseria, G. E. J Chem Phys 2004, 121, 2144.
20. Kuchle, W.; Dolg, M.; Stoll, H.; Preuss, H. J Chem Phys 1994, 100, 7535.
21. Titov, A. V.; Mosyagin, N. S. Int J Quantum Chem 1999, 71, 359.
22. Mosyagin, N. S.; Petrov, A. N.; Titov, A. V.; Tupitsyn, I. I. Progr Theor Chem Phys B 2006, 15, 229.
23. Bunday, B. D. Basic Optimization Methods; Edward Arnold: London, 1984.
24. Press, W. H.; Teukolski, S. A.; Vetterling, V. T.; Flannery, B. P. Numerical Recipes in Fortran 77: The Art of Scientific Computing; Cambridge University Press: Cambridge, 1997.
25. Kresse, G.; Hafner, J. VASP the Guide, University of Vienna, 2007. Available at: http://cms.mpi.univie.ac.at/vasp.
26. Blöchl, P. E. Phys Rev B 1994, 50, 17953.
27. Frisch, M. J.; Trucks, G. W.; Schlegel, H. B.; Scuseria, G. E.; Robb, M. A.; Cheeseman, J. R.; Montgomery, Jr., J. A.; Vreven, T.; Kudin, K. N.; Burant, J. C.; Millam, J. M.; Iyengar, S. S.; Tomasi, J.; Barone, V.; Mennucci, B.; Cossi, M.; Scalmani, G.; Rega, N.; Petersson, G. A.; Nakatsuji, H.; Hada, M.; Ehara, M.; Toyota, K.; Fukuda, R.; Hasegawa, J.; Ishida, M.; Nakajima, T.; Honda, Y.; Kitao, O.; Nakai, H.; Klene, M.; Li, X.; Knox, J. E.; Hratchian, H. P.; Cross, J. B.; Bakken, V.; Adamo, C.; Jaramillo, J.; Gomperts, R.; Stratmann, R. E.; Yazyev, O.; Austin, A. J.; Cammi, R.; Pomelli, C.; Ochterski, J. W.; Ayala, P. Y.; Morokuma, K.; Voth, G. A.; Salvador, P.; Dannenberg, J. J.; Zakrzewski, V. G.; Dapprich, S.; Daniels, A. D.; Strain, M. C.; Farkas, O.; Malick, D. K.; Rabuck, A. D.; Raghavachari, K.; Foresman, J. B.; Ortiz, J. V.; Cui, Q.; Baboul, A. G.; Clifford, S.; Cioslowski, J.; Stefanov, B. B.; Liu, G.; Liashenko, A.; Piskorz, P.; Komaromi, I.; Martin, R. L.; Fox, D. J.; Keith, T.; Al-Laham, M. A.; Peng, C. Y.; Nanayakkara, A.; Challacombe, M.; Gill, P. M. W.; Johnson, B.; Chen, W.; Wong, M. W.; Gonzalez, C.; and Pople, J. A. GAUSSIAN-03, Revision C. 02; Gaussian Inc.: Wallingford, CT, 2004. Available at: http://www.gaussian.com/.
28. Dovesi, R.; Saunders, V. R.; Roetti, C.; Orlando, R.; Zicovich-Wilson, C.M.; Pascale, F.; Civalleri, B.; Doll, K.; Harrison, N. M.; Bush, I.J.; D'Arco, Ph.; Llunell, M. CRYSTAL-06, Users Manual, University of Turin, 2006. Available at: http://www.crystal.unito.it.
29. Monkhorst, H. J.; Pack, J. D. Phys Rev B 1976, 13, 5188.
30. Available at: https://bse.pnl.gov/bse/portal.
31. (a) Kresse, G.; Furthmüller, J. J Comput Mater Sci 1996, 6, 15; (b) Kresse, G.; Furthmüller, J. Phys Rev B 1996, 54, 11169.
32. (a) Kresse, G.; Hafner, J. Phys Rev B 1993, 48, 13115; (b) Kresse, G.; Hafner, J. Phys Rev B 1994, 49, 14251.
33. Boys, S. F.; Bernardi, F. Mol Phys 1970, 19, 553.
34. Evarestov, R. A.; Bandura, A. V.; Alexandrov, V. E. Surf Sci 2007, 601, 1844.

Surface Science 603 (2009) 50–53

Contents lists available at ScienceDirect

Surface Science

journal homepage: www.elsevier.com/locate/susc

First principles calculations of oxygen adsorption on the UN(001) surface

Yu.F. Zhukovskii [a], D. Bocharov [a,*], E.A. Kotomin [b], R.A. Evarestov [c], A.V. Bandura [c]

[a] Institute for Solid State Physics, Kengaraga 8, LV–1063 Riga, Latvia
[b] European Commission, Joint Research Centre, Institute for Transuranium Elements, Hermann von Helmholtz Pl. 1, D-76344 Eggenstein-Leopoldshafen, Germany
[c] Department of Quantum Chemistry, St. Petersburg State University, Universitetsky Prosp. 26, 198504 St. Petergof, Russia

ARTICLE INFO

Article history:
Received 18 August 2008
Accepted for publication 13 October 2008
Available online 22 October 2008

Keywords:
Density functional calculations
Uranium nitride
Chemisorption
Oxygen

ABSTRACT

Fabrication, handling and disposal of nuclear fuel materials require comprehensive knowledge of their surface morphology and reactivity. Due to unavoidable contact with air components (even at low partial pressures), UN samples contain considerable amount of oxygen impurities affecting fuel properties. In this study we focus on reactivity of the energetically most stable (001) substrate of uranium nitride towards the atomic oxygen as one of initial stages for further UN oxidation. The basic properties of O atoms adsorbed on the UN(001) surface are simulated here combining the two first principles calculation methods based on the plane wave basis set and that of the localized orbitals.

The actinide nitrides and carbides, *e.g.,* uranium mononitride (UN) with a face centered cubic (fcc) rock salt structure, belong to the family of non-oxide ceramic nuclear fuels considered as promising candidates for the use in Generation-IV fast nuclear reactors. These materials reveal several advantages over traditional UO_2 fuel (*e.g.*, higher thermal conductivity and metal density) [1]. One of the problems with nitride and carbide fuels is their active interaction with the oxygen which results in an effective fuel oxidation and degradation [2]. This could affect the fabrication process as well as the fuel performance and safety. First experimental studies on O in UN were performed in 80ies ([1] and references therein). These activities were continued recently combining several techniques ([2] and references therein). However, understanding of the atomistic mechanism of fuel oxidation needs first principles theoretical modeling. Thus, to shed more light on this problem, we study here theoretically the interaction of atomic oxygen with the UN(001) surface.

Theoretical simulations of uranium compounds are especially complicated due to a relativistic character of an electron motion in the U atomic core and the strong electron–electron correlation. Moreover, UN is characterized by a mixed metal-covalent chemical bonding. Physical and chemical properties of light actinides are determined by partly localized *5f* electrons, which determine a number of properties, such as mixed valence, magnetism, etc. A series of first principles DFT calculations on pure and defective UO_2 were performed recently (*e.g.*, [3–8]) whereas a number of similar calculations on the nitride fuels is still much more limited [9–15]. In our recent paper [15] the methodology was proposed for LCAO calculations of the UN surface properties. The first results on the pure UN surfaces were presented therein using two approaches based on the basis sets of atomic orbitals (AO) and plane waves (PW), respectively. Use of the two different methods greatly increases the reliability of the results obtained.

To simplify modeling of the oxygen interaction with UN powder surface, we study here only the (001) surface which according to Tasker [16] has the lowest energy. To simulate the perfect UN(001) substrate as well as its interaction with oxygen, we have employed the DFT-PW computer code *VASP 4.6* [17] based on the use of a plane wave basis set and the method of projector–augmented–waves (PAW) for atomic core description. We apply the non-local exchange-correlation functional Perdew-Wang-91 using the generalized gradient approximation (GGA) [18] and the scalar relativistic PAW pseudopotentials representing the U core electrons (with $6s^2 6p^6 6d^2 5f^2 7s^2$ valence shell), N ($2s^2 2p^3$) and O ($2s^2 2p^4$) atoms (containing 14, 5 and 6 valence electrons, respectively). The cut-off energy has been chosen to be 520 eV. We use the Monkhorst–Pack scheme [19] with mainly $8 \times 8 \times 1$ *k*-point meshes in the Brillouin zone (BZ).

As the second method, we have used the *CRYSTAL-06* computer code [20] based on the Gaussian-type functions centered on the atomic nuclei as the basis sets for expansion of the linear combination of atomic orbitals (LCAO). We use the non-local exchange-correlation functional PBE [21]. The oxygen basis set (BS) 8-411G(1*d*) was taken from Ref. [22]. For the N atom, the all-electron BS 6-311G(2*d*) has been used [23]. Finally, for the U atom we have used the energy-adjusted relativistic small core (60 electrons in core) effective potential from Ref. [24]. To get rid of the basis set linear

* Corresponding author. Tel.: +371 67187480; fax: +371 67132778.
E-mail address: bocharov@latnet.lv (D. Bocharov).

0039-6028/$ - see front matter © 2008 Elsevier B.V. All rights reserved.
doi:10.1016/j.susc.2008.10.019

dependence in the *CRYSTAL* LCAO calculations, the diffuse *s*-, *p*-, *d*- and *f*- Gaussian-type orbitals with exponents < 0.2 a.u.$^{-1}$ have been removed from the basis sets. The exponents of other polarization functions have been reoptimized, to restore the required precision in the total energy. High accuracy in both *k*-set mesh and DFT integration grid (XLGRID) has been applied for all *CRYSTAL-06* calculations. Prior to a study of surface properties, the bulk structure optimization of UN crystal has been performed using the LCAO approach. The Monkhorst–Pack scheme [19] with $16 \times 16 \times 16$ *k*-point mesh for the BZ sampling and $32 \times 32 \times 32$ *k*-point Gilat [25] net for the calculation of the Fermi energy and density matrix have been used here.

When modeling the UN(001) surface, we have used symmetric slabs consisting of five atomic layers with regularly alternating uranium and nitrogen atoms [15]. Plane wave computational formalism requires the use of an artificial slab translation in a vertical direction with a period called the *vacuum gap*. The magnitude of the latter (38.8 Å for five-layer UN slab), was found large enough to exclude the interaction between the repeated slabs for all single slab models studied using the PAW approach The slabs in the LCAO calculations have been really two-dimensional. The optimized lattice constant (4.87 for PAW *VASP vs.* 4.81 Å for LCAO *CRYSTAL* calculations) has been used in all further calculations, with an error within 2% of the experimental value (4.89 Å) [1]. Only ferromagnetic UN ground state has been considered in this study as the energetically most preferable state at low temperatures. The calculations of UN bulk structure suggest the magnetic moment on the U cation ~1 μ_B. Thus, for five-layers slab the total magnetic moment of a 2×2 2D supercell (containing 20 U cations and 20 N anions) in both approaches has been fixed at 20 μ_B.

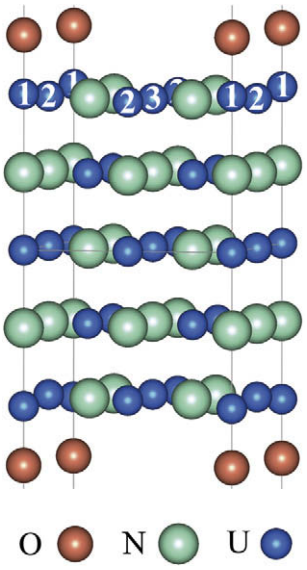

Fig. 1. A model of two-sided periodic adsorption of O atoms (0.25 ML) atop the surface U cations. Numbers enumerate non-equivalent interfacial atoms.

To simulate the O atom adsorption, we have used the same supercell model with a periodic adsorbate distribution. These supercells with the 2×2 extension of surface translation vectors correspond to the atomic O coverage of 0.25 ML. To reduce computational efforts, we have considered symmetric two-sided arrangement of oxygen adatoms (Fig. 1). We have simulated two configurations of atomic adsorption: O atop the surface U cation or N anion (Fig. 1) with the complete structural optimization. For PAW calculations on the O/UN(001) interface using 3D slab model, we should also check whether the vacuum gap of 38.8 Å for a five-layer slab of uranium nitride [15] is large enough for the models additionally containing adsorbed O atoms from both sides.

The binding energy E_{bind} of adsorbed oxygen O_{ads} was calculated with respect to a free O atom

$$E_{bind} = \frac{1}{2}\left(E_{tot}^{UN} + 2E_{tot}^{O_{triplet}} - E_{tot}^{O/UN}\right), \quad (1)$$

where $E_{tot}^{O/UN}$ is the total energy of a fully relaxed O/UN(001) slab for O_{ads} positions atop either the N or U surface ions, $E_{tot}^{O_{triplet}}$ and E_{tot}^{UN} the energies of an isolated O atom in the ground (triplet) state and of a pure relaxed slab. In PAW calculations of free O atom, the cubic box with the same periodicity as for the O/UN(001) and UN(001) 3D slabs has been used. The factor 1/2 before brackets appears since the substrate is modeled by slab with the two equivalent surfaces and O_{ads} is positioned symmetrically with respect to the surfaces.

Due to a mixed metallic-covalent nature of the chemical bonding in UN [10–14], we expect a high affinity of O_{ads} towards the UN(001) substrate. The binding energy *per* O adatom is expected to be closer to that on a regular O/Al(111) and (001) metallic interfaces (~10 eV) [26] than on semiconducting O/$SrTiO_3$(001) interfaces (with two possible SrO- or TiO_2-terminations) (~2eV) [27]. Indeed, we have obtained in the *VASP* calculations the binding energies of 6.9 and 5.0 eV *per* O adatom atop the surface U or N ions, respectively, accompanied with 0.9–1.2 *e* charge transfer from the surface towards the O adatom (Tables 1 and 2). The positively charged surface U cation goes outwards, to the adsorbed O atom whereas in the O configuration atop the N anion the latter is

Table 1
The calculated binding energy (E_{bind}), the distance between O and surface U cation (d_{O-U}), the effective atomic charges (q), and vertical (Δz) U and N displacements from the surface plane for adatom position atop the surface U (Fig. 1). The effective charges of U and N ions on the pure surface are equal to +1.63 *e* for surface U cation and −1.55 *e* for surface N anion in LCAO 5-layer slab calculations as well as +1.66 *e* for surface U cation and −1.63 *e* for surface N anion in PAW 5-layer slab calculations [15].

Method of calculation	E_{bind}, eV	q(O), *e*	q(U1), *e*	q(U2), *e*	q(U3), *e*	q(N), *e*	d_{O-U}, Å	Δz(U1), Å	Δz(U2), Å	Δz(U3), Å	Δz(N), Å
LCAO[a]	8.3	−0.89	1.97	1.66	1.62	−1.56	1.87	+0.15[b]	−0.07	−0.11	−0.04
PAW[c]	6.9	−1.04	1.96	1.86	1.83	−1.60	1.91	+0.135[b]	−0.02	−0.04	−0.05

[a] LCAO–PBE calculations performed with *CRYSTAL-2006* code.
[b] Positive sign corresponds to atom displacement outward from the substrate.
[c] PAW–PW91 calculations performed with *VASP-4.6* code.

Table 2
The calculated parameters for O atom adsorption atop the surface N anion[a]. See caption and footnotes of Table 1 for explanation.

Method of calculation	E_{bind}, eV	q(O), *e*	q(N1), *e*	q(N2), *e*	q(N3), *e*	q(U), *e*	d_{O-N}, Å	Δz(N1), Å	Δz(N2), Å	Δz(N3), Å	Δz(U), Å
PAW	5.0	−1.20	−1.44	−1.56	−1.59	−1.56	2.19	−0.64	+0.065	+0.06	+0.10

[a] Atomic positions of U and N ions are reversed as compared to those shown in Fig. 1.

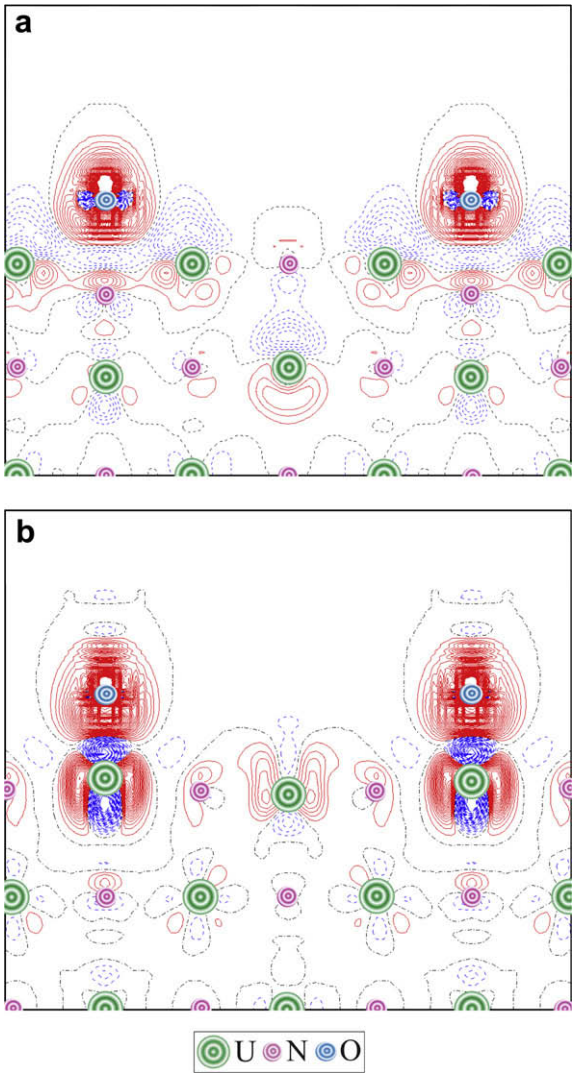

Fig. 2. The difference electron density maps $\Delta\rho$ (**r**) (the total density of the interface minus the densities of substrate and adsorbate with optimized interfacial geometry) for the O adatoms atop the surface: (a) N anions and (b) U cations on the UN(001) surface obtained using results of PAW calculations. Solid (red) and dashed (blue) isolines correspond to positive and negative electron density, respectively. Isodensity increment is 0.003 e Å^{-3}. (For interpretation of the references to color in this figure legend, the reader is referred to the web version of this article).

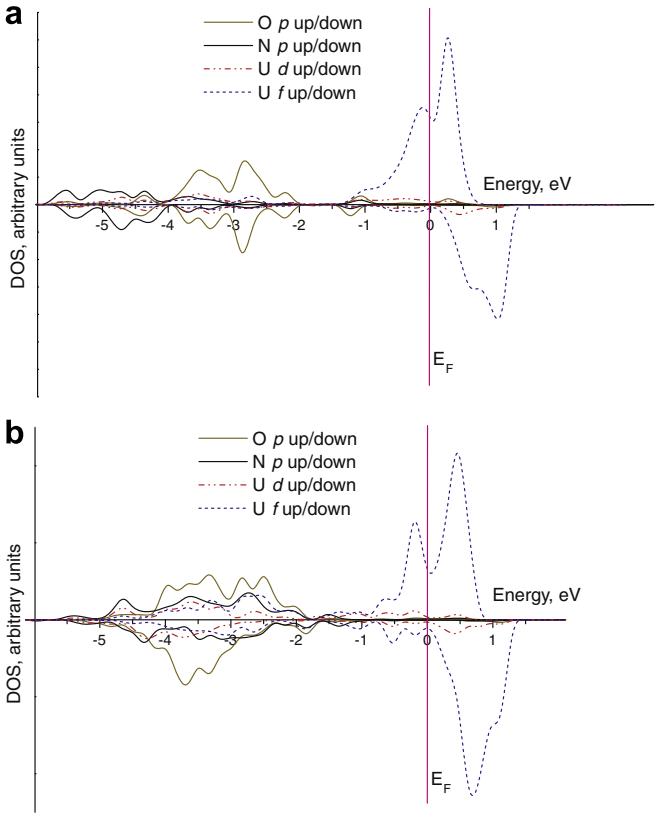

Fig. 3. The total and projected densities of states for O adsorption atop the N anion (a) and the U cation (b) obtained using results of PAW calculations. In the former, we consider the orbital projections of N anion under O atom and one of four nearest neighbouring U cations (Fig. 2a). Analogously, the lower plot presents the orbital projections of U cation beneath adatom and one of four nearest N anions. The largest peaks have been normalized to the same value, whereas a convolution of individual energy levels has been plotted using the Gaussian functions with a half-width 0.2 eV. "O" on energy axis corresponds to Fermi level.

strongly displaced from the adsorbed O atom towards the slab center, due to a mutual repulsion.

The corresponding results of *VASP* and *CRYSTAL* calculations based on the two very different methods demonstrate a good qualitative agreement for O adatom properties atop the surface U ion (Table 1) in all properties: the binding energies (3D slab models usually underestimate this parameter due to a weak repulsion between the adjacent polarized slabs), atomic displacements and even effective charges (which are calculated using the very different Mulliken (LCAO) and Bader (PAW) procedures).

An analysis of the difference electron charge redistributions for both configurations of O_{ads} (Fig. 2) confirms that the O adatom forms a strong chemical bonding with the surface U cation which could be considered as one-site complex. In the case of O adatom atop the surface N anion this is rather multi-center adsorption complex involving four adjacent surface U ions. As follows from Table 1, these cations mostly contribute to the high O binding energy atop the N anion.

Adsorption of O_{ads} atop the surface N or U ions on the UN(001) surface leads to appearance of the specific oxygen bands in the density of states (DOS) (Fig. 3) as compared to DOS for a pure UN(001) surface [15]. For oxygen atop the surface U cation, O *2p* states overlap with the U *6d* and with a well-pronounced tail of U *5f* states in the region of the N *2p* valence band (−2 to −4 eV). This indicates once more a strong oxygen chemical bonding (chemisorption) on U, typical for metal surfaces. However, when O is located atop N, the U *5f* contribution in this energy region diminishes whereas N *2p* states are considerably pushed down to smaller energies, due to N anion repulsion from negatively charged O adatom.

Summing up, the results obtained here for oxygen interaction with UN surfaces demonstrate strong chemisorption typical for metallic surfaces and could serve as the first important step in understanding the initial stage of the oxidation mechanism. The excellent agreement of the results obtained using two very different first principles methods supports their reliability. We continue the study of O_2 dissociation and the diffusion path of O_{ads} on both perfect and defective UN(001) substrates, which is aimed at understanding atomistic mechanism of oxidation by means of substitution of surface N ions for O ions.

Acknowledgements

The authors kindly thank P. Van Uffelen, R. Caciuffo, D. Gryaznov, V. Kashcheyevs, A. Kuzmin, M. Losev, Yu. Mastrikov, S. Piskunov for fruitful discussions and for valuable help with the calculations. This study was partly supported by the Service Contract 205343-2006-07 F1ED KAR LV between ITU, Karlsruhe, and

ISSP, Riga, EC Framework 7 Project F-Bridge, and the proposal N25592 from EMS Laboratory of the PNNL. D. Bocharov gratefully acknowledges support from the European Social Fund (ESF).

References

[1] Hj. Matzke, Science of Advanced LMFBR Fuel, North Holland, Amsterdam, 1986;
P.D. Wilson (Ed.), The Nuclear Fuel Cycle, University Press, Oxford, 1996.
[2] H. Wiame, M. Centeno, S. Pacard, P. Bastian, P. Grange, J. Eur. Ceram. Soc. 18 (1998) 1293;
M. Walter, Oxidation of Inert Matrices, JRC-ITU-TN-2005/35.
[3] T. Petit, C. Lemaignan, F. Jollet, B. Bigot, A. Pasturel, Philos. Mag. B 77 (1998) 779.
[4] J.P. Crocombette, F. Jollet, L. Thien Nga, T. Petit, Phys. Rev. B 64 (2001) 104107.
[5] K. Kudin, G. Scuseria, R. Martin, Phys. Rev. Lett. 89 (2002) 266402.
[6] L. Petit, A. Svane, S. Szotek, W.M. Temmerman, Science 301 (2003) 498.
[7] M. Freyss, T. Petit, J.P. Crocombette, J. Nucl. Mater. 347 (2005) 44.
[8] H.Y. Geng, Y. Chen, Y. Kaneta, M. Kinoshita, Phys. Rev. B 75 (2007) 054111.
[9] M.S.S. Brooks, D. Glötzel, Physica B 102 (1980) 51;
M.S.S. Brooks, J. Phys. F: Met. Phys. 14 (1984) 639.
[10] D. Sedmidubsky, R.J.M. Konings, P. Novak, J. Nucl. Mater. 344 (2005) 40.
[11] E.A. Kotomin, Yu.A. Mastrikov, Yu.F. Zhukovskii, P. Van Uffelen, V.V. Rondinella, Phys. Status Solidi C 4 (2007) 1193.
[12] E.A. Kotomin, R.W. Grimes, Yu.A. Mastrikov, N.J. Ashley, J. Phys.: Cond. Matt. 19 (2007) 106208.
[13] M. Samsel-Czekała, E. Talik, P. de V. Du Plessis, R. Troć, H. Misiorek, C. Sułkowski, Phys. Rev. B 76 (2007) 144426.
[14] R.A. Evarestov, M.V. Losev, A.I. Panin, N.S. Mosyagin, A.V. Titov, Phys. Status Solidi B 245 (2008) 114.
[15] R.A. Evarestov, A.V. Bandura, M.V. Losev, E.A. Kotomin, Yu.F. Zhukovskii, D. Bocharov, J. Comput. Chem. 29 (2008) 2079.
[16] P.W. Tasker, J. Phys. C Solid. State 12 (1979) 4977.
[17] G. Kresse, J. Hafner, VASP the Guide, University of Vienna, 2007, <http://cms.mpi.univie.ac.at/vasp/>.
[18] J.P. Perdew, Y. Wang, Phys. Rev. B 45 (1992) 13244.
[19] H.J. Monkhorst, J.D. Pack, Phys. Rev. B 13 (1976) 5188.
[20] R. Dovesi, V.R. Saunders, C. Roetti, R. Orlando, C.M. Zicovich-Wilson, F. Pascale, B. Civalleri, K. Doll, N.M. Harrison, I.J. Bush, Ph. D'Arco, M. Llunell, CRYSTAL2006 User's Manual, Universita di Torino, Torino, 2006, <http://www.crystal.unito.it/>.
[21] J.P. Perdew, K. Burke, M. Ernzerhof, Phys. Rev. Lett. 77 (1996) 3865.
[22] S. Piskunov, E. Heifets, R.I. Eglitis, G. Borstel, Comput. Mater. Sci. 29 (2004) 165.
[23] M.J. Frisch, J.A. Pople, J.S. Binkley, J. Chem. Phys. 80 (1984) 3265.
[24] W. Kuchle, M. Dolg, H. Stoll, H. Preuss, J. Chem. Phys. 100 (1994) 7535.
[25] G. Gilat, Phys. Rev. B 26 (1982) 2243.
[26] Yu.F. Zhukovskii, P.W.M. Jacobs, M. Causà, J. Phys. Chem. Solids 64 (2003) 1317.
[27] S. Piskunov, Yu.F. Zhukovskii, E.A. Kotomin, E. Heifets, D.E. Ellis, MRS Proc. 894 (2006) LL08-05.

Journal of Nuclear Materials 393 (2009) 504–507

Contents lists available at ScienceDirect

Journal of Nuclear Materials

journal homepage: www.elsevier.com/locate/jnucmat

Chemisorption of a molecular oxygen on the UN(0 0 1) surface: *Ab initio* calculations

Yu.F. Zhukovskii, D. Bocharov *, E.A. Kotomin

Institute of Solid State Physics, University of Latvia, 8 Kengaraga Street, LV-1063 Riga, Latvia

ARTICLE INFO

Article history:
Received 18 November 2008
Accepted 21 July 2009

ABSTRACT

The results of DFT GGA calculations on oxygen molecules adsorbed upon the (0 0 1) surface of uranium mononitride (UN) are presented and discussed. We demonstrate that O_2 molecules oriented parallel to the substrate can dissociate either (i) spontaneously when the molecular center lies above the surface hollow site or atop N ion, (ii) with the activation barrier when a molecule sits atop the surface U ion. This explains fast UN oxidation in air.

1. Introduction

The uranium mononitride (UN), which possesses a rock salt structure and metallic nature, is an advanced material for the non-oxide nuclear fuel considered as a promising candidate for the use in Generation-IV fast nuclear reactors. UN reveals several advantages over a traditional UO_2-type fuel (*e.g.*, higher thermal conductivity and metal density). However, one of important problems with actinide nitrides is their effective oxidation in contact with oxygen which can affect nuclear fuel performance [1].

There was a series of *ab initio* density functional theory (DFT) calculations published in last 10 years on pure and defective UO_2 (*e.g.*, [2–10]). Similar calculations on the UN appeared only recently [11–16]. In our recent papers, we studied both the structure of a perfect UN(0 0 1) surface [17] and chemisorption of oxygen atoms upon it [18]. These DFT calculations were performed using the two quite different computer codes: *VASP 4.6* [19], with plane wave basis set (BS), and *CRYSTAL-06* [20], with the BS of localized atomic orbitals (LCAO approach). In both cases we have applied the non-local exchange-correlation functional by Perdew–Wang-91 (PW91), that is, the generalized gradient approximation (GGA) [21]. The results of these two different methods reveal good agreement [17,18] which supports their reliability. A strong *chemisorption* was observed for a single O atom interaction with the UN surface (~7 eV is the binding energy atop the surface U ion) [18] which is typical for traditional metallic surfaces (*cf.* ~ 10 eV *per* adatom bound on the close-packed Al surfaces [22]). However, to shed more light on the UN oxidation mechanism, we study theoretically in this paper the interaction of *molecular* oxygen with the same defectless UN(0 0 1) surface. The key questions are: whether the O_2 dissociation upon the surface is energetically possible, which adsorption sites are optimal for this, and whether it can occur spontaneously, without energy barrier. These are important issues for understanding the mechanism of the oxidation of uranium nitride in air.

2. Theoretical

We have employed the *VASP 4.6* code [19] with the relativistic PAW pseudopotentials representing the core electrons of U ($6s^2 6p^6 6d^2 5f^2 7s^2$ valence shell), N ($2s^2 2p^3$) and O ($2s^2 2p^4$) atoms as well as the non-local PW91 exchange correlation functional [21]. The cut-off energy has been chosen 520 eV. We have applied the Monkhorst–Pack scheme [23] with $4 \times 4 \times 1$ k-point mesh in the Brillouin zone (BZ). When modeling the UN(0 0 1) surface, we have used the same 3D symmetric slabs as previously [17,18] consisting of five non-polar layers, containing alternating U and N atoms, separated by large vacuum gaps along the z-axis (~36 Å) and thus excluding the direct interaction of oxygen molecules from the neighboring slabs. The lattice constant (4.87 Å) optimized for the bulk has been used in all our slab calculations accompanied by a full structure optimization. The DFT GGA calculations suggest *ferromagnetic* ground state [24] of UN which contradicts the experimental observations of AFM phase at low temperatures [1]. Our test calculations [17] have confirmed that the FM phase is energetically more favorable also for the UN slab.

For simulation of the chemisorption of oxygen molecule, we have used mainly the 2×2 extended surface supercell (containing 20 U cations and 20 N anions), similarly to the previous study on chemisorption of an atomic oxygen [18]. The periodic adsorbate distribution corresponds to the molecular coverage of 0.25 ML (or atomic O coverage of 0.5 ML). To reduce computational efforts, we have used a symmetric two-sided arrangement of oxygen molecules on both surfaces of the slab. The energy gain E_{gain} *per* oxygen atom in the adsorbed molecule $(O_2)_{ads}$ arising after approach of the O_2 molecule towards the UN surface has been calculated as

$$E_{gain} = \frac{1}{4}\left(E^{UN} + 2E^{O_2} - E^{O_2/UN}\right), \quad (1)$$

* Corresponding author. Tel.: +371 67187480; fax: +371 67132778.
E-mail address: bocharov@latnet.lv (D. Bocharov).

0022-3115/$ - see front matter © 2009 Elsevier B.V. All rights reserved.
doi:10.1016/j.jnucmat.2009.07.010

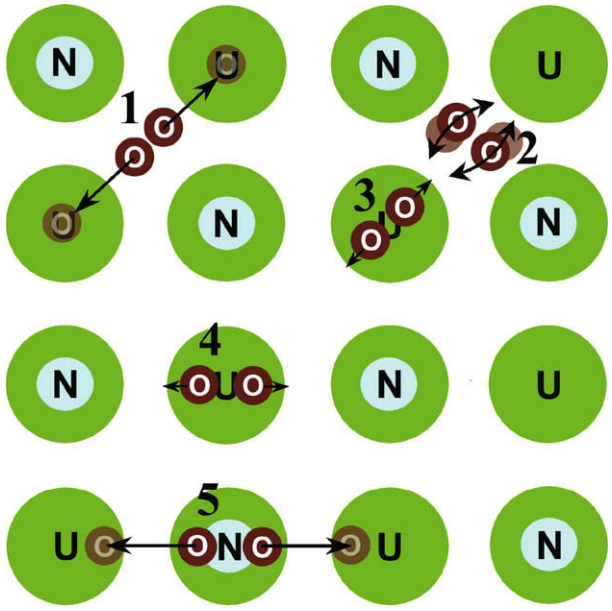

Fig. 1. Schematic view of five different horizontal configurations for the O_2 molecule adsorption on UN surface: (1) atop the hollow site oriented towards the nearest surface U ions, (2) atop the hollow site oriented towards the nearest surface N ions, (3) atop the surface U ions oriented towards the next-nearest surface U ions, (4) atop the surface U ions oriented towards the nearest surface N ions, (5) atop the surface N ions oriented towards the nearest surface U ions. We show, using arrows, that molecule spontaneous dissociation can occur when O_2 is located either atop the hollow site (1) or atop ion N (5).

where $E^{O_2/UN}$ is the total energy of a fully relaxed O_2/UN(0 0 1) slab for several configurations of $(O_2)_{ads}$ upon the substrate (with a center of molecule atop the corresponding surface site as shown in Fig. 1), E_2^O and E^{UN} the total energies of an isolated oxygen molecule in the ground (triplet) state and of a pure relaxed slab, respectively. The factor 1/4 before brackets appears since the substrate is modeled by a slab containing the two equivalent surfaces with $(O_2)_{ads}$ positioned symmetrically relatively to both slab surfaces whereas each molecule before and after dissociation contains two oxygen atoms. Similar analysis was earlier performed by us for various O_2/Al interfaces [22].

To compare the binding energy (E_{bind}) for the atomic oxygen adsorption atop the surface uranium atom calculated by us earlier [18] with the E_{gain} *per* dissociated oxygen adatom (Table 1), one should add about half the binding energy of oxygen molecule to the latter energy. The calculated E_{bind} for a free O_2 molecule in the triplet state is 6.06 eV and a bond length of 1.31 Å (*cf.* with the experimental values of 5.12 eV and 1.21 Å [25], respectively).

3. Main results

When modeling the molecular adsorption, we have analyzed different configurations of an O_2 molecule in the triplet state on the UN(0 0 1) substrate. *Vertical* orientations of the molecule atop the surface N or U ions have been found metastable with respect to molecule reorientation to the *horizontal* configuration, parallel to the surface. We have estimated both the energy gain of molecular adsorption using Eq. (1) and the O_2 dissociation energy (for some configurations), *i.e.*, the difference of the total energies of a slab with an oxygen molecule before and after dissociation, when the two O atoms in the triplet state which sit atop the two nearest surface U ions (Table 1).

3.1. Spontaneous dissociation of O_2 molecules

We have found that a spontaneous, barrierless O_2 dissociation indeed takes place in the two cases: when the molecular center is atop either (i) a hollow site or (ii) surface N ion, with the molecular bond directed towards the two nearest surface U ions (the configurations 1 and 5 in Fig. 1, respectively). The relevant dissociation energies E_{diss} are given in Table 1, along with other parameters characterizing the atomic relaxation and the Bader charge distribution. To estimate energy gain for intermediate molecular adsorption in these two configurations (as present in Table 1) we have fixed the O_2 bond length as in a gas phase allowing the molecule to relax only along a distance from the surface. Geometry and charges for the configurations 1 and 5 after dissociation (Table 1) are in general similar to those obtained in our previous study [18] for UN(0 0 1) substrate covered by chemisorbed O atoms, *e.g.*, surface U atoms beneath the oxygen adatom after dissociation are shifted up in both configurations. An increase of the surface supercell size from 2×2 up to 3×3 results in the 10% growth of the E_{gain} due to a reduced repulsion between the periodically distributed adatoms (Table 1).

We have also identified two other configurations of adsorbed oxygen molecules where the dissociation is energetically possible but with the energy barrier: (i) atop the hollow site when a molecular bond is oriented towards the nearest N ions (the configuration 2 in Fig. 1) and (ii) atop the surface U ion (for any molecular orientation, *e.g.*, the configurations 3 and 4 in Fig. 1). For the configuration 2, we have observed the orientation instability of the adsorbed molecule which easily rotates, *e.g.*, towards the surface U ion with further dissociation. The configurations 3 and 4 could be characterized as rather metastable UO_2 quasi-molecules due to a strong bonding between all three atoms (Fig. 2c) and since the corresponding U ion is noticeably shifted up from its initial positions on surface (Table 1). Meanwhile, the dissociation of $(O_2)_{ads}$ molecule in the configuration 3 is energetically possible but only after overcoming the small (~0.3 eV) activation energy barrier.

Table 1
The calculated energy gains (E_{gain}, Eq. (1)) and dissociation E_{diss} energies (eV), geometry (z, Δz) and charges (q) for configurations of molecular and spontaneous dissociative chemisorption of oxygen molecule above the UN(0 0 1) substrate. Numbers in brackets correspond to the configurations shown in Fig. 1.

Position		E_{gain} *per* O atom, eV	z[a], Å	E_{diss}, eV	q(O), *e*	q(U1[b]), *e*	q(U2[c]), *e*	q(N[d]), *e*	Δz[e](U1), Å	Δz[e](U2), Å	Δz[e](N), Å
Hollow (1)	Molecular adsorption	1.185	1.893	–	−0.465	1.913	1.762	−1.533	−0.0496	−0.0496	0.02498
	After dissociation	4.21	1.957	3.025	−0.978	2.053	1.978	−1.577	0.075	0.068	−0.133
Atop U	Towards next-nearest U (3)	2.15	2.18	–	−0.5905	2.042	1.836	−1.6065	0.176	−0.048	−0.096
	Towards nearest N (4)	2.33	2.14	–	−0.578	2.0485	1.827	−1.6248	0.123	−0.051	−0.106
Atop N (5)	Molecular adsorption	0.82	2.020	–	−0.5685	1.8675	1.8322	−1.3537	−0.0496	−0.0496	0.025
	After dissociation	4.00[f]	1.955	3.18	−0.979	2.115	1.876	−1.580	0.073	0.021	−0.201

[a] z is the height of O atoms respectively the non-relaxed UN substrate.
[b] U1 the nearest surface U ion.
[c] U2 the next-nearest surface U ion.
[d] N the nearest surface N ion.
[e] Δz the additional vertical shifts of the same surface ions from their positions in the absence of adsorbed oxygen.
[f] 4.40 eV for 3×3 extended surface supercell.

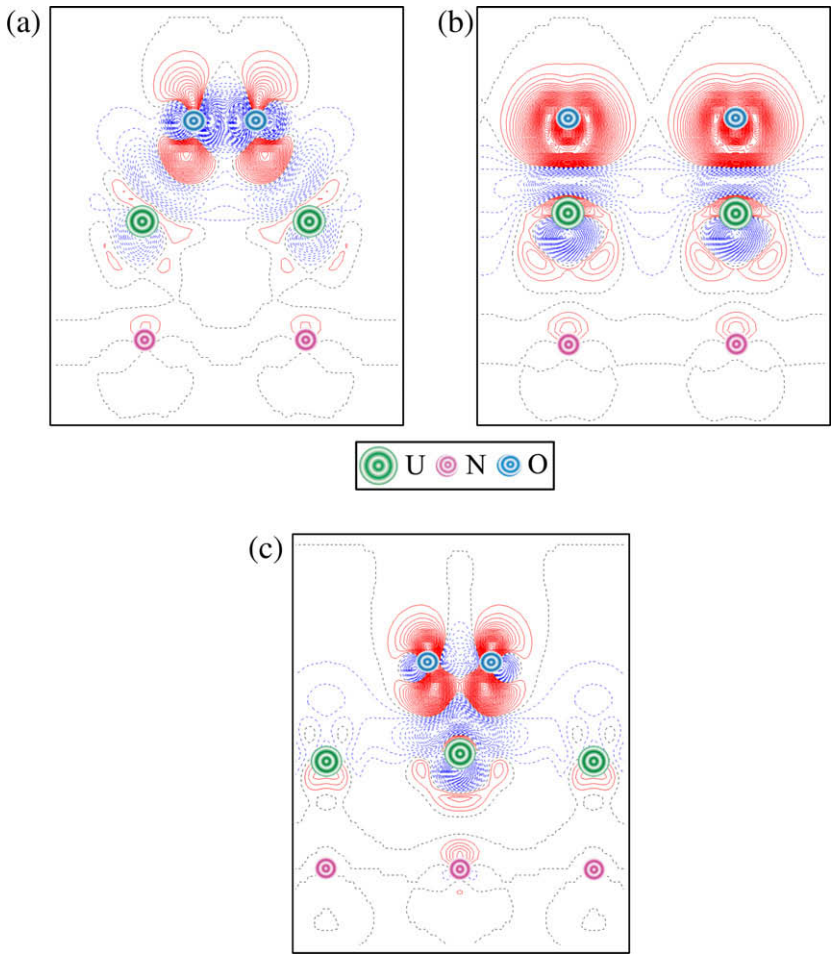

Fig. 2. The difference electron density maps $\Delta\rho$ (r) (the total density of the interface minus the sum of densities of substrate and adsorbate with optimized interfacial geometry) for (a) the O_2 molecule upon the hollow position oriented to the nearest surface U ions, (b) after its dissociation in the configuration 1 (Fig. 1) with O atoms atop the surface U ions and (c) for the O_2 molecule atop the surface U ion in the configuration 3 (Fig. 1). Solid (red) and dashed (blue) isolines correspond to positive (excess) and negative (deficiency) electron density, respectively. Isodensity increment is 0.003 e Å^{-3}. (For interpretation of the references to colour in this figure legend, the reader is referred to the web version of this article.)

3.2. Charge redistribution analysis

Adsorption of an O_2 molecule (in the triplet state) is accompanied by the charge transfer of $\sim$1 e (*per* molecule) from the substrate (Table 1). In Fig. 2 we analyze the difference electron charge redistributions for three configurations of horizontally oriented $(O_2)_{ads}$ upon the surface: (a) molecule adsorbed upon the hollow site (the configuration 1, Fig. 1), (b) molecule dissociated from this configuration with O adatoms located atop the nearest surface U ions, and (c) molecule adsorbed upon the surface U ion (the configuration 3). Spontaneous O_2 dissociation and thus a smooth transition from the charge distribution (a) to (b) can be explained by continuous areas of the electron density (Fig. 2a) parallel to the surface which may be considered as *dissociation channels*, analogously to the density plot for a molecular oxygen upon the Al substrate [22]. After dissociation each O adatom contains an extra charge of $\sim$1 e, *i.e.*, transforms into O^- ion in the triplet state (Fig. 2b). In contrast, when considering the molecular configuration 3, these *dissociation channels* are transformed into *dissociation barriers* (Fig. 2c). Simultaneously, we observe considerably higher electron density, indicating a kind of UO_2 quasi-molecule with a strong bonding between the O_2 molecule and surface U atom beneath. Thus, difference between the electron density plots presented in Fig. 2a and c can explain different dissociation abilities of O_2 molecule in the configurations 1 and 3 (Fig. 1).

3.3. Electronic densities of states (DOS)

For the same adsorbate configurations considered above, we have constructed the total and projected densities of states (DOS) (Fig. 3). Molecular adsorption in these configurations leads to appearance of the specific *oxygen bands* as compared to those for oxygen adatoms upon UN surface [18] and O atom substituted for a host N ion in UN bulk [15]. For a molecular oxygen atop the hollow position (Fig. 3a), O 2*p* peak is observed at -1 eV overlapping with the U 5*f* and 6*d* bands. After O_2 dissociation (Fig. 3b) this peak disappears being replaced by the broad two-peak band in the region of the N 2*p* valence band (-2 to -5 eV), similarly to the DOS for oxygen adatoms on UN(0 0 1) substrate [18]. Some differences are also noticeable between the corresponding U 5*f* and 6*d* peaks in the spectral range above -1 eV (*cf.* Fig. 3a and b) which could be caused by both different arrangement of O and U atoms in these configurations and sensitivity of uranium states to the presence of oxygen, thus indicating once more a strong oxygen chemical bonding (chemisorption). When oxygen molecule is located atop the surface U ion (the configuration 3), the U 5*f* and 6*d* contributions in the energy range above -1 eV are diminished, simultaneously the O 2*p* contribution grows, thus increasing an overlap between all three states and indicating UO_2 quasi-molecular bond formation. As compared to the adsorption of oxygen molecule upon the hollow site (Fig. 3a), we again observe a higher O 2*p* peak

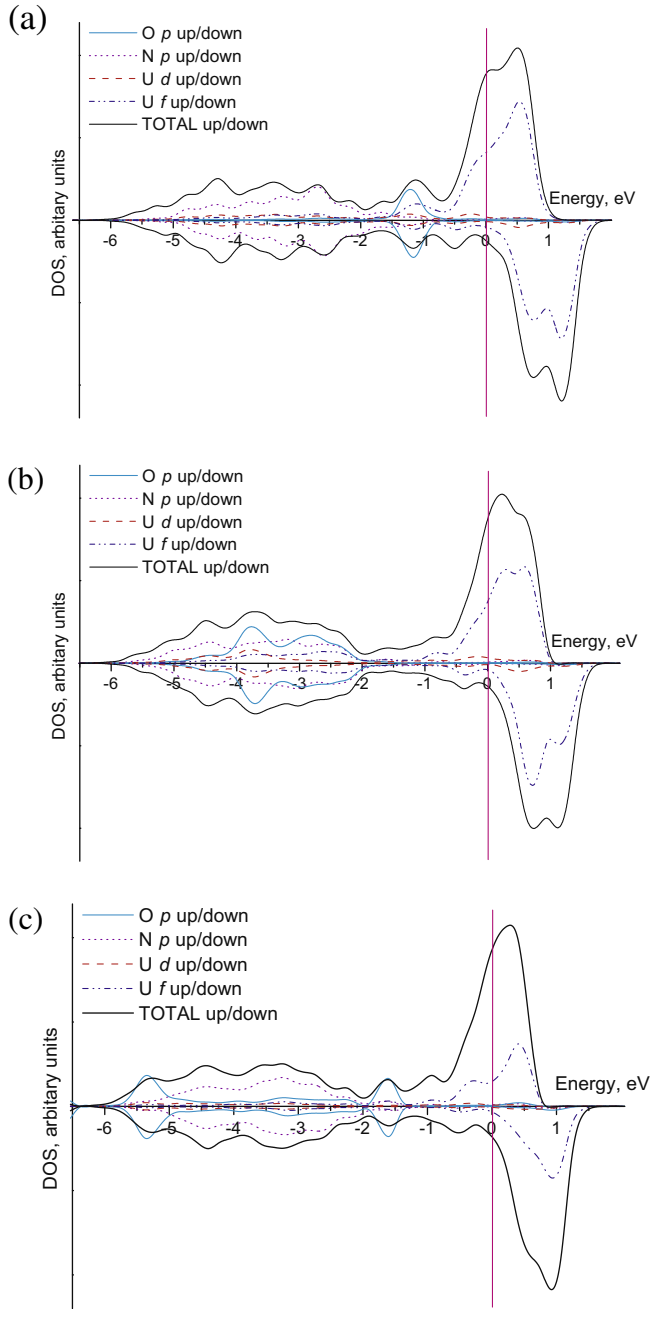

Fig. 3. The total and projected densities of states for three configurations of O_2 molecule as in Fig. 2 (the same a, b and c). The orbital projections of both O atoms as well as the nearest N and U ions are shown. The highest peaks have been normalized to the same value, whereas a convolution of individual energy levels has been plotted using the Gaussian functions with a half-width of 0.2 eV.

(at −1.5 eV) and an additional lower peak of the same O 2*p* (at −5.5 eV) which noticeably overlaps with the U 5*f* and 6*d* subpeaks (Fig. 3c). Similarity with the latter pattern was observed earlier for the projected DOS of O atom substituted for N in UN bulk [15]. In all three DOS (Fig. 3), a broad band corresponding to the N 2*p* projected states does not change drastically which means a weak effect of N ions on the O_2 molecule adsorption on the UN(0 0 1) surface.

4. Conclusions

Summing up, the results of our *ab initio* calculations clearly demonstrate a real possibility for spontaneous dissociation of the adsorbed oxygen molecules upon the perfect UN(0 0 1) surface, analogously to the O_2 dissociation on "traditional" metallic surfaces. This is the important step in understanding the initial stage of the UN oxidation mechanism.

Acknowledgements

This study was partly supported by the European Community FP7 project F-Bridge. D.B. gratefully acknowledges also the support from the European Social Fund (ESF). The authors kindly thank R. Caciuffo, R.A. Evarestov, D. Gryaznov, E. Heifets, Yu. Mastrikov, Hj. Matzke, and P. Van Uffelen for fruitful discussions.

References

[1] (a) Hj. Matzke, Science of Advanced LMFBR Fuel, North Holland, Amsterdam, 1986;
(b) Hj. Matzke, in: P.D. Wilson (Ed.), The Nuclear Fuel Cycle, University Press, Oxford, 1996.
[2] T. Petit, C. Lemaignan, F. Jollet, B. Bigot, A. Pasturel, Philos. Mag. B 77 (1998) 779.
[3] J.P. Crocombette, F. Jollet, L. Thien Nga, T. Petit, Phys. Rev. B 64 (2001) 104107.
[4] K. Kudin, G. Scuseria, R. Martin, Phys. Rev. Lett. 89 (2002) 266402.
[5] L. Petit, A. Svane, S. Szotek, W.M. Temmerman, Science 301 (2003) 498.
[6] M. Freyss, T. Petit, J.P. Crocombette, J. Nucl. Mater. 347 (2005) 44.
[7] F.N. Skomurski, R.C. Ewing, A.L. Rohl, J.D. Gale, U. Becker, Amer. Mineralog. 91 (2006) 1761.
[8] F. Gupta, G. Brillant, A. Pasturel, Philos. Mag. 87 (2007) 2561.
[9] (a) H.Y. Geng, Y. Chen, Y. Kaneta, M. Kinoshita, Phys. Rev. B 75 (2007) 054111; (b) H.Y. Geng, Y. Chen, Y. Kaneta, M. Kinoshita, Phys. Rev. B 77 (2008) 104120.
[10] P. Nerikar, T. Watanabe, J.S. Tulenko, S.R. Phillpot, S.B. Sinnott, J. Nucl. Mater. 384 (2009) 61.
[11] D. Sedmidubsky, R.J.M. Konings, P. Novak, J. Nucl. Mater. 344 (2005) 40.
[12] E.A. Kotomin, Yu.A. Mastrikov, Yu.F. Zhukovskii, P. Van Uffelen, V.V. Rondinella, Phys. Status Solidi (c) 4 (2007) 1193.
[13] E.A. Kotomin, R.W. Grimes, Yu.A. Mastrikov, N.J. Ashley, J. Phys.: Condens. Matter 19 (2007) 106208.
[14] M. Samsel-Czekała, E. Talik, P.V. Du Plessis, R. Troć, H. Misiorek, C. Sułkowski, Phys. Rev. B 76 (2007) 144426.
[15] E.A. Kotomin, Yu.A. Mastrikov, J. Nucl. Mater. 377 (2008) 492.
[16] R.A. Evarestov, M.V. Losev, A.I. Panin, N.S. Mosyagin, A.V. Titov, Phys. Status Solidi (b) 245 (2008) 114.
[17] R.A. Evarestov, A.V. Bandura, M.V. Losev, E.A. Kotomin, Yu.F. Zhukovskii, D. Bocharov, J. Comput. Chem. 29 (2008) 2079.
[18] Yu.F. Zhukovskii, D. Bocharov, E.A. Kotomin, R.A. Evarestov, A.V. Bandura, Surf. Sci. 603 (2009) 50.
[19] G. Kresse, J. Hafner, VASP the Guide, University of Vienna, 2007, <http://cms.mpi.univie.ac.at/vasp/>.
[20] R. Dovesi, V.R. Saunders, C. Roetti, R. Orlando, C.M. Zicovich-Wilson, F. Pascale, B. Civalleri, K. Doll, N.M. Harrison, I.J. Bush, Ph. D'Arco, M. Llunell, CRYSTAL2006 User's Manual, Universita di Torino, Torino, 2006, <http://www.crystal.unito.it/>.
[21] J.P. Perdew, Y. Wang, Phys. Rev. B 45 (1992) 13244.
[22] Yu.F. Zhukovskii, P.W.M. Jacobs, M. Causá, J. Phys. Chem. Solids 64 (2003) 1317.
[23] H.J. Monkhorst, J.D. Pack, Phys. Rev. B 13 (1976) 5188.
[24] R. Atta-Fynn, A.K. Ray, Phys. Rev. B 76 (2007) 115101.
[25] R. Weast, CRC Handbook of Chemistry and Physics, CRC Press Inc., Boca Baton, FL, 1985.

Surface Science 605 (2011) 396–400

Contents lists available at ScienceDirect

Surface Science

journal homepage: www.elsevier.com/ locate/susc

DFT calculations of point defects on UN(001) surface

D. Bocharov [a,b,c,*], D. Gryaznov [a], Yu.F. Zhukovskii [a], E.A. Kotomin [a]

[a] Institute for Solid State Physics, Kengaraga 8, LV-1063 Riga, Latvia
[b] Faculty of Physics and Mathematics, University of Latvia, Zellu 8, LV-1002 Riga, Latvia
[c] Faculty of Computing, University of Latvia, Raina blvd 19, LV-1586 Riga, Latvia

ARTICLE INFO

Article history:
Received 31 August 2010
Accepted 15 November 2010
Available online 27 November 2010

Keywords:
Density functional theory calculations
Uranium mononitride
(001) surface
Surface defects

ABSTRACT

The density functional theory is used in a study of point defects on both UN(001) surface and sub-surface layers. We compare the results for slabs of different thicknesses (both perfect and containing nitrogen or uranium vacancies) with a full geometry, electronic and spin density optimization. The electronic charge density re-distribution, density of states, magnetic moments of U atoms and local atomic displacements around defects are carefully analyzed. It is predicted that the vacancies are formed easier on the surface, whereas the property of sub-surface layer does not differ significantly from the central one in the slab.

1. Introduction

Uranium mononitride (UN) is considered nowadays by the Generation IV International Forum of nuclear reactors [1] as one of the promising nuclear fuels alternative to UO_2. However, it reveals unwanted oxidation in air [2] which could affect the fuel fabrication process and its performance. Atomistic understanding of the oxidation process could help to solve this problem.

Previous first-principles simulations on UN used mostly the density functional theory (DFT) and were focused mainly on bulk properties (for example, [3–9]). To check reliability of these results, we performed recently several calculations on bulk and (001) surface of UN using the two different DFT approaches [10]: linear combination of atomic orbitals (LCAO) applied for construction of basis sets and plane waves (PW) combined with the pseudopotentials representing the core electrons, as implemented in both *CRYSTAL* [11] and *VASP* [12] computer codes. Our basic findings for the bulk and the (001) surface of UN calculated using the *VASP* code were confirmed by *CRYSTAL* calculations [10]. The results of both series of calculations on the lattice constant, bulk modulus, cohesive energy, charge distribution, band structure and density of states (DOS) for UN single crystal were analyzed.

Recently [13,14], we performed first-principles simulations on the atomic and molecular oxygen interaction with the perfect UN(001) surface. It was demonstrated that the O_2 molecules could spontaneously dissociate [14] at the defect-free surface and releasing O adatoms reveal strong chemical interaction with surface ions [13]. It is worth mentioning that all our UN surface calculations [10,13,14] were performed for the fixed magnetic moments of U atoms.

To understand the oxidation mechanism in more detail, one has to take into account surface defects and their interaction with oxygen. So far, only point defects in the UN bulk were calculated [15,16]. In this paper, we study basic properties of surface vacancies. In section 2, a slab model and parameters used in our present spin-polarized PW DFT calculations are described. In section 3, we discuss main results obtained for the N and U vacancies on the surface. A short summary is presented in section 4.

2. Slab model and computational details

UN possesses a rock-salt *fcc* structure over a wide temperature range. We model the (001) surface using the symmetrical slabs containing odd number (5, 7, 9 or 11) of atomic layers separated by the vacuum gap of 38.9 Å which corresponds to 16 inter-layers (Fig. 1). Atomic layers consist of regularly alternating N and U atoms. Our test calculations show that such an inter-slab distance is large enough to exclude spurious interactions between the slabs repeated in the *z*-direction.

To simulate single point defects (either N or U vacancies), we applied a supercell approach using unit cells with 2×2 and 3×3 extensions of surface translation vectors. These supercells contain four and nine pairs of atoms in each layer while periodically distributed surface vacancies for such unit cells correspond to defect concentrations of 0.25 and 0.11 monolayers (ML), respectively. We calculated not only the outer surface defects, but also the sub-surface defects as well as those positioned at the central layer of the slab. To reduce computational efforts, we considered the two-side arrangement of the point defects which is symmetrical with respect to the central (mirror) plane (the atomistic model of surface N vacancies with the 2×2 periodicity is shown in Fig. 2).

* Corresponding author. Institute for Solid State Physics, Kengaraga 8, LV-1063 Riga, Latvia. Fax: +371 67132778.
E-mail address: bocharov@latnet.lv (D. Bocharov).

0039-6028/$ – see front matter © 2010 Elsevier B.V. All rights reserved.
doi:10.1016/j.susc.2010.11.007

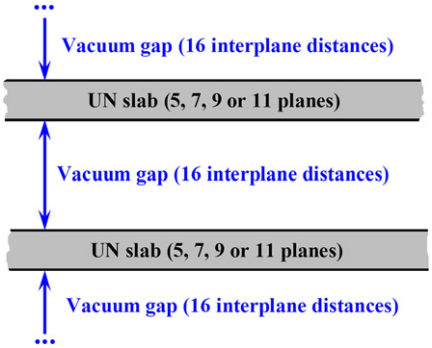

Fig. 1. Cross-section of UN(001) slabs.

For calculations, we used the PW DFT computer code *VASP 4.6* [12,17]. To represent the core electrons (78 electrons for U and 2 electrons for N), the relativistic pseudopotentials combined with the PAW method [18] were used. The Perdew-Wang-91 non-local exchange-correlation (GGA) functional [19] was chosen for calculations. The cut-off energy was fixed at 520 eV. The Monkhorst-Pack *k*-point mesh [20] of $8\times8\times1$ for integration over the Brillouin zone (BZ) was used, whereas the electron occupancies were determined following Methfessel and Paxton [21] as implemented in the *VASP* code. The smearing parameter of 0.2 eV was found to be optimal for reasonable convergences, suggesting the electronic entropy contribution of the order of 10 meV. The total energy of slabs of different thicknesses was optimized with respect to the atomic positions only, with the lattice parameter fixed at its equilibrium value of 4.87 Å for UN bulk. This value is slightly underestimated as compared to the experimental bulk value of 4.89 Å [22]. The ferromagnetic state was chosen for all our slab calculations [3] performed for the self-consistent (relaxed) atomic magnetic moments with no spin-orbit interactions included. Consequently, we calculated both the effective atomic charges and average magnetic moments per atom using the topological Bader analysis [23,24].

3. Main results

3.1. Perfect UN(001) surface

First, the calculations of the effective atomic charges q^{eff}, atomic displacements Δr, average magnetic moments μ_{av} of U atoms, and surface energies E_{surf} for defect-free slabs of different thicknesses

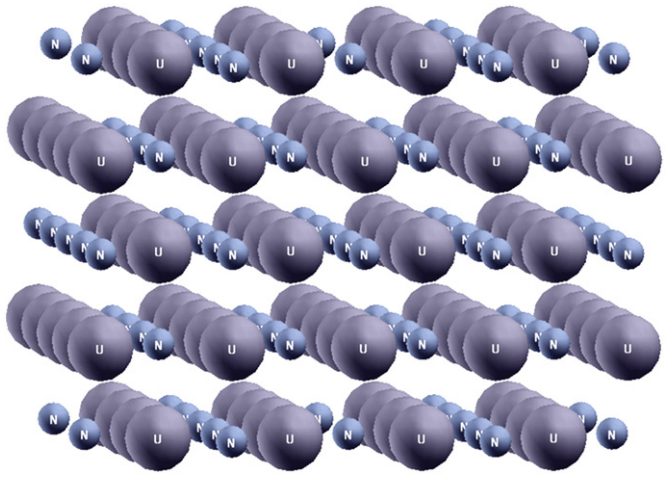

Fig. 2. Five-layer slab containing the two-sided surface N vacancies with a 2×2 periodicity.

Table 1
Surface energies E_{surf} ($\text{J}\cdot\text{m}^{-1}$) for calculations with relaxed and unrelaxed atomic spins as well as averaged magnetic moment (in μ_B) of U atom for the defect-free UN(001) surface.

Number of atomic planes	E_{surf} (spin-unrelaxed slab)	E_{surf} (spin-relaxed slab)	μ_{av}
5	1.69	1.44	1.57
7	1.70	1.37	1.44
9	1.70	1.29	1.37
11	1.69	1.22	1.33

(Tables 1 and 2) were performed, in order to check how these properties depend on atomic spin relaxation (in our previous calculations the total magnetic moment of a slab was fixed [10,13,14]). The spin relaxation leads to considerable change of E_{surf} depending on the number of layers in a slab (Table 1). The largest μ_{av} value was obtained for the U atoms in the 5-layer slab, i.e., μ_{av} slightly decreases with the thickness, suggesting difference of 0.3 μ_B between the 5- and 11-layer slabs. The lattice relaxation energies in spin-optimized calculations turn out to be quite small, i.e., ~0.03 eV.

It is also interesting to analyze q^{eff} values for atoms across the slab as a function of the number of layers in a slab (Table 2). First, q^{eff} shows considerable covalent bonding both on the surface (e.g., sub-surface) and on the central plane since the values are quite far from the formal ionic charges $\pm3e$. Second, the values in Table 2 demonstrate that the surface is slightly positively charged, due to a difference in the N and U charges. Third, the atomic charges are insensitive to both the spin relaxation and the number of layers.

The atomic displacements Δz from perfect lattice sites differ significantly for U atoms positioned at the surface and sub-surface layers (Table 3) being somewhat larger for the 5-layer slab while displacements of nitrogen atoms for all the slabs remain almost unchanged. Note that N atoms at (001) surface are displaced up, whereas U atoms are shifted inwards the slab center which results in the surface rumpling up to 1.2% of the lattice constant.

3.2. Vacancies on the (001) surface

In the present study, we considered the two reference states in calculations of the defect formation energies, both widely used in

Table 2
Atomic Bader charges on a defect-free surface.

Atom	Number of atomic layers			
	5	7	9	11
Surface U	1.68	1.74	1.68	1.72
Sub-surface U	1.67	1.63	1.63	1.67
U in central (mirror) plane	1.69	1.72	1.65	1.66
Surface N	−1.65	−1.67	−1.67	−1.68
Sub-surface N	−1.68	−1.70	−1.70	−1.67
N in central (mirror) plane	−1.74	−1.65	−1.65	−1.63

Table 3
Atomic displacements Δz(Å)* for defect-free surface (spin-relaxed calculations).

Number of atomic planes	U atom displacements		N atom displacements	
	Surface	Sub-surface	Surface	Sub-surface
5	−0.050	−0.012	0.023	0.023
7	−0.046	−0.009	0.024	0.028
9	−0.047	−0.011	0.024	0.028
11	−0.047	−0.011	0.025	0.031

*Negative sign means an inward atomic displacement towards the slab center.

Table 4
The vacancy formation energies (in eV) for the two reference states (see the text for details).

Layer	Number of atomic planes in slab and supercell extension (in brackets)	Reference I, Eqs. (1a)–(2)[a]		Reference II, Eqs. (1a), (1b), (3a) and (3b)[b]	
		U	N	U	N
Surface layer	5 (2×2)	8.63	8.84	1.46	3.70
	7 (2×2)	8.61	8.84	1.44	3.70
	9 (2×2)	8.61	8.84	1.44	3.71
	11 (2×2)	8.60	8.85	1.43	3.71
	5 (3×3)	8.51	8.78	1.34	3.64
	7 (3×3)	8.47	8.78	1.30	3.65
Sub-surface layer	5 (2×2)	10.31	9.38	3.14	4.25
	7 (2×2)	10.29	9.46	3.12	4.33
	9 (2×2)	10.26	9.46	3.09	4.33
	11 (2×2)	10.26	9.46	3.09	4.33
	7 (3×3)	10.18	9.47	3.01	4.34
Central (mirror) layer[c]	5 (2×2)	10.20	9.48	3.03	4.34
	7 (2×2)	10.36	9.57	3.19	4.43
	9 (2×2)	10.34	9.55	3.17	4.42
	11 (2×2)	10.39	9.56	3.22	4.42
	7 (3×3)	10.23	9.55	3.06	4.42

[a] Reference energies I equal to −4.10 eV for U atom and −3.17 eV for N atom.
[b] Reference energies II equal to −11.28 eV for U atom and −8.30 eV for N atom.
[c] Defect formation energies for UN bulk using reference I are 9.1–9.7 eV for N vacancy and 9.4–10.3 for U vacancy [15].

the literature. The point defect formation energy was calculated either as

$$E_{\text{form}}^{\text{N(U)vac}} = \frac{1}{2}\left(E_{\text{def}}^{\text{UN}} + 2E_{\text{ref\_I(II)}}^{\text{N(U)}} - E^{\text{UN}}\right), \tag{1a}$$

for surface and sub-surface vacancies, or

$$E_{\text{form}}^{\text{N(U)vac}} = E_{\text{def}}^{\text{UN}} + E_{\text{ref\_I(II)}}^{\text{N(U)}} - E^{\text{UN}}, \tag{1b}$$

for a vacancy in the central layer of the slab. Here $E_{\text{def}}^{\text{UN}}$ is the total energy of fully relaxed slab containing N (or U) vacancies, E^{UN} the same for a defect-free slab, while $E_{\text{ref\_I(II)}}^{\text{N(U)}}$ is reference energy for N (or U) atom. In our study, we used the two different reference states for both N and U atoms. Note that the pre-factor of ½ in Eq. (1a) arises due to a mirror arrangement of two N (U) vacancies on the surface and sub-surface layers (Fig. 2).

The first reference corresponds to N (U) isolated atom in triplet (quartet) spin states determined by $2p^3$ ($5f^3 6d^1$) valence electron configurations (hereafter reference I as in Table 4) calculated in a large tetragonal box ($28.28 \times 28.28 \times 22$ Å^3), i.e.:

$$E_{\text{ref\_I}}^{\text{N(U)}} = E_{\text{atom}}^{\text{N(U)}} \tag{2}$$

The second reference state (hereafter reference II as in Table 4) represents the chemical potential of N (U) atom which is in general a function of temperature and nitrogen partial pressure. By neglecting these effects, the N chemical potential can be treated as the energy of atom in the molecule N_2. Consequently, the chemical potential of U atom is given by the one-half total energy (per unit cell) of U single crystal in its low-temperature α-phase having the orthorhombic structure [25]. Thus, the corresponding second reference energies can be estimated as:

$$E_{\text{ref\_II}}^{\text{N}} = \mu_{N_2} = \frac{1}{2}E_{\text{tot}}[N_2], \tag{3a}$$

$$E_{\text{ref\_II}}^{\text{U}} = \mu_{\alpha-U} = \frac{1}{2}E_{\text{tot}}[\alpha - U], \tag{3b}$$

where $E_{\text{tot}}[N_2]$ is the total energy of nitrogen molecule while $E_{\text{tot}}[\alpha\text{-U}]$ the total energy of U bulk unit cell containing two atoms. The chemical potentials of N and U, as calculated according to Eqs. (3a) and (3b), represent extreme cases of N (U)-rich conditions [26], i.e., their minimum values were not considered in the present study. The formation energy of N (U) vacancy with respect to the N_2 molecule (or α-U single crystal) and the energy of N (U) isolated atom are closely

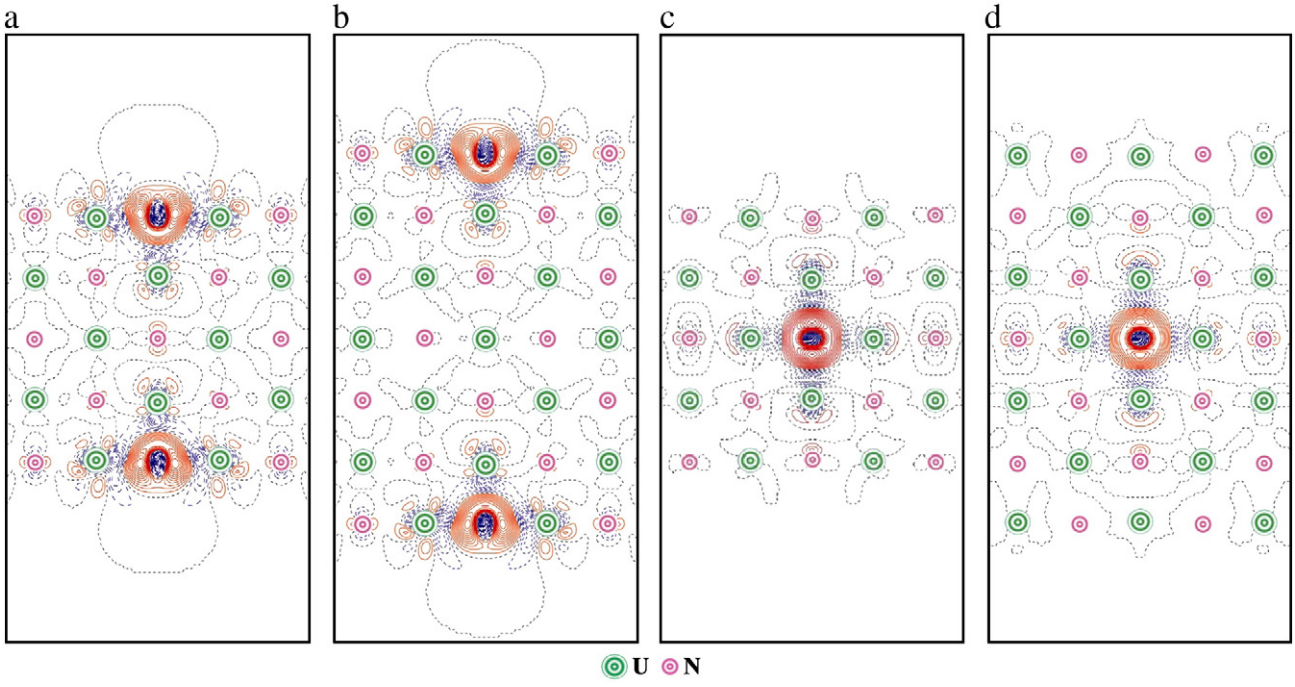

Fig. 3. 2D sections of the electron density redistributions around the nitrogen vacancies in five- and seven-layer UN(001) slabs with 2×2 supercell extension defined as the total electron density of defected surface minus a superposition of the electron densities for both perfect surface and isolated atom in the regular position on the surface: a) N vacancy in a surface plane, five-layer slab, b) the same, 7-layer slab, c) N vacancy in a central plane, five-layer slab, d) the same, 7-layer slab. Solid (red) and dashed (blue) isolines correspond to positive and negative electron density, respectively. Isodensity increment is 0.25 e a.u.$^{-3}$.

related: the former being larger than the latter by half the binding energy of the N_2 molecule or half the cohesive energy of α-U single crystal.

The lattice parameters of α-U were optimized: $a=2.80$ Å, $b=5.88$ Å, $c=4.91$ Å which are slightly underestimated as compared to values obtained experimentally [25] and calculated elsewhere [27,28], except for the parameter b which is in a good agreement with experimental value of 5.87 Å [25] (while $a=2.86$ Å, $c=4.96$ Å [25]). Also, the ratios c/a, b/a as well as the parameter c are well verified by another plane-wave DFT study [29]. Analogously to an isolated nitrogen atom, the N_2 molecule was calculated in the box but of a smaller size ($8\times8\times8$ Å^3). The molecule N_2 is characterized by the bond length of 1.12 Å and the binding energy of 10.63 eV being qualitatively well comparable with the experimental values of 1.10 Å and 9.80 eV [30], respectively.

The formation energies of N and U vacancies ($E_{\text{form}}^{\text{N(U) vac}}$) calculated using Eqs. (1a)–(3b) (with the two reference states as functions of the slab thickness) are collected in Table 4. These are smallest for the surface layer and considerably increase by ~0.6 eV for the N vacancy and by ~1.7 eV for the U vacancy in the sub-surface and central layers, independently of the reference state. This indicates the trend for vacancy segregation at the interfaces (surface or grain boundaries). A weak dependence of $E_{\text{form}}^{\text{N(U) vac}}$ on the slab thickness is also observed. The value of $E_{\text{form}}^{\text{N(U) vac}}$ is saturated with the slab thicknesses of seven atomic layers and more. Moreover, the difference between values of $E_{\text{form}}^{\text{N(U) vac}}$ for the 5 and 7 layer slabs is less for the surface vacancies than for those in the central layer. This difference is the largest for the U vacancy in the central plane (~0.16 eV).

The reference state II leads to smaller $E_{\text{form}}^{\text{N(U) vac}}$ (as compared to those found with the reference state I) and demonstrates a significant difference for two types of vacancies. According to reference II, the U vacancy could be substantially easier formed at $T=0$ K than the N vacancy. Notice that the chemical potentials of O and U atoms used in similar defect studies on UO_2 bulk did not reveal the energetic preference for U vacancy [28,31]. The defect–defect interaction is not responsible for this effect as $E_{\text{form}}^{\text{N(U) vac}}$ decreased by 0.1 eV only with the larger supercell size (3×3 in Table 4). On the other hand, due to the temperature dependence of the chemical potential of a free N_2 molecule [32], we predict reduction of the formation energy of the N vacancy by ~0.8 eV as the temperature increases from RT to 1000 °C. Unlike the reference state II, the reference I results in similar formation energies for both types of the vacancies. In the central slab layer, values of $E_{\text{form}}^{\text{N(U) vac}}$ were found to be similar to those in the bulk (Table 4).

The local atomic displacements around the vacancies are largest for the nearest neighbors of vacancies. The analysis of atomic displacements allows us to suggest that the U vacancy disturbs the structure of the surface stronger than the N vacancy. If the N vacancy lies in the surface layer, displacements of the nearest U atoms in z-direction achieve 0.02–0.05 Å towards the central plane of slab. The displacements of N atom nearest to surface N vacancy achieve 0.05 Å towards the central plane (z-direction) and 0.01 Å in xy (surface) plane. Maximum displacements of neighbor atoms around the N vacancy in the central plane have been found to be 0.04–0.07 Å (nearest U atoms from the neighboring layers are shifted in z-direction towards the vacancy), and do not exceed 0.025 Å for all the other atoms in the slab.

In contrast, the U vacancy results in much larger displacements of neighboring atoms, independently of its position. If the U vacancy is in the surface layer, then the atomic displacements of 0.3–0.32 Å are observed for the nearest N atoms. If the U vacancy lies in the central layer, then the nearest N atoms from this layer are displaced by 0.17 Å, while the N atoms from the nearest layers are not shifted in xy direction, being displaced by 0.15 Å towards the slab surface in the z-direction. Furthermore, the atomic displacements are weakly dependent on the slab thickness. The atomic displacements around the N and U vacancies in the UN bulk have been found to be −0.03 Å and 0.13 Å for N and U vacancies, respectively [15]. These values are close to those found in the present calculations for the vacancies in the central slab layer, which mimics the crystal bulk.

The finite slab-size effects caused by relatively large concentration of defects could be illustrated using the difference electron density redistribution $\Delta\rho(\mathbf{r})$. In Fig. 3, these redistributions are shown for N vacancies positioned at both the outer surface and central (mirror) planes of 5- and 7-layer slabs. Presence of two symmetrically positioned vacancies in the 5-layer slab induces their weak interaction across the slab (Fig. 3a) illustrated by appearance of an additional electron density around the N atoms in the central plane of the slab.

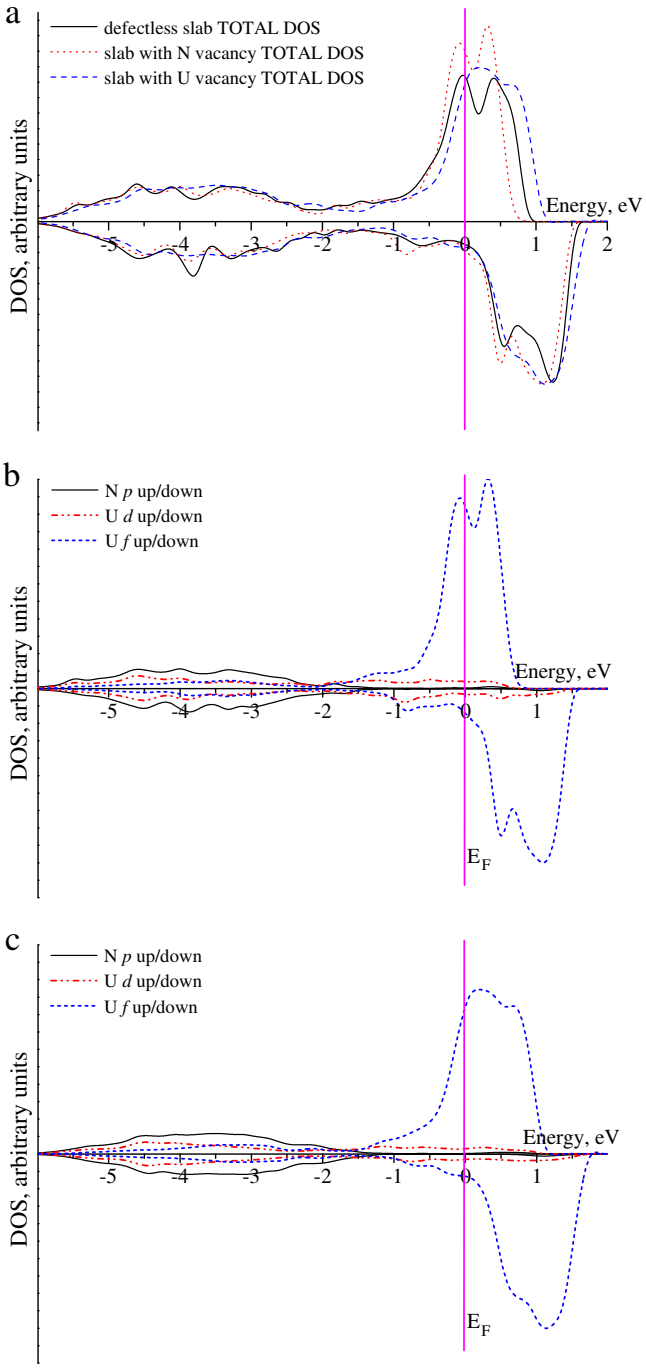

Fig. 4. The total and projected DOSs of 7-layer UN(001) slab (2×2 supercell for vacancy-containing models): a) total DOS of defective and defect-free surfaces, b) projected DOSs for the surface containing N vacancies, c) projected DOSs for the surface containing U vacancies.

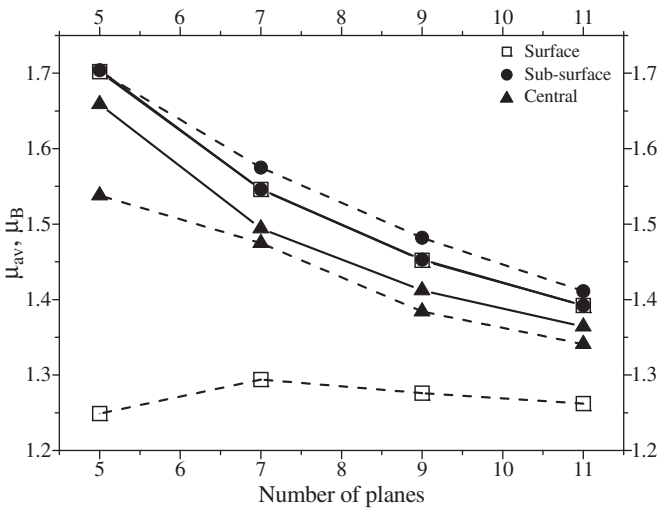

Fig. 5. The average U magnetic moment μ_{av} (in μ_B) in the slab as a function of a number of planes. The dashed curves correspond to U vacancy, whereas the solid curves describe the N vacancy.

Similarly, the vacancy in the mirror plane disturbs the atoms in the surface plane if thin slab contains only 5 layers (Fig. 3c). By increasing the slab thickness, we can avoid the effect of finite slab size (Fig. 3b and d) which explains the stabilization of formation energies calculated for the 7-layer and thicker UN(001) slabs (Table 4).

The densities of states (DOS) are presented in Fig. 4 for perfect and defective 7-layer UN slab. The DOS for other slabs calculated in this study did not demonstrate additional effects and, thus are not shown here. In accordance with previous bulk calculations [10,15], the U(5*f*) electrons occupy the Fermi level (Fig. 4a). These electrons are relatively localized but still strongly hybridized with the N(*2p*) electrons. It confirms the existence of covalent bonding observed in the analysis of Bader charges (Table 2). The N(2*p*) states form a band of the width ~4 eV similar to that obtained in the bulk [10,15]. In contrast, the contribution of U(6*d*) electrons remains insensitive to the presence of vacancies as these are almost homogeneously distributed over a wide energy range including the conduction band.

The analysis of the average magnetic moment of U atoms (μ_{av}^{U}) in the defective UN slabs is done too (Fig. 5). It decreases for both types of vacancies as a function of a number of layers in the slab, except for the U vacancy in the surface layer which remains almost unchanged. On the other hand, μ_{av}^{U} increases significantly when the U vacancy is located in the sub-surface and surface layers. In contrast to the U vacancies, μ_{av}^{U} for the slabs with the N vacancies are less sensitive to the position of defect. Moreover, the values of μ_{av}^{U} for the slabs with the N vacancies in the surface and sub-surface planes are practically identical.

4. Conclusions

In the present study, the basic properties of vacancies on the UN (001) surface were calculated from the first principles. In particular, the formation energies for U and N vacancies were determined using the two reference states, which included the energies of isolated atoms as well as atoms in the metallic α-U phase and N_2 molecule, respectively. The formation energies indicated a clear trend for segregation towards the surface (and probably, grain boundaries) as these energies for surface layer are noticeably smaller than those for sub-surface and central layers (although both latter are very close). However, the magnetic moments in the sub-surface and central layers differ significantly. We demonstrated also a considerable deviation of effective atomic charges from formal charges (caused by a covalent contribution to the U-N chemical bond). The obtained results will be used in the oncoming study of oxygen interaction with real (defective) UN surfaces, in order to understand the atomistic mechanism of UN oxidation.

Acknowledgements

This study was partly supported by the EC FP7 *F-BRIDGE* project and ESF project No.2009/0216/1DP/1.1.1.2.0/09/APIA/VIAA/044. D.B. gratefully acknowledges the doctoral studies support from the European Social Fund (ESF). The authors kindly thank R.A. Evarestov, P. Van Uffelen, and V. Kashcheyevs for fruitful discussions.

References

[1] P.D. Wilson (Ed.), The Nuclear Fuel Cycle, University Press, Oxford, 1996,, www.gen-4.org.
[2] Y. Arai, M. Morihira, T. Ohmichi, J. Nucl. Mater. 202 (1993) 70.
[3] R. Atta-Fynn, A.K. Ray, Phys. Rev. B 76 (2007) 115101.
[4] M.S.S. Brooks, J. Phys. F Metal Phys. 14 (1984) 639.
[5] M. Samsel-Czekała, E. Talik, P. de V. Du Plessis, R. Troć, H. Misiorek, C. Sułkowski, Phys. Rev. B 76 (2007) 144426.
[6] M.S.S. Brooks, D. Glötzel, Physica 102B (1980) 51.
[7] E.A. Kotomin, Yu.A. Mastrikov, Yu.F. Zhukovskii, P. Van Uffelen, V.V. Rondinella, Phys. Stat. Sol. C 4 (2007) 1193.
[8] R.A. Evarestov, M.V. Losev, A.I. Panin, N.S. Mosyagin, A.V. Titov, Phys. Stat. Sol. B 245 (2008) 114.
[9] E.A. Kotomin, Yu.A. Mastrikov, J. Nucl. Mater. 377 (2008) 492.
[10] R.A. Evarestov, A.V. Bandura, M.V. Losev, E.A. Kotomin, Yu.F. Zhukovskii, D. Bocharov, J. Comput. Chem. 29 (2008) 2079.
[11] R. Dovesi, V.R. Saunders, C. Roetti, R. Orlando, C.M. Zicovich-Wilson, F. Pascale, B. Civalleri, K. Doll, N.M. Harrison, I.J. Bush, Ph. D'Arco, M. Llunell, CRYSTAL2006 User's Manual, Universita di Torino, Torino, 2006, http://www.crystal.unito.it/.
[12] G. Kresse, J. Furthmüller, *VASP* the Guide, University of Vienna, 2009, http://cms.mpi.univie.ac.at/vasp/.
[13] Yu.F. Zhukovskii, D. Bocharov, E.A. Kotomin, R.A. Evarestov, A.V. Bandura, Surf. Sci. 603 (2009) 50.
[14] Yu.F. Zhukovskii, D. Bocharov, E.A. Kotomin, J. Nucl. Mater. 393 (2009) 504.
[15] E.A. Kotomin, R.W. Grimes, Yu.A. Mastrikov, N.J. Ashley, J. Phys. Condens. Matter 19 (2007) 106208.
[16] E.A. Kotomin, Yu.A. Mastrikov, S. Rashkeev, P. van Uffelen, J. Nucl. Mater. 393 (2009) 292.
[17] G. Kresse, J. Furthmüller, Comput. Mater. Sci. 6 (1996) 15.
[18] G. Kresse, D. Joubert, Phys. Rev. A 59 (1999) 1758.
[19] J.P. Perdew, J.A. Chevary, S.H. Vosko, K.A. Jackson, M.R. Pederson, D.J. Singh, C. Fiolhais, Phys. Rev. B 46 (1992) 6671.
[20] H.J. Monkhorst, J.D. Pack, Phys. Rev. B 13 (1976) 5188.
[21] M. Methfessel, A.T. Paxton, Phys. Rev. B 40 (1989) 3616.
[22] H.-J. Matzke, Science of Advanced LMFBR Fuels, North Holland, Amsterdam, 1986.
[23] R. Bader, Atoms in molecules: a quantum theory, Oxford University Press, New York, 1990.
[24] G. Henkelman, A. Arnaldsson, H. Jónsson, Comput. Mater. Sci. 36 (2006) 354.
[25] J. Akella, S. Weir, J.M. Wills, P. Söderlind, J. Phys. Condens. Matter 9 (1997) L549.
[26] C.G. Van de Walle, J. Neugebauer, J. Appl. Phys. 95 (2004) 3851.
[27] P. Söderlind, Phys. Rev. B 66 (2002) 085113.
[28] B. Dorado, M. Freyss, G. Martin, Eur. Phys. J. B 69 (2009) 203.
[29] M. Freyss, Phys. Rev. B 81 (2010) 014101.
[30] D.R. Lide (Ed.), CRC Handbook of Chemistry and Physics, 88th Edition, CRC Press, 2007-2008.
[31] M. Iwasawa, Y. Geng, Y. Kaneta, T. Ohnuma, H.-Y. Geng, M. Kinoshita, Mater. Trans. 47 (2006) 014101.
[32] NIST Chemistry Web-book, http://www.webbook.nist.gov/chemistry/2010.

Journal of Nuclear Materials 416 (2011) 200–204

Contents lists available at ScienceDirect

Journal of Nuclear Materials

journal homepage: www.elsevier.com/locate/jnucmat

Ab initio modeling of oxygen impurity atom incorporation into uranium mononitride surface and sub-surface vacancies

D. Bocharov [a,b,c,*], D. Gryaznov [a], Yu.F. Zhukovskii [a], E.A. Kotomin [a]

[a] Institute of Solid State Physics, Kengaraga 8, LV-1063 Riga, Latvia
[b] Faculty of Physics and Mathematics, University of Latvia, Zellu 8, LV-1002 Riga, Latvia
[c] Faculty of Computing, University of Latvia, Raina blvd. 19, LV-1586 Riga, Latvia

ARTICLE INFO

Article history:
Available online 14 December 2010

ABSTRACT

The incorporation of oxygen atoms has been simulated into either nitrogen or uranium vacancy at the UN(0 0 1) surface, sub-surface or central layers. For calculations on the corresponding slab models both the relativistic pseudopotentials and the method of projector augmented-waves (PAW) as implemented in the VASP computer code have been used. The energies of O atom incorporation and solution within the defective UN surface have been calculated and discussed. For different configurations of oxygen ions at vacancies within the UN(0 0 1) slab, the calculated density of states and electronic charge re-distribution was analyzed. Considerable energetic preference of O atom incorporation into the N-vacancy as compared to U-vacancy indicates that the observed oxidation of UN is determined mainly by the interaction of oxygen atoms with the surface and sub-surface N-vacancies resulting in their capture by the vacancies and formation of O–U bonds with the nearest uranium atoms.

1. Introduction

Uranium mononitride (UN) is considered as a promising nuclear fuel for the fast nuclear Generation IV reactors [1]. It has several advantages as compared to the traditional oxide nuclear fuels [2]. The synthesis of UN may be carried out by direct substitution starting from fluorides (*e.g.*, using oxidative ammonolysis of uranium fluorides to uranium nitride [3]). However, oxygen impurities always presented in UN lead to its unwanted pollution and further degradation in air. A number of experiments were performed, in order to understand an influence of oxygen on UN properties and other actinide compounds [4–6]. Various experimental analyses clearly manifested that oxygen contact with the actinide nitride surfaces can result in growth of the oxide [4,5] and, at initial stages, leads to the formation of oxynitrides [6]. The oxynitrides of varying structure (UO_xN_y) can be formed in the reactions of uranium metal with NO_2 [7] or by direct current sputtering upon U target in an Ar atmosphere containing admixture of O_2 and N_2 [8]. This facilitates importance of UO_xN_y for actinide surface studies.

Beginning with 1980s [9,10] a number of *ab initio* calculations on UN bulk [11–16] were performed using formalism of the Density Functional Theory (DFT). It is also worth mentioning that the first-principles calculations on actinide nitride compounds continue attracting great attention, due to improved methods and increasing interest for the fast breeder reactors and for the issues of transmutation of plutonium and minor actinides. Basic bulk properties of actinide nitrides were considered in a few recent studies [17–19], with emphasis on elastic and magnetic properties. The first electronic structure simulations on the perfect UN(0 0 1) *surface* and its reactivity towards the molecular and atomic oxygen were performed only recently [20–22]. These studies clearly show that the O_2 molecule after adsorption on the UN(0 0 1) surface dissociates spontaneously, whereas the newly-produced O atoms demonstrate a strong chemisorption at the surface. For simplicity, we call hereafter O adatoms despite the fact that these are negatively charged ions O^-. Additionally, a considerable attention [14] was paid to the static and dynamic properties of primary defects (vacancies) in UN *bulk* [15] which affect the fuel performance during operation and its reprocessing.

Apart the behavior of empty vacancies, the O atom incorporation into vacancies in bulk UN was considered. Its incorporation into the N-vacancies was found to be energetically more favorable as compared to the interstitial sites [23]. However, the solution energy has shown an opposite effect. The migration energy for the O atom via the interstitial sites along the [0 0 1] direction is 2.84 eV [23,24]. Defective UN surface containing both nitrogen and uranium vacancies disposed at different positions within the UN(0 0 1) slab has been also discussed in a separate paper [25]. In order to shed more light on the mechanism of UN unwanted oxidation, the incorporation of oxygen impurities into the N- and U-vacancies on the UN(0 0 1) surface is focused in this paper.

* Corresponding author at: Institute of Solid State Physics, Kengaraga 8, LV-1063 Riga, Latvia. Fax: +371 67132778.
E-mail address: bocharov@latnet.lv (D. Bocharov).

0022-3115/$ - see front matter © 2010 Elsevier B.V. All rights reserved.
doi:10.1016/j.jnucmat.2010.11.090

2. Computational details

For the simulation of a defective UN(0 0 1) substrate with empty and oxygen-occupied vacancies, the DFT plane wave computer code VASP 4.6 [26–29] was employed. The VASP package is suited for performing first-principles calculations based on the DFT approximation when varying the free energy and evaluating the instantaneous electronic ground state at each quantum-mechanical molecular dynamics time step [26,30]. Ultra-soft pseudopotentials combined with the PAW method [31,32] were used. Computational procedures implemented in this code [26,27] foresee the iterative solution of the Kohn–Sham equations based on both residuum-minimization and optimized charge-density mixing routines [28,29]. The non-local exchange–correlation functional within the Perdew–Wang-91 Generalized Gradient Approximation (PW91 GGA) [33] and the relativistic pseudopotentials for 78 U core electrons (with $6s^2 6p^6 6d^2 5f^2 7s^2$ valence shell), as well as 2 both N and O core electrons (with $2s^2 2p^3$ and $2s^2 2p^4$ valence shells, respectively) were applied in the current study. The Monkhorst–Pack scheme [34] with a $8 \times 8 \times 1$ k-point meshes in the Brillouin zone (BZ) was used while the cut-off energy was set to 520 eV. It became common in last years to use the so-called GGA + U approach to such strongly correlated systems as actinides (*e.g.*, UO_2 [35] and references therein). On the other hand, our test calculations with reasonable U-parameters have shown that the relative variation in the defect formation energies may be ~10% which does not affect main trends and conclusions of the present study. This is why the standard GGA approximation was used which is important for a comparison with previous calculations of defect energies in the UN bulk [15].

For the symmetric UN(0 0 1) substrate possessing the *fcc* rock-salt structure, a slab model was employed. It consists of 5, 7 or 9 atomic layers and containing regularly alternating U and N atoms. The 2D slabs are separated by a vacuum gap of sixteen interlayer distances (38.88 Å) in the z-direction. This inter-slab distance is large enough to exclude the spurious interaction between the slabs. Our calculations supposed the supercells with 2×2 and 3×3 extensions of translation vector for the (0 0 1) surface of UN. Both empty as well as oxygen-occupied N- and U-vacancies were disposed in the surface, sub-surface and central layers of 2D slab. Due to the presence of mirror layers in the symmetric slabs, one can consider the two-sided symmetric arrangement of defects (Fig. 1), except for the central mirror plane, thus, minimizing the computational expenses. Fig. 1 also shows the oxygen-occupied N-vacancies with a 2×2 and 3×3 periodicity disposed on the surface layer. The lattice constant of UN slabs is fixed at 4.87 Å, taken from the lattice relaxation of the UN bulk [20]. In all the calculations, the structural optimization within the supercell of fixed linear dimensions was performed, using the standard procedure of total energy minimization. Our test calculations have shown that the ferromagnetic (FM) phase is energetically slightly more favorable for UN *slabs* than the anti-ferromagnetic (AFM) one. The spin magnetic moment was allowed to relax in all the calculations for the FM spin arrangements on the uranium sub-lattice.

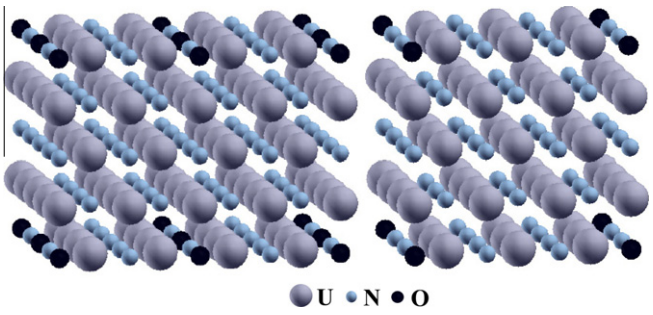

Fig. 1. The symmetrical five-layer UN(0 0 1) slab with a 2×2 (left) and 3×3 (right) periodicity of the oxygen atoms incorporated into the surface N-vacancies.

3. Incorporation and solution energies

The energy balance for the incorporation of an O atom into a vacancy can be characterized by *the incorporation energy* E_I suggested by Grimes and Catlow [36] in the shell model calculations on fission products in UO_2:

$$E_I = E^{N(U)}_{O\_inc} - E^{N(U)}_{vac} - E_O \tag{1a}$$

for the O atom incorporated into the N- and U-vacancy disposed in the central atomic layer and

$$E_I = \frac{1}{2}\left(E^{N(U)}_{O\_inc} - E^{N(U)}_{vac} - 2E_O\right) \tag{1b}$$

for the same incorporation in the surface or sub-surface layers. Here $E^{N(U)}_{O\_inc}$ is the total energy of the supercell containing the O atom at either the N- or U-vacancy $\left(E^{N(U)}_{O\_inc} < 0\right)$, $E^{N(U)}_{vac}$ the energy of the supercell containing an unoccupied (empty) vacancy, and E_O half the total energy of isolated O_2 molecule in the triplet state. It is defined by the oxygen chemical potential at 0 K. Since the value of E_I describes the energy balance for the incorporation into pre-existing vacancies, it has to be negative for energetically favorable incorporation processes.

To take into account the total energy balance, including the vacancy formation energy E_{form} in the defect-free slab, the solution energy [36] was defined as:

$$E_S = E_I + E_{form} \tag{2}$$

where E_{form} is the formation energy of N- or U- vacancy in the slab, calculated as

$$E_{form} = E^{N(U)}_{vac} + E^{N(U)}_{atom} - E^{UN} \tag{3a}$$

for a defect in the central atomic layer of the slab and

$$E_{form} = \frac{1}{2}\left(E^{N(U)}_{vac} + 2E^{N(U)}_{atom} - E^{UN}\right) \tag{3b}$$

for a defect in the surface or sub-surface layer. Here E^{UN} is an energy of the defectless relaxed slab, and $E^{N(U)}_{atom}$ can be defined as chemical potentials of N or U atom, which is, in general, a function of temperature and nitrogen partial pressure. The chemical potential of nitrogen at 0 K is defined by the total energy of N_2 molecule, *i.e.*, $\mu_{N_2} = \frac{1}{2}E_{tot}[N_2]$, while the chemical potential of U atom at 0 K can be estimated as the total energy, *per* atom, for metallic uranium in its low-temperature ortho-rhombic α-phase: $\mu_{\alpha U} = \frac{1}{2}E_{tot}[\alpha U]$. The co-factor of 1/2 in Eqs. (1b) and (3b) as well as multiplication of E_O and $E^{N(U)}_{atom}$ by 2 in the same equations appears due to the symmetric arrangement of incorporated O atoms.

More details on calculations of unoccupied N- and U- vacancies and parameters of calculated of N_2 and α-U are given in Ref. [25]. It is worth mentioning, however, that use of the standard O pseudopotential in our VASP calculations gave good bond length of 1.23 Å for the O_2 molecule but considerable overestimate of the binding energy (6.79 eV *vs.* the experimental value of 5.12 eV). Several corrections were suggested in the literature how to take into account this serious DFT shortcoming [37,38]. Thus, the calculated defect formation and solution energies may be corrected by ~1 eV (its impact is also discussed below).

Table 1
Incorporation (E_I), solution (E_S) energies in eV, average spin magnetic moments of U atoms μ^U_{av} in μ_B and effective charge of O atoms in e^- for O incorporation into the UN(0 0 1) surface. The reference states for calculating the incorporation and solution energies are the chemical potentials of O, N and U calculated for O_2, N_2 molecules and α-U, respectively.

Layer	Supercell size	Number of atomic layers in slab	N-vacancy				U-vacancy			
			E_I (eV)	E_S (eV)	μ^U_{av} (μ_B)	q_{eff} (e^-)	E_I (eV)	E_S (eV)	μ^U_{av} (μ_B)	q_{eff} (e^-)
Surface	2 × 2	5	−6.173	−2.473	1.65	−1.36	−0.339	1.120	1.16	−0.98
		7	−6.181	−2.476	1.49	−1.36	−0.855	0.583	1.36	−1.03
		9	−6.188	−2.479	1.41	−1.36	−0.943	0.493	1.31	−1.06
	3 × 3	5	−6.122	−2.481	1.60	−1.37	−0.683	0.654	1.48	−1.05
		7	−6.126	−2.480	1.46	−1.36	−1.073	0.230	1.38	−1.08
Sub-surface	2 × 2	5	−6.314	−2.068	1.64	−1.42	−1.856	1.284	1.66	−1.10
		7	−6.419	−2.090	1.49	−1.40	−1.823	1.297	1.45	−1.10
		9	−6.417	−2.091	1.41	−1.40	−1.823	1.271	1.38	−1.10
	3 × 3	7	−6.428	−2.093	1.46	−1.39	−2.012	1.000	1.43	−1.10
Central (mirror)	2 × 2	7	−6.611	−2.180	1.47	−1.42	0.736	3.923	1.44	−0.89
		9	−6.608	−2.192	1.39	−1.38	0.669	3.838	1.38	−0.90
	3 × 3	7	−6.599	−2.182	1.45	−1.42	0.317	3.378	1.47	−0.94

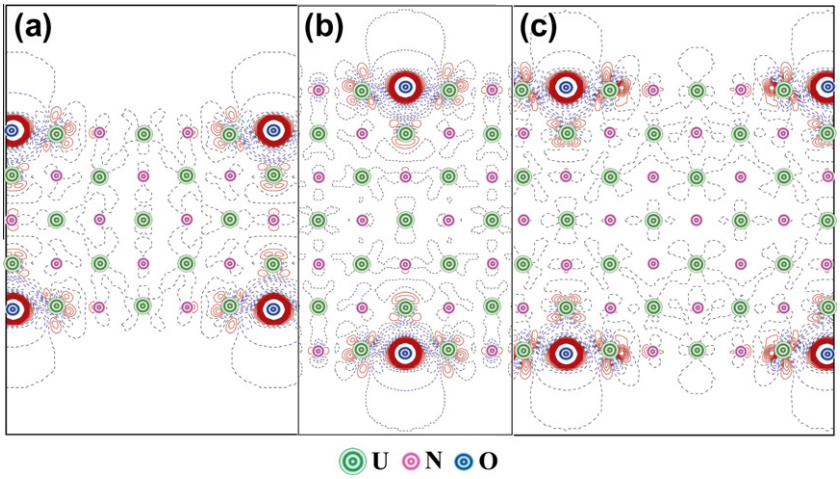

Fig. 2. The 2D sections of the electron charge density redistributions $\Delta\rho(\mathbf{r})$ around the O atoms incorporated into the surface N-vacancies of the five- and seven-layer UN(0 0 1) slabs with 2 × 2 and 3 × 3 supercell extensions. $\Delta\rho(\mathbf{r})$ are defined as the total electron density of the O-containing defected surface minus a superposition of the electron densities of the surface containing the N-vacancies and the O atom in the regular positions on the surface. (a) 3 × 3 periodicity of the oxygen atoms upon the five-layer slab, (b) 2 × 2 periodicity of the oxygen atoms upon the seven-layer slab, (c) 3 × 3 periodicity of the oxygen atoms upon the seven-layer slab. Solid (red) and dashed (blue) isolines correspond to positive and negative electron density, respectively. Dashed black isolines correspond to the zero-level. Isodensity increment is 0.25 e a.u.$^{-3}$. (For interpretation of the references to colour in this figure legend, the reader is referred to the web version of this article.)

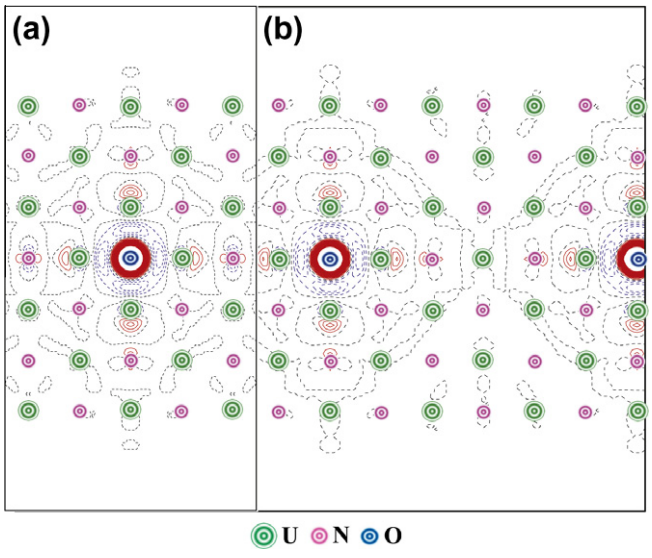

Fig. 3. The 2D sections of $\Delta\rho(\mathbf{r})$ around the O atoms incorporated into the N-vacancies disposed in central layer of the seven-layer UN(0 0 1) slabs with (a) 2 × 2 and (b) 3 × 3 supercell extensions. Other details are given in caption of Fig. 2.

4. Results and discussion

The calculated O atom incorporation into the N-vacancies at the UN(0 0 1) surface is energetically favorable since both values of E_I and E_S are strictly negative (Table 1), thus, being in favor of both creating the N-vacancy and adsorbing the O atom from air. Also, E_I decreases by ∼0.4 eV (becomes more negative) within the slab as compared to the surface layer, whereas E_S is smallest for the N-vacancy just on the surface layer. Contrary, in case of the U-vacancies, the values of E_I calculated for the surface and central layers are found to be close to zero. The sub-surface layer is characterized by E_I which is ∼1 eV smaller than that for the surface and central layers. Our results indicate importance of oxynitride formation. However, E_S is positive and increases for O atoms in the the U-vacancy and the slab centre. Note that the energies in Table 1 do not include the corrections discussed above for the O atoms. However, such corrections may lead to E_I (or E_S) increased by ∼1 eV and, as a result, more positive E_I for the U-vacancy. Table 1 also indicates that solution of the oxygen atoms is energetically more favorable at the surface layers than in the slab. As the supercell size increases (the 3 × 3 extension in Table 1), both E_I and E_S values decrease whereas the slab thickness has no such clear effect. Nevertheless, the U-vacancy appeared to be most sensitive to the

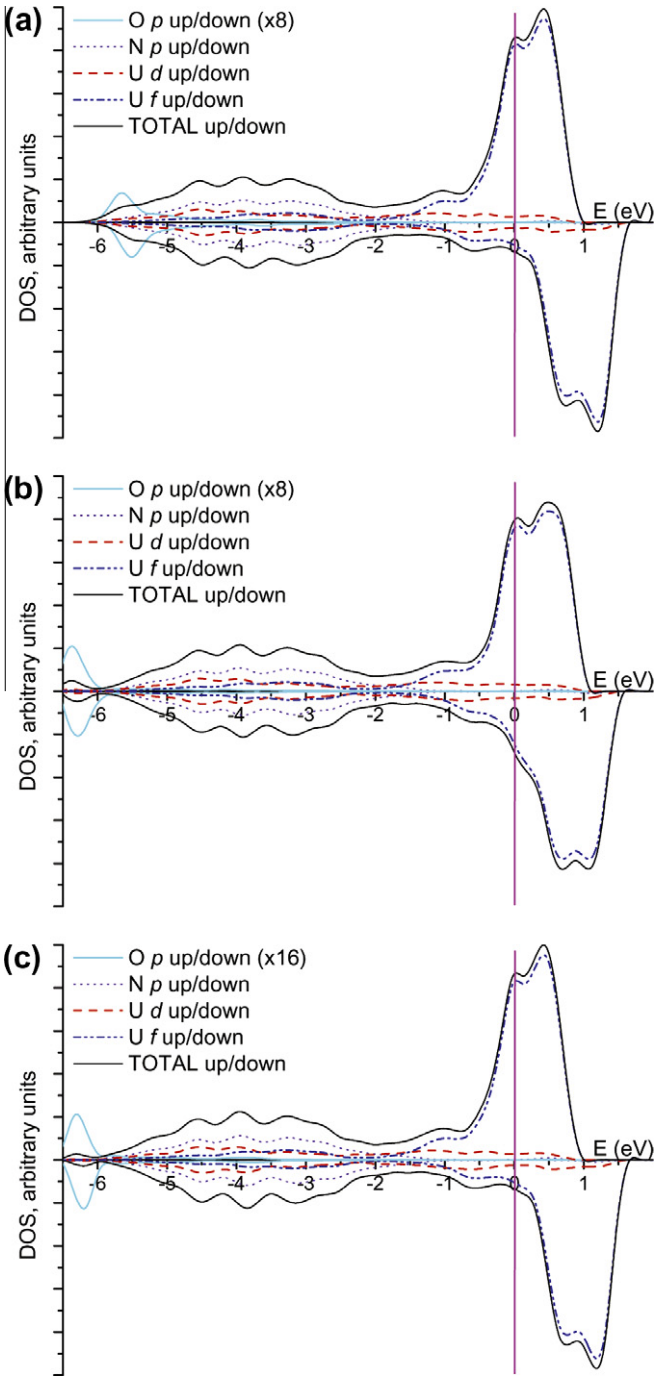

Fig. 4. The total and projected DOS for three positions of O atoms incorporated into the N-vacancies with a 3×3 periodicity across the seven-layer UN(0 0 1) slab: (a) surface layer, (b) sub-surface layer, (c) central layer. The O 2*p* peaks have been normalized to the same value, *i.e.*, these were multiplied by a factor of 8 and 16 for vacancies in the surface (sub-surface) and central layers, respectively (please see figure labels), A convolution of individual energy levels has been plotted using the Gaussian functions with a half-width of 0.2 eV.

supercell size which is related to spurious interactions between the periodically repeated defects. The E_I as well as E_S values may be reduced by 0.15 eV at the average in this case.

Table 1 allows us to analyze also the averaged spin density of U atoms μ_{av}^{U} for different morphologies of defective UN(0 0 1) surfaces with incorporated O atoms. Analogously to defective UN surface with empty vacancies [25], μ_{av}^{U} decreases with a number of layers in the slab for both types of the vacancies (except for the O atom incorporated into the U-vacancy in the surface layer). It is also seen that μ_{av}^{U} is higher in the surface layer for the N-vacancy than for the U-vacancy. The sub-surface and central layers are characterized by similar μ_{av}^{U} for both the vacancies. Interestingly, the effective charge q_{eff} of O atoms is also higher for the N-vacancy and inside the slab. In the case of U-vacancy, however, q_{eff} decreases by almost 0.3 e. The same effect is also seen for the N atoms their effective charge is smaller when the O atom occupies the U-vacancy (not shown here). The overall picture suggests prevalence of the covalent bonding between different species in the system.

Large concentrations of defects (25% for the 2×2 extension in Table 1) causes certain finite-size effects which can be illustrated using the 2D difference electron density redistributions $\Delta\rho(\mathbf{r})$. These redistributions are shown for the O atoms incorporated into the N-vacancies at the surface (Fig. 2) and central layers (Fig. 3). Inside the five-layer slab, a presence of the two symmetrically positioned defects induces their interaction (visible in charge redistribution across a slab in Fig. 2a). An increase of the slab thickness reduces this effect (Fig. 2c). If the supercell size is decreased (the 2×2 extension, Fig. 2b) an additional electron density parallel to the surface layer is observed between the defects. Similar effects are also observed for redistributions of the electron density around defects in the mirror planes (Fig. 3). A perfect spherical negative charge redistribution is observed around the O atom in the U-vacancy in the central plane (not shown here). The effect of supercell size in this case is similar to that discussed for the N-vacancy. However, in the case of surface vacancy more electron density is seen between the O atom and neighbouring N atoms in the sub-surface layer, in a comparison to the N-vacancy. Thus, the effect of slab thickness also may not be underestimated in this case.

In Fig. 4, the total and projected density of states (DOS) is shown for the seven-layer defective UN(0 0 1) surface with the O atom incorporated into the N-vacancy. The system remains conducting throughout all the calculations with the significant contribution from the U 5*f* states at the Fermi level similar to pure UN bulk [20]. The appearance of the specific O 2*p* band with the energy peak at −6 eV is observed. When comparing the DOS for the O atoms incorporated into the N–vacancies, a noticeable shift of the O 2*p* band (by about −1.0 eV) allows one to distinguish the surface layer from the internal layers. Moreover, in the case of the surface layer, this band considerably overlaps with the N 2*p* band, partly mixed with the U 5*f* states (similar effects happen with the O_2 molecule atop the surface U atom [22]). Contrary, the O 2*p* band remains quasi-isolated from the other bands (analogously to the O atom incorporated into the N-vacancy in UN bulk [23]). Note that position of the N 2*p* band is insensitive to the presence of O atoms and lies within energy range of −6 and −1 eV.

5. Conclusions

Summing up the results obtained in this and our recent studies, the following stages for reactivity of oxygen positioned atop the UN(0 0 1) surface could be suggested: (i) spontaneous breaking of the O_2 chemical bond after molecular adsorption [22], (ii) location of the two newly formed O adatoms atop the surface U atoms [21], (iii) incorporation of O adatoms in pre-existing surface N-vacancies (as a result of vacancy surface diffusion), (iv) incorporation of O atoms in existing sub-surface N-vacancies as a result of inter-lattice diffusion. This explains an easy UN oxidation observed in air.

The formation of oxynitrides [8] near the UN(0 0 1) surface is proposed, which can be caused by diffusion of the oxygen atoms within the interlayers of uranium nitride with further capture by nitrogen vacancies, thus, resulting in their stabilization due to formation of the chemical bonds with the nearest uranium atoms. The relevant effects of the electronic charge re-distribution were ana-

lyzed. They demonstrate a quite local nature of the density perturbation caused by the incorporated O atoms. The analysis of density of states shows both overlapping of the O 2*p* states with the N 2*p* states at initial stages of oxidation (*surface incorporation*) and separation of the O 2*p* states from other bands in the case of deeper positioned oxygen atoms (*sub-surface penetration*). The results of this analysis could be used for the interpretation of the experimental ultraviolet photoelectron spectra for uranium oxynitrides [8].

Acknowledgements

This study was partly supported by the European Commission FP7 Project *F*-BRIDGE and ESF Project No. 2009/0216/1DP/1.1.1.2.0/09/APIA/VIAA/044. The corresponding author gratefully acknowledges also the doctoral studies support by the European Social Fund. The authors kindly thank R.A. Evarestov, P. Van Uffelen and V. Kashcheyevs for a numerous fruitful discussions. The technical assistance of A. Gopejenko and A. Kuzmin was the most valuable.

References

[1] P.D. Wilson (Ed.), The Nuclear Fuel Cycle, University Press, Oxford, 1996.
[2] B.J. Jaques, B.M. Marx, A.S. Hamdy, D.P. Butt, J. Nucl. Mater. 381 (2008) 309.
[3] C.B. Yeamans, G.W. Chinthaka Silva, G.S. Cerefice, K.R. Czerwinski, T. Hartmann, A.K. Burrell, A.P. Sattelberger, J. Nucl. Mater. 374 (2008) 75.
[4] Y. Arai, M. Morihira, T. Ohmichi, J. Nucl. Mater. 202 (1993) 70.
[5] H. Wiame, M. Centeno, S. Pacard, P. Bastian, P. Grange, J. Eur. Ceram. Soc. 18 (1998) 1293.
[6] G.P. Novoselov, V.V. Kushnikov, V.A. Baronov, V.P. Serebryakov, N.M. Stepennova, Atom. Energy 53 (1982) 528.
[7] A.F. Carley, P. Nevitt, P. Roussel, J. Alloys Compd. 448 (2008) 355.
[8] M. Eckle, T. Gouder, J. Alloys Compd. 374 (2004) 261.
[9] P. Weinberger, C.P. Mallett, R. Podloucky, A. Neckel, J. Phys. C: Solid State Phys. 13 (1980) 173.
[10] M.S. Brooks, J. Phys. F: Metal Phys. 14 (1984) 639.
[11] D. Sedmidubsky, R.J.M. Konings, P. Novak, J. Nucl. Mater. 344 (2005) 40.
[12] Z. Yongbin, M. Daqiao, Z. Zhenghe, M. Meizhong, Chin. J. Chem. Phys. 18 (2005) 735.
[13] E.A. Kotomin, Yu.A. Mastrikov, Yu.F. Zhukovskii, P. Van Uffelen, V.V. Rondinella, Phys. Status Solidi C 4 (2007) 1193.
[14] R. Atta-Fynn, A.K. Ray, Phys. Rev. B 76 (2007) 115101.
[15] E.A. Kotomin, R.W. Grimes, Yu.A. Mastrikov, N.J. Ashley, J. Phys.: Condens. Matter 19 (2007) 106208.
[16] M. Samsel-Czekała, E. Talik, P.deV. Du Plessis, R. Troć, H. Misiorek, C. Sułkowski, Phys. Rev. B 76 (2007) 144426.
[17] H. Shibata, T. Tsuru, M. Hirata, Y. Kaji, J. Nucl. Mater. 401 (2010) 113.
[18] P.F. Weck, E. Kim, N. Balakrishnan, F. Poineau, C.B. Yeamans, K.R. Czerwinski, Chem. Phys. Lett. 443 (2007) 82.
[19] L. Petit, A. Svane, Z. Szotek, W.M. Temmerman, G.M. Stocks, Phys. Rev. B 80 (2009) 045124.
[20] R.A. Evarestov, A.V. Bandura, M.V. Losev, E.A. Kotomin, Yu.F. Zhukovskii, D. Bocharov, J. Comput. Chem. 29 (2008) 2079.
[21] Yu.F. Zhukovskii, D. Bocharov, E.A. Kotomin, R.A. Evarestov, A.V. Bandura, Surf. Sci. 603 (2009) 50.
[22] Yu.F. Zhukovskii, D. Bocharov, E.A. Kotomin, J. Nucl. Mater. 393 (2009) 504.
[23] E.A. Kotomin, Yu.A. Mastrikov, J. Nucl. Mater. 377 (2008) 492.
[24] E.A. Kotomin, D. Gryaznov, R.W. Grimes, D. Parfitt, Yu.F. Zhukovskii, Yu.A. Mastrikov, P. Van Uffelen, V.V. Rondinella, R.J.M. Konings, Nucl. Instrum. Method B 266 (2008) 2671.
[25] D. Bocharov, D. Gryaznov, Yu. F. Zhukovskii, E.A. Kotomin, Surf. Sci., in press, doi:10.1016/j.susc.2010.11.007.
[26] G. Kresse, J. Furthmüller, VASP the Guide, University of Vienna (2009). <http://www.cms.mpi.univie.ac.at/vasp/>.
[27] (a) G. Kresse, J. Hafner, Phys. Rev. B 48 (1993) 13115;
(b) G. Kresse, J. Hafner, Phys. Rev. B 49 (1994) 14251.
[28] G. Kresse, J. Furthmüller, Comput. Mater. Sci. 6 (1996) 15.
[29] G. Kresse, J. Furthmüller, Phys. Rev. B 54 (1996) 11169.
[30] J. Hafner, Comput. Phys. Commun. 177 (2007) 6.
[31] P.E. Bloechl, Phys. Rev. B 50 (1994) 17953.
[32] G. Kresse, D. Joubert, Phys. Rev. B 59 (1999) 1758.
[33] J.P. Perdew, J.A. Chevary, S.H. Vosko, K.A. Jackson, M.R. Pederson, D.J. Singh, C. Fiolhais, Phys. Rev. B 46 (1992) 6671.
[34] H.J. Monkhorst, J.D. Pack, Phys. Rev. B 13 (1976) 5188.
[35] D. Gryaznov, E. Heifets, E. Kotomin, Phys. Chem. Chem. Phys. 11 (2009) 7241.
[36] R.W. Grimes, C.R.A. Catlow, Phil. Trans. Roy. Soc. A 335 (1991) 609.
[37] Y.-L. Lee, J. Kleis, J. Rossmeisl, D. Morgan, Phys. Rev. B 80 (2009) 224101.
[38] Yu. Mastrikov, R. Merkle, E. Heifets, E.A. Kotomin, J. Maier, J. Phys. Chem. C 114 (2010) 3017.